DOCTOR OF PHILOSOPHY

Advanced avalanche photodiode receivers in optical communications.

Fyath, Raad Sami

Award date:
1990

Awarding institution:
Bangor University

ADVANCED AVALANCHE PHOTODIODE RECEIVERS

IN OPTICAL COMMUNICATIONS

Thesis Submitted in Candidature for the Degree

of Doctor of Philosophy

April 1990

Raad Sami Fyath

School of Electronic Engineering Science

University of Wales-Bangor

United Kingdom

ACKNOWLEDGMENTS

I wish to express my thanks to Professor John J. O'Reilly for his advice and motivation throughout the course of this study and for his help in the final preparation of the thesis. I am also grateful to the University of Basrah (Iraq) for a Postgraduate Scholarship. Finally, my thanks to all the colleagues at the Engineering Department who contributed to my work with many fruitful discussions and continuous encouragement.

SUMMARY

This thesis is concerned with a detailed study of the performance of superlattice avalanche photodiodes (SAPDs) and the implications for high bit rate direct-detection optical fibre communication systems. In these advanced detectors the electron to hole ionisation rate ratio is artificially enhanced through selective heating of the electron distribution to reduce the excess noise associated with the randomness of the avalanche multiplication and to ensure high gain-bandwidth product. Thus SAPDs are suitable for long wavelength applications (1.3-1.6 μm) where most compound semiconductor materials otherwise have comparable electron and hole ionisation rates.

A comprehensive discrete ionisation model is developed to assess the performance of SAPDs; emphasis being placed on the gain, excess noise factor, gain moment generating function (MGF), and gain-bandwidth product. The model is quite flexible and it is found that other device impairments such as dark current and the number of ionisations per stage caused by the injected carrier can be readily incorporated into the formulation. The performance of optical receivers employing SAPDs is examined using a Gaussian approximation (GA) and taking into account the influence of various device impairments. To assess the accuracy of GA a rigorous statistical analysis is developed using a MGF formulation.

New signal designs for optical communications devised specifically for APD receivers are described. These signals achieve simultaneously both zero intersymbol interference and zero telegraph distortion with respect to a depressed optimum threshold and are thus well suited to untimed transmission. Importantly, they also offer improved tolerance to alignment jitter when they used in conventional fully retimed receivers.

CONTENTS

CHAPTER 1

INTRODUCTION

1.1 High Bit Rate Direct Detection Systems

Considerable effort has been invested world-wide in developing high bit rate, long haul direct detection optical communication systems. Increasing the bit rate expands the capacity of the system, whereas increasing the distance between transmitter and receiver ensures a decrease in the number of repeaters which can result in improved system reliability. In both cases, the effort ultimately reduces the cost of the communication system. Systems for 1.6 Gbit/s transmission have already been implemented for practical application [Cohen, 1986] and operating at >10 Gbit/s systems are currently being studied [Fujita et al., 1988; Gimlett et al., 1989].

The straight forward target for achieving longer repeater spacings is improved receiver sensitivity. The photodetectors used in the present 1.55μm wavelength band are based on InGaAs/InP avalanche photodiode (APD) structures with separate absorption and multiplication (SAM) regions [Campbell et al., 1983], or InGaAs pin FETs [Gimlett, 1987]. APDs have the potential benefit of providing internal gain and thereby offering improved sensitivity, especially at high bit rate. However, the performance of an APD is governed by the excess noise associated with statistical fluctuations in the multiplication process. This excess noise is a strong function of the ratio of ionisation rates for electrons and holes, which is about

0.4-0.6 in InP material systems. There is thus considerable interest in artificial enhancement of the ionisation rate of one carrier over the corresponding bulk rate through the use of superlattice structures [Capasso, 1983]. In these devices one type of carrier is selectively heated compared with the other via potential step discontinuities at the heterostructure interfaces. The target is to achieve ionisation rate ratios less than 0.01 in these structures. An improvement of up to 5dB in receiver sensitivity is possible, which corresponds to a 33km extension in the repeater spacing for 0.15 dB/Km fibre [Kimura, 1988].

A further feature of these superlattice APDs (SAPDs) is that carrier multiplication occurs at discrete locations in the device, leading to a reduction in the variability of the number of hole-electron pairs generated per photon. Thus these APDs can be considered as a first step towards a solid state photomultiplier, analogous to a photomultiplier tube. Capasso et al. (1983) have shown that the noise characteristics of staircase SAPDs cannot be calculated using the conventional McIntyre analysis [McIntyre, 1966] since the latter assumes carrier ionisation to be a continuous process, as is appropriate for conventional APDs (CAPDs). In addition, Teich et al. [1986a; 1986b] have found that the theory of discrete ionisation processes proposed by van Vliet and co-workers [1979a; 1979b] for short avalanche region CAPDs is applicant for staircase and other superlattice APDs, assuming single ionisation per initiating carrier per stage. The performance of optical receivers incorporating such advanced structures has been reported for the ideal case of zero dark

current and negligible residual hole ionisation [Teich et al., 1986b]. The effect of these (and other) device impairments on system performance will be discussed in this thesis in detail.

1.2 Thesis Organisation

Following this introductory chapter, an overview of superlattice avalanche photodiodes (SAPDs) is presented in Chapter 2. Consideration is given to the discrete ionisation model used to investigate the noise characteristics of these advanced detectors.

In Chapter 3 formulas are derived for the effective gain and effective excess noise factor associated with dark current generated in SAPDs. This allows us to investigate the performance of optical receivers incorporating SAPDs taking into account the influence of both dark current and residual hole ionisation. The analyses are then extended for conventional avalanche photodiodes (APDs) to examine the influence of dark current generated within the multiplication (avalanche) region.

The performance of a staircase APD is usually analysed assuming that electrons ionise at the steps only while the holes ionise within the graded-gap regions [Capasso et al., 1983]. In Chapter 4 the analysis is extended, in order to consider the effect of carrier (electron and hole) impact ionisation both in the graded-gap regions and at the steps. General formulas for the gain and excess noise factor have been derived relating to three important extreme cases. The performance of a 2 Gbit/s optical receiver employing a ten-stage staircase APD has been examined to assess the influence of various

carrier ionisation probabilities.

Recently interest has been expressed in SAPDs in which multiple ionisations per initiating carrier per stage occur, similar to secondary emission in photomultiplier tubes, thereby greatly enhancing the gain of the device. In Chapter 5 we extend the existing analysis of SAPDs to allow for the production of up to two impact ionisations per initiating carrier per stage. Extension for more than two ionisations is considered in Chapter 6 where a new discrete ionisation model for a solid state photomultiplier (SSPM) is presented and used to predict the gain and excess noise characteristics of these devices. The expressions obtained here are quite general and can be applied to photomultiplier tubes, single ionisation or two-ionisation SAPDs, and CAPDs. The performance of optical receivers based on these advanced APDs is also examined, emphasis being placed on the effect of both dark current and residual hole ionisation.

A Gaussian approximation (GA) has been used in Chapters 3-6 to predict the performance of optical receivers based on SAPDs. This technique make use of the excess noise factor, representing first and second order statistical properties of the gain fluctuations introduced by the multiplication process. A more precise measure for the performance of these systems requires a comprehensive statistical description of the random gain associated with SAPDs. This problem is addressed in Chapter 7. First we present a numerical technique to evaluate the moment generating function (MGF) associated with the multiplication process of nonideal SAPDs (with residual hole ionisation). Secondly, we use the MGF together with a modified

Chernoff bound [Prabhu 1982, da Rocha and O'Reilly, 1982] to predict the performance of SAPD receivers in the presence of dark current. A comparison with the GA is also presented.

In Chapter 8 we direct our attention to the speed of response of SAPDs, and the effect on the performance of high bit rate lightwave receivers. We have shown that the SAPD may be modelled as a CAPD in which the hole and electron ionisation rates exhibit position dependency corresponding to a series of impulses, one per stage. This has enabled us to apply the theory of CAPDs directly to predict the gain-bandwidth product of SAPDs.

Chapter 9 is devoted to overall receiver considerations. We start by comparing the performance of SAPD receivers with that for CAPDs. This is necessary in order to indicate upper bounds on superlattice device non-idealities, which are strongly dependent on the number of stages, below which these advanced APDs can offer improved performance compared with existing long wavelength CAPDs. We then describe new signal designs for optical communications based on APD receivers. These signals achieve simultaneously both zero intersymbol interference (ISI) and zero telegraph distortion (TD) with respect to a depressed optimum threshold encountered with high performance APD receivers. The new signal design targets are thus well suited to untimed transmission whilst also offering improved tolerance to alignment jitter when used in conventional fully retimed optical receivers. The practical realisation is considered to consist of signal shaping networks with responses closely approximating these new designs.

Chapter 10 concludes the thesis, summarising the main findings and identifying areas where further research may be appropriate.

1.3 Contributions

The research reported here sought to provide a detailed and comprehensive assessment of the performance of direct detection optical receivers incorporating superlattice avalanche photodiodes (SAPDs), emphasis being placed on the influence of residual hole ionisation and dark current. The gain and noise characteristics of various SAPDs have been analysed using discrete ionisation models and used as a basis for performance assessment of practical systems. In order to achieve this it has been necessary to produce a number of new derivations and means of analysis, relating both to specific impairments and their combined influence on system performance.

The main contributions of this thesis may be summarised as follows:

(1) Expressions are derived for the effective gain and effective excess noise factor associated with dark current in SAPDs [Fyath and O'Reilly, 1988a]. This allows us to assess the influence of various dark current components on the performance of optical receivers employing these devices [O'Reilly and Fyath, 1988a; Fyath and O'Reilly, 1988e]. The analyses are then extended for CAPDs to investigate the effect of dark current generated within the avalanche region [Fyath and O'Reilly, 1989a].

(2) The performance of optical receivers using a recently proposed new APD, in which multiplication is achieved by single impact ionisation per traversal of the primary carrier through the device, has been investigated. It has been shown that the sensitivity improves as a function of ionisation rates ratio k, a behaviour which is in contrast to that for CAPDs [O'Reilly and Fyath, 1988c].

(3) The existing analysis of staircase APDs has been extended to allow for the possibility of both types of carriers impact ionising at the steps and in the graded regions. We identify and discuss three extreme cases depending on material and structure of the diode. The influence of various carrier ionisation probabilities on receiver performance has been examined [Fyath and O'Reilly, 1988d].

(4) General expressions have been obtained for the average gain and excess noise factor associated with photocurrent and dark current in SAPDs where multiple ionisations per initiating carrier per stage may occur. The performance of optical receivers utilising these advanced detectors has also been examined [Fyath and O'Reilly, 1988b, 1988c, 1988h].

(5) A gain moment generating function (MGF) formulation for SAPDs has been developed and evaluated numerically taking into account the effect of residual hole ionisation. This has been used as a basis for rigorous analysis of optical receivers employing these detectors. We have described a statistical model for the detection process using the modified Chernoff bound which has enabled us to assess accurately receiver performance in the presence of hole ionisation and dark current [Fyath and O'Reilly, 1989b, 1989d].

(6) We have examined in detail the speed of response of SAPDs and its effect on the performance of multigigabit per second lightwave receivers. Particular consideration is given to the avalanche build-up time arising from the regenerative nature of the multiplication process in the presence of residual hole ionisation [Fyath and O'Reilly, 1988f, 1988g; O'Reilly and Fyath, 1989].

(7) We have presented a comparison of the performance of SAPD optical receivers with that for CAPD receivers. This has enabled upper bounds to be indicated on superlattice device non-idealities below which these advanced APDs can offer improved performance compared with existing long wavelength CAPDs [Fyath and O'Reilly, 1989c].

(8) New signal designs developed for optical receivers employing APDs have been presented. These provide zero ISI and zero TD with respect to a depressed optimum threshold and can then be used for both untimed (2R) and fully retimed (3R) repeaters. The effect of alignment timing jitter on the performance of retimed receivers has been considered and the new designs have been shown to offer reduced power penalties compared with widely adopted raised cosine receivers. A fourth-order low pass ladder network filter has been shown to provide a suitable basis for a practical realisable approximation [Fyath and O'Reilly 1987, O'Reilly and Fyath, 1988b].

CHAPTER 2

SUPERLATTICE AVALANCHE PHOTODIODES

2.1 Introduction

Recent years have seen renewed interest in avalanche photodiodes (APDs) as detectors for long haul lightwave communication systems. The internal gain associated with the avalanche process in these devices provides a potential means of overcoming thermal noise limitations in wideband detection [Personick, 1973]. Unfortunately, the performance of an APD is governed by excess noise associated with statistical fluctuations in the multiplication process. Nevertheless, it is widely accepted that APDs can provide substantial improvement in receiver sensitivity compared with PIN photodiodes, the margin provided by the APD increasing with bit rate [Brain, 1982; Smith and Forrest, 1982]. Multiplication noise for conventional APDs (CAPDs) was investigated by Tager [1965] and later by McIntyre [1966]. These results show that it is important for low noise, high gain APDs that carrier feedback in the multiplication process be minimised, that is, the electron and hole ionisation coefficients α and β should be very different, and the carrier species with the highest ionisation rate should initiate the avalanche process. For wavelengths below 1μm the silicon APD represents a near-ideal detector choice for optical fibre communication systems since the hole to electron ionisation rate ratio is less than 1/20 in this material [Webb et al., 1974; Robbins et al., 1985].

The more recent development of optical fibres with low loss and

negligible dispersion in the 1.2-1.6μm wavelength range has led to extensive research on new photodetector materials. These investigations have shown that germanium and most III-V materials sensitive to this wavelength range have nearly equal ionisation coefficients so that they are unsuitable for low noise APDs [Stillman et al., 1984]. There is thus considerable interest in new APD structures in which the ionisation rate ratio can be artificially enhanced.

2.2 APDs with Enhanced Ionisation Rate Ratios

Several principles have either been used or proposed for altering the ionisation rate ratio, among these are the following :

(a) Eliminating the feedback noise associated with residual hole ionisation by trapping the holes in a potential well formed between two heterojunctions [Gordon et al., 1979].

(b) Difference between the ionisation energies and the quasi-electric fields for electrons and holes in graded-gap materials [Capasso, 1981].

(c) The use of superlattice or multilayer structures in which the distribution of one carrier type (electrons in general) is selectively heated to high energy while the hole distribution remains relatively cool such that no subsequent ionisation occurs. Various schemes have been proposed which are based on : use of large asymmetry between conduction and valence-band discontinuities as in multiquantum well APDs [Chin et al., 1980; Capasso et al., 1982] and staircase APDs [Capasso et al., 1983], use of built-in electric field arising from a periodic doping profile in conjunction with band-edge discontinuity as

in doped quantum well APDs [Blauvelt et al., 1982], or the use of sequential resonant tunelling [Brennan and Summers 1987a].

(d) Spatial separation of electrons and holes in materials of different bandgaps such as in channelling APDs [Capasso, 1982a, 1982b; Tanoue and Sakaki, 1982].

(e) Resonant enhancement of impact ionisation in a superlattice, induced by the zone folding effect [Mon and Hess, 1982].

(f) Making use of resonant impact ionisation initiated by holes from the split-off valence band. This occurs when the spin orbit splitting is equal to the bandgap energy which makes the threshold energy for hole initiated impact ionisation reach the smallest possible value and the ionisation process occurs with zero momentum. This leads to a strong increase of hole ionisation coefficient. An ionisation rate ratio of about 0.1 has been reported in AlGaSb [Hildebrand et al., 1981] and HgCdTe [Alabedra et al., 1985].

(g) By using silicon as the avalanche material in SAM (separate absorption and multiplication) structures. This material has small impact ionisation rate ratio suitable for low noise carrier multiplication. Avalanche gain as high as 50 has been measured at a wavelength of 1.3μm in Ge_xSi_{1-x}/Si heterostructure photodiodes [Pearsall et al., 1986]. The absorption of the infrared radiation occurs in a GeSi/Si strained-layer superlattice which serves as a waveguide core, and the avalanche multiplication takes place in one of the Si-cladding layers.

The superlattice APDs (SAPDs) mentioned in (c) have attracted increasing interest in the literature as promising long wavelength detectors with ionisation rate ratio below 0.01. The prediction of

enhancement of ionisation rate ratio has been clarified experimentally [Capasso et al., 1982; Juang et al., 1985; Yu et al., 1987] and theoretically using both Monte Carlo simulation [Brennan, 1985a; Brennan and Wang, 1988] and lucky drift theory [Ridley, 1985; Marsland and Woods, 1987; MacBean, 1990b].

2.3 Examples of SAPDs

SAPDs have in general a p-i-n form where the superlattice "i" region consists of a periodic structure of alternating layers of different bandgaps. The engineering of this region and the material used are responsible for the enhancement of the ionisation rate ratio in these devices.

2.3.1 Quantum well APDs

This structure was first proposed by Chin et al. (1980) and it is illustrated schematically in Fig. 2.1 along with its corresponding energy band diagram. The avalanche region consists of alternating layers of wide and narrow bandgap materials. In addition, the majority of the bandgap discontinuity occurs in the conduction band. In this structure an electron is accelerated by the electric field through the wide bandgap material (barrier) until it reaches the small bandgap material (well). When it enters the well, it abruptly gains an energy equal to the conduction-band, discontinuity ΔE_c. It is important to stress the ballistic nature of this energy gain. The threshold of impact ionisation of electrons in the small bandgap material is effectively lowered by ΔE_c. However, the valence-band discontinuity ΔE_v is not large enough to supply a similar energy boost

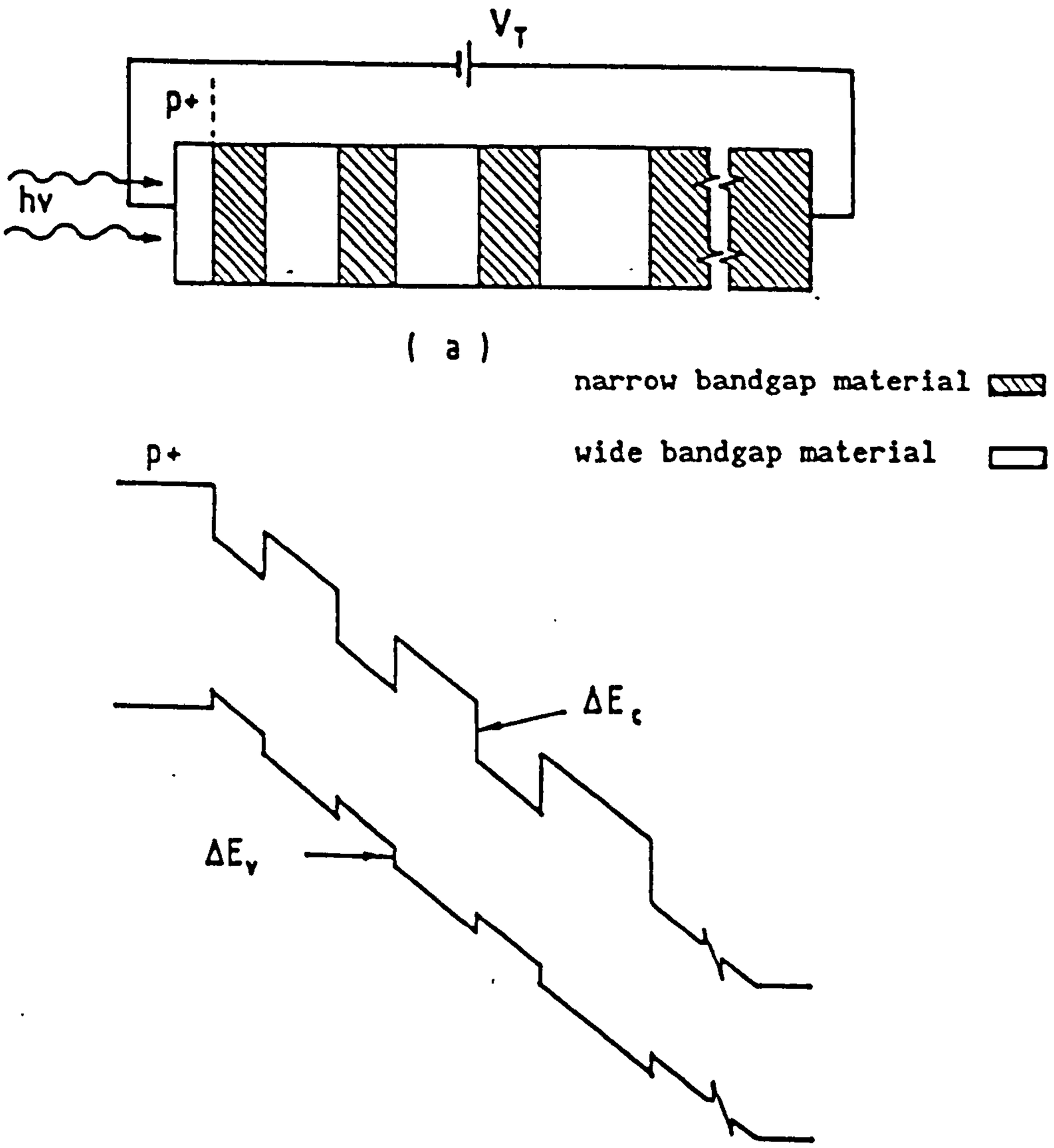

Fig. 2.1 Quntum well avalanche photodiode.
(a) schematic diagram
(b) energy band-diagram

to free holes (for semiconductor heterostructures where $\Delta E_c > \Delta E_v$). Since the impact ionisation rate depends exponentially on the impact ionisation threshold, the electron ionisation rate α is enhanced much more than that for holes, β.

A quantum well APD similar to the one proposed by Chin et al. was fabricated by Capasso et al. [1982] and consisted of 50 alternating $Al_{0.45}Ga_{0.55}As$ (550Å) and GaAs (450Å) layers with a doping concentration of $2x10^{14}cm^{-3}$. They obtained electron to hole ionisation rate ratio α/β of 7 to 8, which represents an improvement of a factor of 3 to 4 over α/β in GaAs bulk material. Brennan et al. [1985a] have reported on Monte Carlo calculations of the ionisation rate coefficient in a superlattice of AlGaAs/GaAs ide n tical to the one used by Capasso et al. [1982]. They found an excellent fit to the electron ionisation rate data of Capasso et al. if ΔE_c is taken to be 0.75 of the bandgap difference. The calculated hole ionisation rate, on the other hand, is comparable to the bulk value, which is again in agreement with experimental data.

Other authors have also observed an enhancement of the α/β ratio in AlGaAs/GaAs superlattices [Juang et al. 1985; Kagawa et al., 1989]. Osaka et al. [1986] have reported an enhancement of β by a factor of four over the bulk value in $Ga_{0.47}In_{0.53}As$/InP superlattices due to the large value of ΔE_v. Yu et al. [1987] have measured β/α equal to 6 in InGaAs/InAlAs SAPDs.

Recently Capasso et al. [1986] have observed a new avalanche phenomenon in superlattices, namely, impact ionisation across band-edge discontinuities of carriers confined in the wells. This ionisation phenomenon was briefly discussed by Smith et al. [1983] and

later Chuang and Hess [1986] have proposed it independently and calculated the ionisation rates. In this ionisation effect only one type of carrier is created so that the positive feedback of impact ionisation of the other carrier species eliminated, leading to the possibility of a quiet avalanche with small excess noise. This has been confirmed experimentally by Capasso et al. [1986] on both AlInAs/GaInAs and AlSb/GaSb superlattices, and by Allam et al. [1987] on AlInAs/GaInAs systems. In the latter structure ionisation rate ratio β/α in excess of 50 have been measured, which is the highest ionisation rate ratio measured to date in III-V materials.

2.3.2 The graded-gap staircase APD

This detector has been devised by Capasso et al. [1983] as a semiconductor analogue to the photomultiplier tube. It is also based on the physical concept of impact ionisation assisted by a band edge discontinuity. In a staircase APD, however, the entire ionisation energy may be acquired at the conduction band steps. Fig. 2.2 illustrates the staircase APD, along with its associated energy band diagram. Each stage is linearly graded in composition from a low (E_{g1}) to a higher (E_{g2}) bandgap, with an abrupt step back to low bandgap material. The conduction band discontinuity shown accounts for most of the bandgap difference. The materials are chosen for a conduction band discontinuity ΔE_c comparable to, or greater than, the electron ionisation energy E_{ie} in the low gap material following the step.

The band structure of the staircase APD under reverse biased is shown in Fig. 2.2c. Consider that a photoelectron is generated

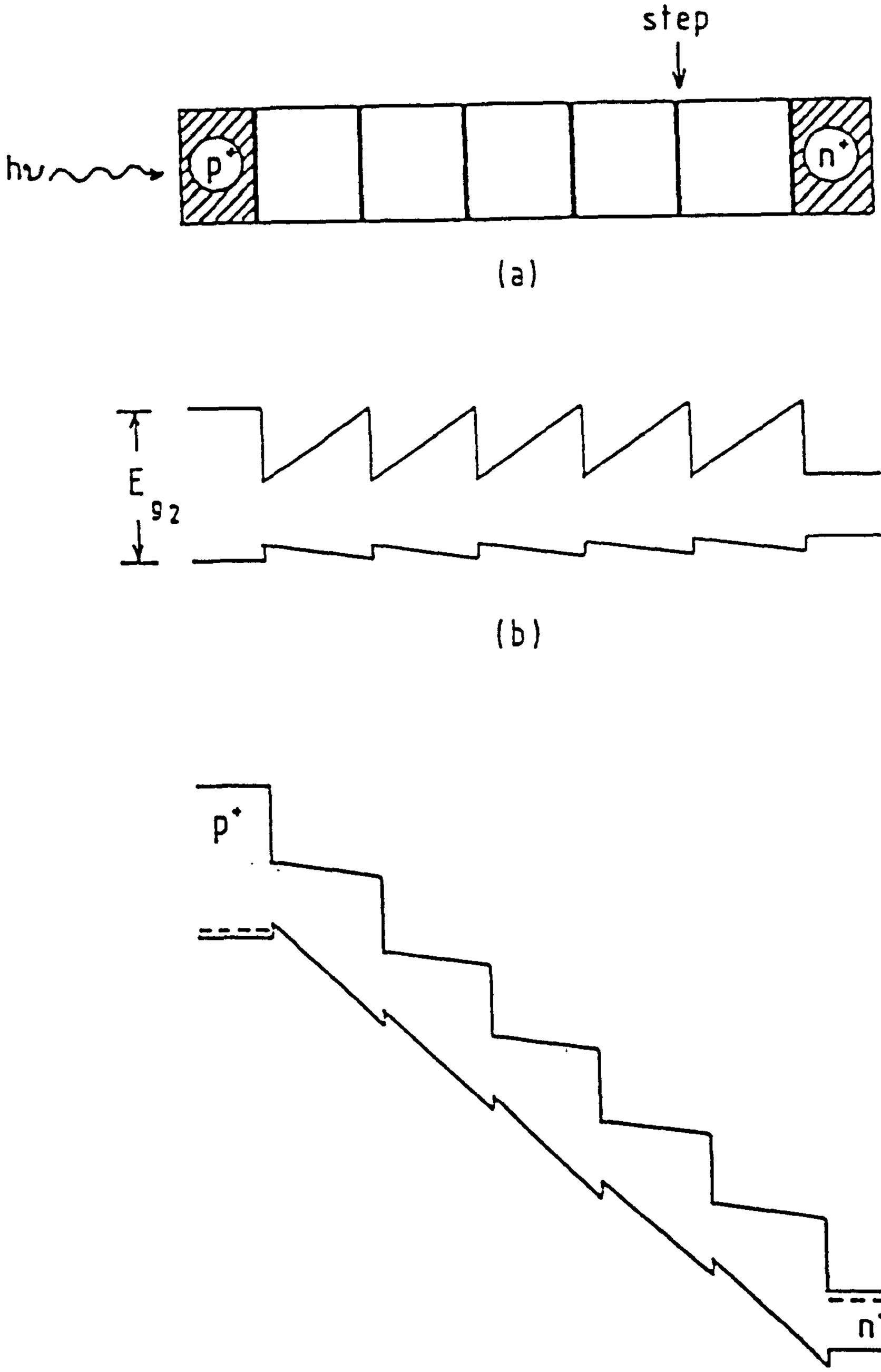

Fig. 2.2 Graded-gap staircase avalanche photodiode.
(a) schematic diagram
(b) energy band-diagram under zero bias
(c) energy band-diagram under reversed bias

next to the p^+ region. Under the combination of the biasfield F and the grading field $\Delta E_c/L$ (L is the width of the graded region), it drifts towards the first conduction-band step. The effective electric field in the graded region $F-\Delta E_c/L$ is small enough so that the electron does not impact ionise before it reaches the step [Williams et al., 1982; Capasso et al., 1983]. After the step, since $\Delta E_c \cong E_{ie}$, the electron impact ionises; this ballistic ionisation process is repeated in each stage. In this structure the valence-band steps are of the wrong sign to assist ionisation. Thus any residual hole ionisation can only be caused by the effective electric field in the graded region, which is chosen so that holes cannot ionise them. For electron transport across the graded region, the bias field must be sufficiently high to cancel the $\Delta E_c/L$ quasi- electric field and provide a small extra component to assure drift rather than diffusion transport. Ideally, only electrons impact ionise in this structure and hence the multiplication process is virtually noise-free, even at high gain. For long wavelength photodetectors, two material systems are presently of interest: Al/GaAsSb/GaSb on GaSb substrate and HgCdTe lattice matched to CdTe or InSb substrates [Capasso 1985].

A further feature of SAPDs is that carrier multiplication occurs at discrete locations in the device - the narrow bandgap layers in multiquantum well APDs and conduction band steps in staircase APDs - leading to a reduction in the variability of the number of hole-electron pairs generated per photon. Thus these APDs can be considered as a first step towards a solidstate photomultiplier, analogous to a photomultiplier tube. Capasso et al. (1983) have shown that the noise characteristics of staircase APDs cannot be calculated

using the conventional McIntyre analysis [McIntyre, 1966] since the latter assumes carrier ionisation to be a continuous process, as is appropriate for CAPDs. Thus a discrete ionisation model is required to investigate the noise characteristics of these advanced APDs. The features of this model will be discussed in the following section.

2.4 Discrete Ionisation Model

The avalanche multiplication process in semiconductor devices has usually been analysed using standard "continuous" device physics, involving differential or integral equations for position-dependent multiplied carrier fluxes. For two-carrier multiplication processes such as occur in bipolar devices, a detailed theory for the multiplication factors and noise was given by Tager [1965] for the case that ionisation coefficients of electrons and holes are equal, and by McIntyre [1966] for the general case that the ionisation coefficients for electrons and holes are different. A simple theory for the avalanche process in JFETs, where only majority carriers participate in the multiplication process, was given later by van der Ziel and Chenette [1978], although the result was known earlier to Tager. In these papers it is assumed that the avalanche region is very long compared to the mean free path for an impact ionisation to occur, so that the number of ionisations per carrier transit is extremely large. Only under these conditions can one justify the use of continuous ionisation rates per unit length, $\alpha(x)$ for electrons and $\beta(x)$ for holes. When the avalanche region is short the above theories cannot be relied on. This was first observed by Lukaszek et al. [1976] in which they showed that for low-breakdown-voltage diodes the

number of possible ionisations per carrier transit through the avalanche region is often no more than one or two. They used a rather complex statistical theory to derive new expressions for the multiplication and the noise, presuming no more than one ionisation or two ionisations per carrier transit. The theoretical results were in good agreement with their experimental data. Experimental results conducted by other works also support the discrete ionisation approach in short avalanche region devices [Rucker and van der Ziel, 1978; Campbell et al., 1989a].

Van Vliet et al. [1979a, 1979b] have developed a comprehensive analysis for the gain and excess noise in short avalanche region devices. The theory involves consideration of the discrete statistical process whereby N ionisations can occur per carrier transit in the avalanche region. As N tends to ∞ they recovered McIntyre's results [1966] for continuous ionisation in CAPDs. Further for N=1, which is applicable for submicrometer devices under the influence of extremely high electric field, they recovered Lukaszek's results [1976]. Later Teich et al. [1986a, 1986b] found that the theory of discrete ionisation processes developed by van Vliet and co-workers is applicable to staircase APDs and other superlattice APDs, assuming single ionisation per initiating carrier per stage. For a N-stage SAPD the average gain and excess noise factor for pure electron injection can be expressed as

$$\langle M_e \rangle \equiv \langle g_N \rangle = \frac{(1+p)^N (p-u)}{p(1+u)^{N+1} - u(1+p)^{N+1}} \qquad (2.1)$$

$$F_e \equiv F_N = 1 + \frac{(1-1/<g_N>)(p-u)}{p(2+u+p)}\left[-p + \frac{2(1-up)}{(1+u)}\left[\frac{u(1+p)<g_N>}{p-u} + \frac{1}{1+p}\right]\right] \qquad (2.2)$$

where p and u represent the impact ionisation probability per stage for electrons and holes respectively (assumed to be identical for various stages). For N=1 eqns. 2.1 and 2.2 reduce to

$$<M_e> = \frac{1+p}{1-kp^2} \qquad (2.3)$$

$$F_e = \frac{1+3p+3kp^2+kp^3}{(1+p)^2} \qquad (2.4)$$

in accord with Lukaszek's results [1976]. Here $k \equiv u/p$. For conventional APDs, we let $N \to \infty$ and set $p = \alpha.\Delta x$ and $u = \beta.\Delta x$ with Δx the width of the stage and α and β the ionisation rates per unit length for electrons and holes, respectively. Using these expressions for u and p with eqns. 2.1 and 2.2, and letting $\Delta x \to 0$ we obtain McIntyre's results [1966] for uniform CAPDs:

$$<M_e> = \frac{(1-k)\ \exp[\alpha W(1-k)]}{1-k\ \exp[\alpha W(1-k)]} \qquad (2.5)$$

$$F_e = <M_e>\left[\left[1-(1-k)\ [(<M_e>-1)/<M_e>]^2\right]\right] \qquad (2.6)$$

where W is the width of the avalanche region, $k = \beta/\alpha$, and we make use

of the relation [van Vliet et al. 1979b].

$$\lim_{N\to\infty} [(1+p)/(1+u)]^N = \exp[W(\alpha-\beta)] \tag{2.7}$$

It is also interesting to examine eqns. 2.1 and 2.2 for two extreme cases according to the value of k: k=0 (very-low noise device) and k=1 (high-noise device). For the first case we have

$$\langle g_N \rangle = (1+p)^N \tag{2.8a}$$

$$F_N = [(1-p)/(1+p)]\left[1+[1-(1+p)^{-N}]\right] \tag{2.8b}$$

Note that $F_N=1$ in two cases p=0 and p=1 since the gain will be deterministic. For k=1 such that u=p eqns. 2.1 and 2.2 reduce to:

$$\langle g_N \rangle = 1/(1-Np) \tag{2.9a}$$

$$F_N = (1-Np^2)/(1-Np) \tag{2.9b}$$

In order to address the general case, we plot in Fig. 2.3 the gain of a SAPD as given by eqn. 2.1, as a function of p for different values of k≡u/p and number of stages N. This indicates that when k≠0, the average gain will increase without limit for certain parameter values (i.e. avalanche breakdown will occur). We also know that as k decreases, larger values of p are possible at fixed N before avalanche breakdown occurs. From eqn. 2.1, avalanche breakdown will occur in a

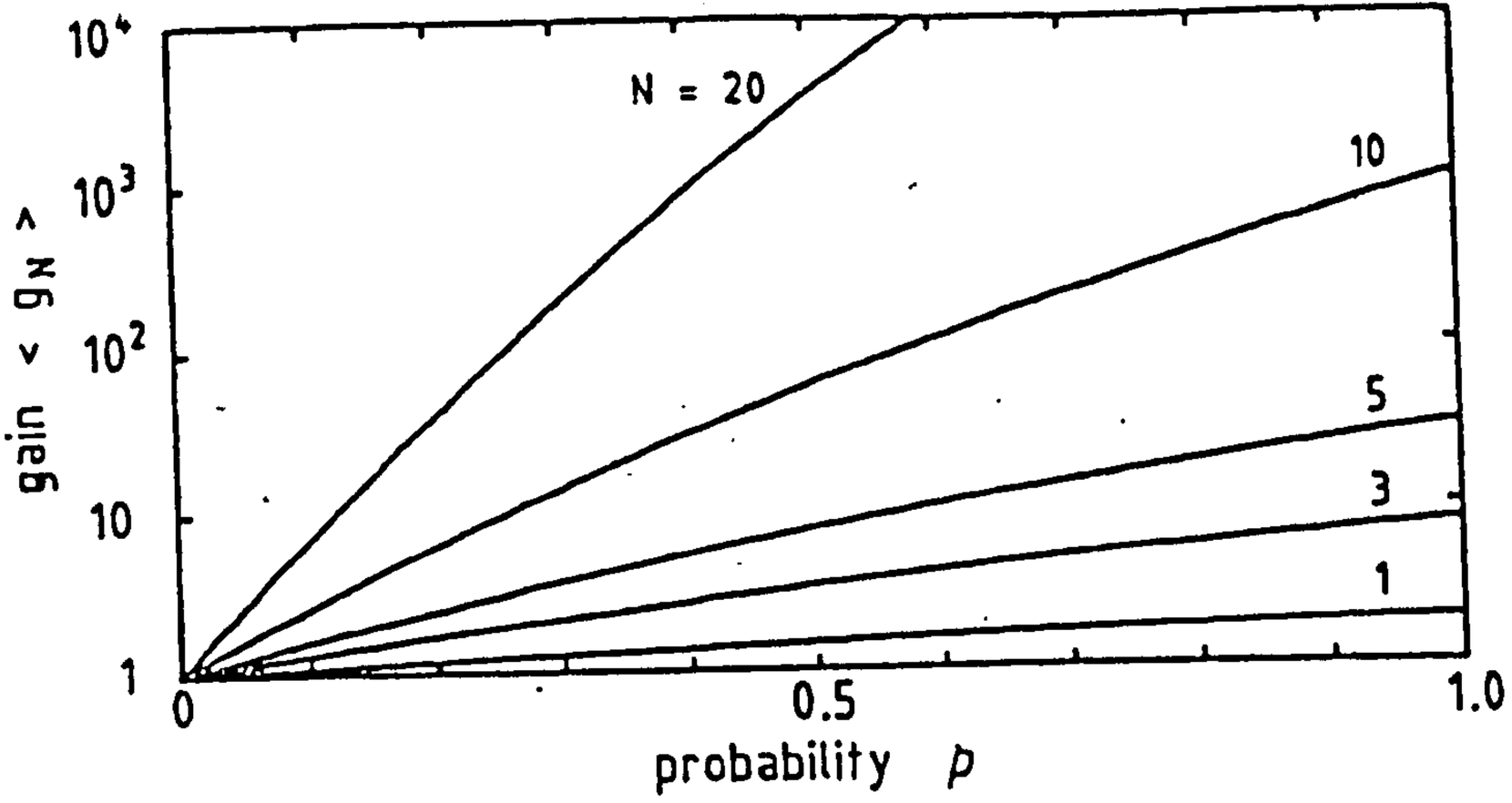

(a)

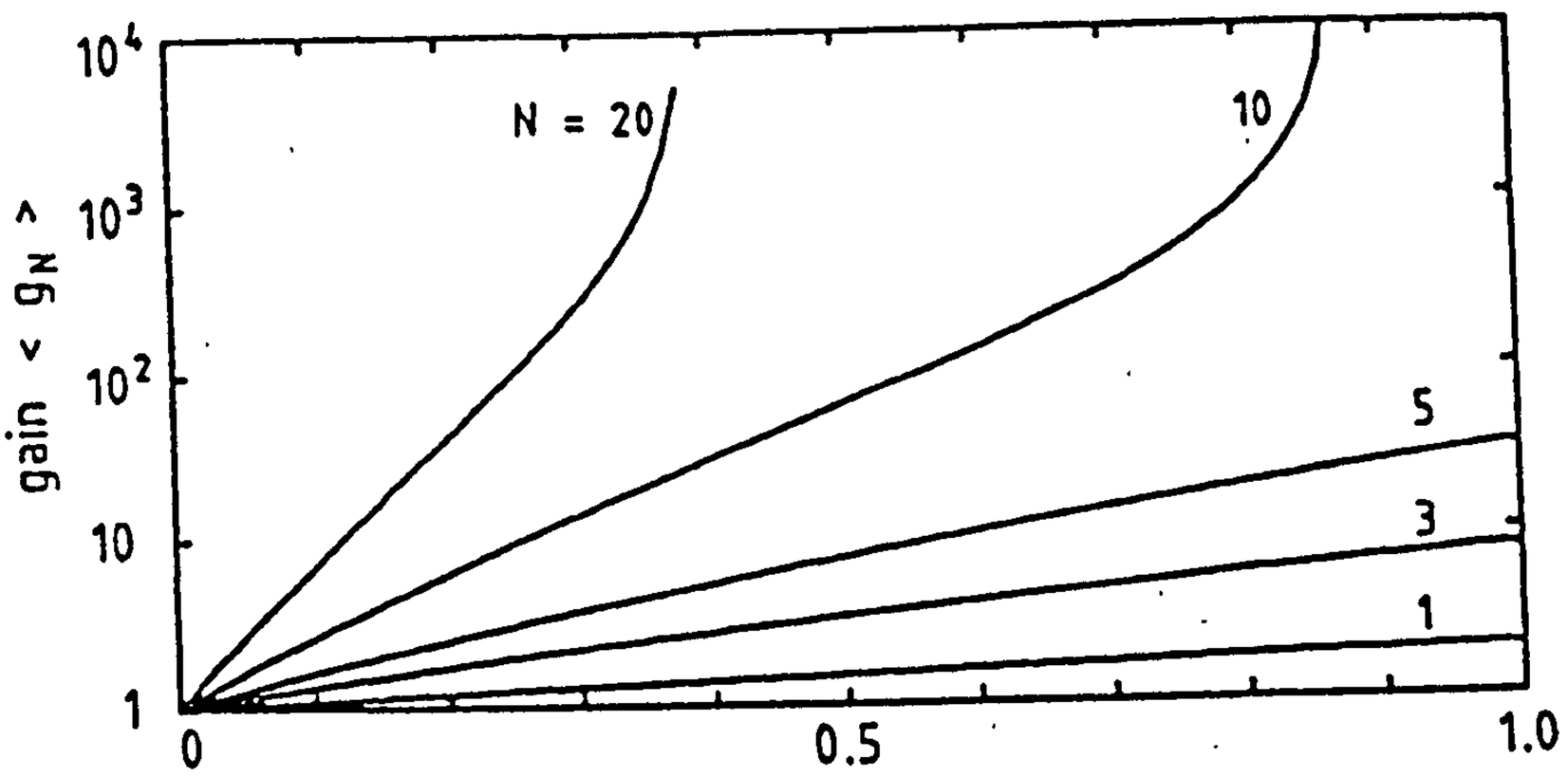

(b)

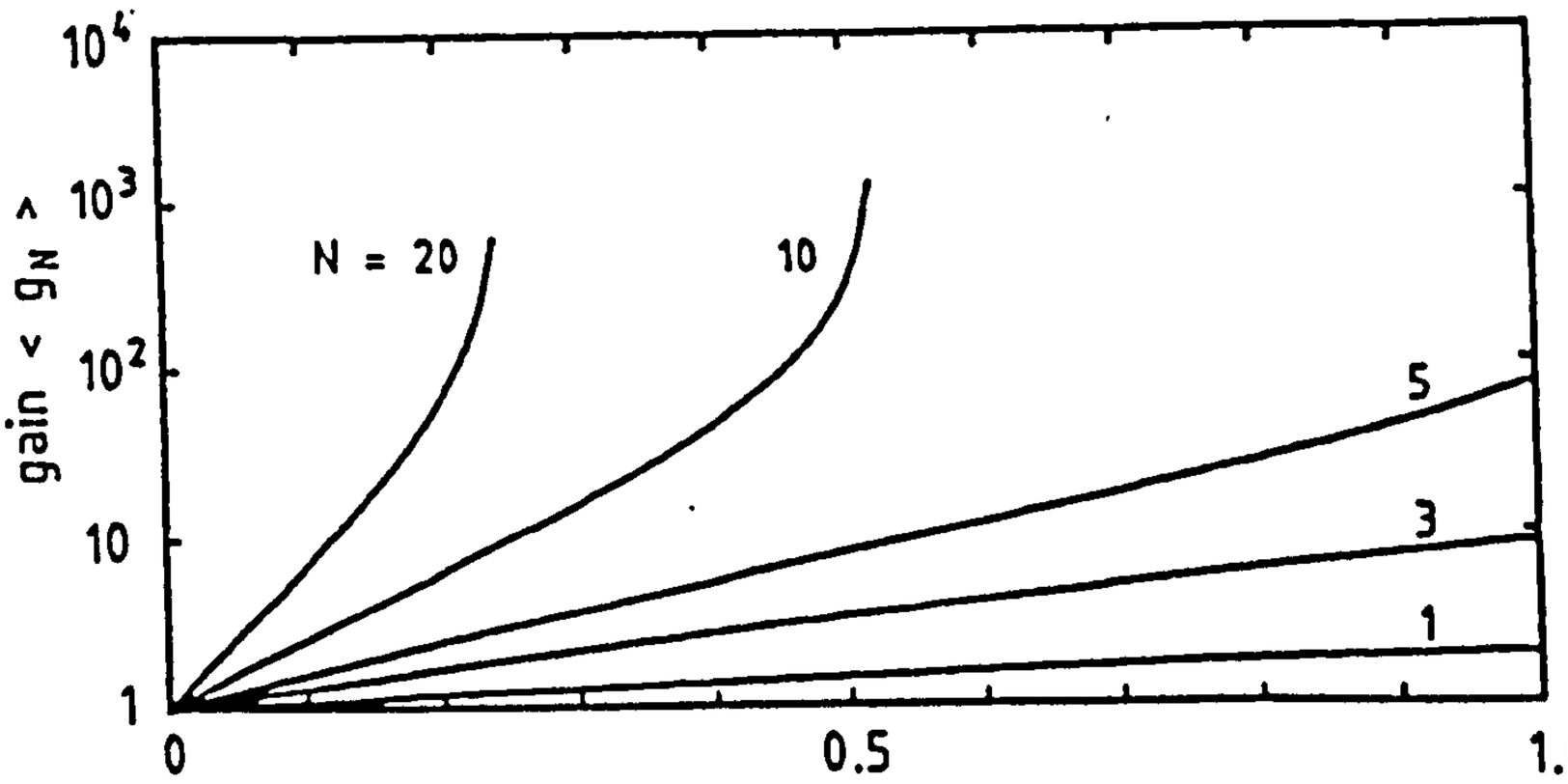

(c)

Fig. 2.3 Average gain associated with photogenerated carriers against electron ionisation probability per stage.
(a) k=0.0 (b) k=0.001 (c) k=0.01

SAPD if:

$$p(1+u)^{N+1} \leq u(1+p)^{N+1} \quad \text{for } p>u,\ u\neq 0$$

or

$$u(1+p)^{N+1} \leq p(1+u)^{N+1} \quad \text{for } p<u,\ p\neq 0 \qquad (2.10)$$

or

$$p \geq 1/N \quad \text{for } p=u,\ u\neq 0$$

For $u=0$ (or $p=0$) no avalanche breakdown will occur with a finite number of stages. From the conditions of eqn. 2.10, the maximum allowable value of p (for $p>u$) is presented in Fig. 2.4 as a function of N. Note that Fig. 2.5 illustrates the variation of the excess

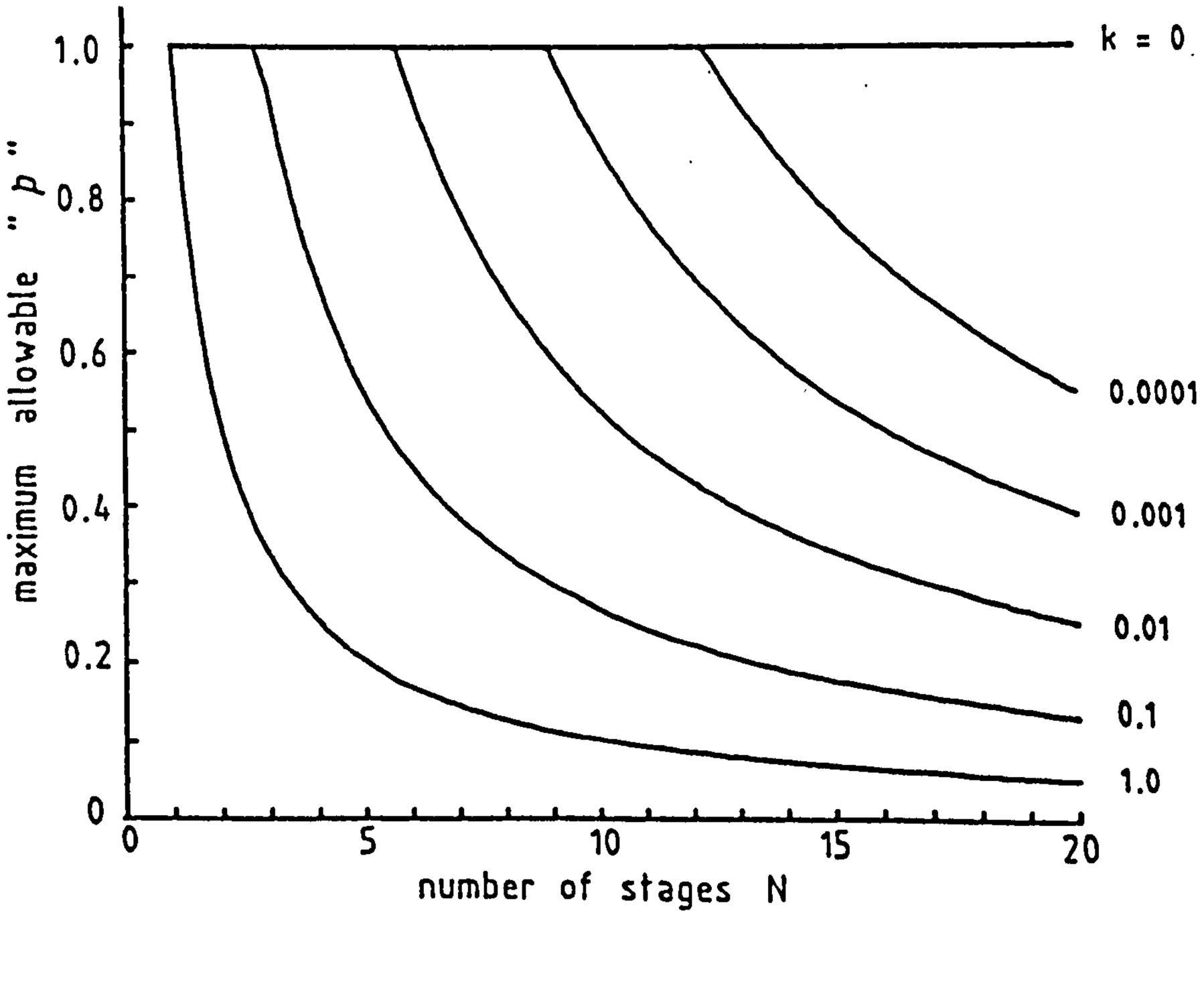

Fig. 2.4 Maximum allowable electron ionisation probability per stage versus number of stages.

noise factor of a SAPD as a function of electron ionisation probability taking k and N as parameters. Note that even a small non-zero value of k leads to a large increase in the excess noise factor, especially when N is large. This is in accord with previously published results [Teich et al., 1986a; Brennan, 1986c]. These results provide a limit on the residual hole ionisation that is tolerable in a SAPD. Brennan [1986c] has estimated k to be of the order of 10^{-3} for GaInAs/AlInAs doped quantum well devices with much higher values being predicted for other structures [Brennan, 1985a].

Teich et al. [1986a] have compared the gain and noise characteristics of SAPDs with those for CAPDs and photomultiplier tubes. They have also investigated the performance of optical receivers incorporating these advanced APDs assuming both zero dark current and negligible residual hole ionisation. In the next chapter we will extend the existing analyses relating to SAPDs taking into account the influence of these device impairments and investigate the performance implications for optical receivers.

It should be noted that while the results developed in the following chapters are based on staircase APDs, they are also applicable to other superlattice structures in which the carrier transport is perpendicular to the superlattice planes. However, they do not apply to the channelling APD [Capasso, 1982b, Brennan, 1985b] in which the carriers are spatially separated by means of a transverse field, with transport taking place in the plane of the layers.

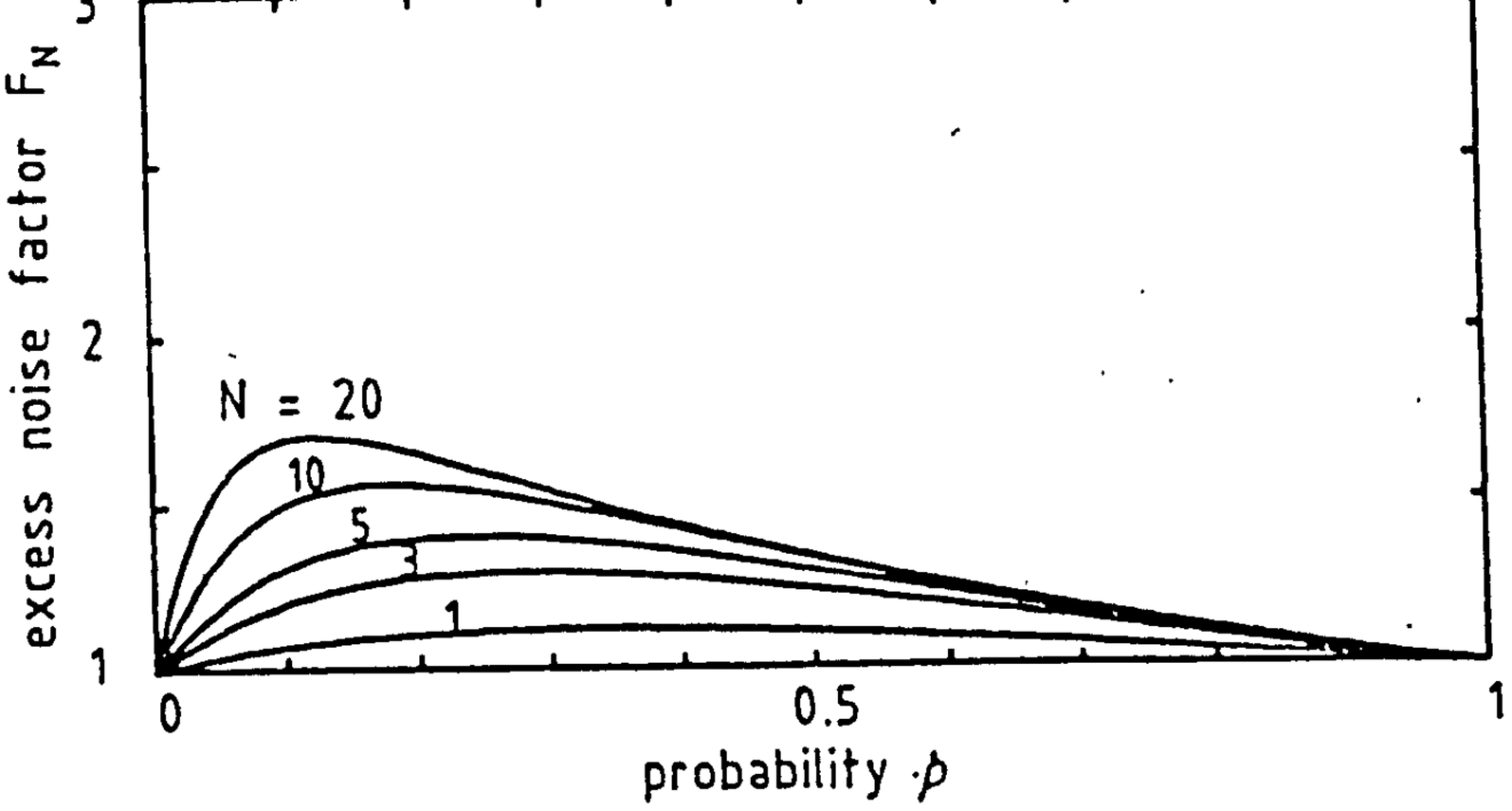

(a)

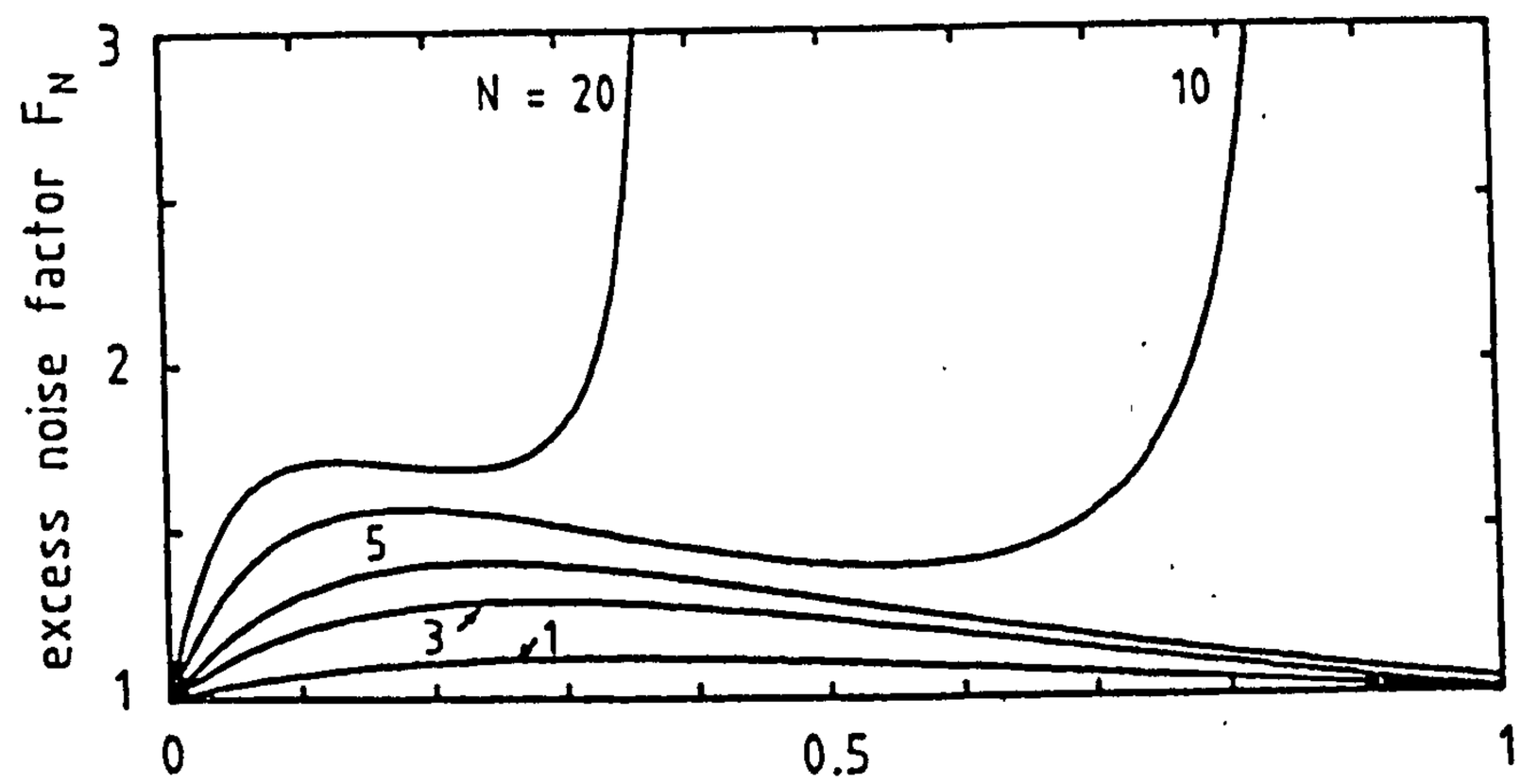

(b)

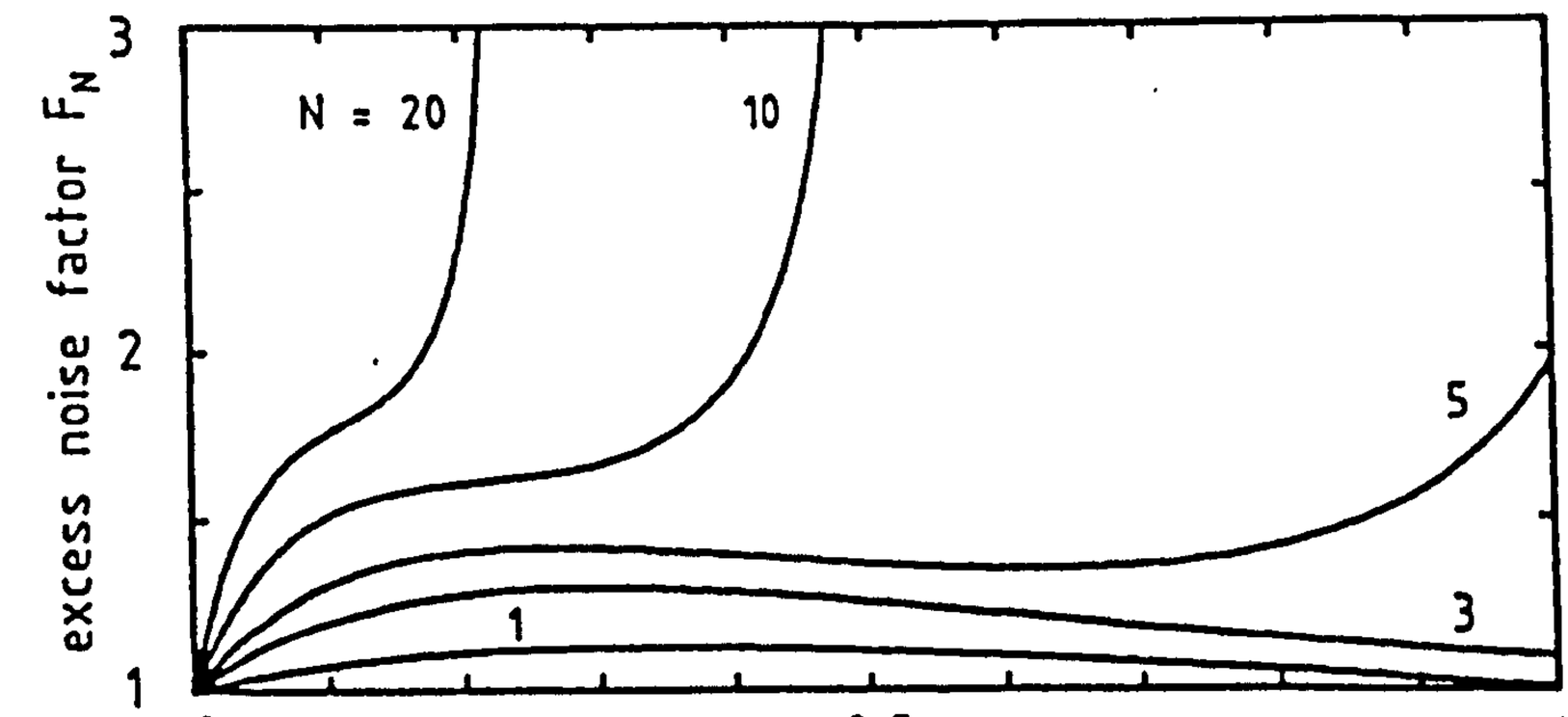

(c)

Fig. 2.5 Excess noise factor associated with photogenerated carriers against electron ionisation probability per stage.
(a) k=0.0 (b) k=0.001 (c) k=0.01

CHAPTER 3

DARK CURRENT CONSIDERATIONS

Rather high levels of dark current have been observed in many superlattice APDs, fabricated by variety techniques, especially at room temperature [e.g. Capasso et al., 1986; Allam et al., 1987; Beltram et al., 1987]. This high level of dark current, associated with the high gain of these devices, can lead to substantial degradation in receiver sensitivity and it is therefore important to analyse the influence of dark current in these structures. From the point of view of receiver sensitivity we can decompose the dark current into essentially three components :

(a) A surface component which, since it does not enter the multiplication process, can be taken into account as leakage current associated with the front-end amplifier following the APD.

(b) Dark current components resulting from minority carriers diffusing from the p^+ and/or n^+ regions into the depletion layers. These will experience the same gain and excess noise factor as is associated with photocarriers generated in the same regions.

(c) Dark current generated within the multiplication region (i.e. in different stages), attributed mainly to tunnelling through the various heterointerfaces. In this case, the distribution of dark current among the various stages must be taken into account in order to deduce the total noise associated with this component.

In this chapter, we direct our attention to determining the effective gain and effective excess noise factor corresponding to the third component since it contributes predominently to the multiplied dark current, [Capasso et al., 1986; Li et al., 1987]. The

performance of optical receivers incorporating SAPDs is determined, allowing for the influence both of residual hole ionisation and dark current components. The analysis is then extended to conventional APDs to investigate the influence of dark current generated within the multiplication region.

3.1 Generalised Formulas for the Gain and Excess Noise Factor

Since thermally generated dark current carriers may originate at any position within the device, it is necessary to extend existing analyses relating to gain and excess noise factor for photogenerated current [e.g. Teich et al., 1986a] to include the position of the initiating hole-electron pair.

Consider a hole-electron pair generated in the position A in the device. This position will be labelled by A(j), where j denotes the number of possible ionisations which the initiating electron can induce while moving to the n^+ region. Thus the primary hole can induce N-j possible ionisations when moving to the p^+ region, where N is the total number of stages and a single ionisation per initiating carrier per stage is assumed. Extension for more than one ionisation is considered in detail in Chapters 5 and 6

Let p and u represent the impact-ionisation probability per stage for electrons and holes respectively. The average gain $<g_j>$ and the excess noise factor F_j associated with hole-electron pair initiation at point A(j) are shown in Appendices A and B respectively to be given by

$$<g_j> = <g_N> Q^{j-N} \qquad (3.1)$$

$$F_j = Q^{N-j} F_N - \frac{2(1-up)}{(1+u)^2 Q} (Q^{N-j} - 1) \tag{3.2}$$

where

$$Q = (1+p)/(1+u) \tag{3.3}$$

Here $<g_N>$ and F_N are, respectively, the gain and excess noise factor associated with a hole-electron pair generated at the p^+ region (i.e. pure electron injection) and they are defined in eqns. 2.1 and 2.2.

It is instructive to examine eqns. 3.1 and 3.2 for two extreme cases: u=0 (very low noise device) and u=p (high noise device). For the first case (i.e. u=0) we have

$$<g_j> = (1+p)^j \tag{3.4}$$

$$F_j = 1 + [1-1/(1+p)^j][(1-p)/(1+p)] \tag{3.5}$$

from which we note that the gain and the excess noise factor depend only on the number of stages crossed by the electron (i.e. j only). Eqns. 3.4 and 3.5 are identical to the gain and excess noise factor results for a j-stage device when u=0. This is anticipated since the multiplication process is unilateral in this instance. For u=p eqns. 3.1 and 3.2 reduce to

$$<g_j> = 1/(1-Np) \tag{3.6}$$

$$F_j = (1-Np^2)/(1-Np) \tag{3.7}$$

and $<g_j>$ and F_j are independent of the position of the initiating hole-electron pair.

In order to address the general case, we consider first the

influence of the position of the initiating hole-electron pair on the gain and excess noise factor. Figs. 3.1 and 3.2 show, for a 5-stage device, the variation of $<g_j>$ and F_j, respectively, as a function of j, taking p and the ionisation rate ratio k (≡ u/p) as parameters. For p>u, the gain $<g_j>$ decreases exponentially with the distance (i.e. number of stages) from the p^+ region where the initiating hole-electron pair generation occurs. For k=0 the excess noise factor F_j decreases slightly as j decreases. This result may also be deduced from Fig. 2.3a by replacing N by j since u=0. For k > 0 F_j will behave in similar manner when p = 0.1 (Fig. 3.2a), but for large p it increases strongly as j decreases (Figs. 3.2b and 3.2c). For k=1, both $<g_j>$ and F_j are independent of j as stated previously. Also from these figures we see that for fixed j both $<g_j>$ and F_j increase with k.

An interesting point to note here is that for small value of p, for example p=0.1, a lower noise device can be obtained when the less strongly ionising carrier (hole in this case) initiates the multiplication process, corresponding to the light being incident on the n^+ region of the device. This is in marked contrast to the McIntyre theory [McIntyre, 1966] for CAPDs. However, the reduction in the excess noise factor in this case is small compared with F_N and is associated with lower gains; this does not, therefore, seem to be of practical significance.

3.2 Noise-Variance Analysis of Dark Current

In staircase APDs and other supperlattice structures, the multiplication region is distributed across the stages and hence the dark current carriers generated in each stage will .experience a different gain and excess noise factor. In order to treat the dark

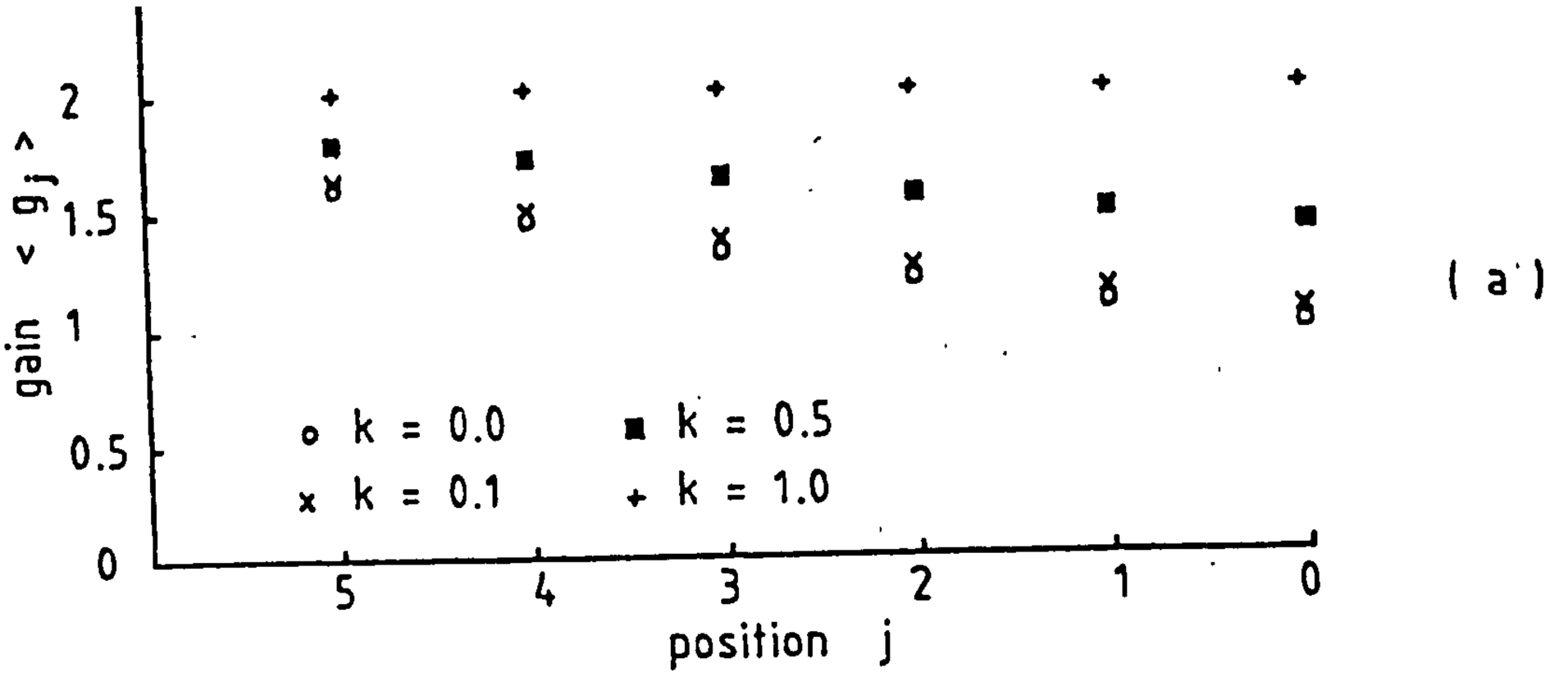

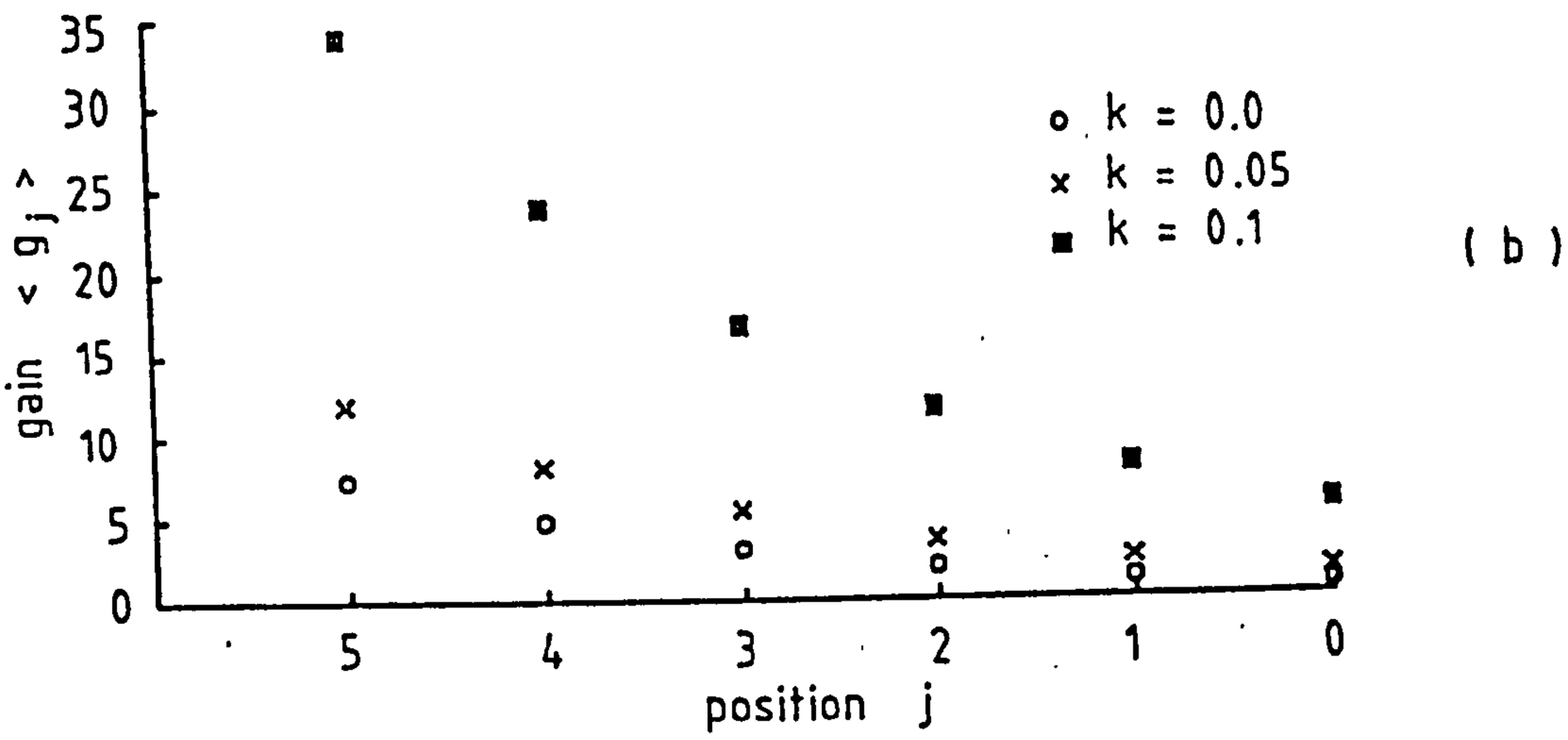

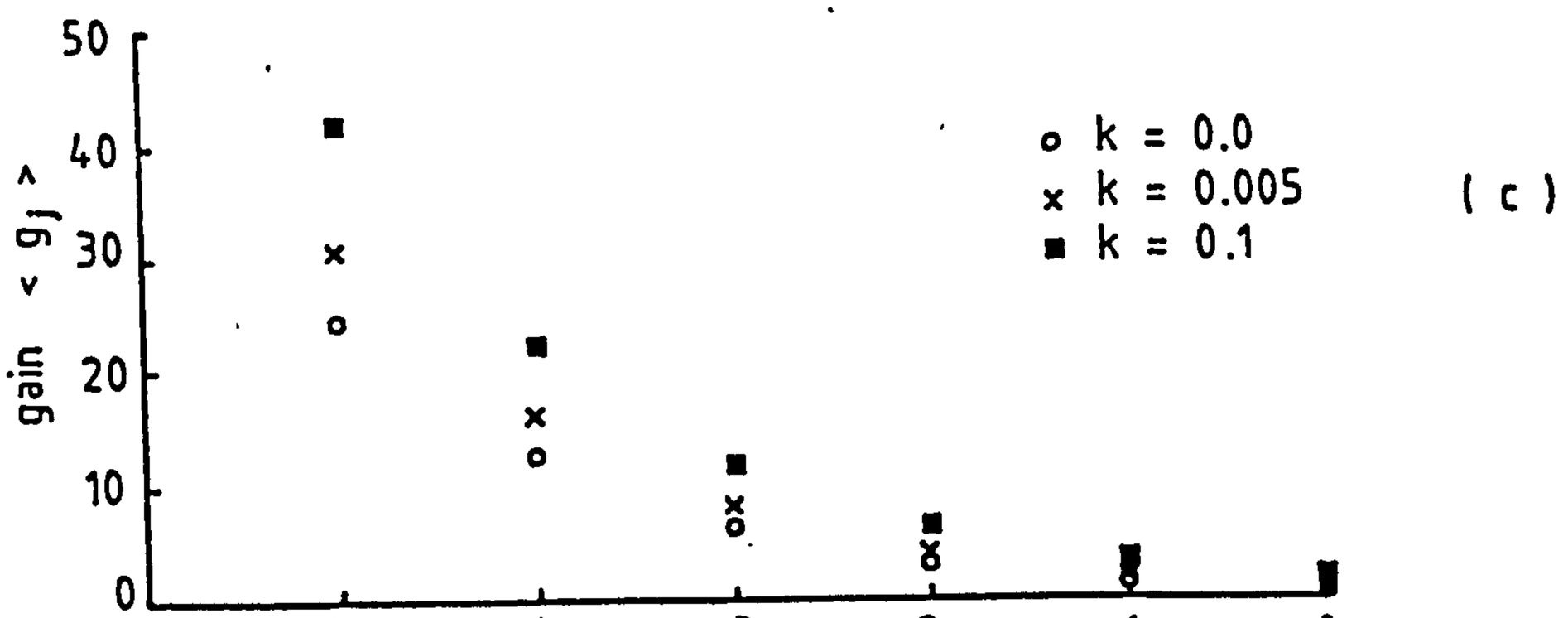

Fig. 3.1 Average gain associated with hole-electron pair initiated at position A(j).
(a) p=0.1 (b) p=0.5 (c) p=0.9

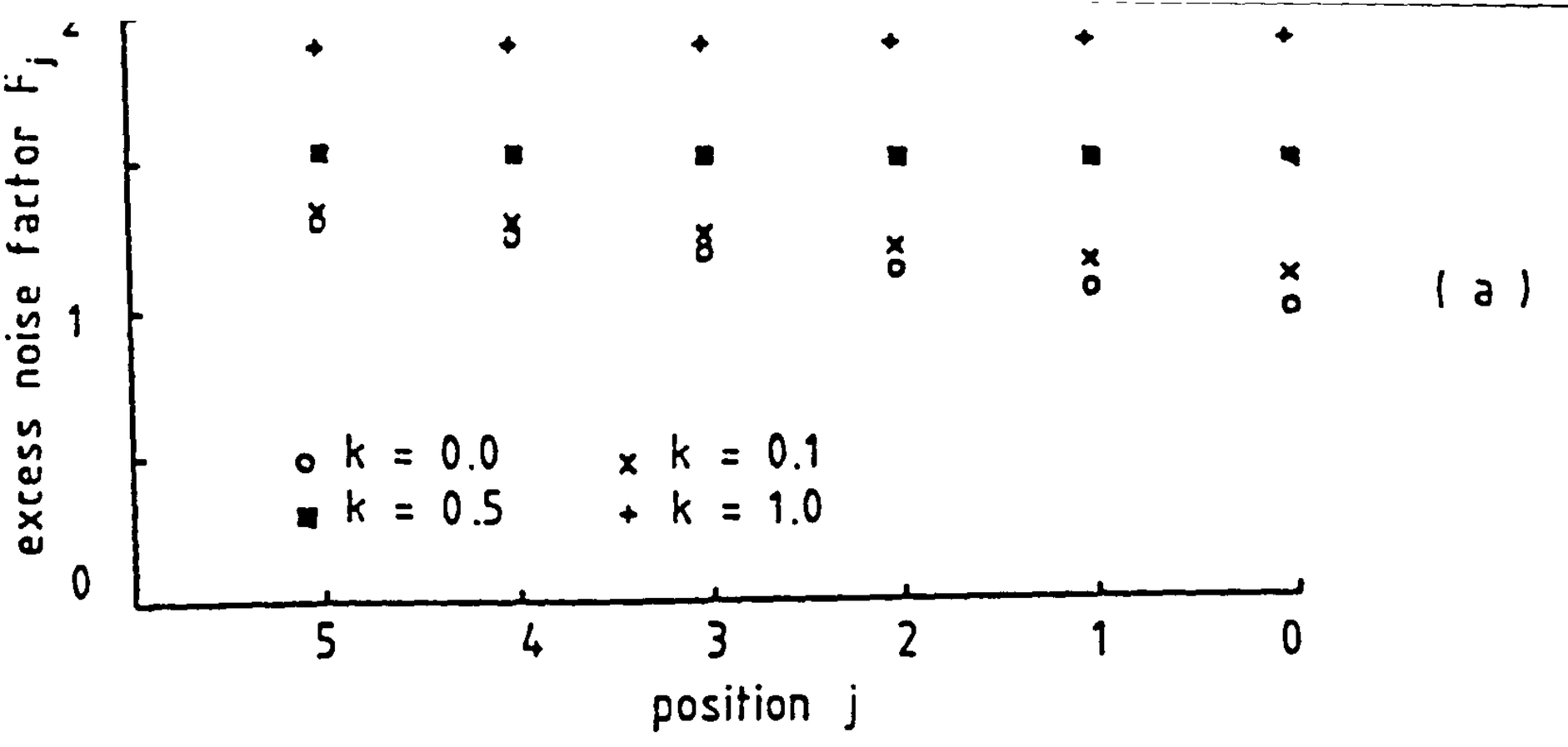

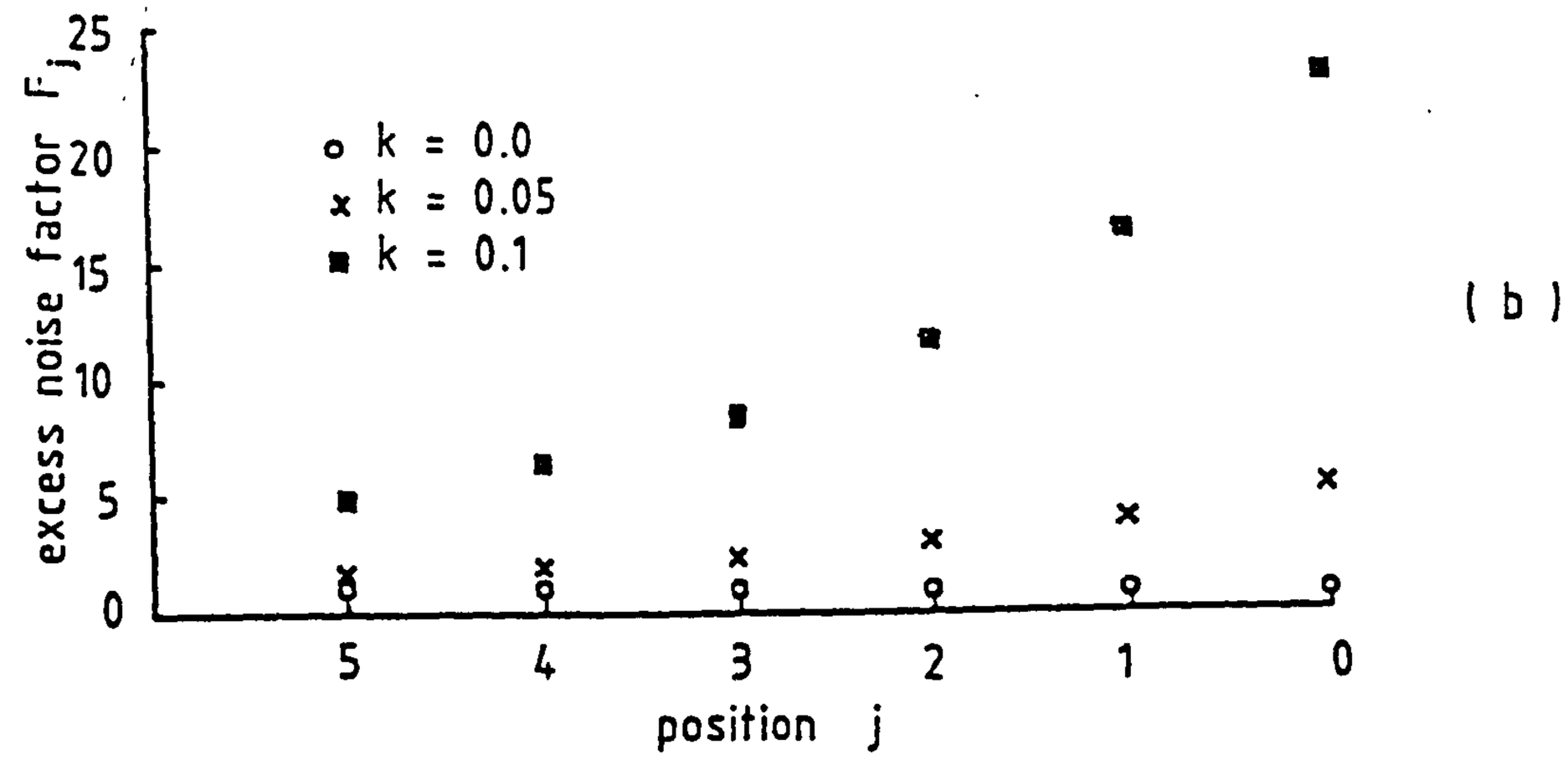

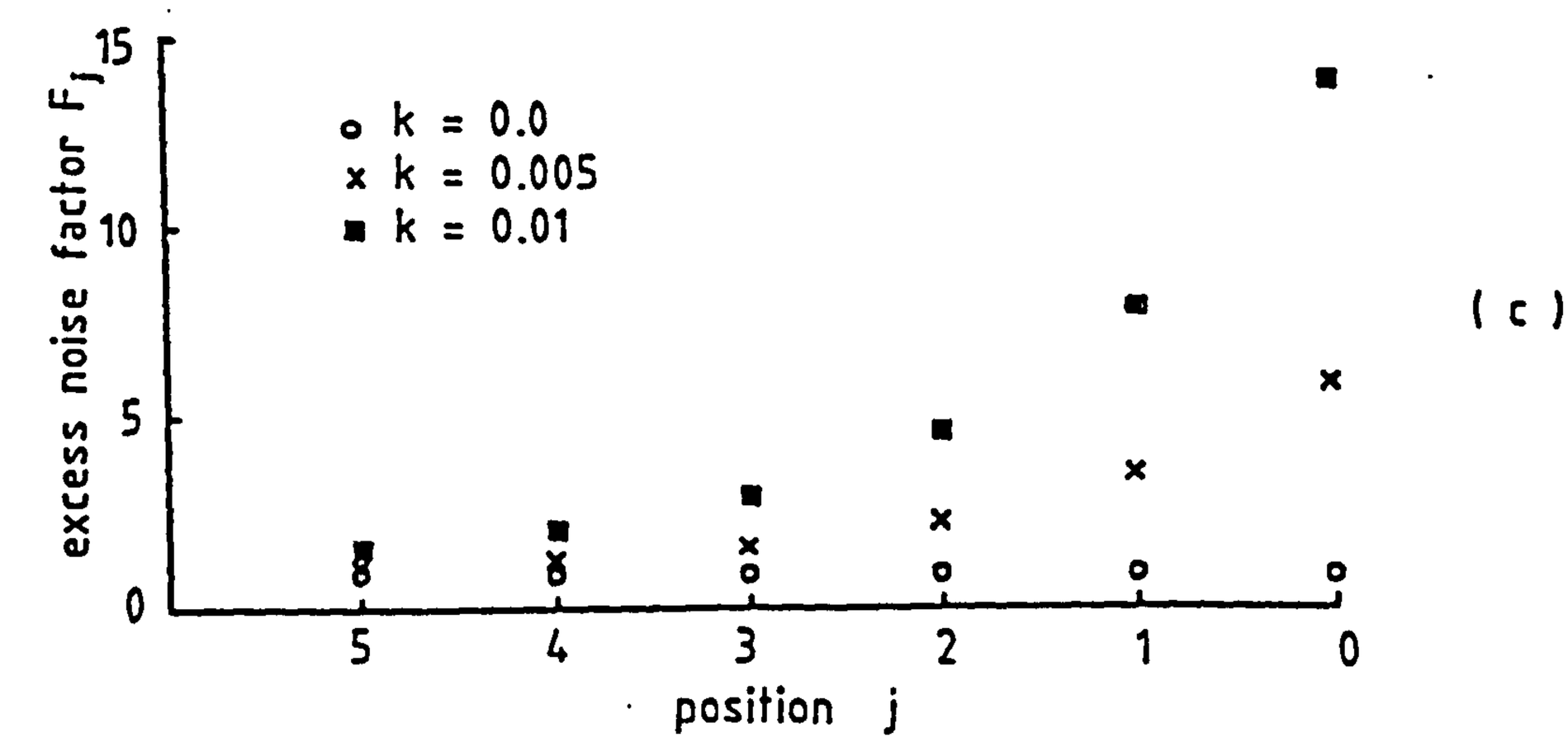

Fig. 3.2 Excess noise factor associated with hole-electron pair initiated at position A(j).
(a) p=0.1 (b) p=0.5 (c) p=0.9

current generated within the multiplication regionin a similar way to photogenerated current we introduce the effective gain g_{eff} and effective excess noise factor F_{eff}. These differ from $<g_N>$ and F_N and are chosen such that for the given primary dark current, if we treat this as initiated at the p^+ region, the same values of average and variance of dark current are realised at the output.

3.2.1 Modelling the Problem

Let x_j be the dark current generated randomly at the position A(j). This current will enter the multiplication process (which is governed by the random gain g_j) to give an output current y_j. Let I_o represent the total output dark current due to all stages, given by

$$I_o = \sum_{j=1}^{N} y_j \tag{3.8}$$

In a similar manner the primary dark current I_d can be written as

$$I_d = \sum_{j=1}^{N} x_j \tag{3.9}$$

If we assume that the individual dark current components are statistically independent then [Cattermole, 1984]

$$<I_o> = \sum_{j=1}^{N} <y_j> \tag{3.10}$$

$$S(I_o) = \sum_{j=1}^{N} S(y_j) \tag{3.11}$$

where $S(.)$ denotes the mean square current spectral density. $<y>$ and $S(y)$ can be expressed as [Teich et al. 1986a]:

$$\langle y_j \rangle = \langle g_j \rangle \langle x_j \rangle \tag{3.12a}$$

$$S(y_j) = S(x_j) \langle g_j \rangle^2 F_j \tag{3.12b}$$

where a Poisson distribution for the thermally generated carriers associated with each dark current component is assumed [Buckingham, 1983]. In eqn. 3.12b $S(x_j)$ is the shot noise spectral density associated with x_j:

$$S(x_j) = 2q \langle x_j \rangle \tag{3.13}$$

Here q is the electronic charge.

3.2.2 Effective Gain and Effective Excess Noise Factor

To treat the dark current in a similar manner to photocurrent generated at the p^+ region we introduce the effective gain g_{eff} and the effective excess noise factor F_{eff} such that the same values of $\langle I_o \rangle$ and $S(I_o)$ are realised at the output. Hence

$$g_{eff} = \frac{\langle I_o \rangle}{\langle I_d \rangle} = \frac{\sum_{j=1}^{N} \langle g_j \rangle \langle x_j \rangle}{\sum_{j=1}^{N} \langle x_j \rangle} \tag{3.14}$$

$$F_{eff} = \frac{S(I_o)}{2q \langle I_d \rangle g_{eff}^2} = \frac{\sum_{j=1}^{N} \langle x_j \rangle \langle g_j \rangle^2 F_j}{g_{eff}^2 \sum_{j=1}^{N} \langle x_j \rangle} \tag{3.15}$$

For the case of individual dark current components in each stage

having identical mean values, then eqns. 3.14 and 3.15 reduce to

$$g_{eff} = \frac{1}{N} \sum_{j=1}^{N} \langle g_j \rangle \tag{3.16}$$

$$F_{eff} = \frac{N \sum_{j=1}^{N} \langle g_j \rangle^2 F_j}{[\sum_{j=1}^{N} \langle g_j \rangle]^2} \tag{3.17}$$

With the aid of eqns. 3.1 and 3.2 the expressions for g_{eff} and F_{eff} can be simplified further

$$g_{eff} = \frac{\langle g_N \rangle}{N} \sum_{j=1}^{N} Q^{j-N}$$

$$= \frac{\langle g_N \rangle}{N} \left[\frac{1-1/Q^N}{1-1/Q} \right] \tag{3.18}$$

$$F_{eff} = \frac{N \sum_{j=1}^{N} Q^{2j} F_j}{\left[\sum_{j=1}^{N} Q^j \right]^2}$$

$$= N \frac{(Q^2-1)Q^N F_N - 2(p-uQ^2)(1+u)(Q^{N-1}-1)}{Q(Q+1)(Q^N-1)} \tag{3.19}$$

For N=1, g_{eff} and F_{eff} will be identical to those of photogenerated current $\langle g_N \rangle$ and F_N respectively. Eqns. 3.18 and 3.19 can be examined for two extreme cases.

(i) k=0

$$g_{eff} = \frac{1+p}{Np} [(1+p)^N - 1] \tag{3.20}$$

$$F_{eff} = Np \frac{2(1+p)[(1+p)^N+1] - (1-p)(2+p)}{(2+p)(1+p)^2[(1+p)^N-1]} \quad (3.21)$$

(ii) $k=1$

$$g_{eff} = \langle g_N \rangle = 1/(1-Np) \quad (3.22)$$

$$F_{eff} = F_N = (1-Np^2)/(1-Np) \quad (3.23)$$

In this latter case the dark current will behave in a similar manner to photocurrent generated in the p^+ region.

Figs. 3.3 and 3.4 show g_{eff} and F_{eff} respectively as a function of p for different values of N and k. Curves corresponding to $\langle g_N \rangle$ and F_N (solid lines) are also shown for comparison. These results indicate that for $N>1$ the effective gain g_{eff} experienced by dark current is always less than that for photogenerated current $\langle g_N \rangle$, while the effective excess noise factor F_{eff} is higher than F_N especially for high values of p. Also both g_{eff} and F_{eff} increase in general as a function of p, k and N. An interesting point to be noted is that even for $p=1$ and $k=0$, representing a noiseless device for photocurrent (since $F_j=1$), for dark current F_{eff} will be greater than 1 for $N>1$ since $\langle g_j \rangle$ is a function of j. From the above discussion it is clear that the effect of dark current on the performance of SAPD receivers increase with p, k and N since these contribute to higher values of g_{eff} and F_{eff}.

3.3 Calculation of Receiver Sensitivity

Teich et al. (1986b) have calculated the bit error rate (BER) for a staircase APD receiver, with $k=0$, neglecting the dark current, using

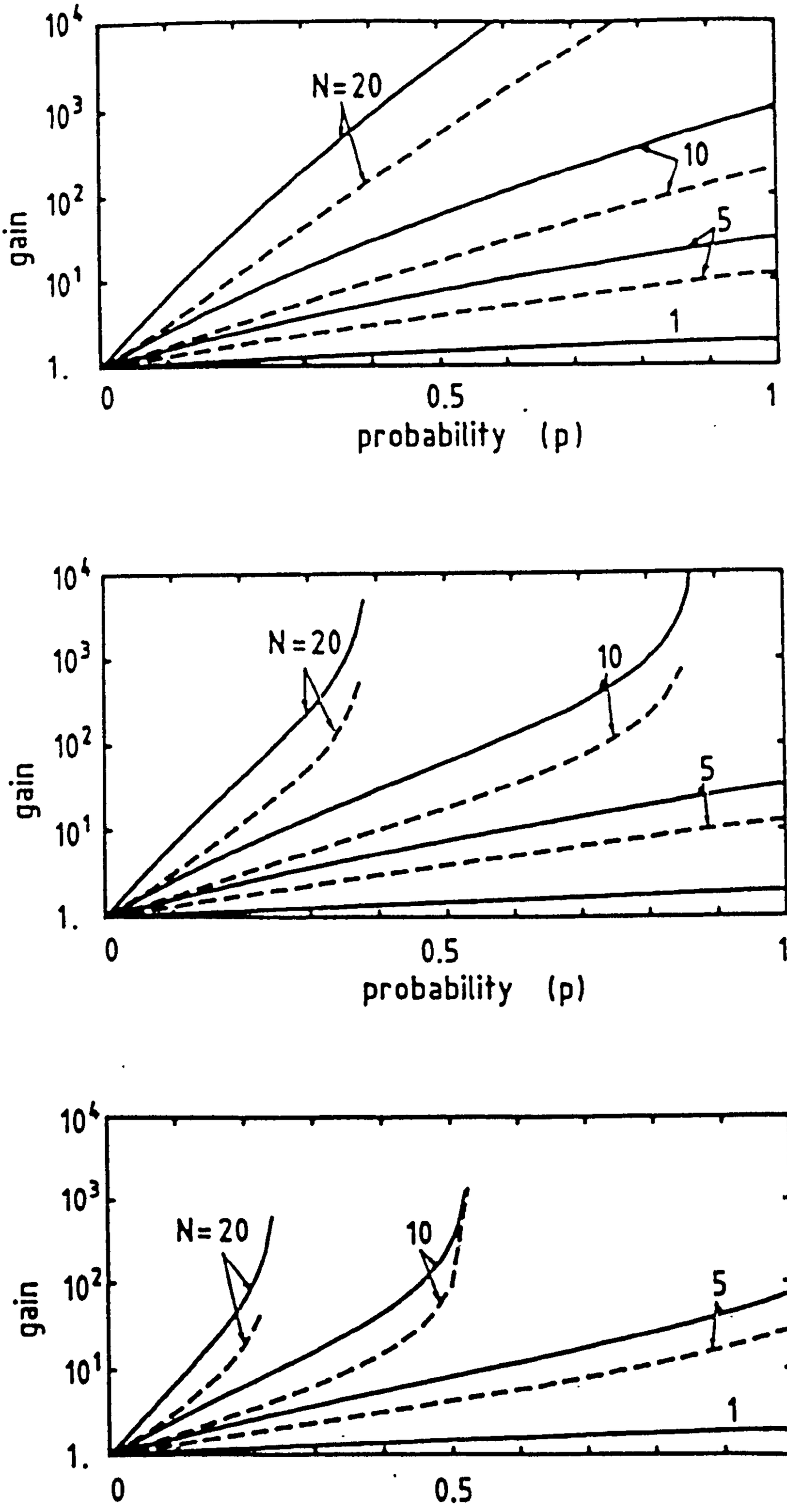

(a)

(b)

(c)

Fig. 3.3 Average gain as a function of electron ionisation probability per stage. (a) k=0.0 (b) k=0.001 (c) k=0.01

——— $\langle g_N \rangle$ --- g_{eff}

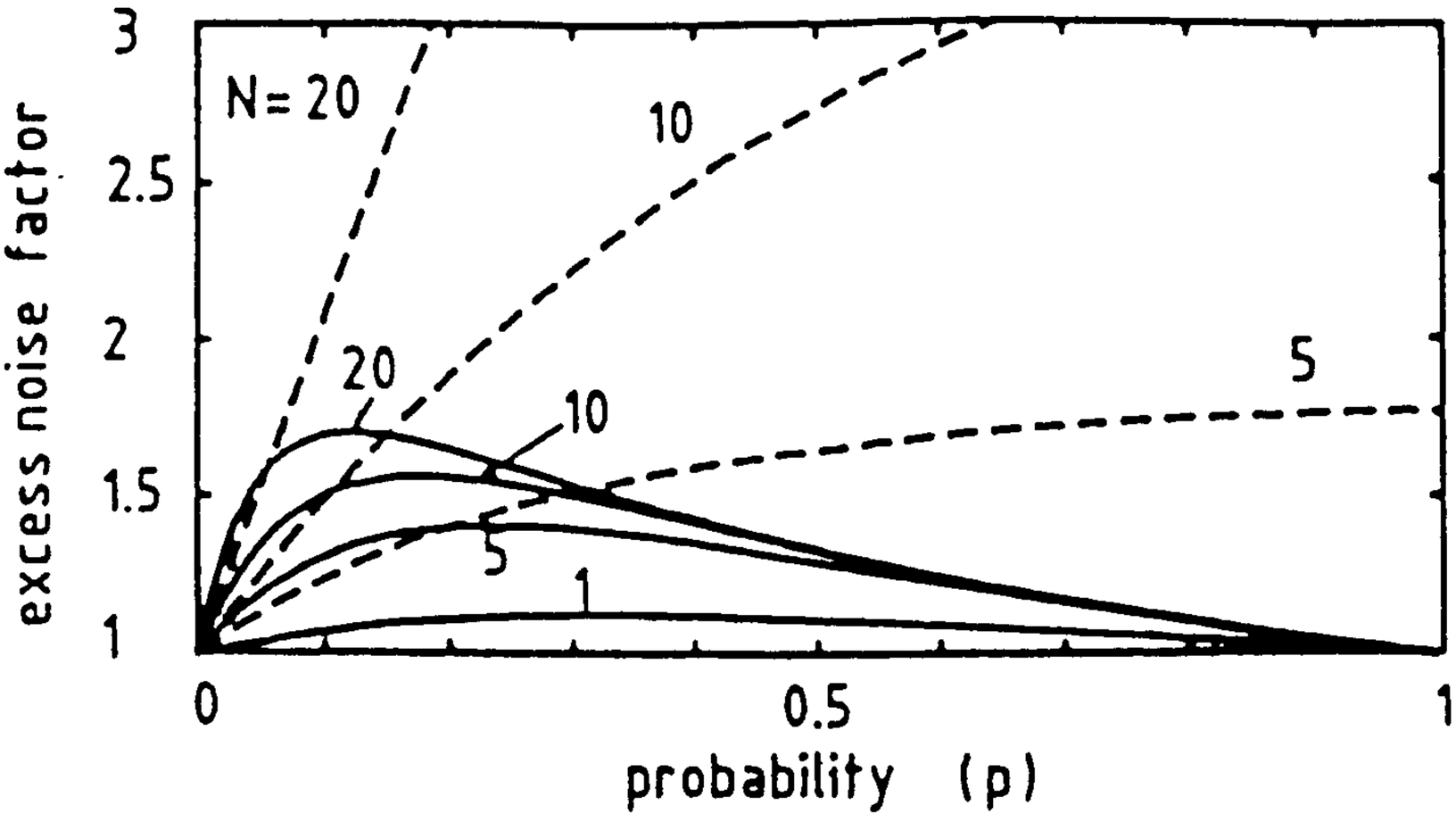

(a)

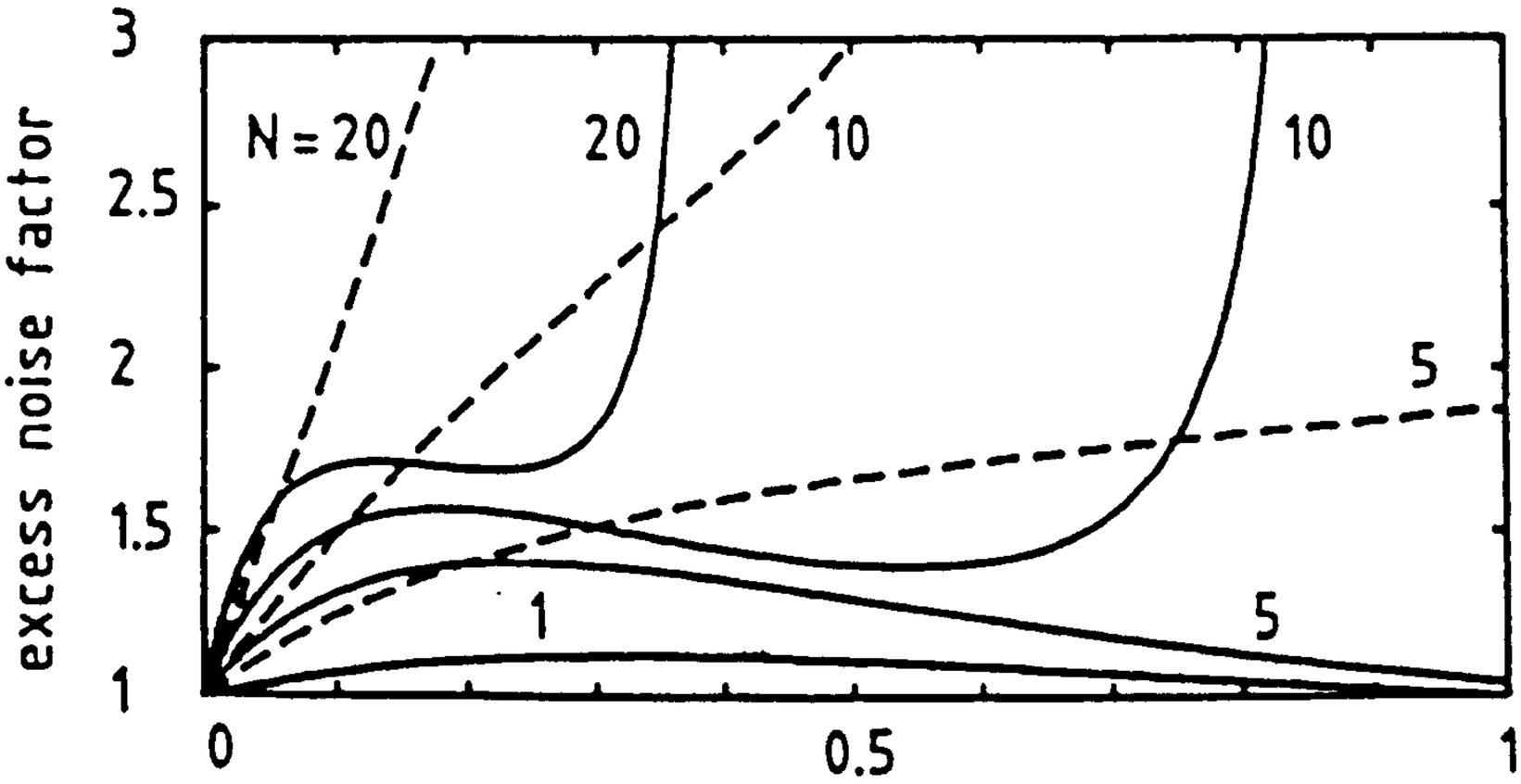

(b)

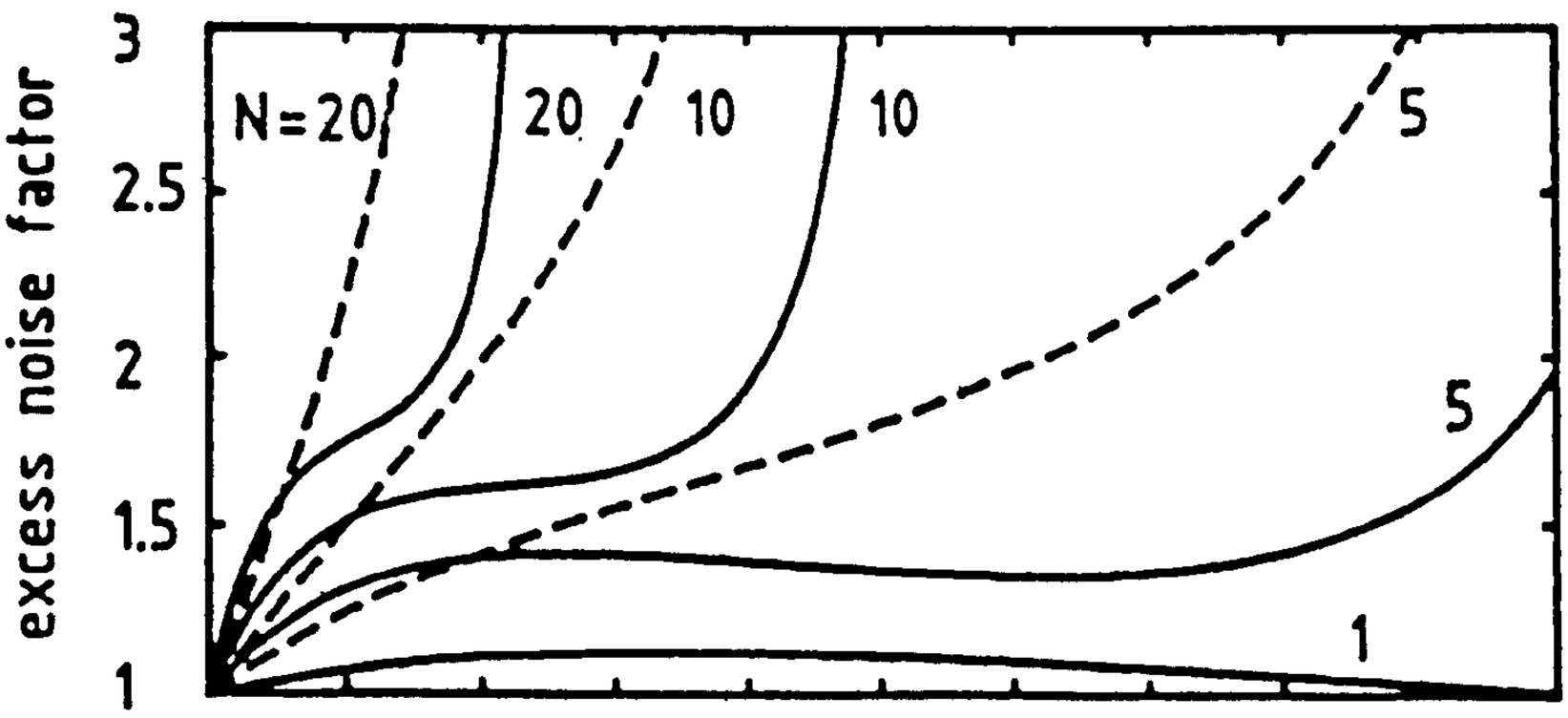

(c)

Fig. 3.4 Excess noise factor as a function of electron ionisation probability per stage. (a) k=0.0 (b) k=0.001 (c) k=0.01

—— F_N - - - F_{eff}

the electron counting distribution and assuming maximum-likehood detection. They showed that such a receiver will exhibit improved sensitivity compared with CAPD receivers with identical gain and circuit noise. In this section we will discuss the influence of dark current on the performance of these new APD receivers taking into account the effect of residual hole ionisation. We shall make use of Personick's approach [Personick, 1973; Smith and Personick, 1980] based on a Gaussian noise approximation. Although it is an approximation, there is a wealth of evidence available in the literature substantiating it as accurate when it is compared with exact methods [Personick et al., 1977; Fyath and O'Reilly, 1989d]. Exact calculations based on a gain moment generating function formulation will be discussed in Chapter 7. Further we shall assume in the subsequent analysis that the gain-bandwidth product of the diode is extremely high, such that it is not a limiting factor receiver performance. This effect will be considered in Chapter 8.

The receiver sensitivity $\bar{P}$, expressed in terms of the average detected optical power required at the receiver input for a desired error rate, is given by [Smith and Personick, 1980]:

$$\eta\bar{P} = \frac{Q_o h\upsilon}{q} \left[Q_o qBI_1F_N + (<i_{na}^2> + <i_{nd}^2>)^{1/2}/<g_N> \right] \qquad (3.24)$$

where η is the external quantum efficiency of the detector, $h\upsilon$ is the photon energy, Q_o is a parameter related to the desired bit error rate ($Q_o=6$ for BER$=10^{-9}$) and $<i_{na}^2>$ is the input equivalent amplifier mean square noise current at the given operating bit rate B. The parameter $<i_{nd}^2>$ represents the dark current noise contribution:

$$\langle i_{nd}^2 \rangle = 2qBI_2[I_{ds}+I_{dd}\langle g_N \rangle^2 F_N + I_{da}\, g_{eff}^2\, F_{eff}] \qquad (3.25)$$

where I_{ds} is the surface dark current that does not experience the multiplication process, I_{dd} is the diffusion dark current, owing to minority carriers thermally generated outside the multiplication region, and I_{da} is the dark current component generated in various stages and is associated with effective gain g_{eff} and effective excess noise factor F_{eff} as given by eqns. 3.18 and 3.19 respectively.

The amplifier noise $\langle i_{na}^2 \rangle$ for a FET amplifier is given by [Smith and Personick, 1980].

$$\langle i_{na}^2 \rangle = [\frac{4K\theta}{R_L}(1+\frac{\Gamma}{g_m R_L}) + 2q\, I_g]\, I_2 B + 4K\theta\Gamma\, \frac{(2\pi C_t)^2}{g_m} I_3 B^3 \qquad (3.26)$$

where 1/f amplifier noise is neglected. Here K is Boltzmann's constant and θ is the absolute temperature. Other parameters are defined in Table 3.1.

The parameters I_1, I_2 and I_3 appearing in the above equations are weighting functions which are dependent only on the shapes of the optical pulse at the input to the receiver and the equalised output pulse [Personick, 1973].

3.4 Performance Assessment of SAPD Receivers

Illustrative results will be presented for a 2 Gbit/s receiver operating at $\lambda = 1.5\mu$m. The receiver sensitivity is estimated for BER$=10^{-9}$ at room temperature (300K), and assuming 50% return-to-zero (RZ) input format and full raised-cosine output signal spectrum. The receiver parameters used in the calculations are listed in Table 3.1. The equivalent input noise current spectral density of the amplifier is estimated to be 2.124 pA/Hz$^{1/2}$.

TABLE 3.1

Parameters of APD/FET receiver used as thebasis for sensitivity calculations.

Parameter		Value
Wavelength, λ		1.5μm
FET gate leakage current, I_g		2nA
FET transconductance, g_m		40mS
FET noise factor, Γ		1.78
Receiver input capacitance, C_t		1pF
Load resistance, R_L		22kΩ
Personick integrals for 50% return-to-zero (RZ) input format and raised-cosin output signal spectrum	I_1	0.5
	I_2	0.403
	I_3	0.0361
Temperature, θ		300K

3.4.1 Effect of Number of Stages

In this section we look at the effect of the number of stages N on receiver sensitivity. Fig. 3.5 shows the variation of receiver sensitivity $\eta\bar{P}$ as a function of APD gain $<g_N>$ for two values of N, i.e. 5 and 10, and assuming zero dark current. At low values of k (0 and 0.001) a better optimum sensitivity can be obtained with the 10-stage SAPD, while as k increases, the 5-stage device offers a very slightly improved performance. Note that the 5-stage SAPD will have a wider bandwidth compared with N=10 device since the bandwidth is inversely proportional to the number of stages, all other factors

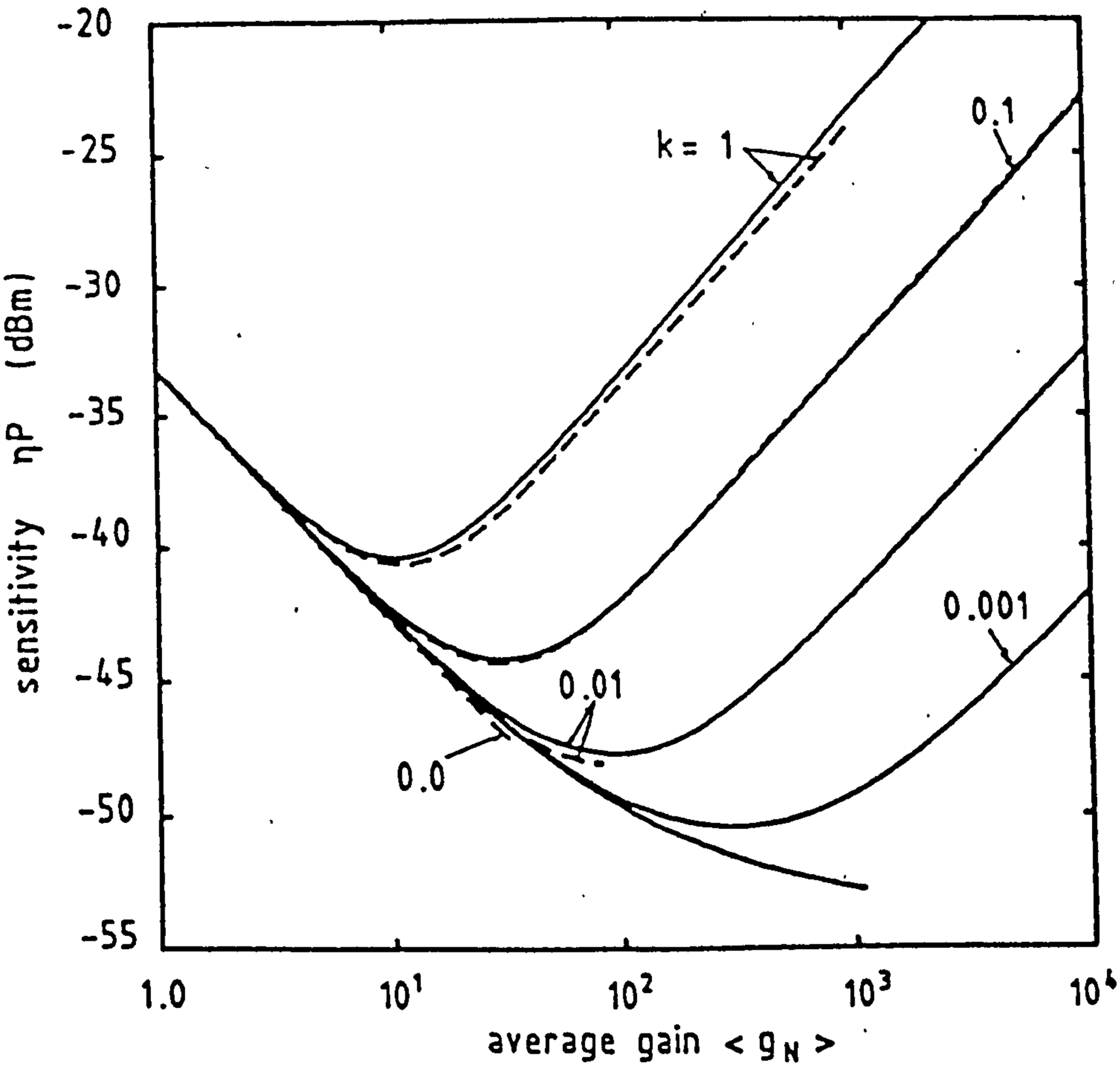

Fig. 3.5 Receiver sensitivity $\eta\bar{P}$ as a function of APD gain $<g_N>$, assuming zero dark current.

--- N=5 ——— N=10

being equal [Matsuo et al., 1985]. Fig. 3.5 also indicates that at lower values of k (e.g. 0 for N=10 and less than 0.01 for N=5) there is no optimum gain at which the detectable optical power for a given BER is minimum. Hence the diode continues to give improved sensitivity as the gain increases so that the optimum sensitivity will occur at p=1. For higher values of k there is an optimum gain. This is owing to avalanche breakdown associated with higher values of ionisation rate ratio, leading to a strong increase in the excess noise factor as the gain increases.

We are unable to present a general expression for the optimum

gain $\langle g_N \rangle_{opt}$, but it can be shown that for k=1 and neglecting all dark current components

$$\langle g_N \rangle_{opt} = \left[\frac{N \langle i_{na}^2 \rangle^{1/2}}{Q_o q B I_1 (N-I)} - \frac{1}{N-I} \right]^{1/2} \quad \text{for } N > 1 \qquad (3.27)$$

and the value of the electron ionisation probability per stage at which $\langle g_N \rangle_{opt}$ occurs is given by:

$$p_{opt} = (1 - 1/\langle g_N \rangle_{opt})/N \qquad (3.28)$$

3.4.2 Effect of Ionisation Rate Ratio k

From the previous section, it is clear that for single carrier multiplication (i.e. k=0), the sensitivity increases with N for fixed p, a behaviour similar to that for a photomultiplier tube, while for k>0 this is not always the case. Here we shall investigate the influence of residual hole ionisation on system performance for different values of N. Three values of N are considered, i.e. 1, 5 and 10. The single stage SAPD (N=1) has attracted attention recently as high aspeed photodiode with low excess noise-to-gain ratio [Hollenhorst, 1986; Jindal, 1987].

Fig. 3.6 presents the variation of receiver sensitivity as a function of hole-to-electron ionisation probability ratio k, assuming both zero dark current and 100nA dark current generated uniformly in the various stages. The gain of the diode is adjusted for each set of parameters to give the best attainable value of sensitivity. If we compare the different curves, the following can be stated:

(i) As k increases the sensitivity degrades for the 10-stage SAPD, while it improves for a single stage device. For N=5 there is a

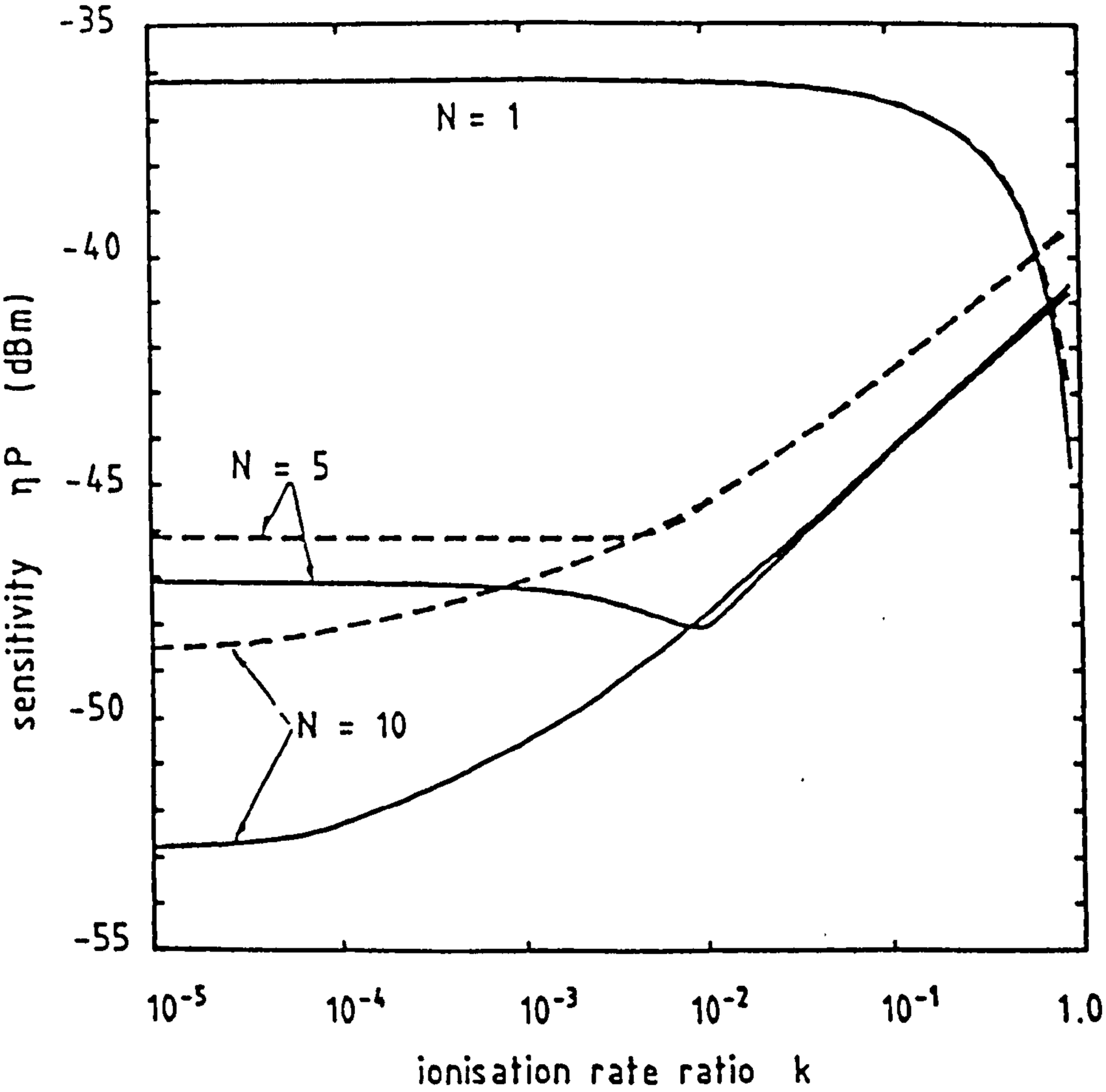

Fig. 3.6 Receiver sensitivity $\eta\bar{P}$ against ionisation rate ratio k.

—— I_{da}=0 - - - I_{da}=100 nA

certain value of k where the sensitivity approaches the best value, and this can be explained with the aid of eqn. 3.24. If we neglect the dark current for a moment, the receiver sensitivity $\eta\bar{P}$ is the sum of two terms: one directly proportional to F_N, and the other inversely proportional to $<g_N>$. As k increases, both F_N and $<g_N>$ increase, but to different extents. It is worthwhile noting here that the behaviour of the 10-stage SAPD is identical to that of a conventional photodiode [Smith and Forrest, 1982; Muoi, 1984].

(ii) At lower values of k, the best sensitivity can be obtained with N=10. For high values of k, near 1, a single stage device offers the

best performance.

(iii) The 10-stage device is more significantly affected by dark current, especially at low values of k. For the N=1 receiver the influence of dark current is negligible unless k is near 1. This is clear from Fig. 3.7 which is a plot as a function of k of the sensitivity penalty due to 100nA dark current.

(iv) Although a single stage SAPD is useful for high speed operation, it will not offer a significant advantage over a PIN diode unless k is high. In this case, the best sensitivity can be obtained when both k and p approach 1, which requires ballistic injection of carriers across the gain region [Hollenhorst, 1986].

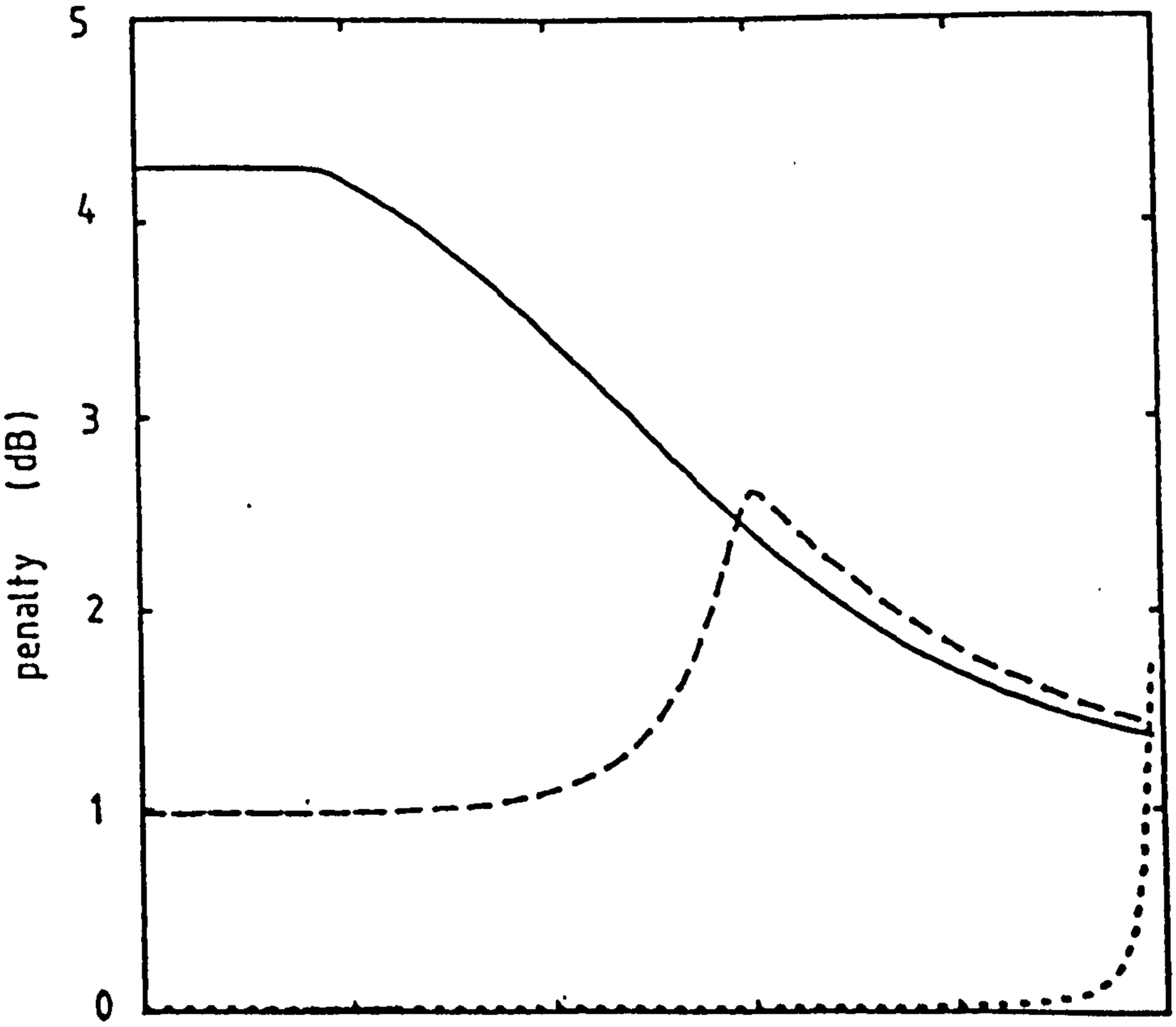

Fig. 3.7 Degradation in receiver sensitivity owing to 100 nA dark current generated uniformly in the different stages.

····· N=1 — — — N=5 ——— N=10

The optimum gain $<g_N>_{opt}$ and the optimum ionisation probability per stage p_{opt} used in the previous calculations (Fig. 3.6) are given in Figs. 3.8 and 3.9 respectively. At lower values of k, a higher optimum gain is required for the 10-stage device. Note that for N=1, $<g_N>_{opt}$ increases with k in contrast to the N=10 case. The existence of dark current reduces the required optimum gain for the range of k where avalanche breakdown occurs. Note also that $<g_N>_{opt}$ usually occurs, as in CAPDs, in the vicinity of the breakdown region, hence additional circuitry must be used with these APDs to ensure stable operation in the presence of temperature and voltage variations.

3.4.3 Effect of Various Dark Current Components

In the following, we will predict the sensitivity degradation for various dark current components. The effect of unmultiplied dark current, such as surface leakage current I_{ds}, is in general not significant compared with multiplied dark current components. Also, its effect can be taken as a leakage current associated with the following amplifier, i.e. its effect added to $<i_{na}^2>$. Here, we focus on I_{da} and I_{dd} components.

Fig. 3.10 compares the relative multiplication noise spectral density associated with both dark current components on the 10-stage SAPD, using k as a parameter. When k=0, the multiplication noise due to I_{dd} is greater than that for I_{da} of the same mean value, at all values of diode gain $<g_N>$. As k increases the difference reduces, and it vanishes at k=1. Note that at k=1, the gain and excess noise factor are no longer dependent on the position of the initiating carrier.

Fig. 3.11 displays the sensitivity against dark current for the 10-stage SAPD. Notice that for all values of k<1, I_{dd} is more

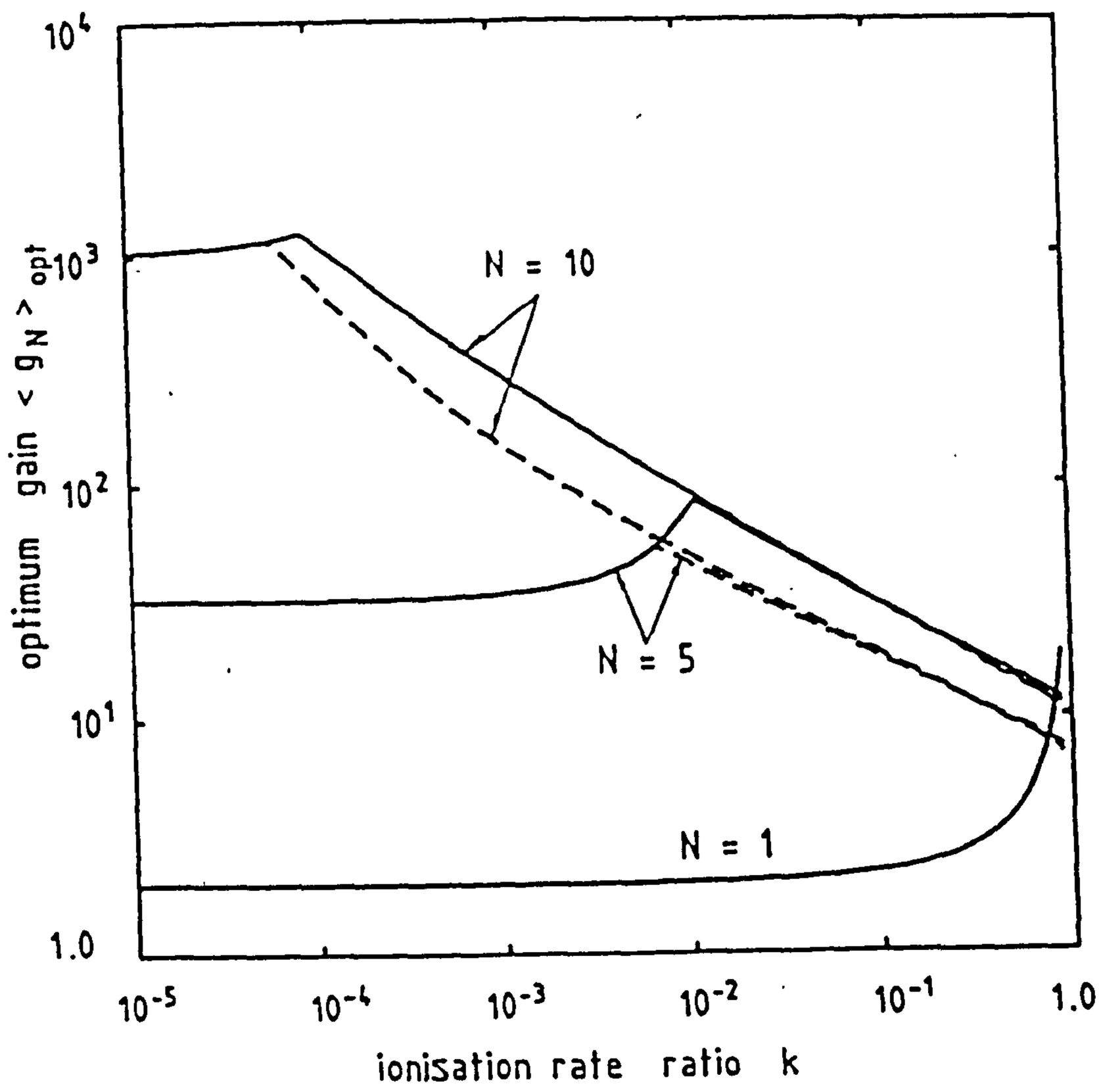

Fig. 3.8 Optimum gain $\langle g_N \rangle_{opt}$ against ionisation rate ratio.

—— I_{da}=0 - - - I_{da}=100 nA

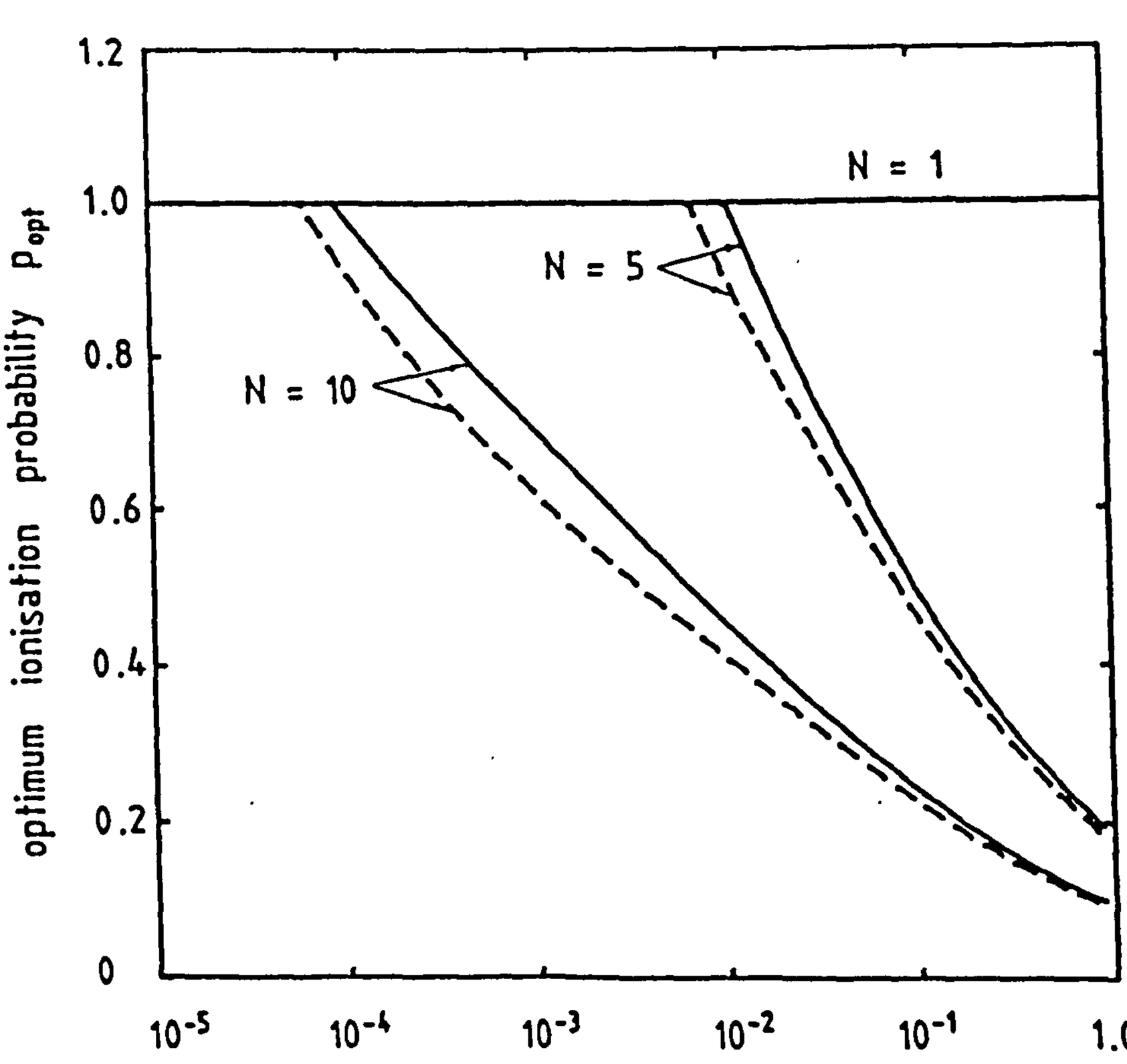

Fig. 3.9 Electron ionisation probability per stage required to achieve optimum sensitivity.

—— I_{da}=0 - - - I_{da}=100 nA

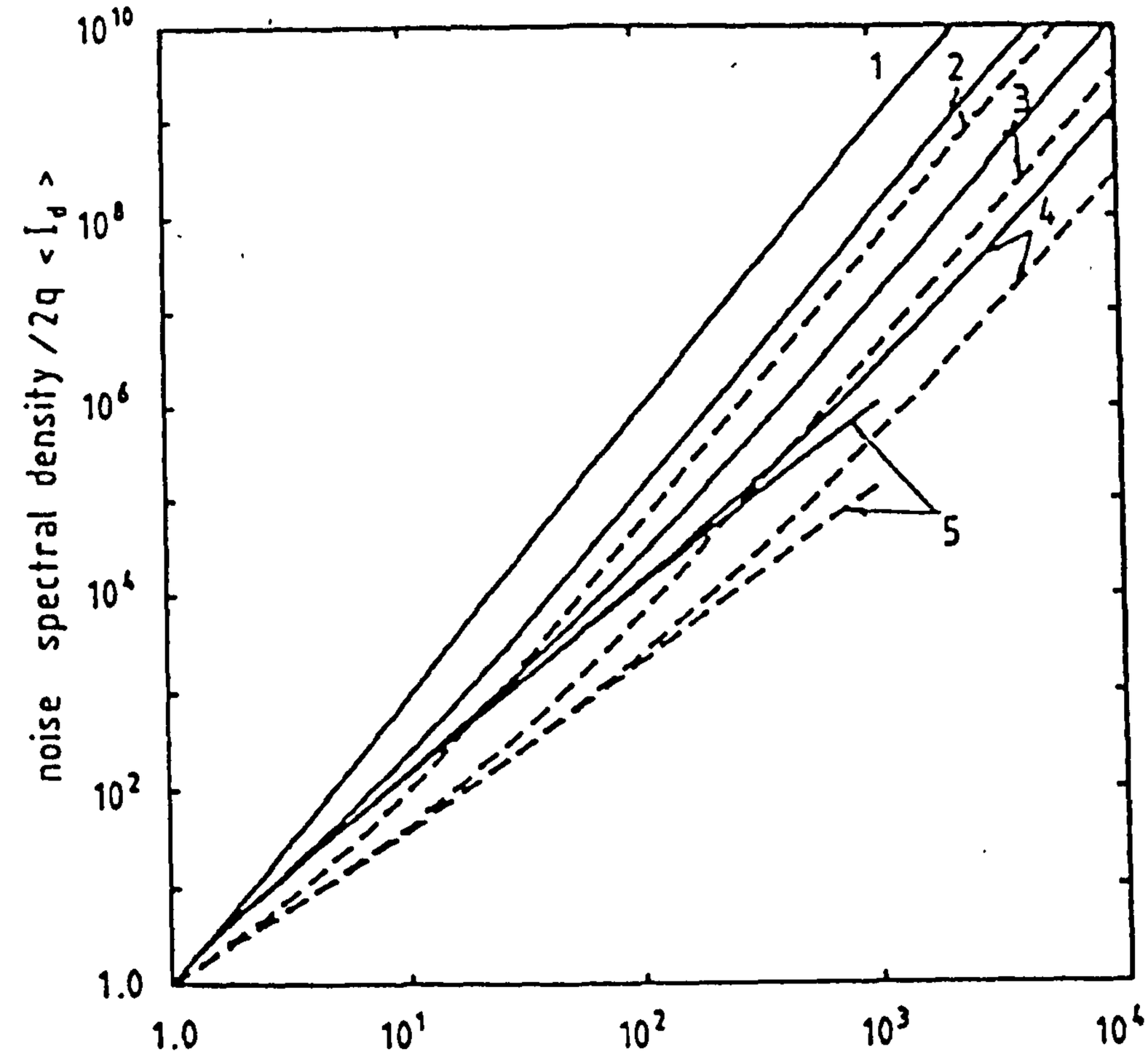

Fig. 3.10 Relative multiplication noise spectral density as a function of gain for 10-stage SAPD.

——— for photocurrent (and dark current component I_{dd})

— — — for dark current component I_{da}

1: k=1 2: k=0.1 3: k=0.01 4: k=0.001 5: k=0.0

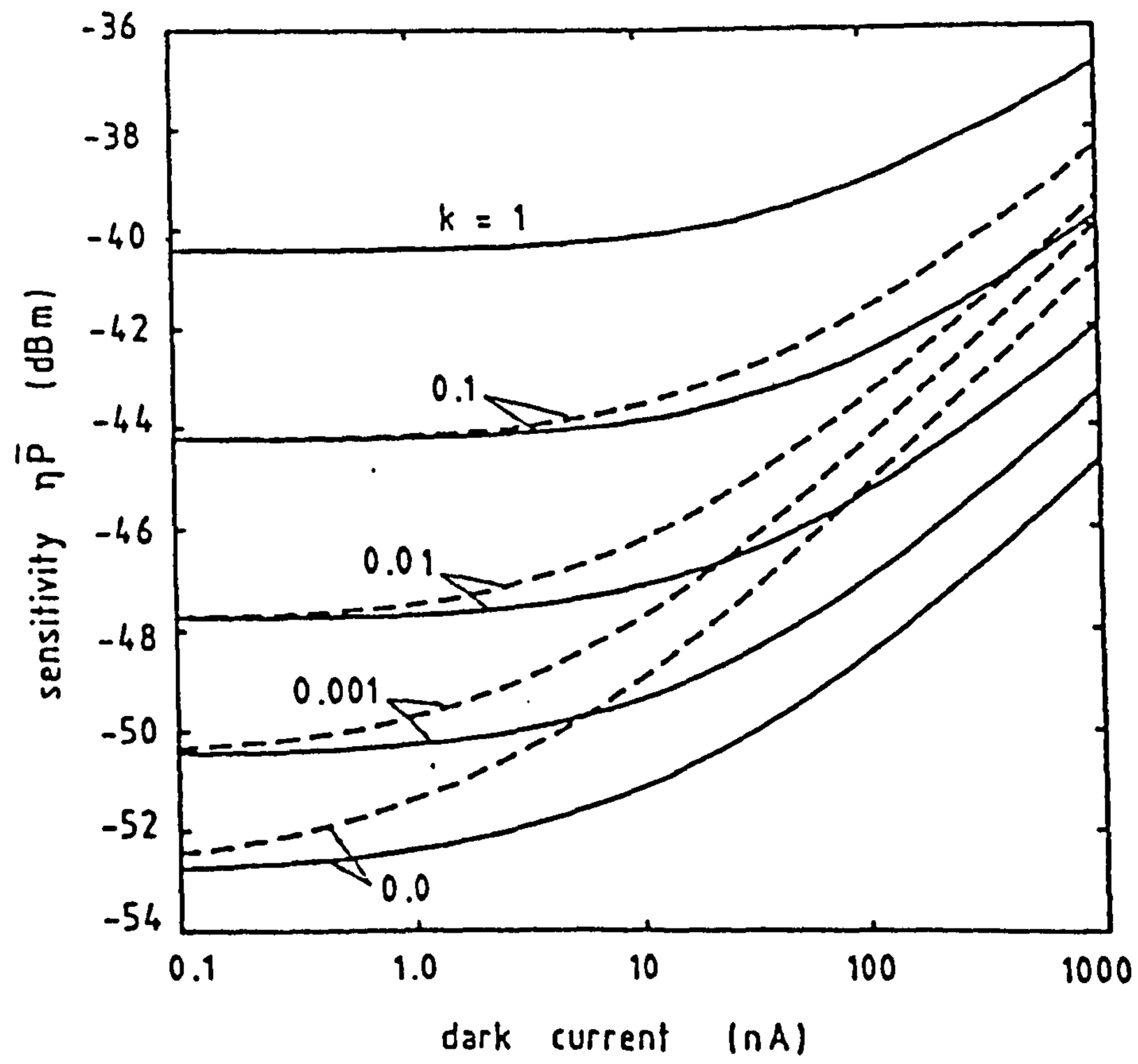

Fig. 3.11 Effect of dark current components on sensitivity of optical receiver employing 10-stage SAPD.

——— I_{dd}=0, $<I_d>=I_{da}$ — — — I_{da}=0, $<I_d>=I_{dd}$

significant than I_{da}, and the difference between receiver sensitivity obtained when I_{dd} dominates, compared with the case when I_{da} is dominant, increases with the mean value of dark current. Figs. 3.12a and 3.12b compare the performance of N=5 and N=10 SAPD receivers under the influence of both dark current components I_{da} and I_{dd}, respectively. It is clear that the value of k, after which the 10-stage device gives no significant performance improvement over that for the 5-stage device, depends on both the average value and the type of dark current component.

3.5 Performance of Single Stage SAPD Receiver

Recently new APD structures have been proposed [Hollenhorst, 1986; Jindal, 1987] in which the avalanche multiplication can be achieved with only one ionising collision per traversal of the primary carrier through the device (i.e. N=1). Hence high speed and low noise operation can be achieved even with equal hole and electron ionisation probabilities. Moreover, such devices can offer improved sensitivity as k tends to 1 as seen from section 3.4.2. In the following we will investigate further the impact of using such advanced APDs in optical receivers.

The average gain and the excess noise factor associated with a single stage SAPD (for pure electron injection) can be expressed as

$$\langle M_e \rangle \equiv \langle g_N \rangle = \frac{1+p}{1-kp^2} \tag{3.29a}$$

$$F_e \equiv F_N = \frac{1+3p+3kp^2+kp^3}{(1+p)^2} \tag{3.29b}$$

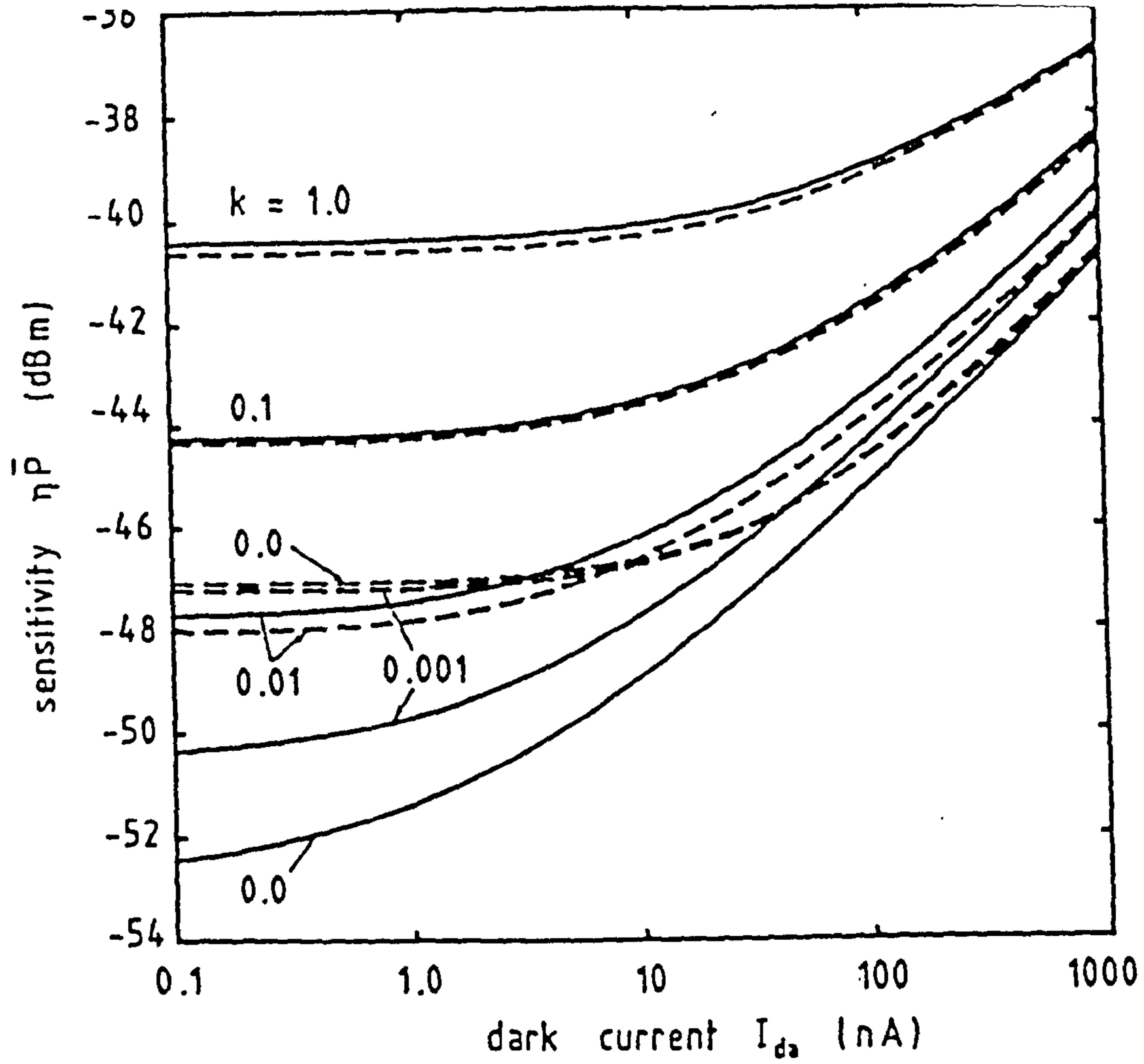

(a)

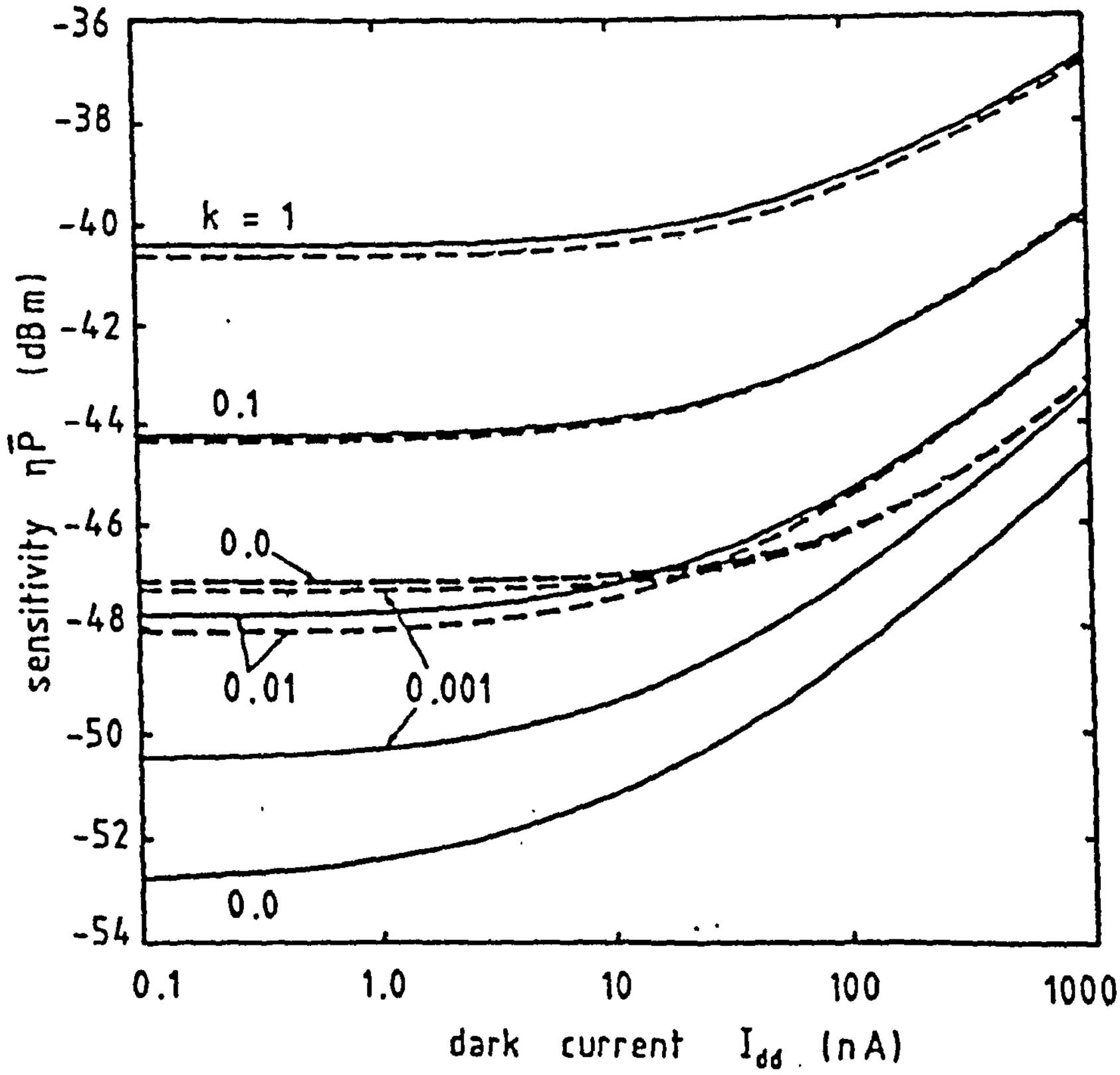

(b)

Fig. 3.12 Receiver sensitivity against dark current.

(a) I_{dd}=0 (b) I_{da}=0

— — — N=5 —— N=10

Note that for k=1, $F_e = 2 - \frac{1}{<M_e>}$ which is exactly the same function of gain as that for a CAPD with k=0. The noise properties of these new APDs have been investigated by Hollenhorst (1986) and Jindal (1987). Here we shall turn our attention to receiver sensitivity. It can be shown that the receiver sensitivity is improved as p increases for fixed value of k and dark current. Hence the best attainable sensitivity occurs at p=1 leading to:

$$<M_e> = 2/(1-k) \tag{3.30}$$

$$F_e = 1+k \tag{3.31}$$

The optimum sensitivity for zero dark current can be expressed as

$$(\eta \bar{P})_{opt} = \frac{Q_o h\upsilon}{q} [(1+k)A + (1-k)<i_{na}^2>^{1/2}/2] \tag{3.32}$$

where $A=Q_o qBI_1$. Thus for $k \to 1$, $(\eta \bar{P})_{opt} = 2Q_o h\upsilon A/q$ independent of the amplifier noise since the gain tends to an extremely large value. Eqn. 3.32 indicates that the optimum sensitivity varies linearly with k. Hence we can usefully discuss three cases (see Fig. 3.13):

(i) $<i_{na}^2>^{1/2} = 2A$, which gives $(\eta \bar{P})_{opt} = 2Q_o h\upsilon A/q$ independent of k.

(ii) $<i_{na}^2>^{1/2} < 2A$, for which the sensitivity degrades as k increases. This behaviour is identical to that for a CAPD. Note in this case that a very small value of k is required for best performance.

(iii) $\langle i_{na}^2 \rangle^{1/2} > 2A$, for which the sensitivity improves as k increases, and the best performance can be obtained as k→1. This case requires ballistic injection of both carriers across the gain region to achieve p=k=1 as proposed by Hollenhorst [1986].

Note that (i) can offer the best performance among the three cases at k=0, but it requires an extremely low noise amplifier. If we consider a 2 Gbit/s receiver operating with 50% RZ input format and full raised-cosine output signal, the amplifier input noise density must be less than 4.3×10^{-2} pA/Hz$^{1/2}$, which is very difficult to achieve practically.

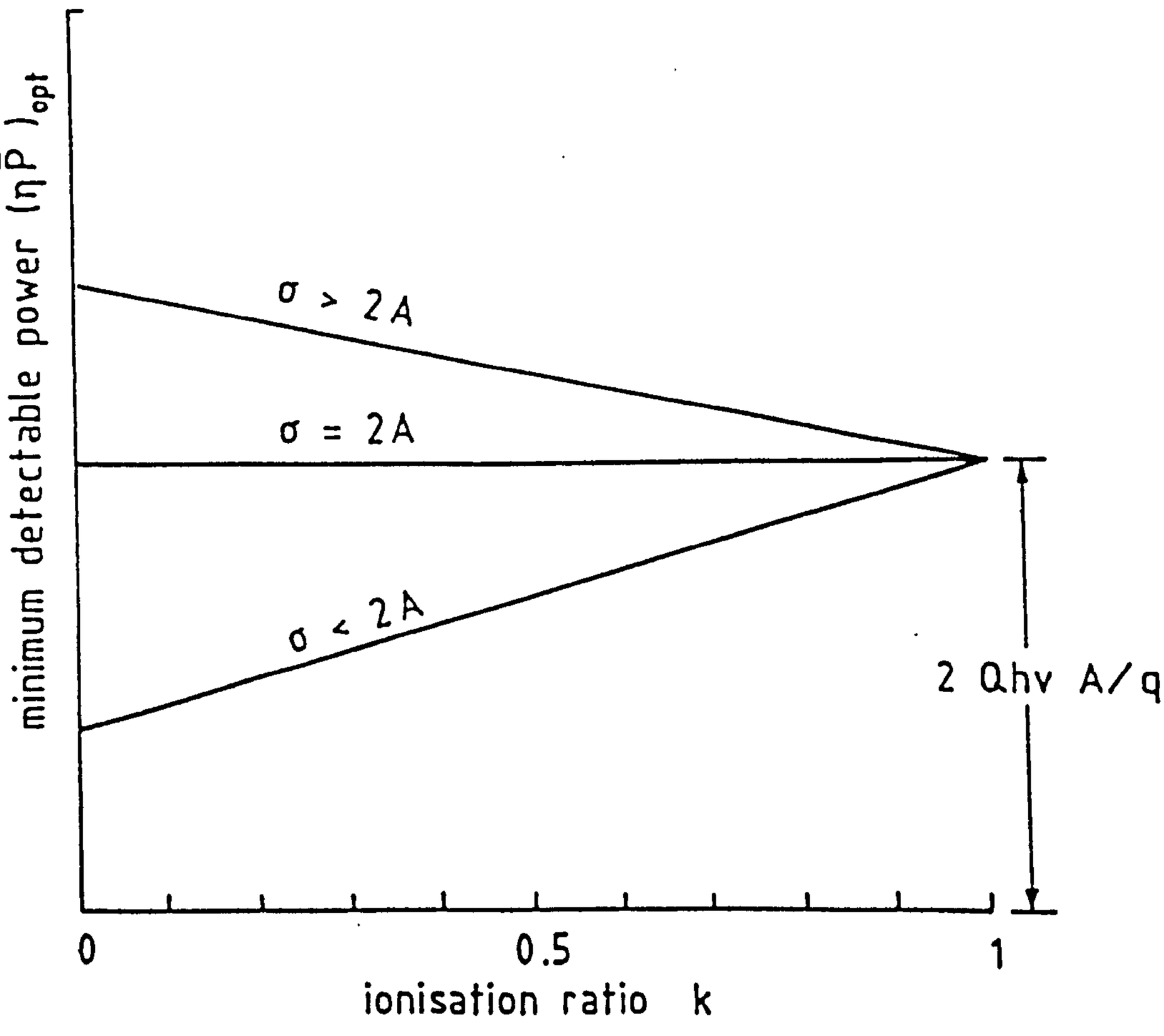

Fig. 3.13 Variation of optimum sensitivity of the new APD receiver with ionisation rate ratio k, assuming zero dark current. Note there are three modes of operation according to the amplifier noise $\sigma \equiv \langle i_{na}^2 \rangle^{1/2}$ relative to the parameter A.

To illustrate the foregoing analyses, we consider the 2 Gbit/s receiver described in section 3.4. Fig. 3.14 presents the sensitivity versus the ionisation ratio k for both zero and 100nA dark current. Results for a CAPD receiver are also shown for comparison. In these calculations the gain of the APD is adjusted, for each set of parameters, to obtain the optimum sensitivity. The sensitivity of the new APD receiver improves with increasing k, in contrast to a CAPD, although , at fixed k and dark current, the latter offers better sensitivity except at high values of k (e.g. $k>0.7$ for zero dark current). The existence of dark current affects only very slightly the sensitivity of the new receivers unless k is close to 1. This is clear from Fig. 3.15 where the sensitivity penalty due to 100 nA dark current is given as a function of k. Again the penalty is an increasing function of k, in contrast to the behaviour of a CAPD.

It is worth noting here that since most CAPDs sensitive to the wavelength range 1.3-1.6 μm have in general ionisation rate ratios around 0.3-0.5, they can lead to a better receiver sensitivity compared with the new APD structures except when k for the latter devices is made very large ($k>0.9$). Thus from a practical point of view we conclude that the only advantage to be gained from these advanced APDs is the high speed of operation due to the short length of the avalanche region [Hollenhorst, 1986; Jindal, 1987].

3.6 Performance Degradation of CAPD Receivers due to Dark Current Generated within the Multiplication Region

Several theoretical studies have been reported on the influence of dark current on the performance of CAPD receivers [e.g. Personick, 1973; Mazo and Salz, 1976; Smith and Forrest, 1982]. It has generally

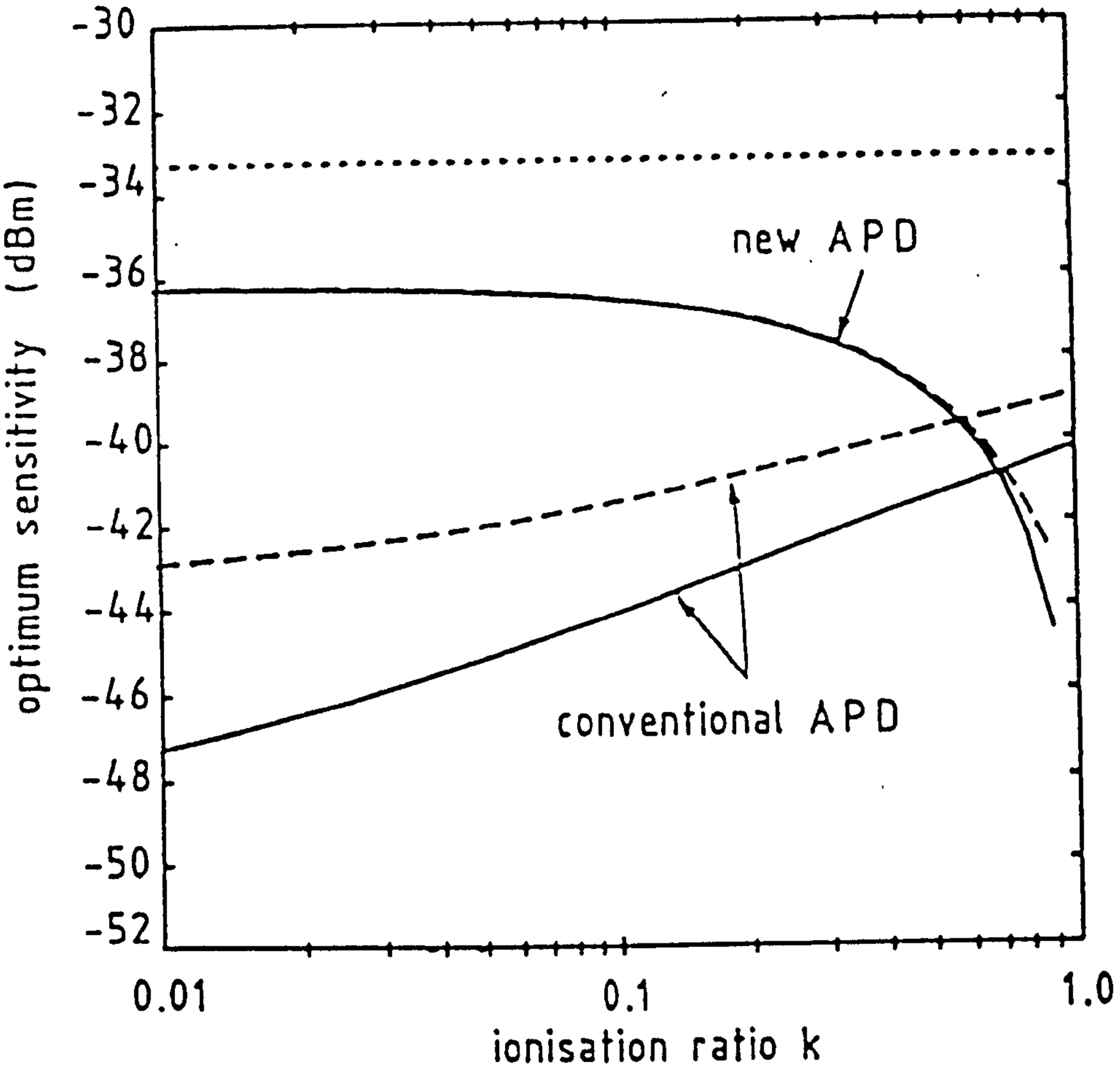

Fig. 3.14 Receiver sensitivity $(\eta\bar{P})_{opt}$ versus ionisation rate ratio k.

—— $\langle I_d \rangle$=0 --- $\langle I_d \rangle$=100 nA

····· for PIN receiver with zero dark current.

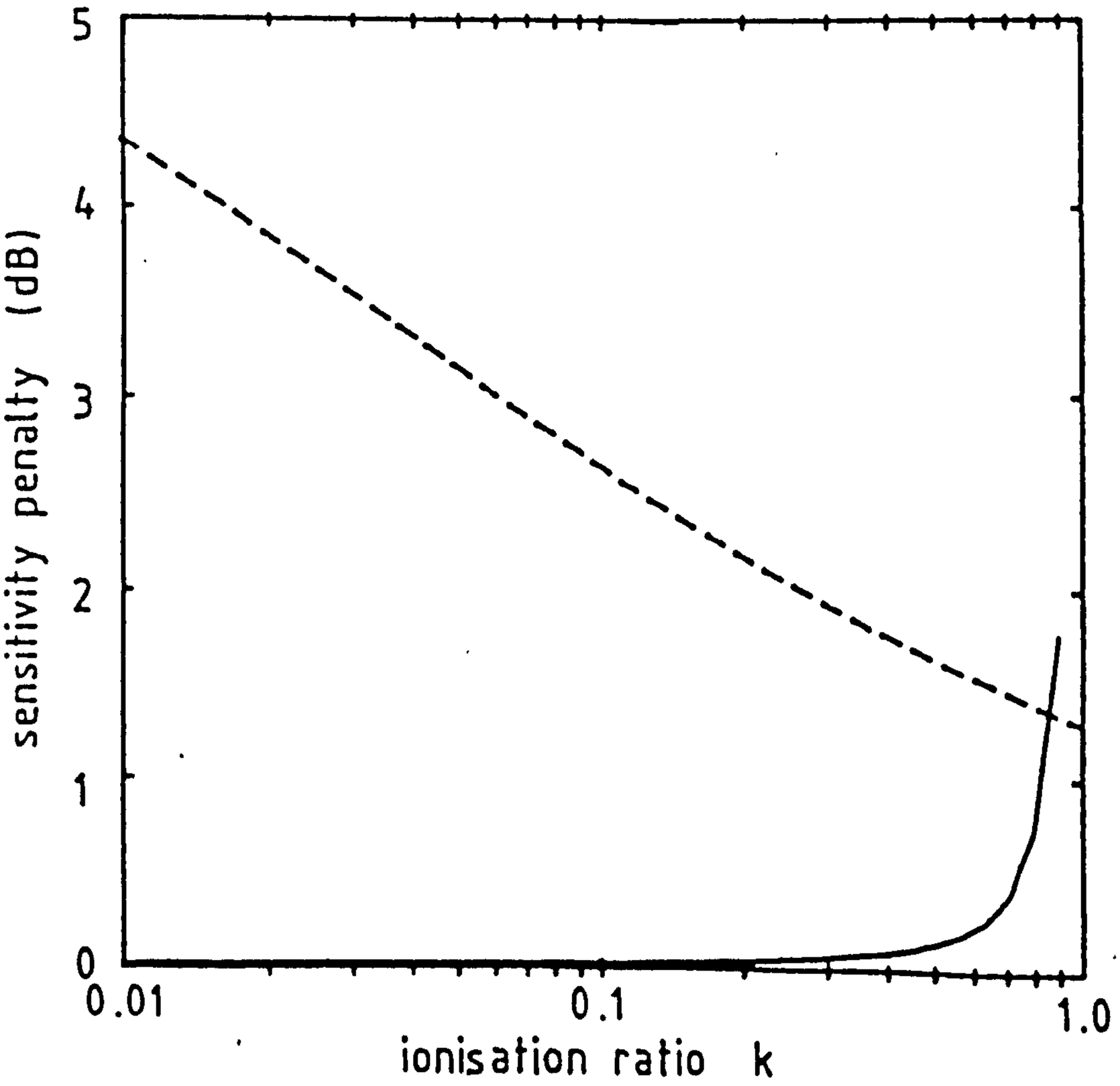

Fig. 3.15 Sensitivity penalty against ionisation rate ratio.

--- conventional APD —— single stage SAPD

been assumed that dark current is generated outside the avalanche region (diffusion type), where it can be modelled by an equivalent photocurrent source in the absorption layer. It is not then necessary to consider the positional distribution of dark current outside the multiplication region since all the initial hole-electron pairs are subject to the same random gain process. However, experimental studies show that the average gain and excess noise factor associated with dark current are different from those of photogenerated carriers since some of the dark current carriers are thermally generated within the multiplication region [Brain, 1979, 1981; Knabe and Grosskopf, 1980]. Also Knabe et al. [1981] have observed experimentally that I_{da} could be more significant than I_{dd} in some germanium APD structures.

For more substantial analysis of the influence of dark current I_{da}, its distribution within the avalanche region must be considered since the gain and the noise associated with a hole-electron pair initiated at the avalanche region exhibit positional dependence. Recently Fujihashi [1987] has studied the effect of this type of dark current, with the restriction that its rate of generation is proportional to the electron ionisation rate at the same position. Hence the excess noise factor for dark current is given in a form similar to the signal multiplication noise.

In this section we analyse the dark current generated within the multiplication region for CAPDs by applying the same approach used earlier to investigate the dark current in SAPDs. In this treatment I_{da} is replaced by an equivalent photocurrent source in the absorption layer, but has associated with it effective average gain and effective excess noise factors, which differ from those for photogenerated current, to include the position-dependence of both the random gain

and the primary dark current distribution in the high field region. The theory is then applied to a uniformly multiplying APD (p-i-n avalanche photodiode) in which the dark current is taken to be uniformly distributed within the avalanche region.

3.6.1 Theory

Consider a reverse biased APD in which the high-field region extends from x=0 to x=W as shown in Fig. 3.16. The direction of the electric field is such that the electrons travel in the positive x direction and the holes travel in the opposite direction, as shown. The electrons and holes traversing the high-field region have impact ionisation probabilities per unit length equal to α and β,

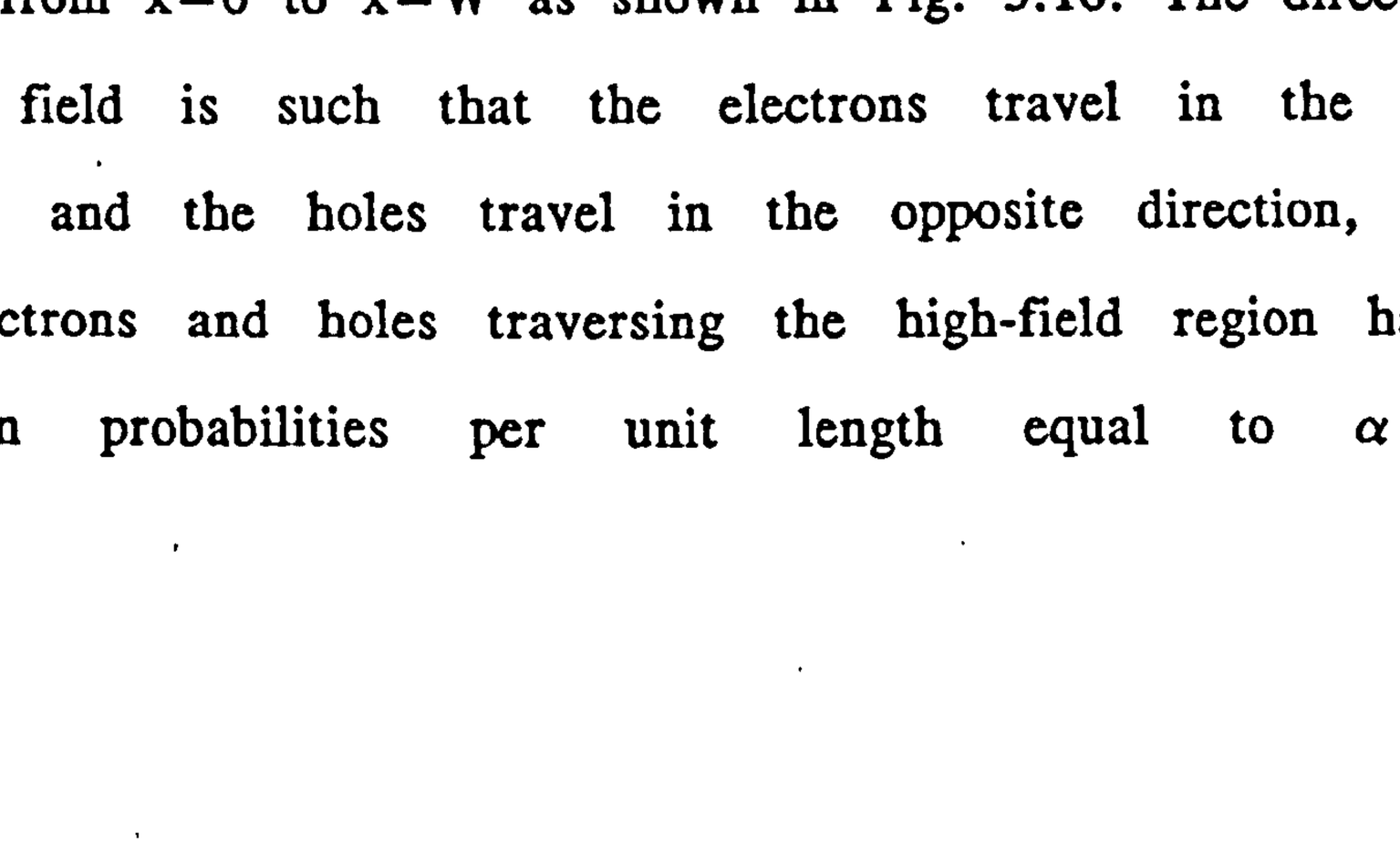

Fig. 3.16 Schematic diagram of the high-field region of APD.

respectively, which are functions of the electric field. The spectral density of the noise generated in the APD can be calculated for any distribution of the injected carriers [McIntyre, 1966]:

$$\Phi = 2q \left[2 \left[I_e(0).M^2(0) + I_h(W).M^2(W) + \int_0^W R_g(x).M^2(x).dx \right] + I \left[\int_0^W \alpha(x).M^2(x).dx - M^2(0) \right] \right] \quad (3.33)$$

where $I_e(0)$, $I_h(W)$ are the electron and hole currents entering the depletion region at $x=0$ and $x=W$, respectively, $R_g(x)$ is the rate per unit length at which the hole-electron pairs are generated (thermally and/or optically) in the depletion region, and $M(x) \equiv \langle g(x) \rangle$ is the average gain associated with a hole-electron pair initiated at position x:

$$M(x) = \frac{\exp\left[\int_x^W (\alpha-\beta)\, dx' \right]}{1 - \int_0^W \beta \exp\left[\int_{x'}^W (\alpha-\beta)\, dx'' \right] dx'} \quad (3.34)$$

Further, I is the total current (including multiplication) flowing through the diode

$$I = I_e(0).M(0) + I_h(W).M(W) + \int_0^W R_g(x).M(x)\, dx \quad (3.35)$$

Let us concern ourselves with dark current generated within the depletion region. By setting $I_e(0) = I_h(W) = 0$ and assuming $R_g(x)$ is

due to thermal excitation, eqn. 3.35 reduces to:

$$\Phi_{da} = 2q \left[2\int_0^W R_g(x).M^2(x).dx + \left[\int_0^W R_g(x).M(x).dx \right]. \right.$$

$$\left. \left[2 \int_0^W \alpha(x).M^2(x).dx - M^2(0) \right] \right] \qquad (3.36)$$

where Φ_{da} is the noise spectral density associated with dark current generated in the region $0<x<W$. The primary dark current will be given by

$$I_{da} = \int_0^W R_g(x).dx \qquad (3.37)$$

while the mean value of the dark current at the output

$$(I_{da})_{out} = \int_0^W R_g(x).M(x).dx \qquad (3.38)$$

We may replace the distributed dark current by an equivalent photocurrent source in the p^+ region with the same mean value I_{da} by introducing an effective average gain M_{eff} and effective excess noise factor F_{eff} defined by

$$M_{eff} \equiv g_{eff} = (I_{da})_{out}/I_{da}$$

or

$$M_{eff} = \left[\int_0^W R_g(x).M(x).dx \right] / \left[\int_0^W R_g(x).dx \right] \qquad (3.39)$$

and

$$F_{eff} = \Phi_{da} \; / \; (2qI_{da}M_{eff}^2)$$

or

$$F_{eff} = \left[\int_0^W R_g(x).dx \right] \left[2 \int_0^W R_g(x).M^2(x).dx + \left(\int_0^W R_g(x).M(x).dx \right). \right.$$

$$\left. \left(2 \int_0^W \alpha(x).M^2(x).dx - M^2(0) \right) \right] \; / \; \left[\int_0^W R_g(x).M(x).dx \right]^2 \qquad (3.40)$$

Eqns. 3.39 and 3.40 are general expressions for M_{eff} and F_{eff} associated with dark current distributed in the multiplication region. Evaluation of these parameters requires information on R_g, α and β as functions of position x.

We will consider specifically the following three cases:

(i) The hole and electron ionisation coefficients are equal [i.e. $\alpha(x) = \beta(x)$]. Hence

$$M_{eff} = 1/\left[1 - \int_0^W \alpha(x).dx \right] \qquad (3.41)$$

$$F_{eff} = M_{eff} \qquad (3.42)$$

These results are the same as for photocurrent injected into the depletion region [Tager, 1965; McIntyre, 1966], since the gain is no

longer a function of x.

(ii) Let $R_g(x)$ be given by a delta function located at x=0 (i.e. $R_g(x) = R_0.\delta(x)$, where $\delta(.)$ is the Dirac delta function) then eqns. 3.39 and 3.40 reduce to the same expressions given by McIntyre [1966] for electron current injected into the depletion region at x=0.

(iii) If the dark current is generated uniformly along the multiplication region [i.e. $R_g(x) = R_o$, independent of x], then

$$M_{eff} = \frac{1}{W}\int_0^W M(x)dx \tag{3.43}$$

$$F_{eff} = \frac{2\int_0^W M^2(x).dx + \left[\int_0^W M(x).dx\right]\left[2\int_0^W \alpha(x).M(x).dx - M^2(0)\right]}{\frac{1}{W}\left[\int_0^W M(x).dx\right]^2} \tag{3.44}$$

independent of R_o, the rate of generation of dark current Eqn. 3.43 corresponds to the expression given by Howard [1962] for the multiplication for space-charge generated current in an APD since the conditions assumed in both cases are identical.

3.6.2 PIN Avalanche Diode

To compare the noise properties of distributed dark current with those of diffusion type (or injected electron) current, we consider a p-i-n diode in which the electric field is constant within the depletion region such that α and β are no longer dependent on x. For diffusion electron dark current, the gain $\langle M_o \rangle \equiv M(0)$ and the excess

noise factor F_o will be given by eqns. 2.5 and 2.6 respectively. For dark current generated uniformly in the depletion region, eqns. 3.43 and 3.44 reduce to:

$$M_{eff} = \frac{1-\exp\,[-\alpha W(1-k)]}{\alpha W(1-k)}\, M(0) \qquad (3.45)$$

where $k \equiv \beta/\alpha$ is the ionisation rate ratio. Or

$$M_{eff} = \frac{1}{\alpha W(1-k)}\,[M(0) - M(W)] \qquad (3.46)$$

since $M(W) = M(0) \exp\,[-\alpha W(1-k)]$ for a p-i-n structure. Also

$$F_{eff} = \frac{\alpha W(1-k) M(0).M(W)}{M(0) - M(W)} \qquad (3.47)$$

or

$$F_{eff} = \frac{M(0).M(W)}{M_{eff}} \qquad (3.48)$$

Fig. 3.17 shows the variation of the average gains $<M_o>$ and M_{eff} as a function of αW for different values of ionisation rate ratio k. This figure indicates that the effective gain experienced by the dark current generated within the high-field region is less than that for diffusion dark current $<M_o>$, when $0 \leq k < 1$. This is in agreement with previously published experimental results [Kanbe et al., 1981]. The difference between $<M_o>$ and M_{eff} is higher for $k=0$ and reduces to zero at $k=1$. For $k<1$, M_{eff} will be greater than $<M_o>$ since the carriers of lowest ionisation rate are injected into the multiplication region to initiate the avalanche process. This is undesirable for practical

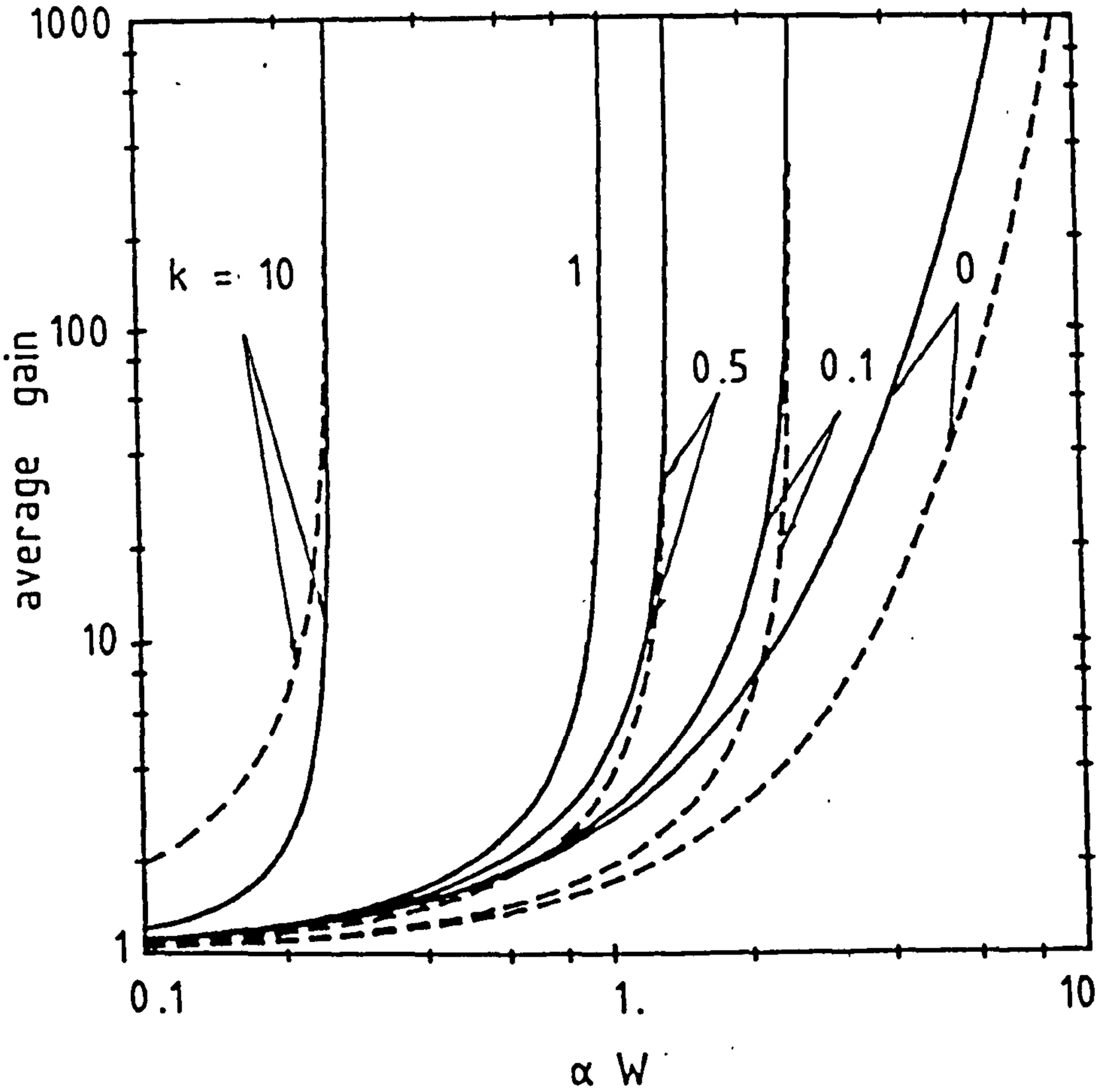

Fig. 3.17 Average gain of PIN avalanche photodiode as a function of αW. —— $\langle M_e \rangle$ – – – M_{eff}

APDs since it results in higher signal-multiplication noise. It will thus not be considered further. An interesting point to be noted here is that both $\langle M_e \rangle$ and M_{eff} tend to infinity (avalanche breakdown occurs) at the same value of αW, at fixed k (see eqn. 3.45).

The excess noise factors F_e and F_{eff} are compared in Fig. 3.18. It is clear that F_{eff} is higher than F_e especially at higher values of αW, when $0 \leq k < 1$. Again the difference between the two parameters is a decreasing function at k. Fig. 3.19 shows that F_{eff} is higher than F_e when the average gain $\langle M_e \rangle$ is less than 4 for all values of $k < 1$. Once again, the higher excess noise factor associated with dark current is

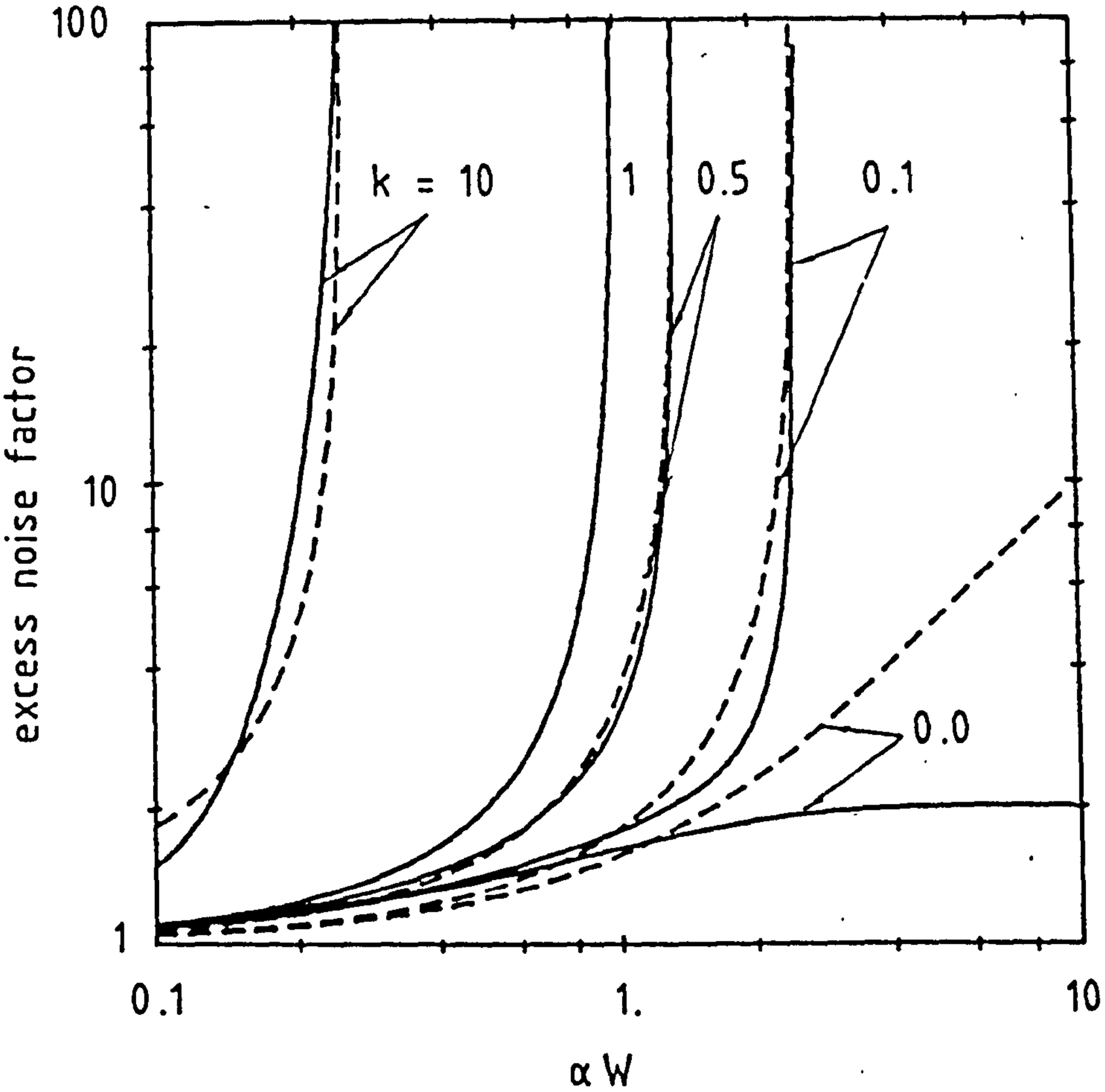

Fig. 3.18 Excess noise factor of PIN avalanche photodiode as a function of αW. —— F_e - - - F_{eff}

in agreement with experimental results [Brain, 1981; Knabe et al., 1981].

To investigate the performance degradation caused by various dark current components, we consider a 2 Gbit/s receiver operating at $\lambda=1.5\mu$m with an amplifier equivalent input noise current density of 2.124 pA/Hz$^{1/2}$, as described in Section 3.4. Fig. 3.20 shows the BER curves for different values of dark current. Two values of k are considered, k=0.025 which represents a low noise APD and k=0.5 which is a reasonable value for APDs made from III-V semiconductor compounds. It is clear that diffusion dark current affects the

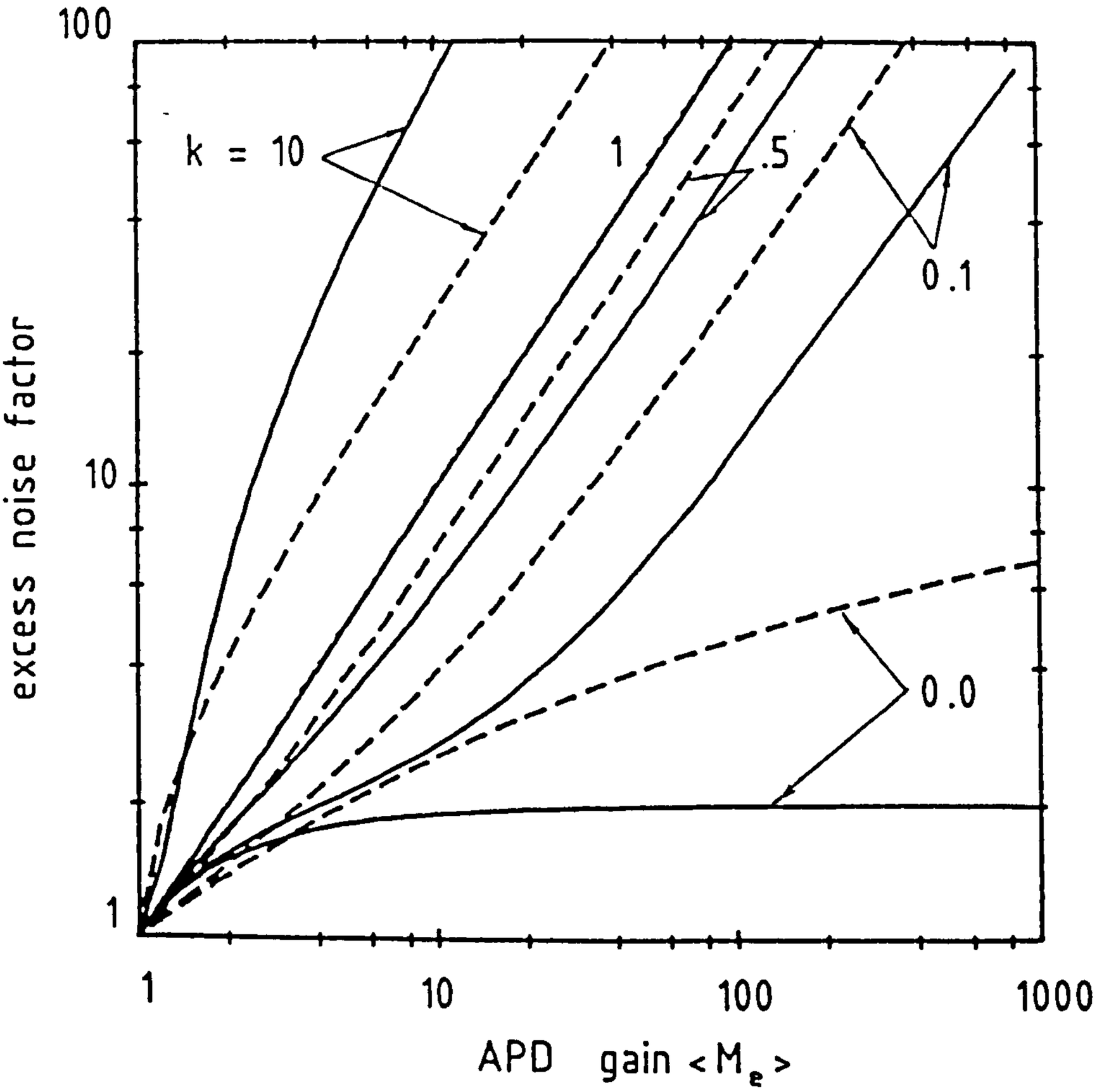

Fig. 3.19 Dependence of excess noise factors F_e(solid) and F_{eff} (broken) on APD gain $\langle M_e \rangle$.

receiver sensitivity more than does I_{da}, especially when k=0.025. In addition, it has been found that the difference between the sensitivity for the receiver with I_{da} and that with I_{dd} is an increasing function of the mean value of dark current, at fixed k [Fyath and O'Reilly, 1989a].

Fig. 3.21 shows the variation of the receiver sensitivity with APD gain $\langle M_e \rangle$ for different values of k. The optimum gain is reduced when dark current exists, but the reduction is greater for diffusion dark current at fixed k. For k=0.5 the difference between the optimum gains for the two types of dark current is small.

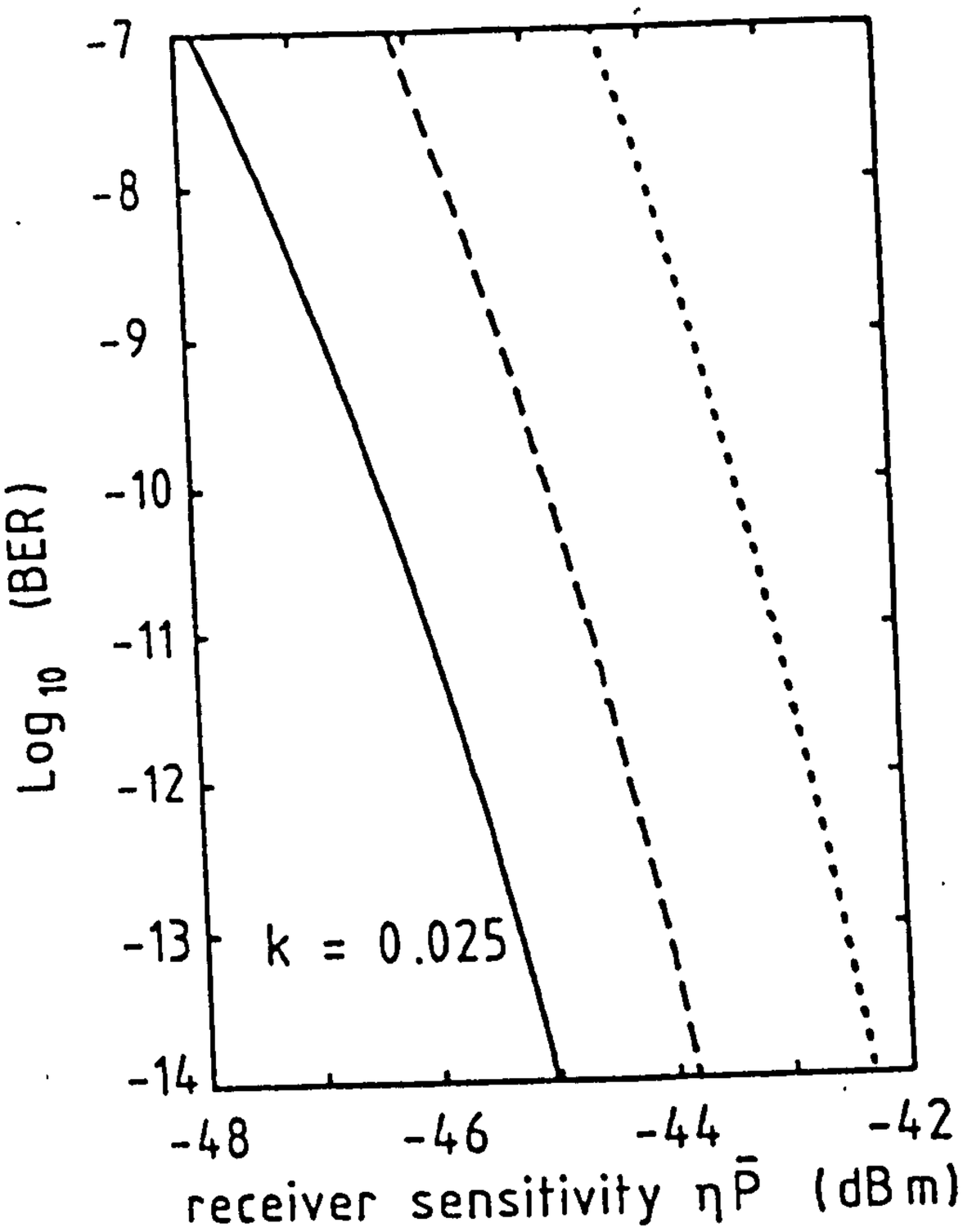

(a)

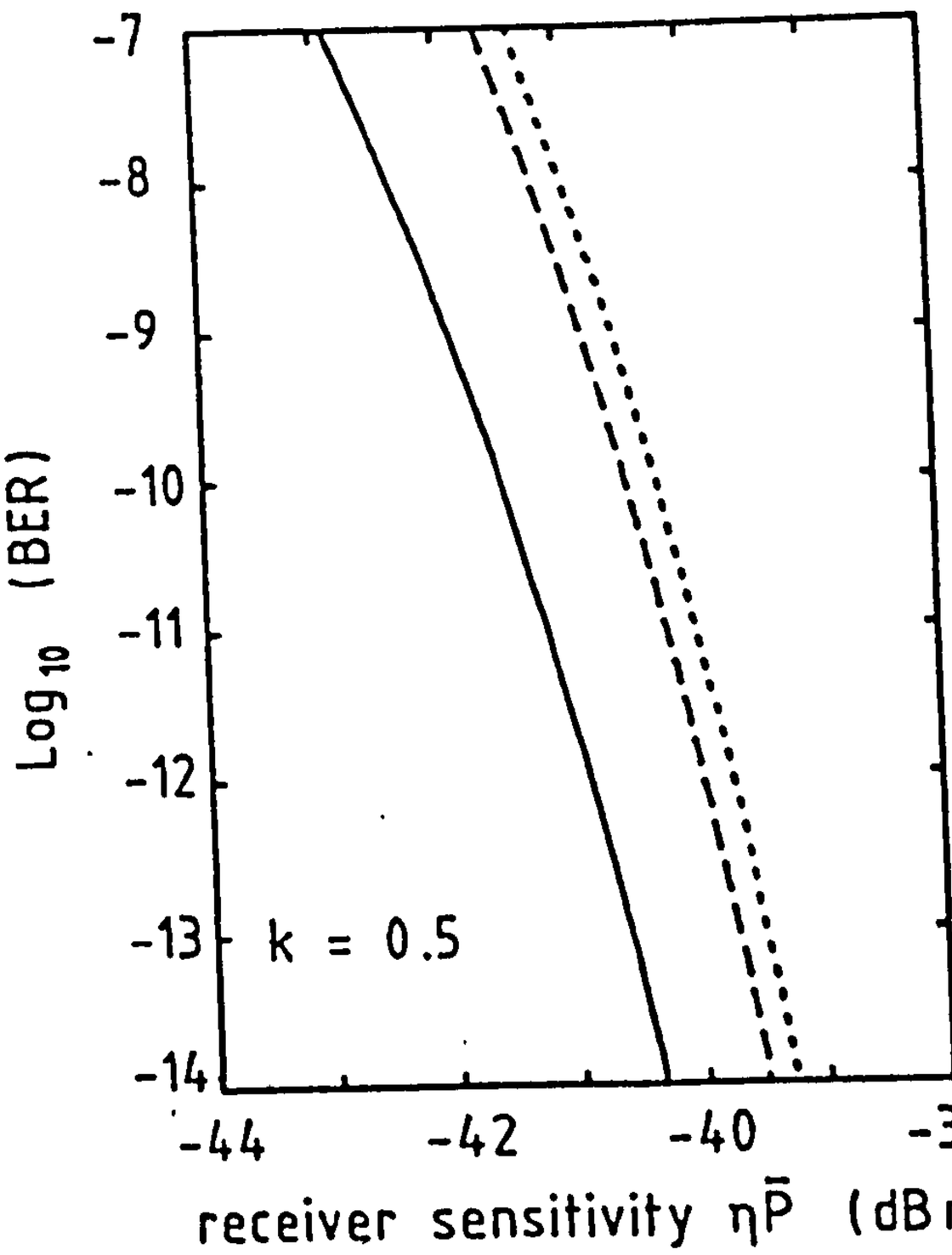

(b)

Fig. 3.20 Bit error rate (BER) versus receiver sensitivity.
(a) k=0.025 (b) k=0.5
——— $I_{dd}=I_{da}=0$ — — — $I_{dd}=0$, $I_{da}=50$ nA
----- $I_{dd}=50$ nA, $I_{da}=0$

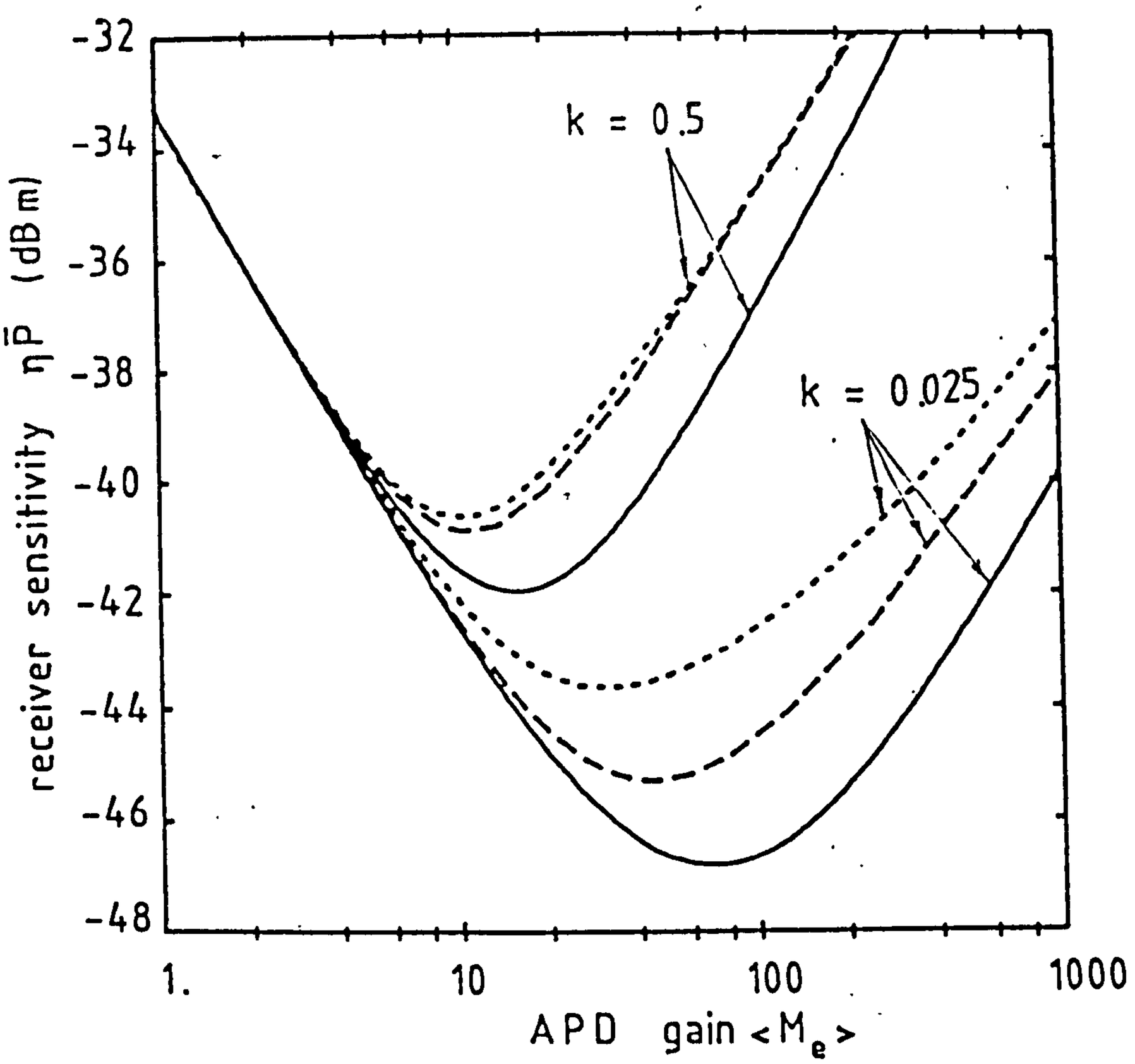

Fig. 3.21 Receiver sensitivity as a function of APD gain.

——— $I_{dd}=I_{da}=0$ — — — $I_{dd}=0$, $I_{da}=50$ nA

····· $I_{dd}=50$ nA, $I_{da}=0$

It is clear from the above discussions that for APDs with low k values (e.g. silicon APDs), care must be taken to distinguish between thetwo types of dark current. For germanium and III-V APDs however, where $k>0.3$ in general all dark current can reasonably be treated as if it was of diffusion type since the effects of both types of dark current are almost the same in these cases.

3.7 Summary

Formulas for the gain and excess noise factor have been derived for superlattice avalanche photodiodes (SAPDs), taking into account

the position of the initiating hole-electron pair. This has enabled the effective gain and effective excess noise factor for the dark current (generated in the various stages) to be determined. The performance has been investigated of optical receivers incorporating SAPDs allowing for both residual hole ionisation and different components of dark current. It has been shown that at low values of hole-to-electron ionisation rate ratio k, a SAPD with a larger number of stages will give improved sensitivity, but will be influenced significantly by dark current. As k increases, best performance (high sensitivity and wide bandwidth operation) is obtained with a smaller number of stages.

The analysis has been extended to accommodate conventional avalanche photodioes (CAPDs). General formulas have been presented for the effective gain and effective excess noise factor associated with dark current generated within the multiplication region of CAPDs. The expressions have been used to study the influence of dark current on the uniformly multiplying APD receiver. The results show that dark current generated within the multiplication region has less influence on system performance than does diffusion dark current of the same value, especially when k is very small. As k increases towards 1, the difference between the effects of the two types of dark current is reduced, approaching zero at k=1.

The analysis of SAPDs given here is applicable for staircase APDs assuming that the electrons ionise at the steps only while the holes ionise within the graded regions, as proposed by Capasso et al. [1983]. In the next chapter the analysis is extended, in order to consider the effect of carrier (electron and hole) impact ionisations both in the graded regions and at the steps. The modelling procedure

adopted represents an expedient simplication, selected to render tractable a complex subject, and tailoring potential physical device models leads to consideration of three extreme cases.

CHAPTER 4

PERFORMANCE OF STAIRCASE APD RECEIVERS

The analyses of the performance of a staircase APD are usually based on the assumption that the effective electric field in the graded-gap region is sufficiently small that the electrons do not impact ionise before they reach the step, while the holes will not ionise at the step since the value of the valence band discontinuity (ΔE_v) is small and of wrong sign to assist hole ionisation [Capasso et al., 1983]. Under these conditions, with electrons ionising at the steps only and holes impact ionising at a very small rate due to the residual electric field in the graded regions, the theory of discrete impact ionisations [van Vliet et al., 1979a; 1979b] can be applied directly by treating, as an approximation, both the graded region and the step as a single stage.

In general, however, there could be in principle finite but different probabilities for electrons to ionise both at the steps and in the graded regions and similarly, with different probabilities, for holes. It is appropriate, therefore, to develop analyses to encompass this situation. We do so initially without reference to specific physical device models seeking to provide a flexible general frame-work for subsequent study of practical cases. Three extreme cases will be identified depending on the material and the structure of the diode. The results indicate that electron ionisation in the graded region can lead to improved receiver sensitivity provided the residual hole ionisation in both the graded region and at the step is

kept to an ultralow value.

It is worth noting here that while the analyses given in the following sections are applied specifically to the staircase APD, they can be also used to investigate other superlattice APDs.

4.1 Modelling Assumptions

From practical considerations different assumptions are required to relate discrete probability models to physical device models. The modelling procedure adopted represents an appropriate expedient simplification, selected to render tractable a complex subject; tailoring this to potential physical device models leads to consideration of three extreme cases, as follows:

Case i: Here it is assumed that when an electron impact ionises at the step, it and its associated secondary electron will also have the possibility of causing ionisation with relatively small probability within the next graded region. The above conditions are satisfied if the electron, injected at zero energy into the graded region, can gain the required ionisation energy from the effective electric field therein. In other words, the collision-free mean path D is less than the width L of the graded region (see Fig. 2.2):

$$D < L \tag{4.1}$$

where

$$D = \frac{E_{ie}(D)}{[qF - dE_c/dx] - \langle n \rangle E_p} \tag{4.2}$$

Here, $E_{ie}(D)$ is the electron ionisation energy in the graded region at distance D from the previous step, F is the applied electric field, dE_c/dx is the quasi-electric field intensity expressed as the gradient of the conduction band discontinuity, $<n>$ is the average number of phonons emitted per unit length, and E_p is the phonon energy. Thus, eqn. 4.1 is satisfied when the length of the graded region is relatively large, or when the staircase APD is made from a material system of low ionisation threshold such as InAsSb.

Case ii: It is assumed here that if an electron impact ionise at the step, it may still further impact ionise at the following graded region but that there is no chance of the secondary electron generated at the step causing ionisation within this graded region. These conditions may occur in a staircase APD made from material in which ΔE_c can be made much greater than the electron ionisation energy (such as $Hg_xCd_{1-x}Te$). Note that Capasso [1984; 1985] has previously proposed the use of HgCdTe material system to fabricate a staircase APD to create more than one hole-electron pair per initiating carrier per dynode.

Case iii: Here the assumption is that only these electrons that do not cause ionisation at the step are able to gain the extra energy required to undergo an ionising collision in the next graded region. Other electrons, have just undergo ionising collisions at the step, or which have just been created there, are unable to gain the required energy to ionise within the graded region. This may occur when eqn. 4.1 is not satisfied.

In each of the above cases, similar assumptions may be made for the holes.

4.2 Gain and Noise Characteristics

In the following sections expressions for the average gain and the excess noise factor associated with a staircase APD are derived for each of the above cases.

4.2.1 Case I

let

p_s = electron ionisation probability in the step

p_g = electron ionisation probability in the graded region

u_s = hole ionisation probability in the step

u_g = hole ionisation probability in the graded region

Note that for practical realisations u_g, $p_g << 1$. Here, the N-stage staircase APD will be treated as 2N-stage device by considering each step and graded region as an individual stage. Since in general $p_s \neq p_g$ and $u_s \neq u_g$, the expressions given in the literature for the gain and excess noise factor of SAPDs with identical stages [Capasso et al., 1983; Teich et al., 1986a] cannot be applied directly to this case. In the following paragraphs, these analyses are extended to accommodate nonidentical stages and are then applied specifically to the staircase APD.

Referring to Fig. 4.1, consider a hole-electron pair incident at position A. This position will be labelled by A(j), where j denotes the number of possible ionisation that can be caused by the electron when moving to the right (at B_1, B_2, ..., B_j). Thus the primary hole will cause 2N-j possible ionisations while moving to the left (at C_1, C_2, ..., C_{2N-j}), where N is the total number of stages. The electron moving to the right has a *prior* probability p_{i+1} of impact ionisation

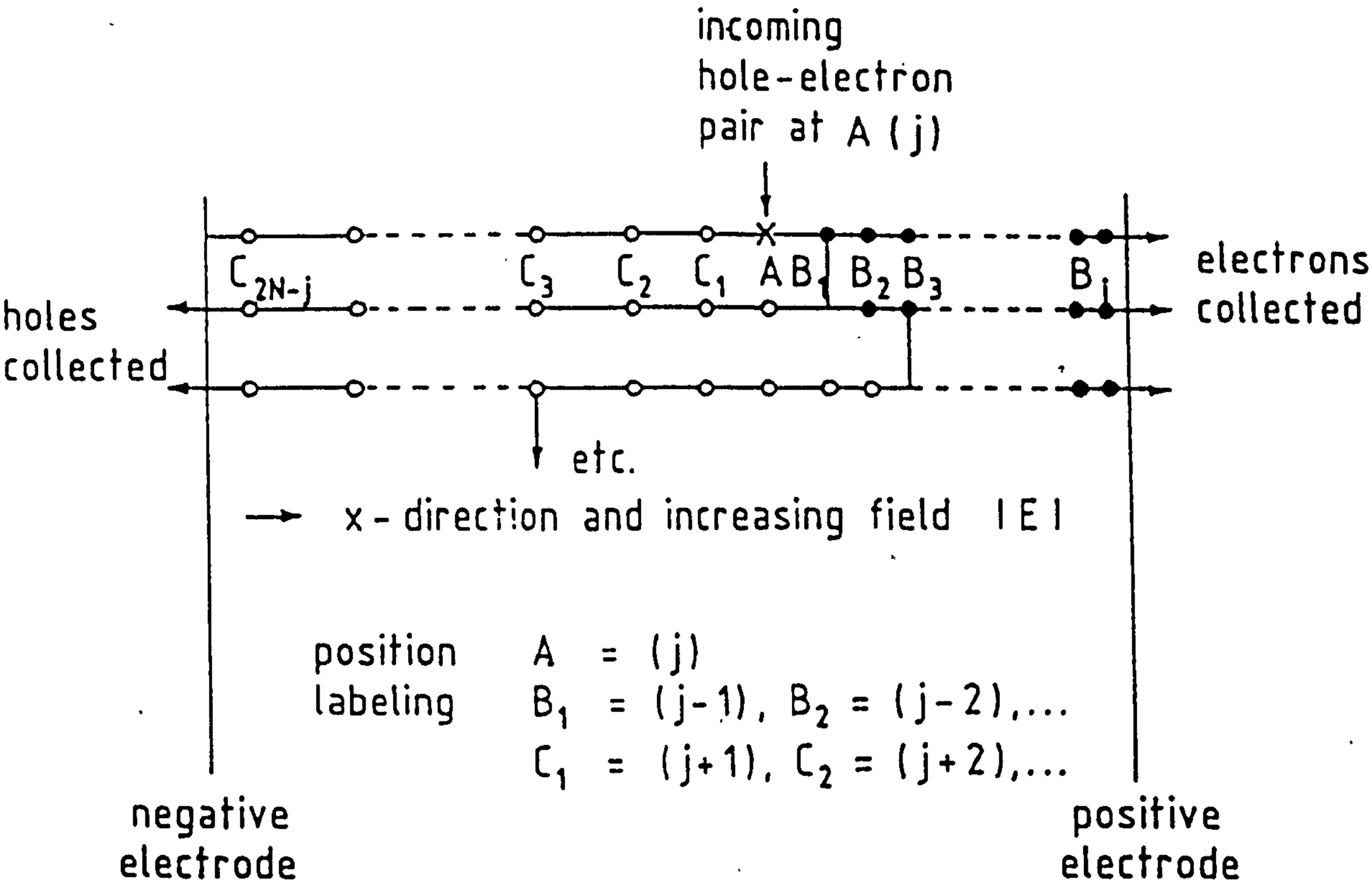

Fig. 4.1 Schematic diagram of the avalanche multiplication process.
● ionisation by electrons O ionisation by holes

at B_1 while the hole may cause ionisation at C_1 with probability u_{i-1}, where i=2N-j. Hence

$$p_i = \begin{cases} p_s & i \text{ even} \\ p_g & i \text{ odd} \end{cases} \qquad 1 \le i \le 2N \tag{4.3}$$

$$u_i = \begin{cases} u_s & i \text{ odd} \\ u_g & i \text{ even} \end{cases} \qquad 0 \le i \le 2N-1$$

let $\phi_j(z)$ be the probability generating function for the total number

of hole-electron pairs generated due to an initial hole-electron pair at position A(j), including this original pair. Following the analysis given in [van Vliet et al., 1979b], general expressions for the average gain <g> and the excess noise factor F_e can be derived; assuming the light in absorped at the p^+ region.

$$<g> = \phi'_{2N} = \frac{\prod_{i=1}^{2N} Q_i}{1 - \sum_{i=1}^{2N} u_{i-1} \prod_{j=1}^{2N} Q_j} \tag{4.4}$$

where ϕ'_{2N} is the derivative with regard to z of $\phi_{2N}(z)$ evaluated at z=1 and

$$Q_i = (1+p_i)/(1+u_{i-1}) \tag{4.5}$$

With the aid of eqn. 4.3, eqn. 4.4 can be written as

$$<g> = \frac{Q^N}{1-Q(u_g+u_s/Q_g)\left[\frac{Q^N-1}{Q-1}\right]} \tag{4.6}$$

where

$$Q = Q_s Q_g \tag{4.7a}$$

$$Q_s = (1+p_s)/(1+u_s) \tag{4.7b}$$

$$Q_g = (1+p_g)/(1+u_g) \tag{4.7c}$$

and

$$Q_i = \begin{cases} Q_s & i \text{ even} \\ Q_g & i \text{ odd} \end{cases} \qquad 1 \le i \le 2N \tag{4.8}$$

From eqn. 4.6 we note that $<g>$ is nonpositive finite when

$$Q(u_g + u_s/Q_g[(Q^N-1)/(Q-1)] \ge 1 \tag{4.9}$$

which corresponds to occurrence of avalanche breakdown.

The excess noise factor F_e is defined as [Teich et al., 1986a; van der Ziel, 1986]:

$$\begin{aligned} F_e &= <g^2>/<g>^2 \\ &= 1+\mathrm{Var}(g)/<g>^2 \end{aligned} \tag{4.10}$$

where [Cattermole, 1984]

$$\mathrm{Var}(g) = \phi''_{2N} - <g>^2 + <g> \tag{4.11}$$

where ϕ''_{2N} is the second derivative with regard to z of $\phi_{2N}(z)$ evaulated at z=1. From eqns. 4.10 and 4.11

$$F_e = \phi''_{2N}/<g>^2 + 1/<g> \tag{4.12}$$

ϕ''_{2N} can be expressed as

$$\phi''_{2N} = \left[\phi''_0 \prod_{i=1}^{2N} Q_i\right] + \left[\sum_{i=1}^{2N} 2S_i\left[\prod_{n=i+1}^{2N} Q_n^2\right]\prod_{j=1}^{i-1} Q_j\right]\phi'^2_0 \tag{4.13}$$

where

$$\phi_0'' = \Bigg[2 \sum_{j=1}^{2N} u_{2N-j}\phi_j' + \sum_{j=1}^{2N} u_{2N-j}\phi_j' \sum_{i=1}^{2N} u_{2N-i}\phi_i' + \sum_{j=1}^{2N} u_{2N-j} \Bigg[\sum_{i=2N-j+1}^{2N} 2S_i \Bigg[\prod_{n=2N-j+1}^{2N} Q_n^2 \Bigg] \cdot \prod_{m=2N-j+1}^{i-1} Q_m \Bigg] \phi_0'^2 \Bigg] \Big/ \Bigg[1 - \sum_{j=1}^{2N} u_{2N-j} \prod_{i=2N-j+1}^{2N} Q_i \Bigg] \qquad (4.14)$$

Also

$$\phi_j' = \langle g \rangle \prod_{i=1}^{2N-j} Q_i^{-1} \qquad 1 \le j \le 2N \qquad (4.15)$$

which represents the average gain associated with an initial hole-electron at position A(j) and

$$S_i = (p_i - u_{i-1}Q_i^2)/(1+u_{i-1}) \qquad (4.16)$$

Again ϕ_j' and ϕ_j'' represents the first and the second derivatives with regard to z of $\phi(z)$ evaluates at z=1. For the staircase APD considered here, eqn. 4.16 reduces to

$$S_i = \begin{cases} S_g = (p_g - u_g)/(1+u_g) & i \text{ even} \\ S_g = (p_g - u_g)/(1+u_g) & i \text{ odd} \end{cases} \qquad 1 \le i \le 2N \qquad (4.17)$$

Note that eqns. 4.4 and 4.12 through 4.16 are general expressions that can be used to determine the average gain and the excess noise

factor of 2N-stage SAPDs in which the electron (an hole) ionisation probabilities are not the same for the different stages. It is illuminating to examine these expressions for certain special cases for which formulations have previously been reported:

(a) Both electrons and holes impact ionise in the step only (i.e. $u_g = p_g = 0$). Eqn. 4.6 reduces to

$$\langle g \rangle = \frac{(1+p_s)^N (p_s - u_s)}{p_s(1+u_s)^{N+1} - u_s(1+p_s)^{N+1}} \tag{4.18}$$

Also the excess noise factor can be deduced from eqns. 4.12-4.14 (Fyath and O'Reilly, 1988d].

$$F_e = 1 + \frac{(1-1/\langle g \rangle)(p_s - u_s)}{p_s[2+u_s+p_s]} \left[-p_s + \frac{2(1-u_s p_s)}{1+u_s} \left[\frac{u_s(1+p_s)\langle g \rangle}{(p_s - u_s)} + \frac{1}{1+p_s} \right] \right] \tag{4.19}$$

Eqns. 4.18 and 4.19 are similar to the formula given in the literature [van Vliet et al., 1979b; Teich et al., 1986a] for the average gain and excess noise factor of an APD with N identical stages, as required. These expressions are also applicable to a staircase APD when both carriers impact ionise in the graded region only (i.e. $u_s = p_s = 0$), in which case u_g and p_g replace u_s and p_s, respectively in eqns. 4.18 and 4.19.

(b) The electrons impact ionise only at the steps while the holes ionise only at the graded region ($u_s = p_s = 0$). These are the conditions used by Capasso et al. [1983] to study the characteristics

of staircase APDs. In this case, eqns. 4.6 and 4.12 will reduce to the form of eqns. 4.18 and 4.19, respectively, except that u_s is replaced by u_g.

4.2.2 Case II

This case can be treated in a similar way to a staircase APD with two ionisations per initiating carrier per stage [Fyath and O'Reilly, 1988b; 1988c]. The performance of two ionisation SAPD will be addressed in detail in the next chapter.

Let $W_e(m)$ and $W_h(m)$ be the probability distribution function of m, the number of ionisations per stage caused by a single electron or hole, respectively, entering the stage. Hence

$$W_e(m) = \begin{cases} 0 & m > 2 \\ p_s p_g \equiv p_2 & m = 2 \\ p_s + p_g - 2p_s p_g \equiv p_1 & m = 1 \\ 1 - p_1 - p_2 & m = 0 \end{cases} \qquad (4.20)$$

A similar expression can be written for $W_h(m)$ by replacing p by u. Following the analysis given in Chapter 5, the average gain and the excess noise factor for electron injection can be expressed as

$$\langle g \rangle = \frac{Q^N (Q-1)}{(Q-1) - Q(Q^N-1)(u_1 + 2u_2)} \qquad (4.21)$$

$$F_e = \frac{2(u_1+2u_2)(Q^N-1)}{(Q-1)Q^{N-1}} + \frac{(u_1+2u_2)^2 (Q^N-1)^2 \langle g \rangle}{(Q-1)^2 Q^{2N-2}}$$

$$+\left[\frac{2(u_1+2u_2)S}{Q-1}+Q\,[2u_2-(u_1+2u_2)^2]\right]\left[\frac{(Q^{2N}-1)<g>}{(Q^2-1)Q^{2N-1}}\right.$$

$$-\frac{2(u_1+2u_2)(Q^N-1)<g>}{(Q-1)^2Q^{2N}}+\frac{2S(Q^N-1)}{(Q-1)Q^{N+1}}+1/<g> \qquad (4.22)$$

where

$$Q = (1+p_1+2p_2)/(1+u_1+2u_2) \qquad (4.23)$$

$$S = \frac{(p_1+3p_2)-Q^2(u_1+3u_2)}{1+u_1+2u_2} \qquad (4.24)$$

4.2.3 Case III

The conditions given for this case lead to an electron probability distribution function W(m) given by

$$W_e(m) = \begin{cases} 0 & m > 1 \\ p_s+p_g-p_sp_g \equiv p_{av} & m = 1 \\ 1-p_{av} & m = 0 \end{cases} \qquad (4.25)$$

A similar expression can be written for $W_h(m)$ by replacing p by u. Hence, this case can be treated as a conventional staircase APD with electron ionising at the step only with probability p_{av} and the holes ionising at the graded region with probability u_{av}. The gain and the excess noise factor can be calculated with the aid of eqns. 4.18 and 4.19.

4.3 Illustrative Results

The expressions given in the previous section can be used to study the influence on the performance of staircase APDs of the various parameters: u_s, u_g, p_s, p_g and N. The special case when $u_s = p_g = 0$ has been investigated in the previous chapter. Here we will concern ourselves with the effect of electron ionisation in the graded region. Illustrative results will be presented for an N=10 device, operating specifically under the conditions given in case I. Similar conclusions can be drawn from consideration of the other cases.

The avalanche breakdown condition given in eqn. 4.7 is displayed in Fig. 4.2. Here the maximum allowable value of p_g is calculated as a function of p_s for different values of u_g and $k_s \equiv u_s/p_s$. When both u_g and k_s are zero, no avalanche breakdown occurs and hence both p_g and p_s can be varied between zero and one. The existence of residual hole ionisation will limit the maximum value of p_g and p_s that can be achieved. As p_g increases, lower values of p_s must be used for given k_s and u_g. Also the maximum allowable value of p_g reduces as u_g, k_s, and p_s increases.

The average gain $\langle g \rangle$ is calculated as a function of p_s for $k_s = 0$ in Fig. 4.3a and for $k_s = 0.001$ in Fig. 4.3b with u_g and p_g taken as parameters. These figures indicate that, for a given u_g, k_s and p_s, the gain increases as p_s increases. The same conclusion applies for the excess noise factor F_e as shown in Fig. 4.4. Note that any small deviation of u_s and u_g from zero will lead to a rapid increase in the gain and the excess noise factor, especially at higher values of p_s and p_g.

The effect of various carrier ionisation probabilities on the

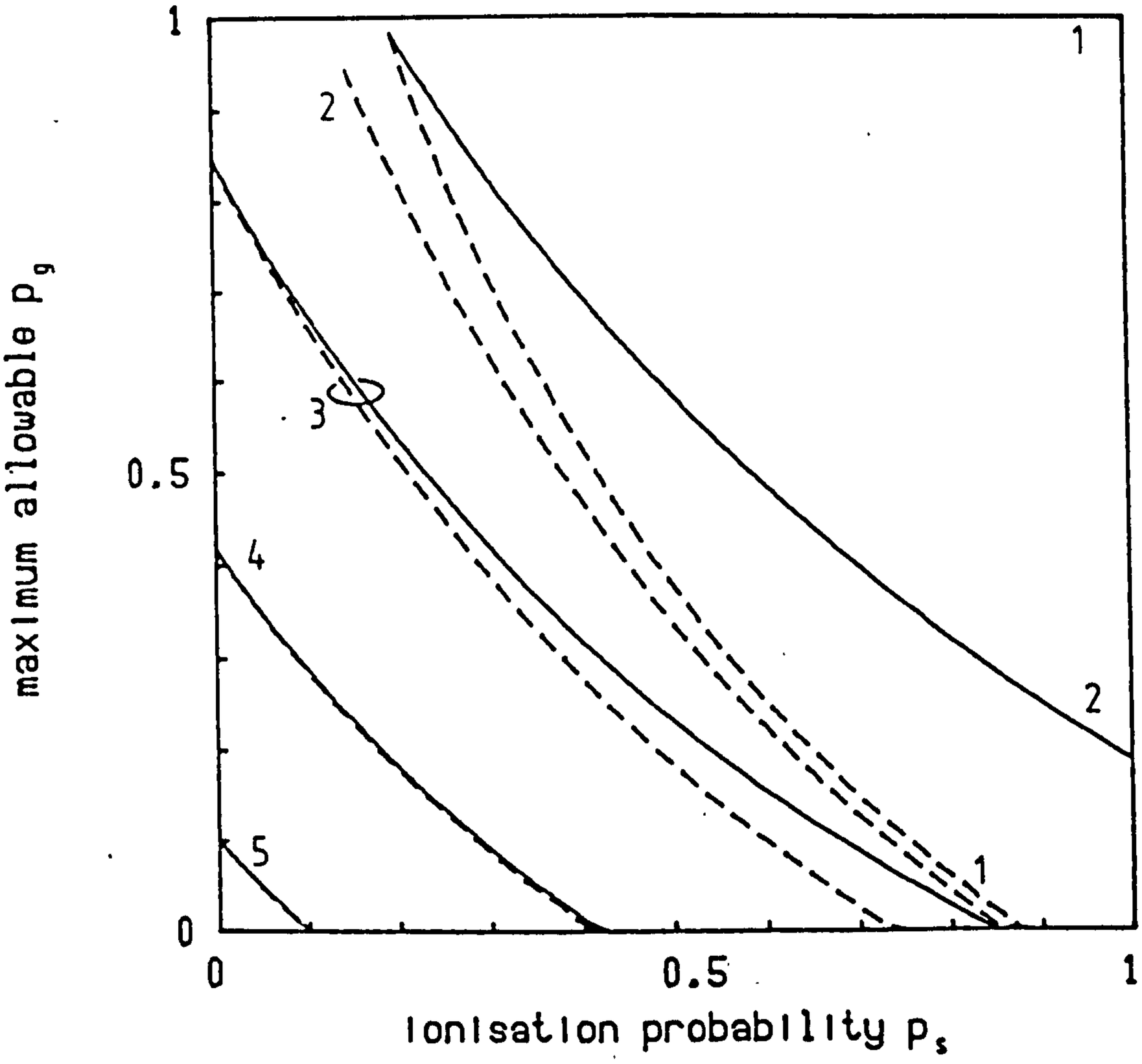

Fig. 4.2. Maximum allowable value of electron ionisation probability in the graded region.

——— k_s=0.0 – – – k_s=0.001

1: u_g=0.0 2: u_g=.0001 3: u_g=.001 4: u_g=.01 5: u_g=.1

performance of an optical receiver employing a staircase APD may also be examined. We consider a 2Gbit/s receiver operating at λ=1.5μm with an amplifier equivalent input noise current density of 2.124pA/HZ$^{1/2}$. Other receiver parameters are given in Table 3.1. The receiver sensitivity $\eta\bar{P}$ is estimated following Smith and Personick [1980] for a bit error rate of 10^{-9}. The results are illustrated in Fig. 4.5. Considering the case of no hole ionisation, represented by the curve 1 of Fig. 4.5a, we note for p_g=0.1, indicated by the broken line, a higher sensitivity is generally obtained compared with the case of

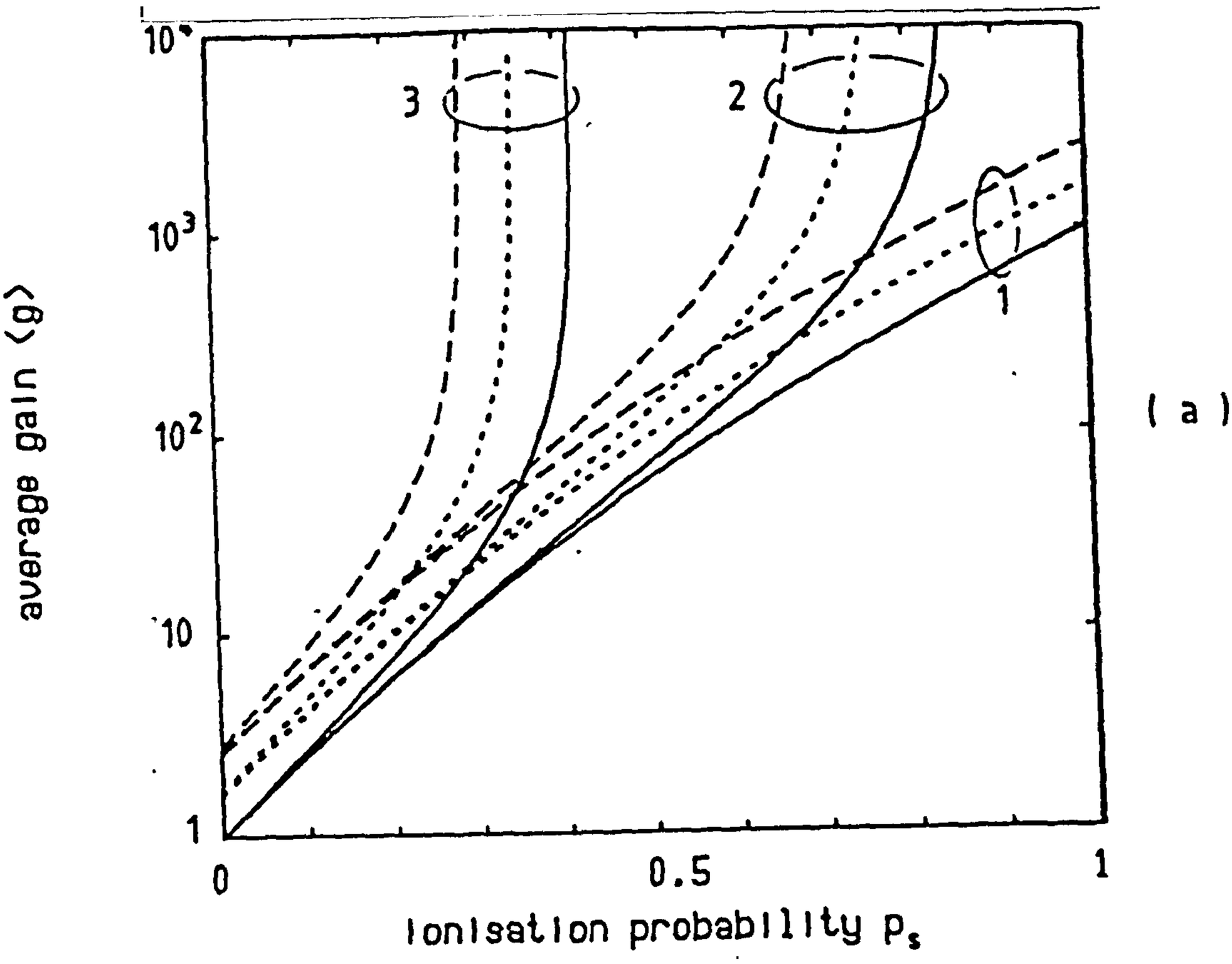

Fig. 4.3 Average gain versus electron ionisation probability at the step. (a) k_s=0.0 (b) k_s=0.001

—— p_g=0.0 ····· p_g=0.05 — — — p_g=0.1

1: u_g=0.0 2: u_g=0.001 3: u_g=0.01

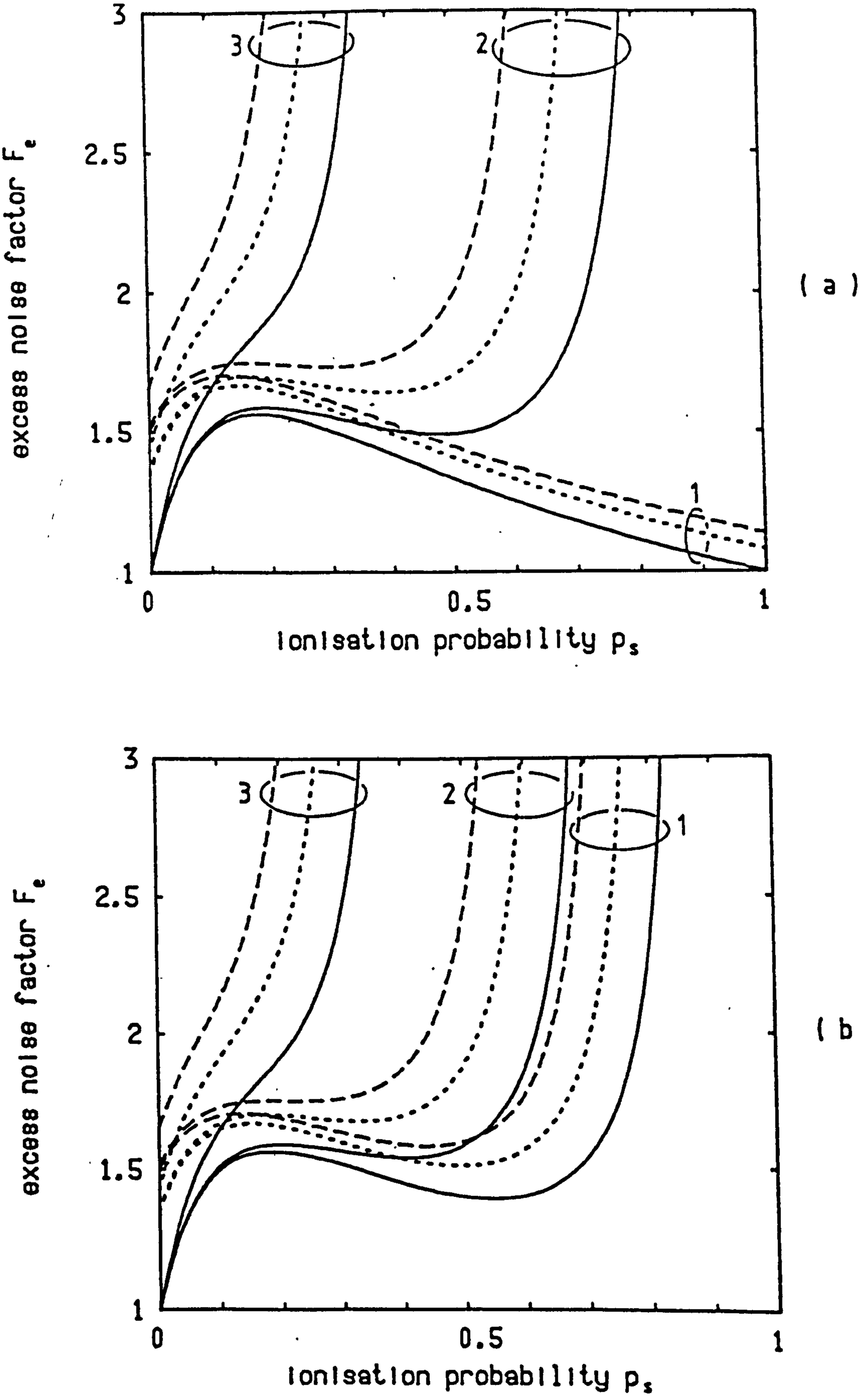

Fig. 4.4 Excess noise factor versus electron ionisation probability at the step. (a) k_s=0.0 (b) k_s=0.001

—— p_g=0.0 ····· p_g=0.05 - - - p_g=0.1

1: u_g=0.0 2: u_g=0.001 3: u_g=0.01

$p_g=0$, indicated by the solid line. This holds true for all values of p_s except near $p_s=1$; the deviation arises since the multiplication process becomes deterministic for $p_g=0$, $p_s=1$ leading to a lower values of the excess noise factor ($F_e=1$). Note also that the difference in the sensitivity between the two cases decreases as p_s increases, becoming negative for p_s greater than 0.9. In fact, the difference is 4dB at $p_s=0$ and -0.24dB at $p_s=1$. When holes impact ionise in the graded regions, at the steps, or both, the case of $p_g=0.1$ still provides higher sensitivity for a fixed p_s compared with that of $p_g=0$ provided that the APD is not operating close to the avalanche breakdown region. Near avalanche breakdown there will be a marked decrease in the sensitivity as p_s increases for a given u_g and k_s.

From the above discussions it is clear that electron ionisation in the graded region can lead to improved receiver performance if holes do not impact ionise in both regions. Without this restriction on hole ionisation it will tend to lead to a sensitivity degradation, especially when the APD is operating near the avalanche breakdown region.

4.4 Summary

Existing analyses of staircase APDs have been extended to allow for the possibility of both types of carriers impact ionising at the steps and in the graded-gap regions. General formulas for the gain and excess noise fsctor have been derived relating to three important extreme cases. The performance of a 2 Gbit/s optical receiver employing a ten-stage staircase APD has been examined to assess the influence of various carrier ionisation probabilities. It has been

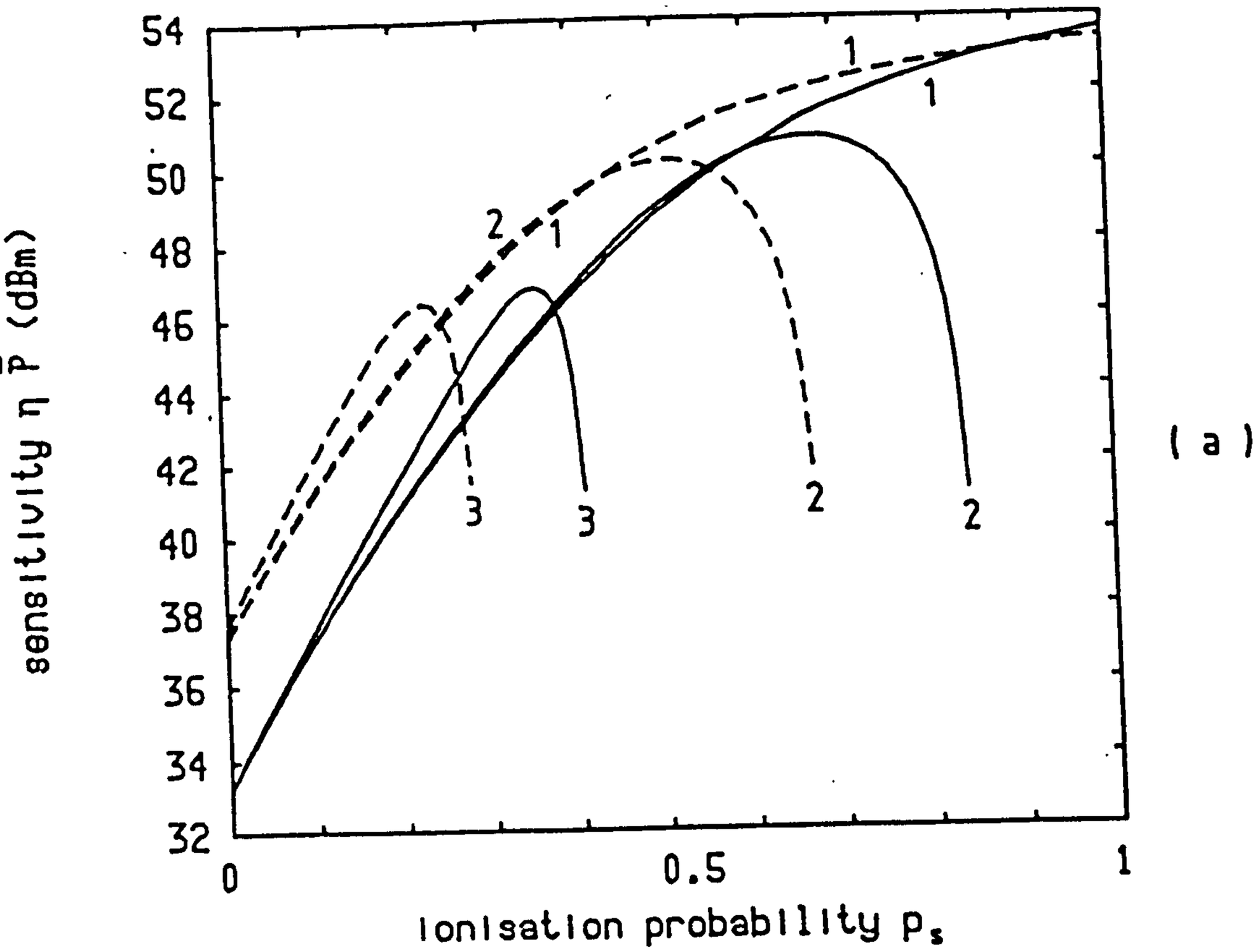

Fig. 4.5 Effect of various carrier ionisation probabilities on the sensitivity of 10-stage APD receiver at 2 Gbit/s bit rate.
(a) k_s=0.0 (b) k_s=0.001 —— p_g=0 - - - p_g=.1
1: u_g=0.0 2: u_g=0.001 3: u_g=0.01

found that electron ionisation in the graded region leads to higher sensitivity when the device is operating prior to avalanche breakdown with improved performance being obtained when the hole ionisation both at the steps and in the graded regions is vanishingly small. These observations are clearly of potential significance for the design of advanced APD structures - an assessment for the implications for specific practical cases will require a detailed consideration of the material systems and device structures involved, with the present analyses providing the necessary framework.

Recently there has been interest in SAPDs in which an electron can cause more than one ionisation per initiating carrier per stage. In the next chapter the previous analyses of the gain and noise properties of SAPDs are extended to allow for the production of up to two ionisations per carrier per stage. Extension for more than two ionisations will be discussed in Chapter 6.

CHAPTER 5

TWO-IONISATION SUPERLATTICE AVALANCHE PHOTODIODES

Recently there has been interest in SAPDs in which an electron can produce by impact ionisation more than one secondary hole-electron pair per stage, as a further step towards a solid-state photomultiplier. For example, Capasso [1984; 1985] has suggested to the use of $Hg_xCd_{1-x}Te$ to fabricate staircase APDs. For heterojunctions made in this material system, a bandgap difference is predominantly in the conduction band (bandgap can vary from 0 eV in HgTe to 1.6 eV in CdTe). Hence carrier multiplication per stage of greater than two can be obtained. As a second example we note that Brennan and Summers [1987a] have proposed a new SAPD, based on sequential resonant tunnelling [Summers and Brennan, 1986; Brennan and Summers, 1987b]. Once again, more than one secondary carrier can be produced per initiating carrier per stage.

Multiple ionisations per stage, similar to secondary emission in a photomultiplier tube, is a desirable requirement for the design of high performance APDs with small number of stages. This is necessary to achieve a wide bandwidth photodetector since the bandwidth of ideal SAPDs (single carrier-type ionisation) is inversely proportional to the number of stages and the sum of the transit times for both carrier to cross a single stage [Matsuo et al., 1985]. Note that the stage length cannot be shortened too much owing to the effects of spatial quantisation in narrow bandgap materials which increases the effective impact ionisation threshold [Brennan, 1986a; 1987c]. Also, it may be necessary to have minimum distance over which the electrons can be heated by the built-in field (and the holes cooled by phonon

scattering), especially in doped quantum well structures [Brennan, 1986b; 1986c]. A small number of stages is also required if on-chip photodetector is to be realised, operated at low bias voltage (5V). It has been shown that in this case, the number of stages is limited in general to 3-5 [Capasso, 1984; Brennan, 1987a; Brennan, 1987b].

In this chapter the noise properties of SAPDs will be investigated allowing for two ionisations per carrier per stage. The sensitivity of optical receivers employing these advanced APDs is calculated taking into account the influence of both residual hole ionisation and dark current. The results indicate clearly that multiple ionisations per stage will lead generally to higher gain, but higher excess noise factor. Receiver sensitivity studies indicate that dark current and hole ionisation are of increased significance in these devices, but if the effects are sufficiently small, improved performance is obtained.

5.1 Gain and Noise Characteristics

We shall direct our attention to the practically significant case of up to two ionisations per initiating electron per stage. The general extension to multiple ionisations will be discussed in Chapter 6.

Let us assume that the initiating electron can obtain enough energy to cause one or two ionisations per stage with probability p_1 and p_2, respectively, while the initiating hole can impact a single ionisation per stage with probability u. It is also assumed that the secondary electrons are unable to cause impact ionisation in the same stage in which they are generated. This is quite practical, since most of the energy gained by the electron is derived from the

potential step discontinuity. Let p_1 and p_2 be related to new parameters, p and r according to

$$p_1 = p/(1+r) \tag{5.1a}$$

$$p_2 = rp/(1+r) \tag{5.1b}$$

where $p = p_1+p_2$ represents the total probability for an electron to cause one or two ionisations per stage, while $r = p_2/p_1$. Hence there are two extreme cases:

(i) $r=0$ (i.e. $p_2=0$) in which the electron can induce only a single ionisation per stage with probability p; this case has been investigated in Chapter 3.

(ii) $r=\infty$ (i.e. $p_1=0$) in which the electron can cause two ionisations per stage with probability p. In this case there is zero probability of an electron causing just one ionisation per stage.

Other values of r, between 0 and ∞, represents the situation where both one and two ionisations per stage are possible. Let k represent the ratio of the average number of ionisations per stage for a hole and an electron given by

$$k = u/(p_1+2p_2)$$

$$= \frac{u}{p[(1+2r)/(1+r)]} \tag{5.2}$$

Consider a hole-electron pair injected into a stage. This entry position will be labelled by A(j), where j represents the number of stages crossed by the electron while moving towards the n^+ region (positive contact). Hence the number of stages crossed by the hole

while moving towards the p^+ region is equal to N-j, where N is the total number of stages. The average gain $<g_N>$ and the excess noise factor F_N associated with hole-electron pair photogenerated in the p^+ region will be given by (see Appendices C and D):

$$<g_N> = \frac{(p_1-2p_2-u)Q^N}{(p_1+2p_2)(1+u)-u(1+p_1+2p_2)Q^N} \tag{5.3}$$

$$F_N = \frac{2u(Q^N-1)}{(Q-1)Q^{N-1}} + \frac{u^2(Q^N-1)^2<g_N>}{(Q-1)^2Q^{2N-2}}$$

$$+ \left[2uS/(Q-1) - u^2Q\right]\left[\frac{(Q^{2N}-1)<g_N>}{(Q^2-1)Q^{2N-1}} - \frac{2uS(Q^N-1)<g_N>}{(Q-1)^2Q^{2N}}\right]$$

$$+ \frac{2S(Q^N-1)}{(Q-1)Q^{N+1}} + 1/<g_N> \tag{5.4}$$

where

$$Q = (1+p_1+2p_2)/(1+u) \tag{5.5a}$$

$$S = (p_1+3p_2-uQ^2)(1+u) \tag{5.5b}$$

For $p_2=0$ (r=0) eqns. 5.3 and 5.4 reduces to the results given by Teich et al. [1986a] for single ionisation per carrier per stage- SAPDs. Note that the gain of the device (eqn. 5.3) depends on the average electron ionisation per stage (p_1+2p_2).

For the ideal case where there is no hole ionisation (i.e. u=0), eqns. 5.3 and 5.4 reduce to

$$\langle g_N \rangle = (1+p_1+2p_2)^N \tag{5.6a}$$

$$F_e = \frac{(1+3p_1+8p_2)-(1+p_1+2p_2)^2}{(p_1+2p_2)(1+p_1+2p_2)} \left[1-(1+p_1+2p_2)^{-N}\right] \tag{5.6b}$$

Eqns. 5.6a and 5.6b are identical to the average gain and excess noise factor, respectively, for a photomultiplier tube with N identical stages [Teich et al., 1986a] in which $\langle \delta \rangle = 1+p_1+2p_2$ and $\langle \delta^2 \rangle = 1+3p_1+8p_2$, where δ is the random gain of a single stage. Eqn. 5.6b shows that when p=1, the excess noise factor F_N will equal 1 only when r=0 or r=∞, since the gain will be deterministics. Other values of r will give slightly higher values of F_N at p=1.

Figs. 5.1 and 5.2 show the variation of the average gain $\langle g_N \rangle$ and the excess noise factor F_N as a function of electron ionisation probability p, for different values of N, r, and k. Fig. 5.1 indicates that, at fixed p, N, and k, higher values of r lead to higher average gain. The noise factor will behave in a similar manner except for high values of p when k=0. This is clear from Fig. 5.3 in which the effects of different parameters on F_N for a 5-stage device are given. For p=1 and k=0, the r=1 case gives slightly higher excess noise factor compared with r=0 or r=∞, as stated previously. These figures indicate that even a small deviation of k from zero leads to a large increase in gain and excess noise factor; this effect will be higher for high values of r, at fixed N. Note also that as k decreases higher values of p are possible, for given N and r, before avalanche breakdown occurs. This maximum allowable value of p will be lower for high values of r at the same conditions. This is clear since avalanche breakdown depends on the average electron ionisations per stage [i.e. $p_1+2p_2 = p(1+2r)/(1+r)$]. Thus when r=∞, breakdown

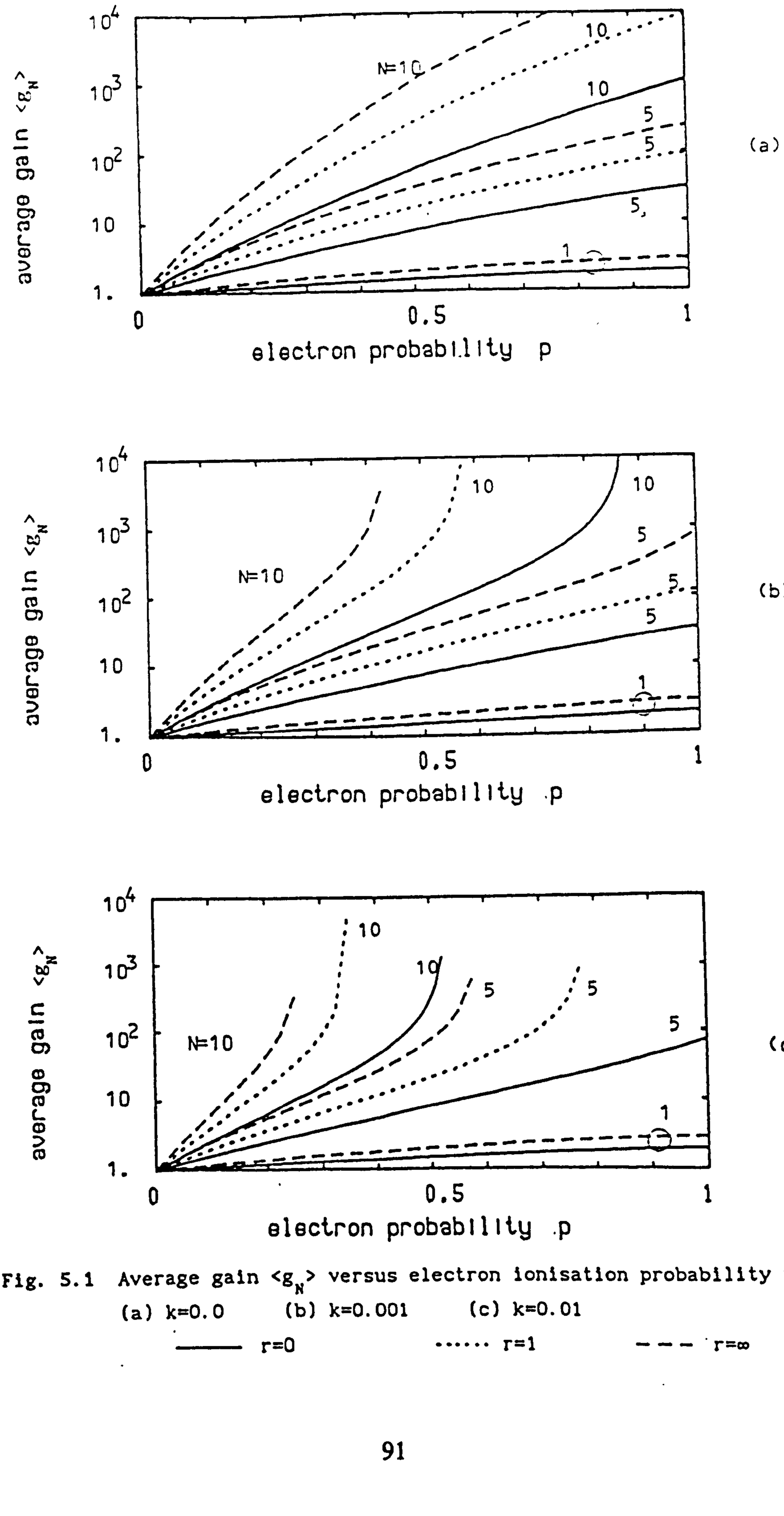

Fig. 5.1 Average gain $\langle g_N \rangle$ versus electron ionisation probability p.
(a) k=0.0 (b) k=0.001 (c) k=0.01
——— r=0 ····· r=1 — — — r=∞

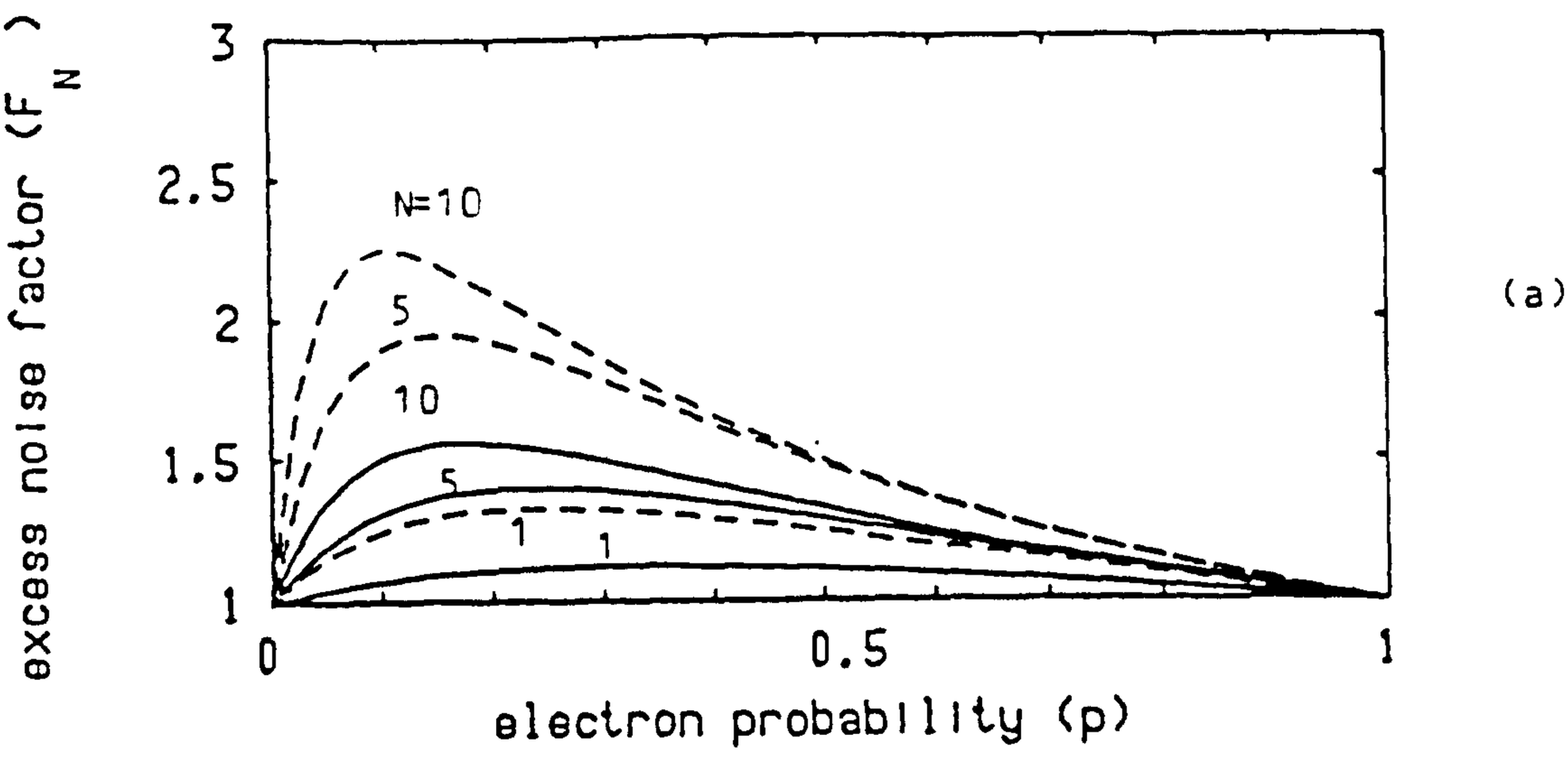

(a)

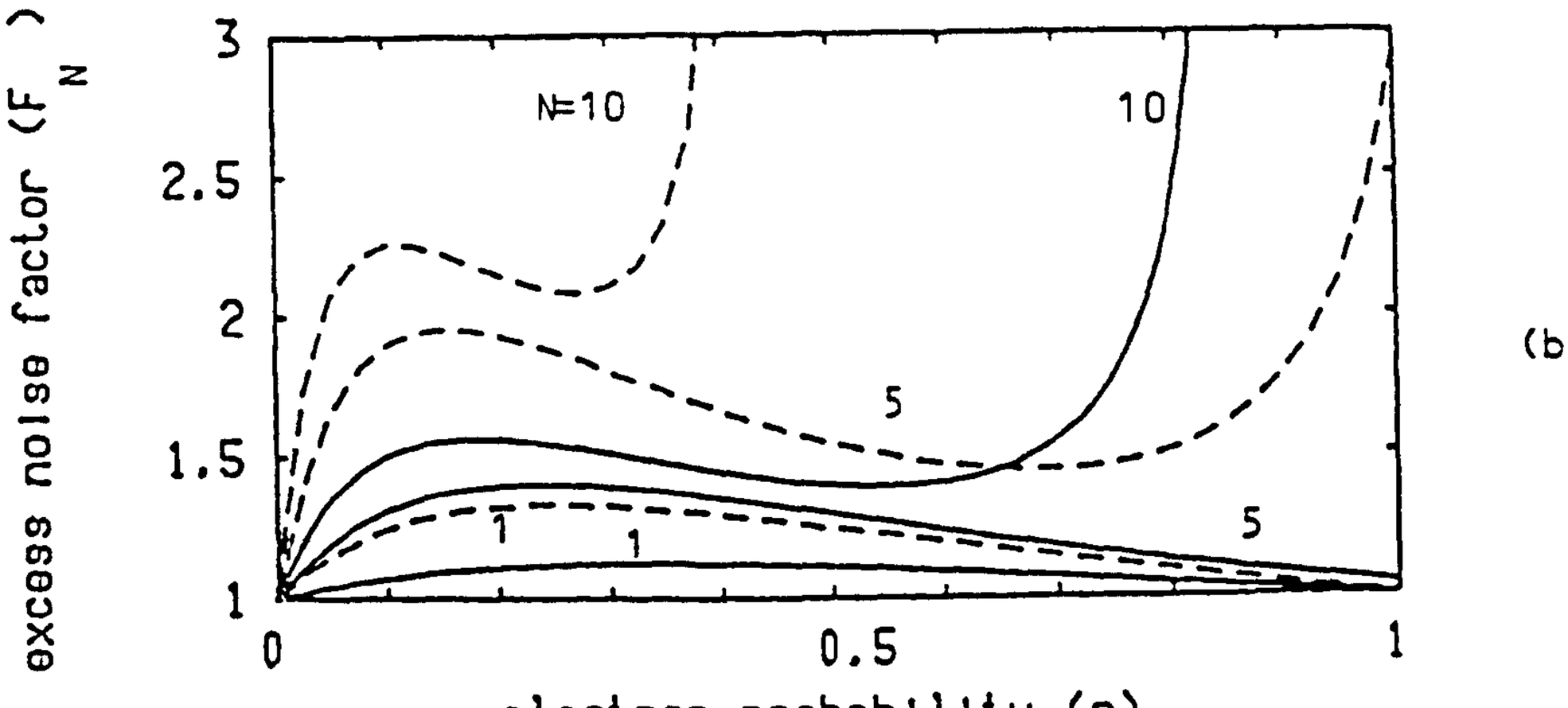

(b)

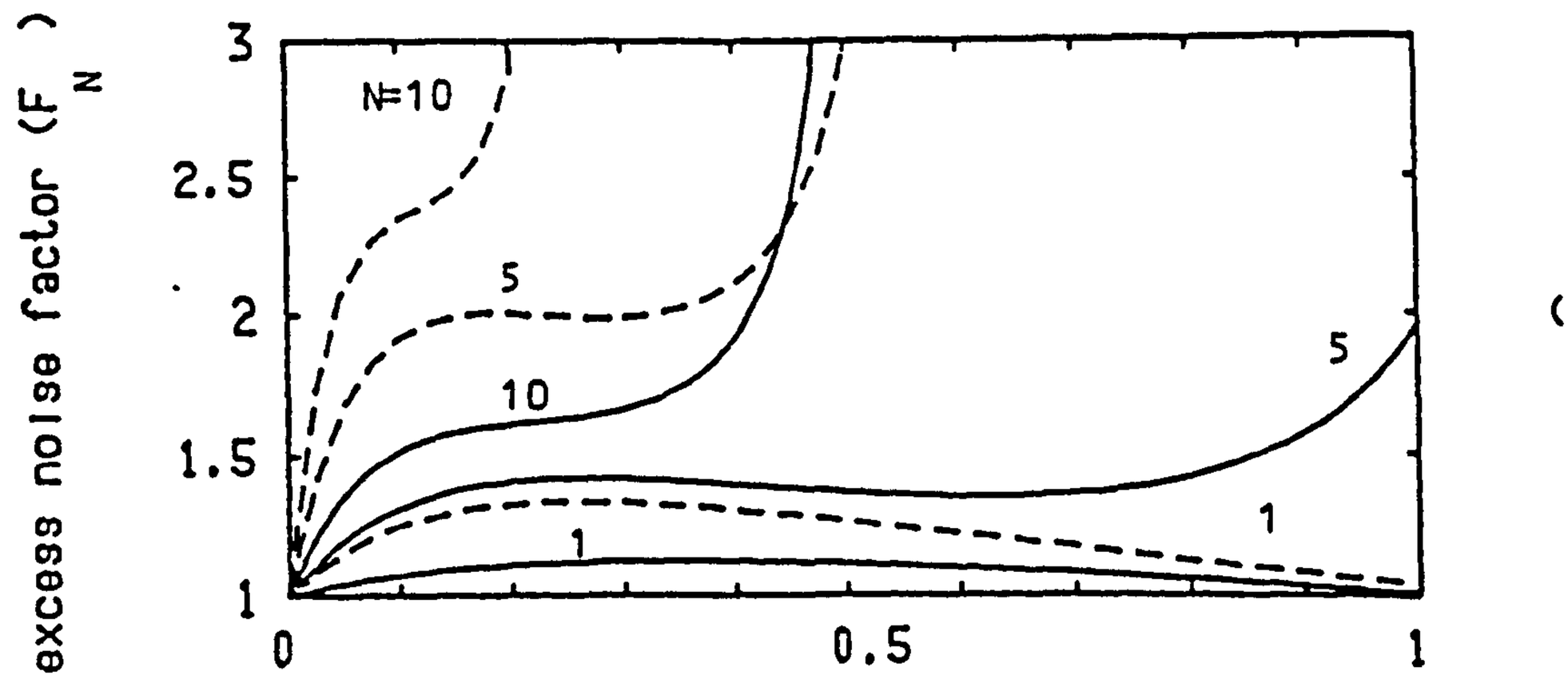

(c)

Fig. 5.2 Excess noise factor F_N versus electron ionisation probability p. (a) k=0.0 (b) k=0.001 (c) k=0.01

——— r=0 — — — r=∞

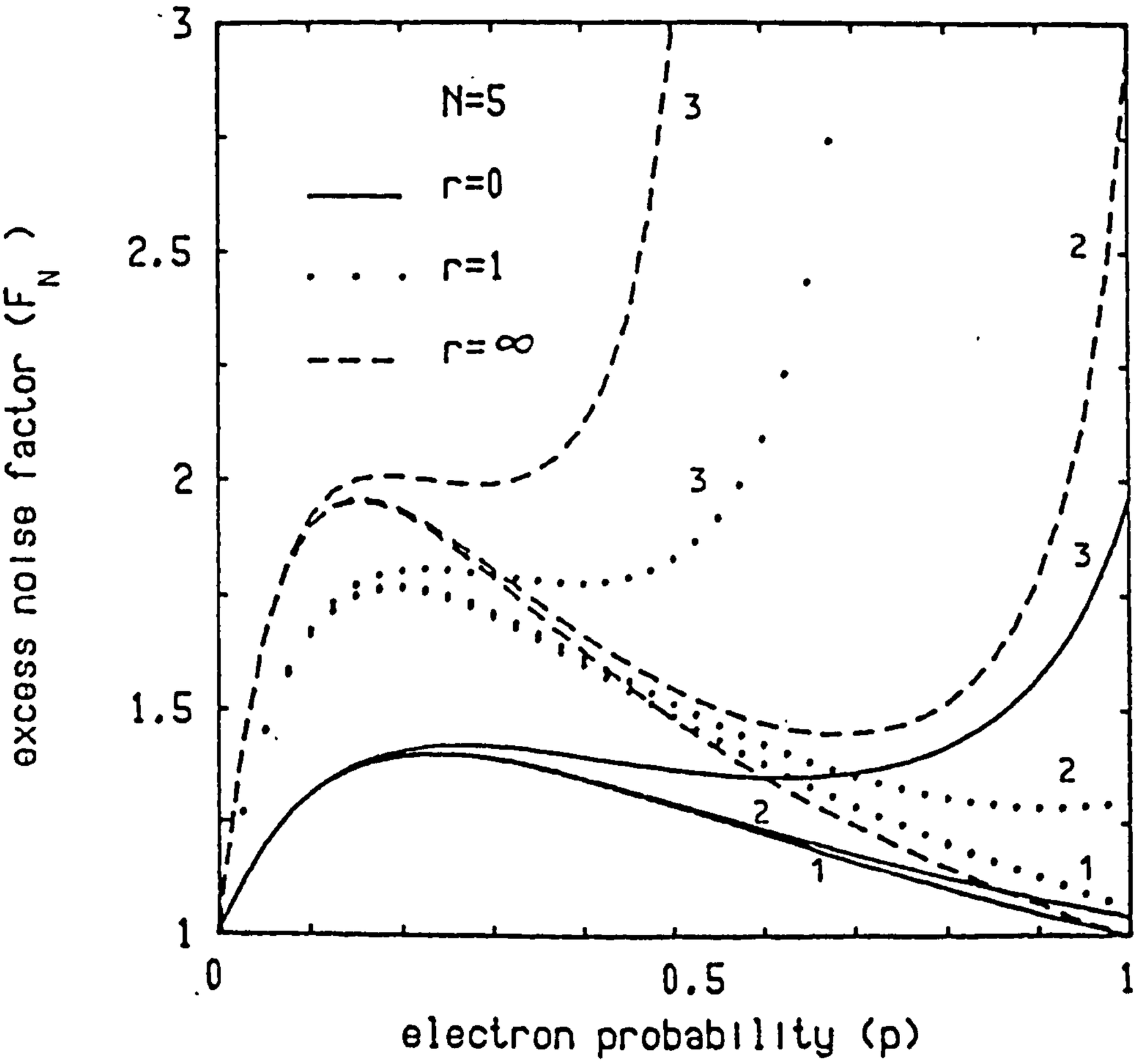

Fig. 5.3· Excess noise factor F_N of 5-stage SAPD as a function of electron ionisation probability p.
1: k=0.0 2: k=0.001 3: k=0.01

will occur at certain value of p equal to half that at r=0, assuming all other parameters are identical.

Fig. 5.4 shown F_N versus $<g_N>$ for a 5-stage APD, with k and r taken as parameters. Even higher gain can be achieved with larger value of r, but this will correspond to higher ratio of F_N to $<g_N>$. Thus, from the point of view of receiver sensitivity, it is better to design APDs operating at lower values of r if the required gain can be obtained in this case.

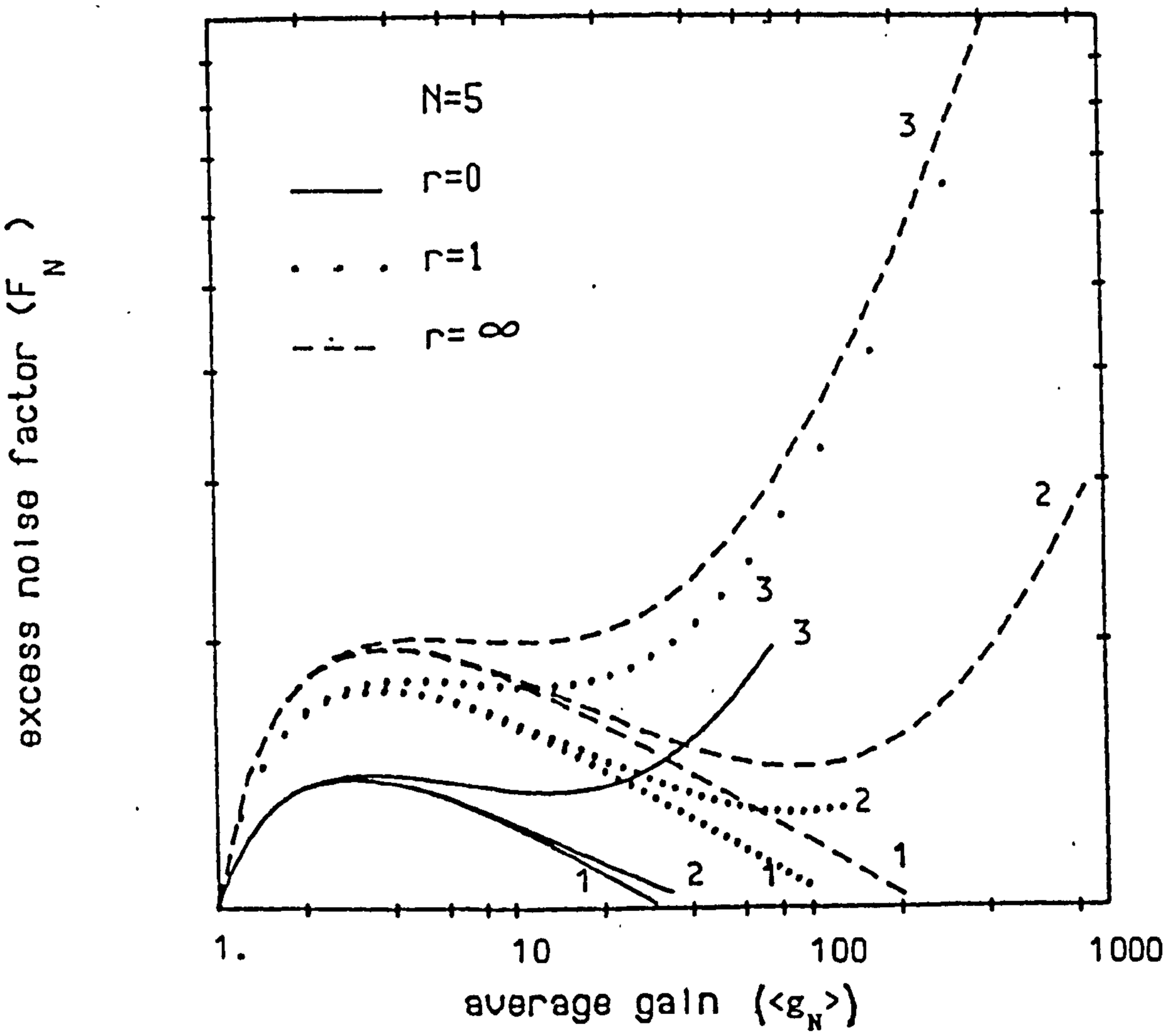

Fig. 5.4 Excess noise factor F_N against average gain $<g_N>$ for 5-stage SAPD 1: k=0.0 2: k=0.001 3: k=0.01

5.2 Effect of Dark Current

The multiplication noise associated with dark current can be analysed in a similar way to that described in Section 3.2. The effective gain g_{eff} and the effective excess noise factor F_{eff} associated with dark current generated in various stage can be expressed as

$$g_{eff} = \frac{\sum_{j=1}^{N} < g_j >}{N} \tag{5.7}$$

$$F_{eff} = \frac{\sum_{j=1}^{N} \langle g_j \rangle^2 F_j}{N.\, g_{eff}^2} \tag{5.8}$$

where we assume that the individual dark current components, generated in different stages, as statistically independent, and have the same mean value. Here $\langle g_j \rangle$ and F_j are the average gain and excess noise factor associated with an initiating hole-electron pair of position A(j). These are given by (see Appendices C and D).

$$\langle g_j \rangle = Q^{j-N} \langle g_N \rangle \tag{5.9}$$

$$F_j = Q^{N-k} F_N - \frac{2S(Q^{j-N}-1)}{Q(Q-1)} \tag{5.10}$$

Substituting eqn. 5.9 into eqn. 5.7, and eqn. 5.10 into eqn. 5.8 yields

$$g_{eff} = \frac{\langle g_N \rangle Q(1-Q^{-N})}{N(Q-1)} \tag{5.11}$$

$$F_{eff} = N \frac{(Q^2-1)\, Q^N F_N - 2S(Q^{N-1}-1)}{Q(Q+1)(Q^N-1)} \tag{5.12}$$

Eqns. 5.11 and 5.12 are displayed in Figs. 5.5 and 5.6, respectively. Curves correspond to $\langle g_N \rangle$ and F_N (solid lines) are also shown for comparison. The results indicate that, at fixed k, p and r the effective gain experienced by dark current, g_{eff}, is always less than that for photogenerated current, $\langle g_N \rangle$, while the effective excess noise factor F_{eff} higher than F_N, especially at higher values of p. An interesting point to be noted is that both g_{eff} and F_{eff} increase

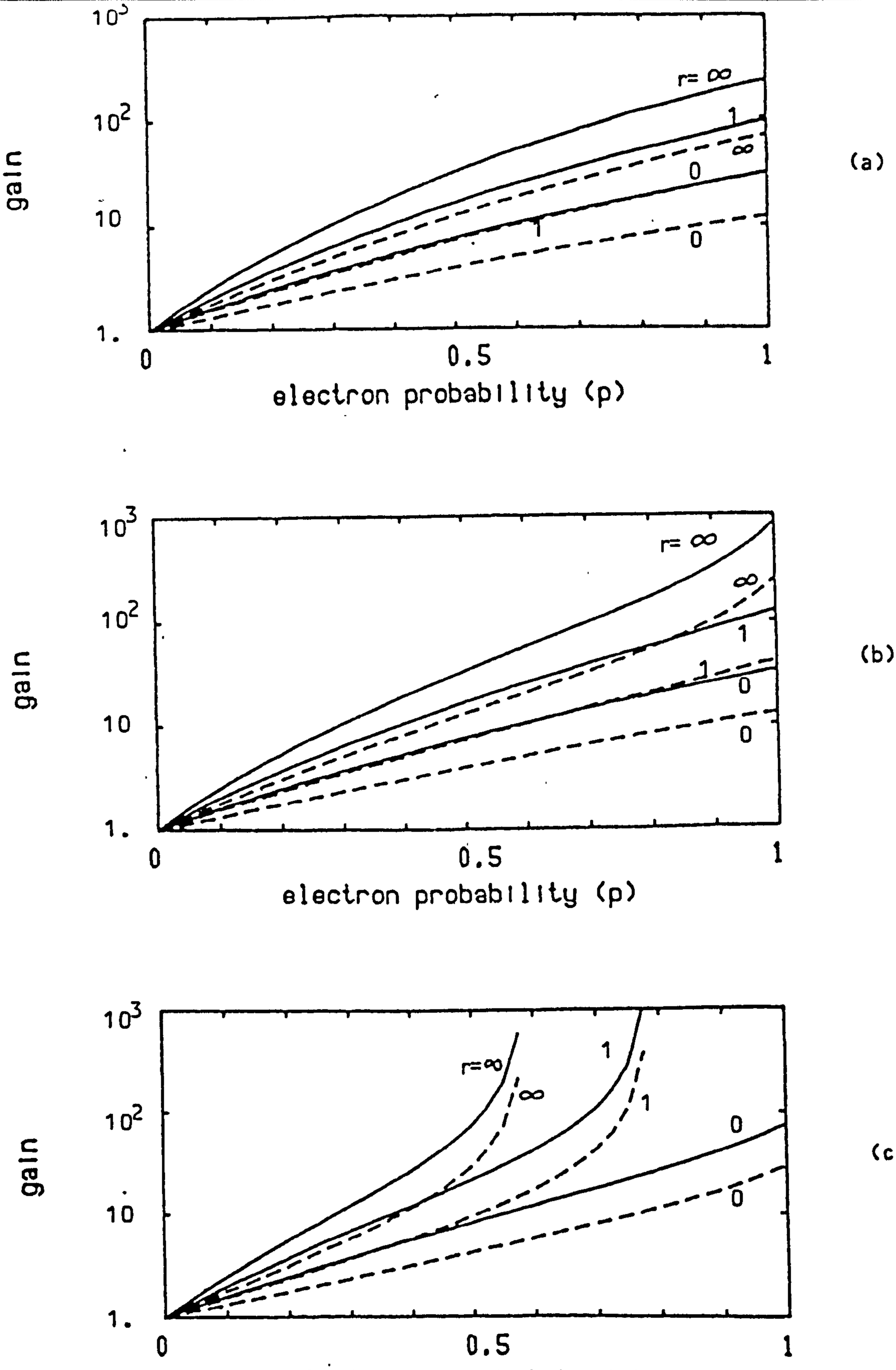

Fig. 5.5 Effective gain associated with dark current versus electron ionisation probability for 5-stage device.

(a) k=0.0 (b) k=0.001 (c) k=0.01

– – – g_{eff} ——— $\langle g_N \rangle$

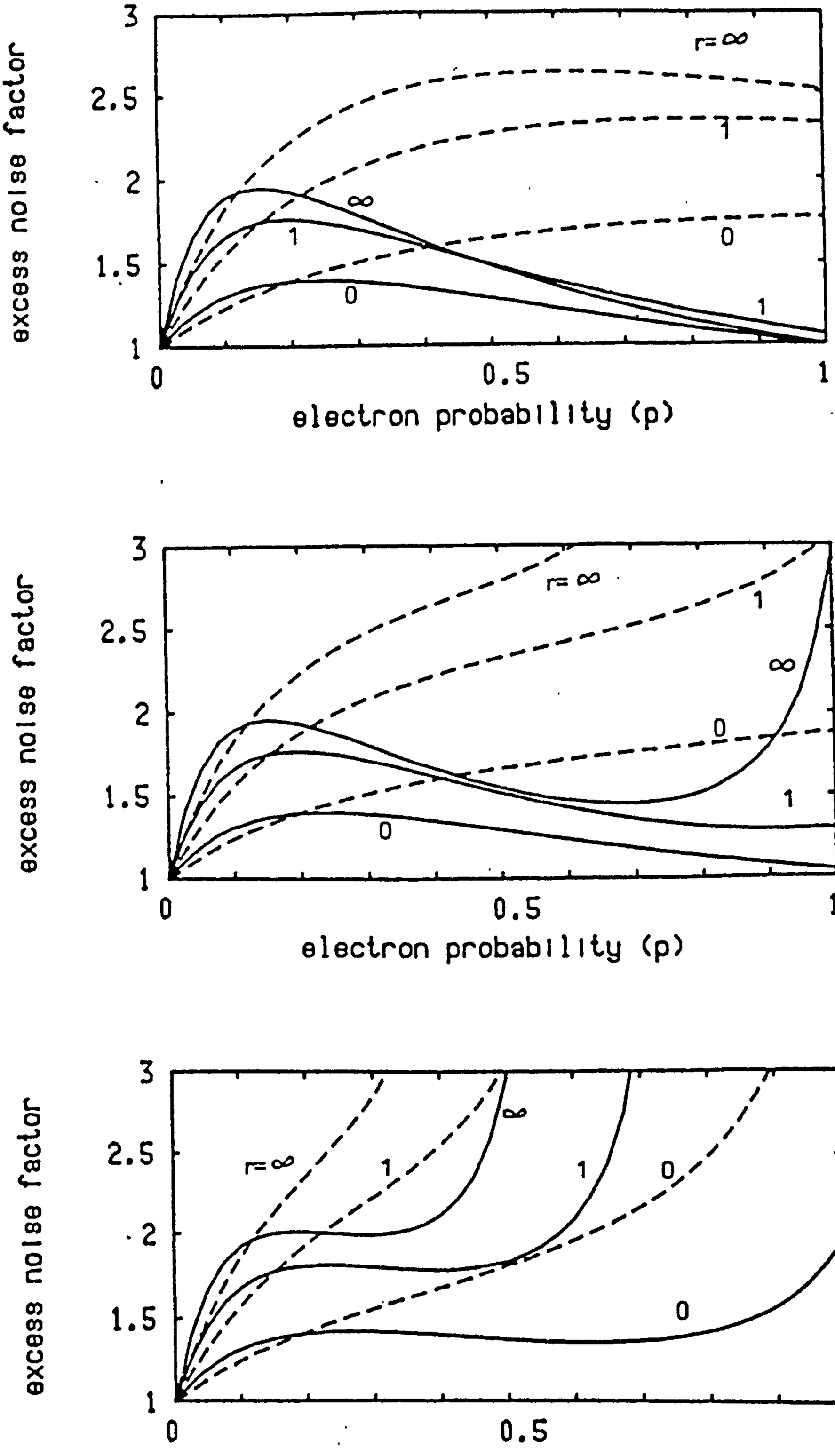

Fig. 5.6 Effective excess noise factor associated with dark current versus ionisation probability for 5-stage device.

(a) k=0.0 (b) k=0.001 (c) k=0.01

– – – F_{eff} ——— F_N

as a function of r, assuming all other parameters are fixed. This indicates that r=0 case is less affected by dark current compared with r>0 cases under the same conditions. Also both g_{eff} and F_{eff} are strongly affected by the residual hole ionisation and this effect increases with r.

5.3 Calculation of Receiver Sensitivity

It is clear that from the previous sections that higher values of r will affect the performance of SAPD in two different ways:

(i) Higher gain can be obtained which may lead to higher receiver sensitivity.

(ii) Higher excess noise factor will in general result and the performance of the APD is more affected by residual hole ionisation and background current. This may lead to sensitivity degradation.

Thus the receiver sensitivity will increase or decrease with r according to the net effect of both factors. In the following paragraphs we will discuss the influence of r on the performance of an optical receiver, taking into account both dark current and hole ionisation. The receiver sensitivity is estimated for bit error rate (BER) of 10^{-9} using Gaussian approximation [Personick, 1973].

Fig. 5.7 shows the sensitivity, $\eta\bar{P}$ of a 2 Gbit/s receiver as a function of p for two different values of N, N=5 (Fig. 5.7a) and N=10 (Fig. 5.7b), and assuming 22kΩ load resistance (R_L) and zero dark current. Other receiver parameters used in the calculations are given in Table 3.1. Note that at p=0 the sensitivity ($\cong$ -33dBm), is nearly independent on N, k and r since the receiver behaves like a PIN/FET receiver (i.e. $<g_N>=1$, $F_N=1$). Fig. 5.7a indicates that for k=0, the receiver sensitivity is an increasing function of r over all the range

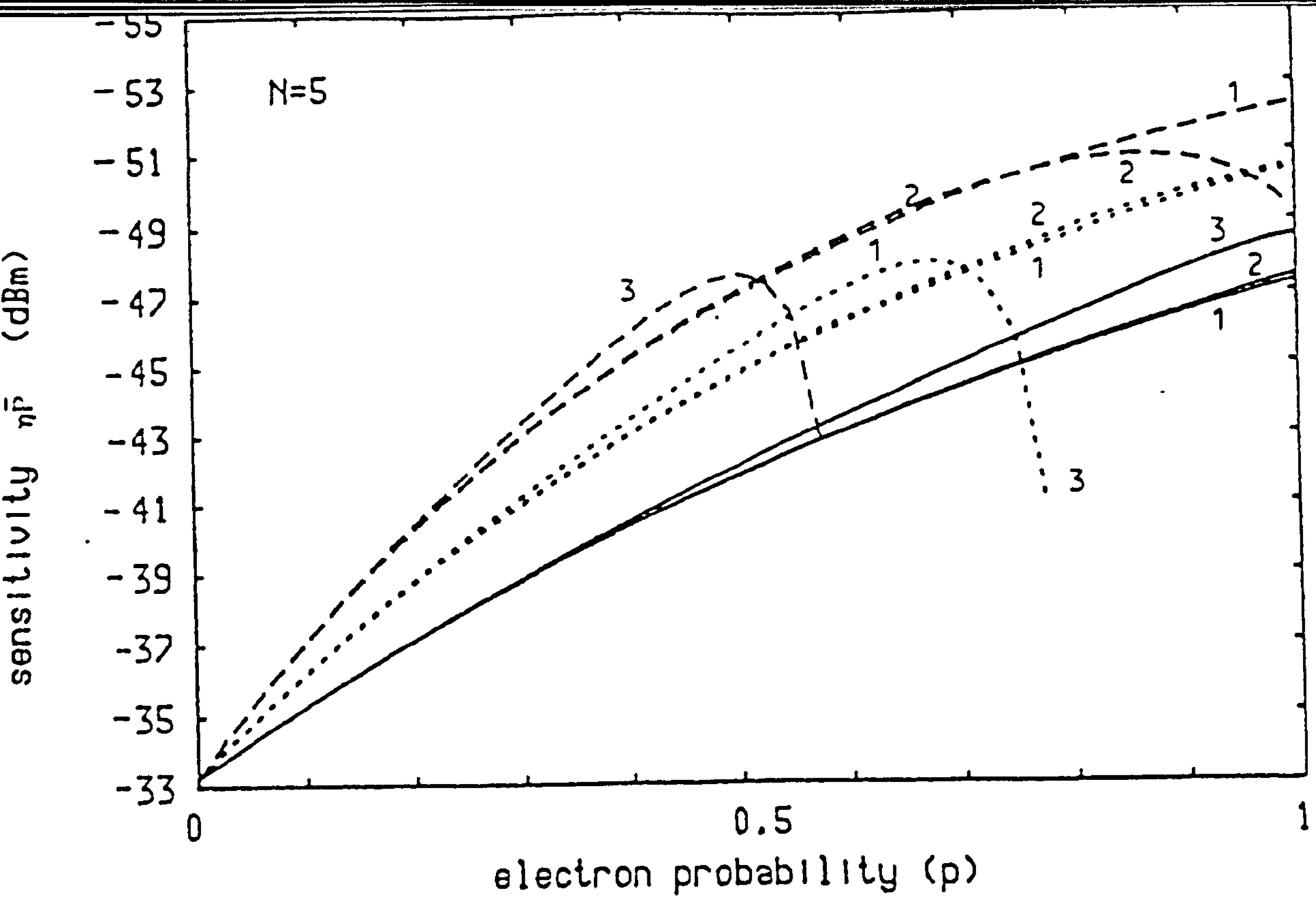

(a)

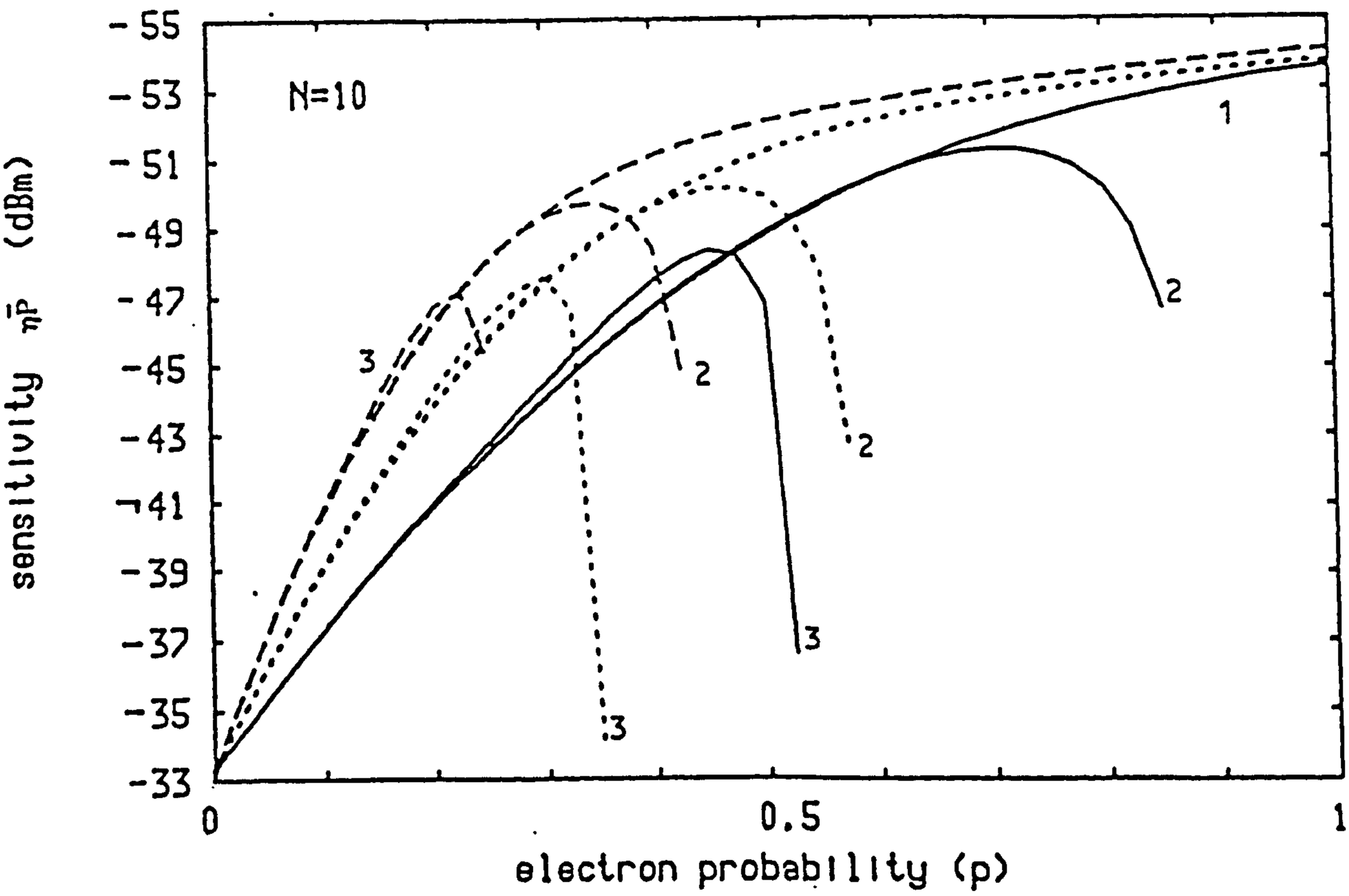

(b)

Fig. 5.7 Receiver sensitivity $\eta\bar{P}$ as a function of ionisation probability p. (a) N=5 (b) N=10

——— r=0 ····· r=1 — — — r=∞

1: k=0.0 2: k=0.001 3: k=0.01

of p, and also increases with p for fixed r. The existence of residual hole ionisation will lead to slightly increased sensitivity, at a given r, and the increment is higher for higher values of k, in the region prior to avalanche breakdown. As p increases near the breakdown region, a sharp reduction in the sensitivity occurs due to the greatly increased excess noise factor. Hence higher values of r will give better sensitivity, at fixed p and k, only when the device is operating away from the breakdown region. Note that for r=0 no breakdown occurs for the given values of k, and the device continues to give a better sensitivity with k over all values of p.

The 10-stage receiver is more significantly affected by residual hole ionisation (Fig. 5.7b), but it gives better sensitivity compared with the 5-stage device under the same conditions, once more assuming that the device is operating away from the breakdown region. Note that at k=0 the the increase in the sensitivity with r will be less at higher values of p. In fact $\eta\bar{P}$ is nearly the same for the three values of r given, when p approaches 1. This is due to the high gain achieved with N=10, p=1 which results in the sensitivity being determined mainly by the first term of eqn. 3.24. Also F_N is equal (or nearly equal) to 1 at p=1, k=0, for $0<r<\infty$. For the same reason, the increase in the sensitivity for $r=\infty$, is less than that for r=0, when N is varied from 5 to 10 at k=0.

The variation of the sensitivity of the 5-stage receiver with bit rate B is illustrated in Fig. 5.8 for two values of k, assuming p=0.8 and 50 nA dark current, assumed to be generated equal in the various stages. Curves for zero dark current are also shown for comparison (solid lines). An appropriate value of R_L is selected in accordance with $R_L.B=1M\Omega.MHz$ [Brain, 1982; Forrest, 1984]. Comparing the various

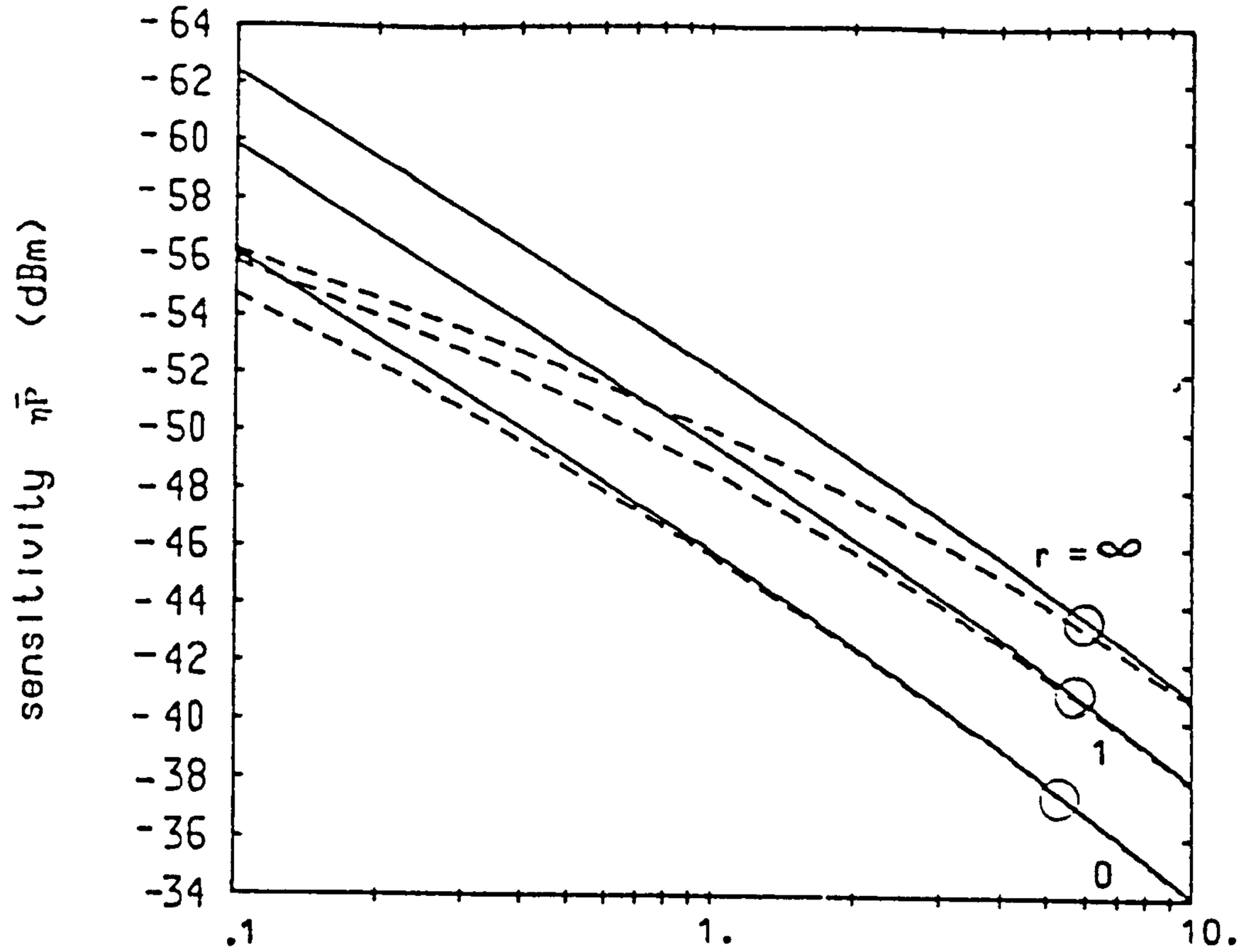

(a)

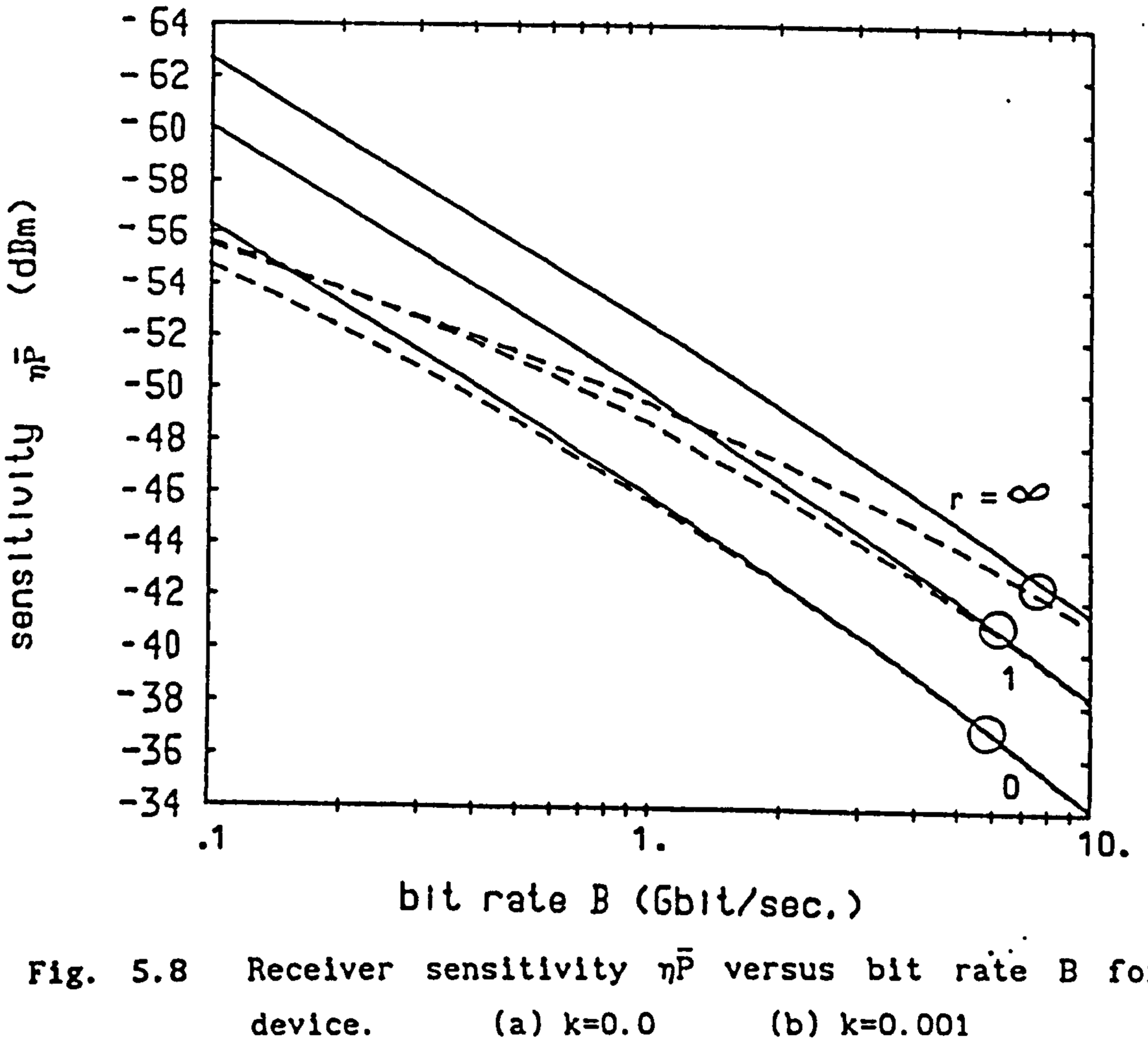

(b)

Fig. 5.8 Receiver sensitivity $\eta\bar{P}$ versus bit rate B for 5-stage device. (a) k=0.0 (b) k=0.001

——— $\langle I_d \rangle$=0 — — — $\langle I_d \rangle$=50nA

curves we conclude that the sensitivity of the high-r receiver is more affected by dark current, and this degradation in performance increases as k increases. Note that at $r=\infty$ the dark current affects the sensitivity over a wider range of bit rate than other values of r.

It is clear from Figs. 5.7a and 5.7b that in the presence of residual hole ionisation there is a well-defined optimum gain where the detected optical power required to achieve certain value of BER is minimum. To illustrate the variation of minimum detectable power required for BER=10^{-9} with k, we plot Figs. 5.9a and 5.9b for N=5 and N=10 respectively. Two values of dark current are considered, zero and 100nA, assumed to be generated equally in various stages. In these calcuations B=2Gbit/s, $R_L=22k\Omega$, and the gain of the APD is adjusted for each set of parameters to obtain the minimum detectable power (assuming k does not vary with p). It is clear from Fig. 5.9a that r=0, which represents a normal SAPD, still give the best performance provided k is greater than 0.0056 for zero dark current and greater than 0.0022 for 100nA dark current. Note also that low values of k, $r=\infty$ receivers are particularly strongly affected by dark current, reducing the benefits which can be gained from using multiple emission SAPDs. We also conclude from Fig. 5.9b that even at the very low value of $k\cong10^{-5}$, the r=0 case still gives the best sensitivity.

5.4 Summary

Superlattice avalanche photodioes in which an electron can cause up to two ionisations per stage, have investigated taking into account residual hole ionisation and dark current. Expressions for the average gain and excess noise factor associated with photogenerated and thermally generated carriers have been represnted, and used to

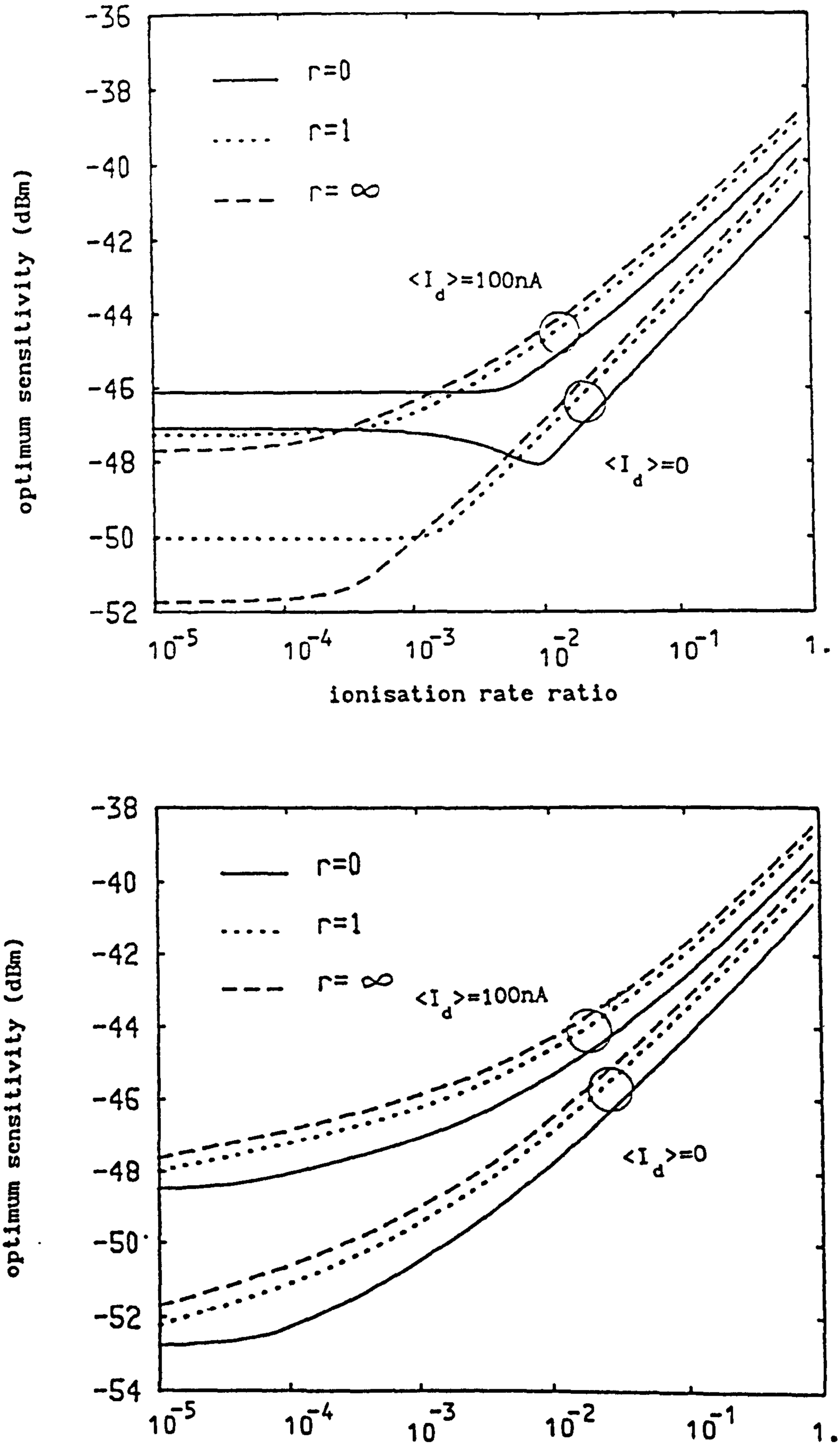

Fig. 5.9 Optimum sensitivity versus ionisation rate ratio k.
(a) N=5 (b) N=10

evaluate the performance of optical receivers employing these advanced APDs. The influence of multiple ionisation per carrier per stage can be summarised as follows:

(i) Higher gain APDs can be realised, or the same gain can be obtained with smaller number of stages leading to high bandwidth and low bias detectors. Unfortunately, there is also an increase in the excess noise factor.

(ii) Receiver performance is more affected by residual hole ionisation which leads to increase strongly both the gain and the excess noise factor of the APD. The maximum allowable value of p, which can be achieved without avalanche breakdown, is reduced in the presence of two ionisations ($r = \infty$).

(iii) Higher sensitivity is obtained for zero dark current and single carrier-type multiplication (no hole ionisation), but considerable degradation is experienced if these conditions do not apply.

In the next chapter we will extend the existing analysis of SAPDs beyond that of two ionisation per initiating carrier per stage.

CHAPTER 6

ANALYSIS OF NONIDEAL SOLID-STATE PHOTOMULTIPLIER (SSPM)

Recently new SAPD structures have been proposed in which multiple ionisations per initiating carrier per stage occur, thereby greatly enhancing the gain of the device. Brennan and Summers [1987a] have proposed new GaAs/GaAlAs multiquantum well APDs based on sequential resonant tunnelling through a variably-spaced superlattice energy filter. In this scheme, the electron distribution is selectively heated to produce up to four secondary carriers per stage. Moreover, Petroff et al. [1987] have demonstrated a new solid-state device capable of detection of individual photons via impurity-impact ionisation. They have reported a very high gain at 7K without residual hole ionisation.

From the previous discussion it is clear that it is necessary to extend the existing analyses of SAPDs beyond that of two ionisations per stage. This could be achieved by considering individual instances, in which the number of ionisations per stage is three, four, etc., but it is more useful if a general analysis can be obtained, applicable to a wide range of different schemes and encompassing specific devices. This is the subject of this chapter. In particular, the analysis of van Vliet et al. [1979a, 1979b] is extended to allow for multiple emission per initiating carrier per stage. General formulas are obtained to describe the average gain and the excess noise factor: these reduce to the previously published results for specific cases such as the photomultiplier tube, single ionisation and two ionisation SAPDs. We find that the noise

characteristics of a solid-state photomultiplier (SSPM) can be expressed using four parameters: the means and variances of both the hole and electron ionisation rate per stage, and these may in principle be determined experimentally from measurement of the average and the variance of the gain for both pure hole and pure electron injection currents. Furthermore, general expressions are obtained for the effective gain and effective excess noise factor associated with dark current generated in the different stages. This facilitates a study of the influence of both dark current and residual hole ionisation on the performance of optical receivers employing SSPMs. The results indicate that when hole ionisation exists the gain per stage must be limited to a low value to prevent avalanche breakdown and to attain optimum sensitivity.

6.1 General Model of SSPM

We consider a reverse-biased p-i-n diode with intrinsic layer fully depleted by the external electric field. Let the depletion region consist of N identical stages, as shown in Fig. 6.1. As a convenient and appropriate approximation we model the situation as follows:

An electron traversing any stage from left to right will encounter essentially two regions: region *a* in which the electron gains sufficient energy to cause a series of impact ionisations, these taking place in the next region, *b*. We assume there is no possibility of the injected electron producing ionisation at region *a*. (For example, this region may be made from wide-bandgap material). Let us assume further that the secondary electrons do not undergo any impact ionisation in the same stage as that in which they are generated.

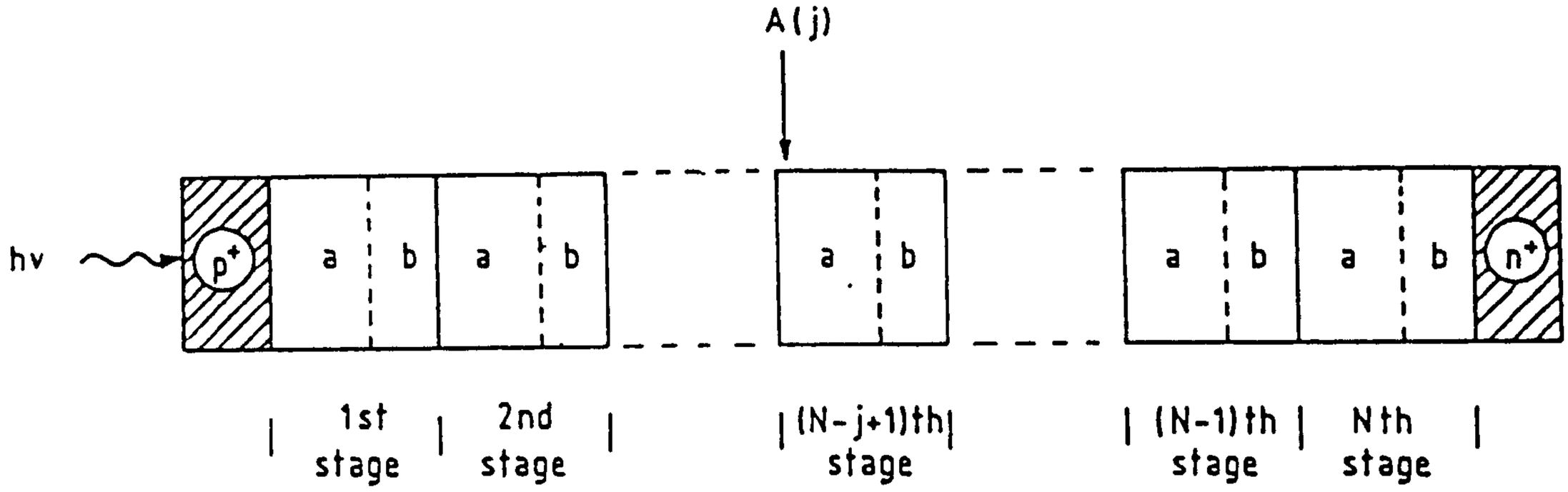

Fig. 6.1 Schematic diagram of a solid-state photomultiplier.

This assumption is entirely appropriate when the net electric field in region *a* is low enough for the secondary electrons to be unable to attain the required ionisation threshold energy from the field therein. For the sake of generality, similar assumptions are made for the holes entering the stage from the right. Here the holes will pass through two regions per stage (not shown in Fig. 6.1). For low-noise operation, the energy gained by the hole from the first region must be kept to a minimum, and other regions could be added to cool the hole distribution, as in doped quantum well APDs. It is worth noting here that the above assumptions are usually met in the various superlattice APD structures proposed by various workers, except that the number of ionisations per initiating carrier per stage has to date generally been limited to one.

Let

g_j = total number of hole-electron pairs generated due to a hole-electron pair initiated at position A(j), including the

original pair.

w_e = number of ionisations per stage caused by a single electron entering the stage from the left.

w_h = number of ionisations per stage caused by a hole entering the stage from the right.

Here g_j, w_e and w_h are random variables with probability generating functions $\phi_j(z)$, $\phi_e(z)$ and $\phi_h(z)$, respectively.

Under these circumstances and following the explanation given in [van Vliet et al., 1979b], we can show that g_j may be decomposed into the original pair plus the first-generation subtrees, which occur at the (N-j+1)th, (N-j+2)th, ..., Nth stage due to electron-triggered events and at (N-j)th, (N-j-1)th, ..., 1st stage due to hole triggered events. Hence we have

$$g_j = 1 + \sum_{i=1}^{j} y_{j-i} + \sum_{i=1}^{N-j} y_{j+i} \qquad (6.1)$$

where the symbol y is used to denote the subtrees. Here the random variable $y_{j-i}(i>0)$ corresponds to the gain process g_{j-i} driven by the random variable w_e. These have probability generating function $\phi_{j-i}(z)$, $\phi_e(z)$, respectively and hence from the theory of compound randomness [Cattermole, 1984] the probability generating function for y_{j-i} is given by $\phi_e(\phi_{j-i}(z))$. In a similar way the probability generating function of y_{j+i} $(i>0)$ is given by $\phi_h(\phi_{j+i}(z))$. Thus from eqn. 6.1 we have:

$$\phi_j(z) = z \prod_{i=1}^{j} \phi_e(\phi_{j-i}(z)). \prod_{i=1}^{N-j} \phi_h(\phi_{j+i}(z)). \qquad (6.2)$$

where the $\phi_e(z)$ and $\phi_h(z)$ are assumed to be identical for the various stages. Extension for nonidentical stages is also possible but will not be considered here explicitly. Eqn. 6.2 provides the key formula for the derivation of gain and noise properties of these devices.

6.2 Gain and Noise Characteristics for SSPM

In this section the gain and noise characteristics of the SSPM are evaluated using discrete ionisation models. The treatment which follows is based on the assumption that the detector and receiver integrating time is sufficiently long for the entire current pulse to be captured as a charge impulse. The analysis thus provides a white noise model

6.2.1 Average Gain

For pure hole injection, corresponding to the light being absorbed in the n^+ region, j=0 and eqn. 6.2 reduces to

$$\phi_0(z) = z \prod_{i=1}^{N} \phi_h(\phi_i(z)) \tag{6.3}$$

Also, for pure electron injection j=N and

$$\phi_N(z) = z \prod_{i=1}^{N} \phi_e(\phi_{N-i}(z)) \tag{6.4}$$

Now, eqn. 6.2 can be expressed in terms of the following recurrence relation:

$$\phi_j(z).\ \phi_e(\phi_j(z)) = \phi_{j+1}(z).\ \phi_h(\phi_{j+1}(z)) \tag{6.5}$$

Differentiating eqn. 6.5 with respect to z and evaluating the result at z=1 yields

$$\phi_j' \ [1+\phi_e'] \ = \ \phi_{j+1}'[1+\phi_h' \ ] \tag{6.6}$$

where ϕ_j' , ϕ_e' , and ϕ_h' denote the first derivative with respect to z of ϕ_j, ϕ_e, and ϕ_h, respectively evaluated at z=1. Starting with j=0 we find that

$$\phi_j' \ = \ Q^j \phi_0' \tag{6.7}$$

$$\phi_N' \ = \ Q^N \phi_0' \tag{6.8}$$

where

$$Q = \frac{1+\phi_e'}{1+\phi_h'} \ = \ \frac{1+<w_e>}{1+<w_h>} \tag{6.9}$$

since the first derivative of the probability generating function at z=1 corresponds to the mean value. Differentiating eqn. 6.3 with respect to z and setting z=1 we get

$$\phi_0' \ = \ 1+\phi_h' \sum_{i=1}^{N} \phi_i' \tag{6.10}$$

Substituting from eqn. 6.7, ϕ_0' can be expressed as

$$\phi_0' \equiv <M_h> \ = \ \frac{1}{1-\phi_h' \sum_{i=1}^{N} Q^i}$$

$$= \frac{(Q-1)}{(Q-1) - \phi_h' Q(Q^N-1)} \qquad (6.11)$$

where $M_h \equiv g_0$ is the gain for pure hole injection. Substituting eqn. 6.10 into eqn. 6.8 yields

$$\phi_N' \equiv \langle M_e \rangle = \frac{Q^N(Q-1)}{(Q-1) - \phi_h' Q(Q^N-1)} \qquad (6.12)$$

where $M_e \equiv g_N$ is the gain for pure electron injection. In general, the average gain associated with a hole-electron pair injected at position A(j) is given by

$$\langle g_j \rangle = Q^{j-N} \langle M_e \rangle \qquad (6.13)$$

which will be used later to evaluate the effective gain associated with dark current. The above equations indicate that the average gain of these devices is determined by the first order statistics of the ionisation process, $\langle w_e \rangle$ and $\langle w_h \rangle$.

At this point it is convenient to define the ionisation rate ratio k as

$$k \equiv \phi_h' / \phi_e' = \langle w_h \rangle / \langle w_e \rangle \qquad (6.14)$$

Hence for k = 1 (very high noise device), eqn. 6.13 reduces to

$$\langle g_j \rangle = \langle M_e \rangle = 1/[1 - N\phi_e'] \qquad (6.15)$$

which is independent of the position A(j) of the injected pair.

It is clear from the previous analysis that to avoid the occurrence of avalanche breakdown in these devices (i.e. to keep the average gain a positive finite number) the following conditions must be satisfied

$$\begin{aligned} Q(Q^N-1)\phi'_h &< (Q-1) && \text{for } k < 1 \\ Q(Q^N-1)\phi'_h &> (Q-1) && \text{for } k > 1 \\ \phi'_e = \phi'_h &< 1/N && \text{for } k = 1 \end{aligned} \qquad (6.16)$$

Again, this condition is independent of position of injection A(j). For k = 1 the above conditions indicate that for stable operation the average number of total ionising collisions per traversal of the primary carrier through the whole depletion region must be less than one, a condition similar to that for conventional APDs [Stillman and Wolfe, 1977).

6.2.2 Noise Characteristics

The excess noise factor associated with pure electron injection is given by

$$F_e \equiv F_N = 1 + \frac{Var(M_e)}{<M_e>^2} \qquad (6.17)$$

where Var(.) denotes the variance, related to the probability generating function by [Cattermole, 1984].

$$Var(M_e) = \phi''_N - \phi'^2_N + \phi'_N \qquad (6.18)$$

where ϕ''_N is the second derivative with respect to z of $\phi_N(z)$ evaluated at z = 1. From eqns. 6.17 and 6.18 we have

$$F_e = \frac{\phi''_N}{<M_e>^2} + \frac{1}{<M_e>} \tag{6.19}$$

The derivation of an expression for ϕ''_N is rather long and accordingly it is given in Appendix E. Using eqn. E9 from Appendix E with eqn. 6.12, F_e can be expressed as

$$F_e = \frac{2\phi'_h\,(Q^N-1)}{(Q-1)Q^{N-1}} + \frac{\phi'^2_h\,(Q^N-1)^2}{(Q-1)^2 Q^{2N-2}} <M_e>$$

$$+ \left[\frac{2\phi'_h\, S}{(Q-1)} + Q(\phi''_h - \phi'^2_h) \right]$$

$$x \frac{(Q^{2N}-1)}{(Q^2-1)Q^{2N-1}} <M_e> - \frac{2\phi'_h S(Q^N-1)}{(Q-1)^2 Q^{2N}}$$

$$x <M_e> + \frac{2S(Q^N-1)}{(Q-1)Q^{N+1}} + \frac{1}{<M_e>} \tag{6.20}$$

where

$$S = \frac{2\phi'_e + \phi''_e - Q(2\phi'_h + \phi''_h)}{2(1+\phi'_h)} \tag{6.21}$$

Again, ϕ''_e and ϕ''_h are the second derivatives with respect to z of $\phi_e(z)$ and $\phi_h(z)$, respectively, evaluated at z = 1 and given by

$$\phi''_e = <w_e^2> - <w_e> \tag{6.22a}$$

$$\phi''_h = \langle w_h^2 \rangle - \langle w_h \rangle \qquad (6.22b)$$

In general, the excess noise factor associated with a hole-electron pair initiated at position A(j) is given by (see Appendix E).

$$F_j = Q^{N-j} F_e - \frac{2S}{Q(Q-1)} [Q^{N-j} - 1] \qquad (6.23)$$

It is interesting to examine eqn. 6.23 for the special case of k = 1.

$$F_j = F_e - (N - j) \frac{(\phi''_e - \phi''_h)}{1 + \phi'_e} \qquad (6.24a)$$

where F_e is given by

$$F_e = \frac{1 - N\phi'^2_e}{1 - N\phi'_e} + N\left[\frac{\phi''_e - \phi''_h}{2(1+\phi'_e)}\right] \times \left[\frac{2 - N\phi'_e}{1 - N\phi'_e}\right] + \frac{N\phi''_h}{1 - N\phi'_e} \qquad (6.24b)$$

Eqn. 6.24a indicates clearly that for k = 1 the excess noise factor is still dependent on the position A(j) where the primary pair is initiated. Here, F_j will increase or decrease linearly with j depending on the values of both ϕ''_e and ϕ''_h. If these two parameters are equal then $F_j = F_e$ for all values of j. This occurs in a single-ionisation APD where $\phi''_e = \phi''_h = 0$. Note that for conventional APDs, it is usually assumed that the excess noise factor is independent of the position of injection for the case of unit ionisation rate ratio.

We may now make the following observations:

(i) The gain and noise characteristics of photomultiplier tubes

are usually expressed using the average and the variance of the random gains for the different stages (or the random gain per stage in the case of identical stages). For a SSPM it is difficult to define a gain per stage due to the feedback effect which arises from residual hole ionisation. We have found here that it is more appropriate to define two random gains per stage δ_e for injected electrons (assuming no residual hole ionisation) and δ_h for injected holes (assuming no electron ionisation). The probability generating functions of these gains are given by $z\phi_e(z)$ and $z\phi_h(z)$, respectively. It can then be shown that

$$<\delta_e> = 1+\phi_e' = 1+<w_e> \qquad (6.25a)$$

$$\text{Var}\ (\delta_e) = \phi_e'' - \phi_e'^2 + \phi_e' \qquad (6.25b)$$

Similar expressions may be written for $<\delta_h>$ and Var (δ_h). These expressions can be used to express the average gain and excess noise factor of a SSPM in terms of the new parameters $<\delta_e>$, $<\delta_h>$, Var(δ_e), and Var(δ_h). This is useful for comparison with the photomultiplier tube.

(ii) It is clear from the previous analysis that four parameters are required to determine the noise characteristics of a SSPM: ϕ_e', ϕ_e'', ϕ_h' and ϕ_h''. This is different from conventional APDs or single ionisation-superlattice APDs, where the excess noise factor can be determined using two parameters only (i.e. the average rates of hole and electron ionisation per unit length or per stage). These latter parameters can be determined experimentally either from the average gains for pure hole injection $<M_e>$ [Stillman and Wolfe, 1977; Capasso

et al., 1983] or from noise measurements of $Var(M_h)$ and $Var(M_o)$ [Yu et al., 1987]. The four parameters arising in our SSPM analysis can in principle be determined from measurements of the quantities $<M_h>$, $<M_o>$, $Var(M_h)$, and $Var(M_o)$. This is demonstrated in Appendix F for reference purposes.

6.2.3 Special Cases

It is interesting to examine the new general expressions obtained here for the average gain and excess noise factor in relation to special cases for which results have been previously reported.

(i) When there is no hole ionisation (i.e. $\phi_h' = \phi_h'' = 0$), eqns. 6.12 and 6.20 reduce to

$$<M_o> = (1 + \phi_o')^N \tag{6.26}$$

$$F_o = \frac{(\phi_o'' + 2\phi_o')[(1+\phi_o')^N - 1]}{\phi_o' (1+\phi_o')^{N+1}} + \frac{1}{(1+\phi_o')^N}$$

$$= \frac{Var(\delta_o)}{1 + <\delta_o>(<\delta_o> - 1)} \left[1 - \frac{1}{<\delta_o>^N}\right] \tag{6.27}$$

where $<\delta_o>$ and $Var(\delta_o)$ are related to ϕ_o' and ϕ_o'' through eqns. 6.25. Eqns. 6.26 and 6.27 are identical to those given in the literature for an N identical stages photomultiplier tube with random gain δ_o per stage (Teich et al., 1986a].

(ii) For single ionisation SAPDs, $\phi_o(z) = 1 - p_1 + p_1 z$ and $\phi_h(z) = 1 - u_1 + u_1 z$, where p_1 (u_1) is the probability for electron (hole) ionisation in a single stage. If we use these expressions in eqns. 6.12 and 6.20, we recover the same results reported previously for these APDs (eqns. 2.1 and 2.2). It is appropriate to note here also

that van Vliet et al. [1979b] have shown that in the limit of $N \to \infty$ and $p_1, u_1 \to 0$, McIntyre's results for conventional APDs can be recovered.

(iii) For two-ionisation SAPDs $\phi_o(z) = 1 - p_1 - p_2 + p_1 z + p_2 z^2$, where p_1, p_2 represent the probability per stage for an electron to impact one or two ionisation per stage, respectively. Similar expressions can be written for $\phi_h(z)$. Making these substitutions in eqn. 6.12 and 6.20, we recover our previous results reported in Chapter 5.

6.3 Influence of Dark Current

The influence of dark current can be taken into account using the same approach discussed in section 3.2. It can be shown [Fyath and O'Reilly, 1988h] that the expressions for the effective gain and effective excess noise factor associated with dark current generated equally in various stages are identical to those reported in Section 5.2 (eqns. 5.11 and 5.12). Here Q and S are defined in eqns. 6.9 and 6.21, respectively. Thus eqns. 5.11 and 5.12 represent general expressions; they reduce to those identified previously for special cases if the appropriate expressions for Q and S are used.

For the limiting case of k=1, we have

$$g_{eff} = \langle M_o \rangle \tag{6.28}$$

$$F_{eff} = F_o - \frac{(N-1)\,(\phi''_o - \phi''_h)}{2(1+\phi'_o)} \tag{6.29}$$

Thus, for $N > 1$, $F_{eff} = F_e$ only when $\phi''_o = \phi''_h$, as expected.

6.4 Diode Performance

A photomultiplier tube is frequently analysed under the

assumption that due to high gain associated with these devices the variance of δ, the random gain of a single stage, is given by [Engstrom, 1980; Teich et al., 1986a].

$$\mathrm{Var}(\delta) = <\delta> + <\delta>^2/D \tag{6.30}$$

D is a constant which if set to ∞ results in $\mathrm{Var}(\delta)=<\delta>$ corresponding to a Poisson distribution for the gain δ. It has been found that the above formula is not appropriate for SSPMs, principally for two reasons:

(i) The proposed realisation schemes for SSPM are limited to a small number of ionisations per initiating carrier per stage.

(ii) The above equation does not predict zero variance for the case where there is no impact ionisation ($\delta=1$).

In the following, we circumvent these difficulties, for the purpose of illustration, by considering

$$\mathrm{Var}(\delta_e) = A_e[<\delta_e> - 1] \tag{6.31a}$$

$$\mathrm{Var}(\delta_h) = A_h[<\delta_h> - 1] \tag{6.31b}$$

where A_e and A_h are arbitrary positive constants. When $<\delta_e> >> 1$ and assuming $A_e = 1$, eqn. 6.31a is consistent with a Poisson distribution for δ_e. With the aid of both parts of eqn. 6.25, eqns. 6.31a and 6.31b can be written in the following form:

$$\phi_e'' = (A_e-1)\phi_e' + \phi_e'^2 \tag{6.32a}$$

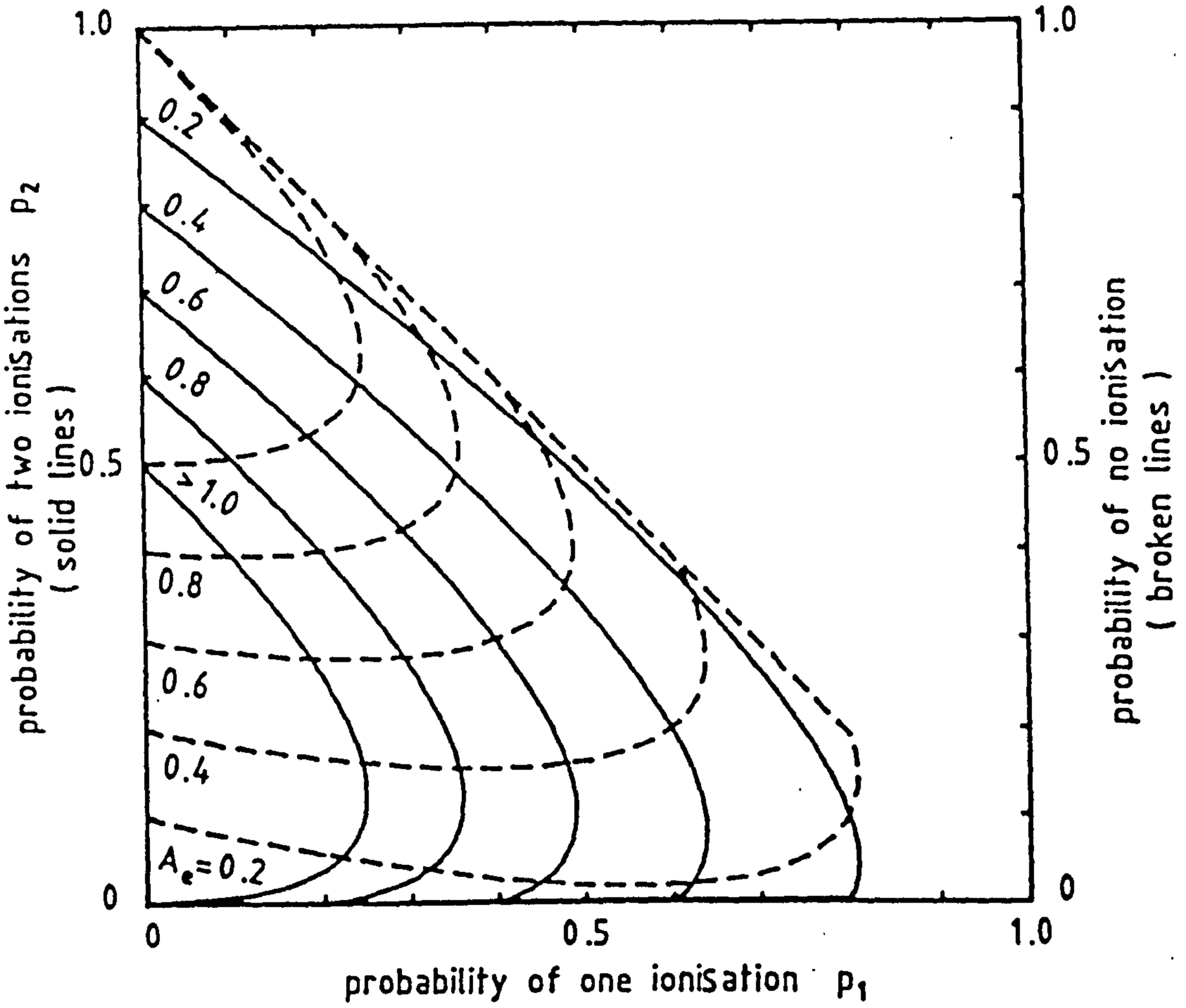

Fig. 6.2 Graph illustrating conditions under which eqn. 6.31a can be satisfied for two-ionisation SAPDs.

——— relation between p_1 and p_2

– – – probability of no ionisation $(1-p_1-p_2)$

$$\phi''_h = (A_h-1)\phi'_h+\phi'^2_h \qquad (6.32b)$$

It has been found that both parts of eqn. 6.31 (or 6.32) can be satisfied in SSPM when the initiating carrier is able to impact two or more ionisations per stage. Fig. 6.2 shows the relation between p_1 and p_2 required to satisfy the above formulas in two-ionisation APDs, taking A_e as a parameter, and Fig. 6.3 presents the same relation for three-ionisation APDs taking A_e and p_3 as parameters. Note that p_i represents the probability for an electron to cause i ionisations per stage.

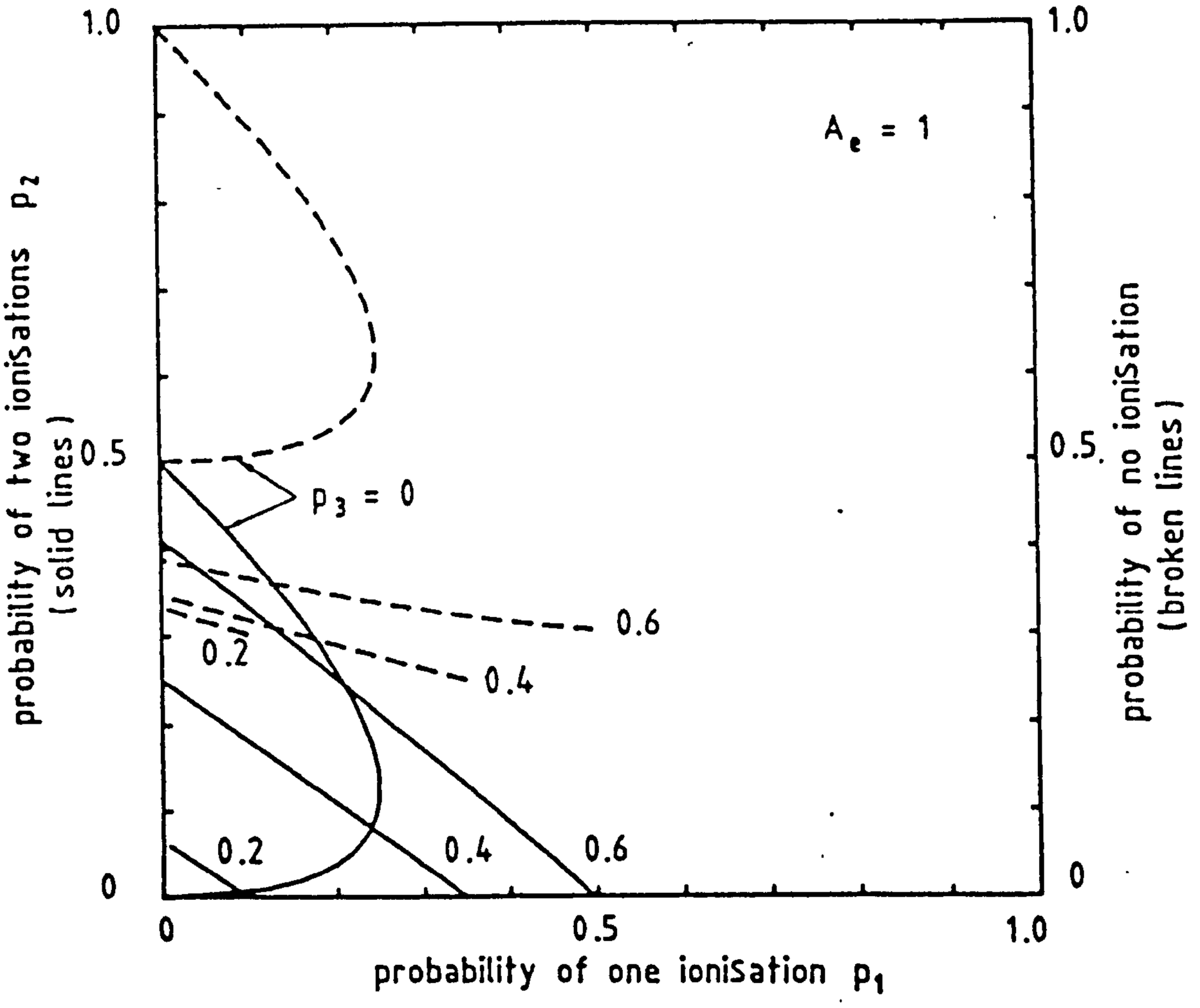

Fig. 6.3 Graph illustrating conditions under which eqn. 31a is satisfied in three-ionisation SAPDs assuming A_e=1.

——— relation between p_1 and p_2

— — — probability of no ionisation $(1-p_1-p_2-p_3)$

Fig. 6.4 shows the maximum value of $<\delta_e>$ which can be used without causing avalanche breakdown. The calculation is based on eqn. 6.16. It is clear that as the ionisation rate ratio k increases, lower values of $<\delta_e>$ must be used to preserve stable operation, and this value is a decreasing function of the number of stages for a given k. Thus, there seems to be little point in designing multiple ionisation SSPMs unless the hole ionisation is reduced to extremely low values, especially when the number of stages is large.

The average gain $<g_N> \equiv <M_e>$ and the effective gain g_{eff} experienced by dark current generated equally in various stages are

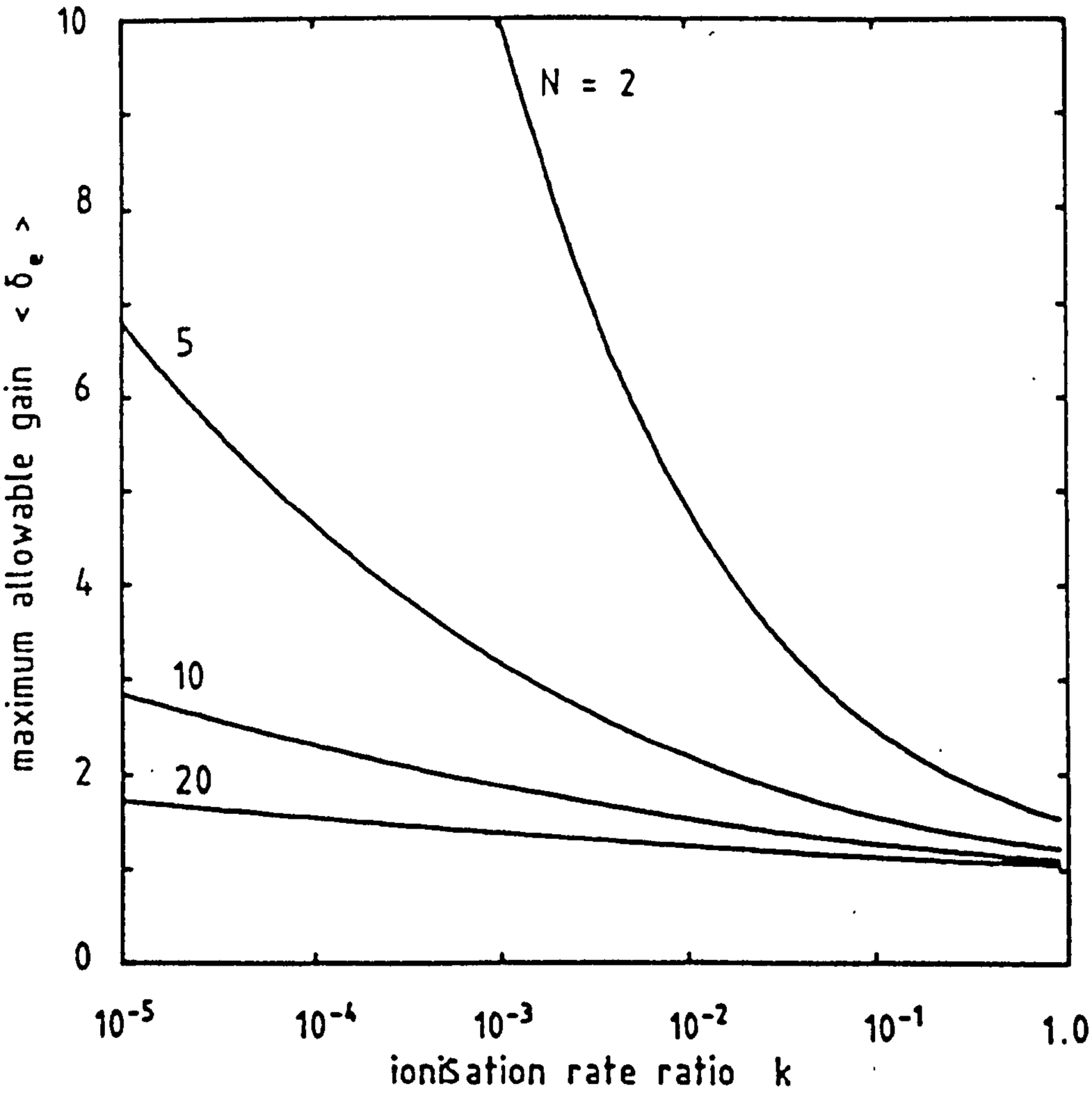

Fig. 6.4 Maximum allowable gain per stage $\langle\delta_e\rangle$ required to prevent avalanche breakdown as a function of ionisation rate ratio k.

displayed in Fig. 6.5. Note that g_{eff} is usually less than $\langle M_e \rangle$ and both of them increase with N, all other parameters being equal. It is clear that the existence of even slight residual hole ionisation results in substantial increase in the average gain and this effect becomes more pronounced as N increases. A similar conclusion can be drawn from Fig. 6.6 for $A_e = A_h$, except that F_{eff} for dark current is generally higher than $F_e \equiv F_N$ for pure electron injection. A comparison between F_e and F_{eff} is also provided by Fig. 6.7, shown as a function of the device gain $\langle M_e \rangle$. This indicates that a higher excess noise factor is associated with dark current except for low gain values.

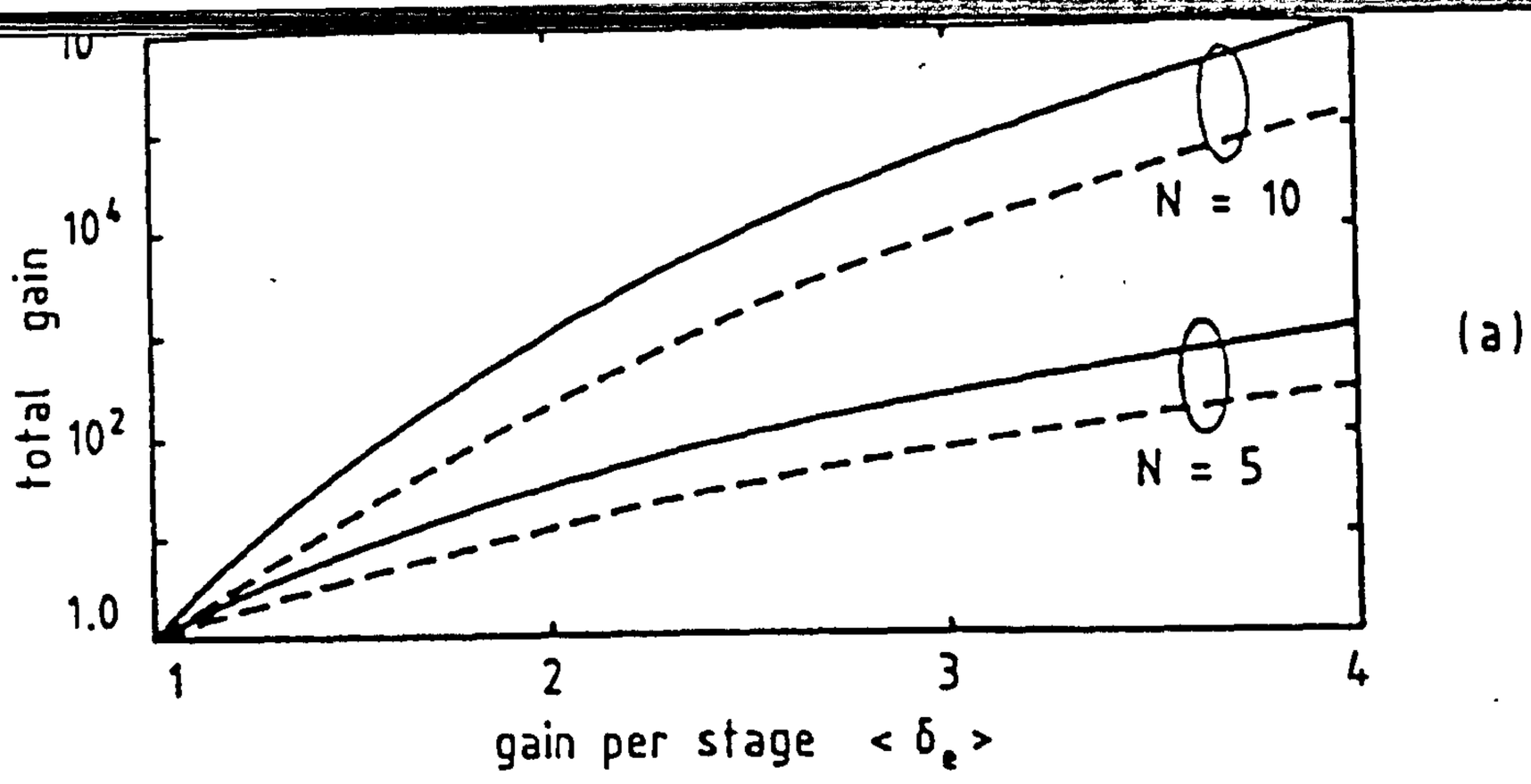

Fig. 6.5 Effect of residual hole ionisation on gain characteristics of SSPM. (a) k=0.0 (b) k=0.001 (c) k=0.01

——— $\langle M_e \rangle$ - - - g_{eff}

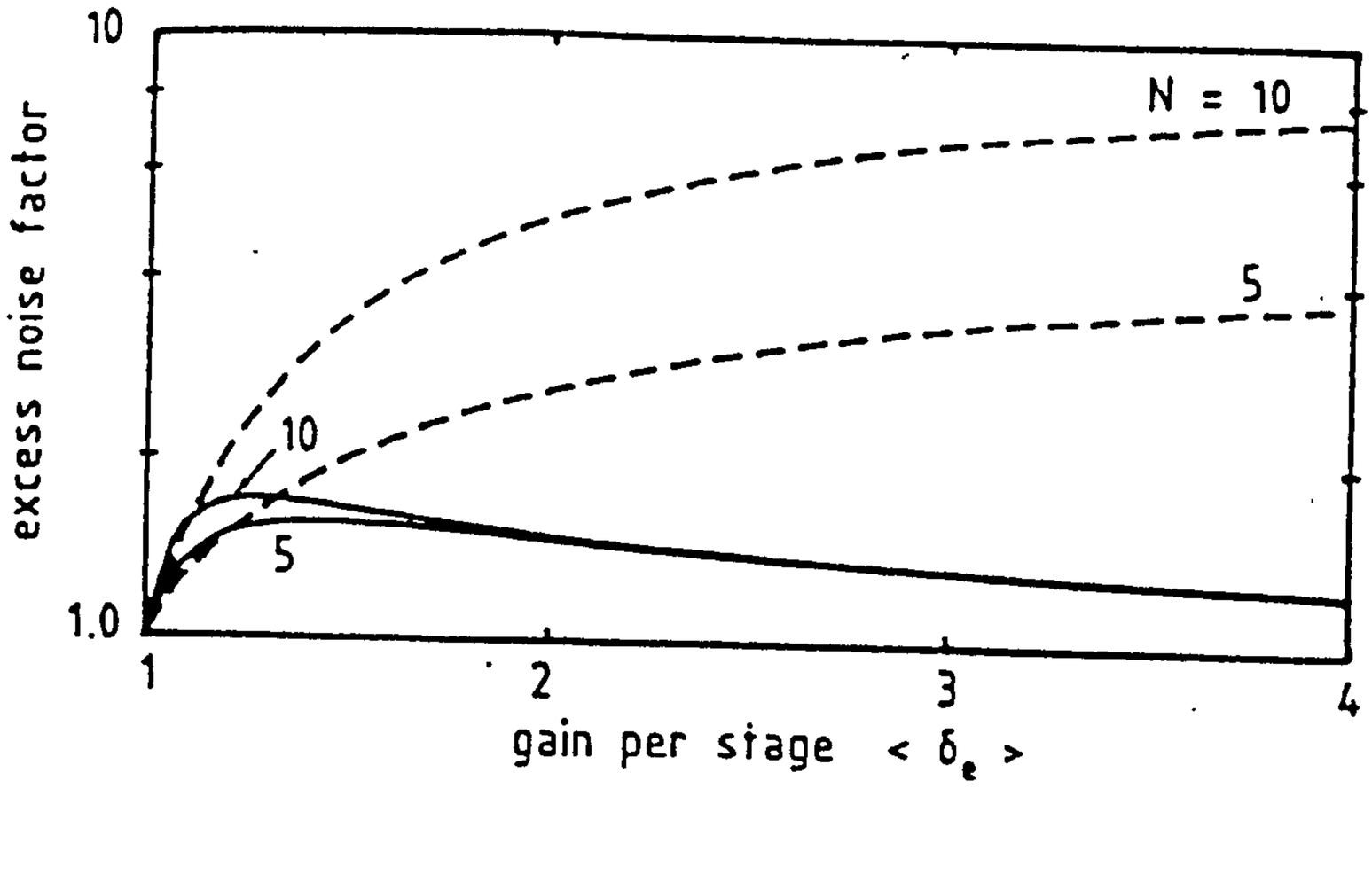

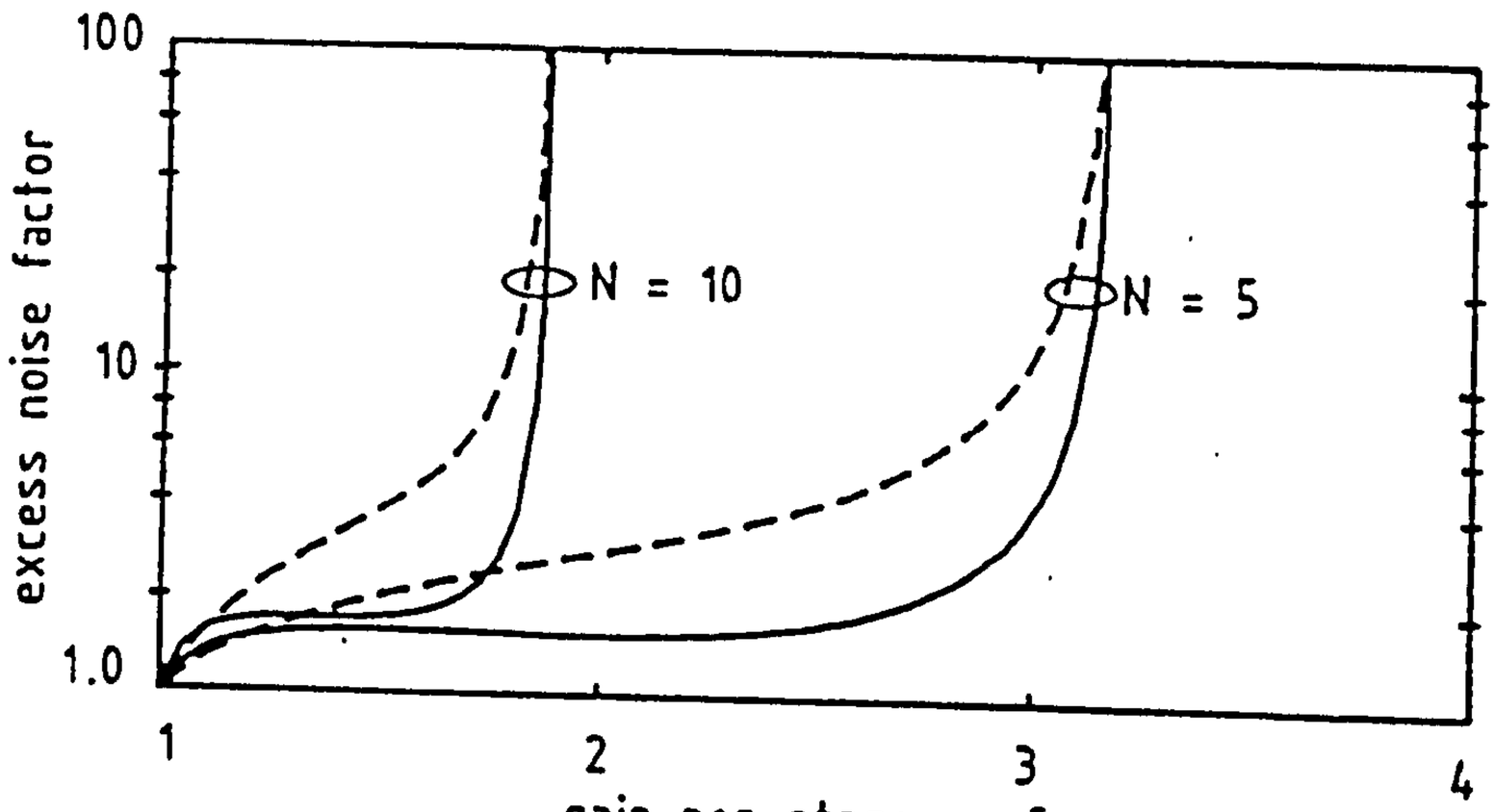

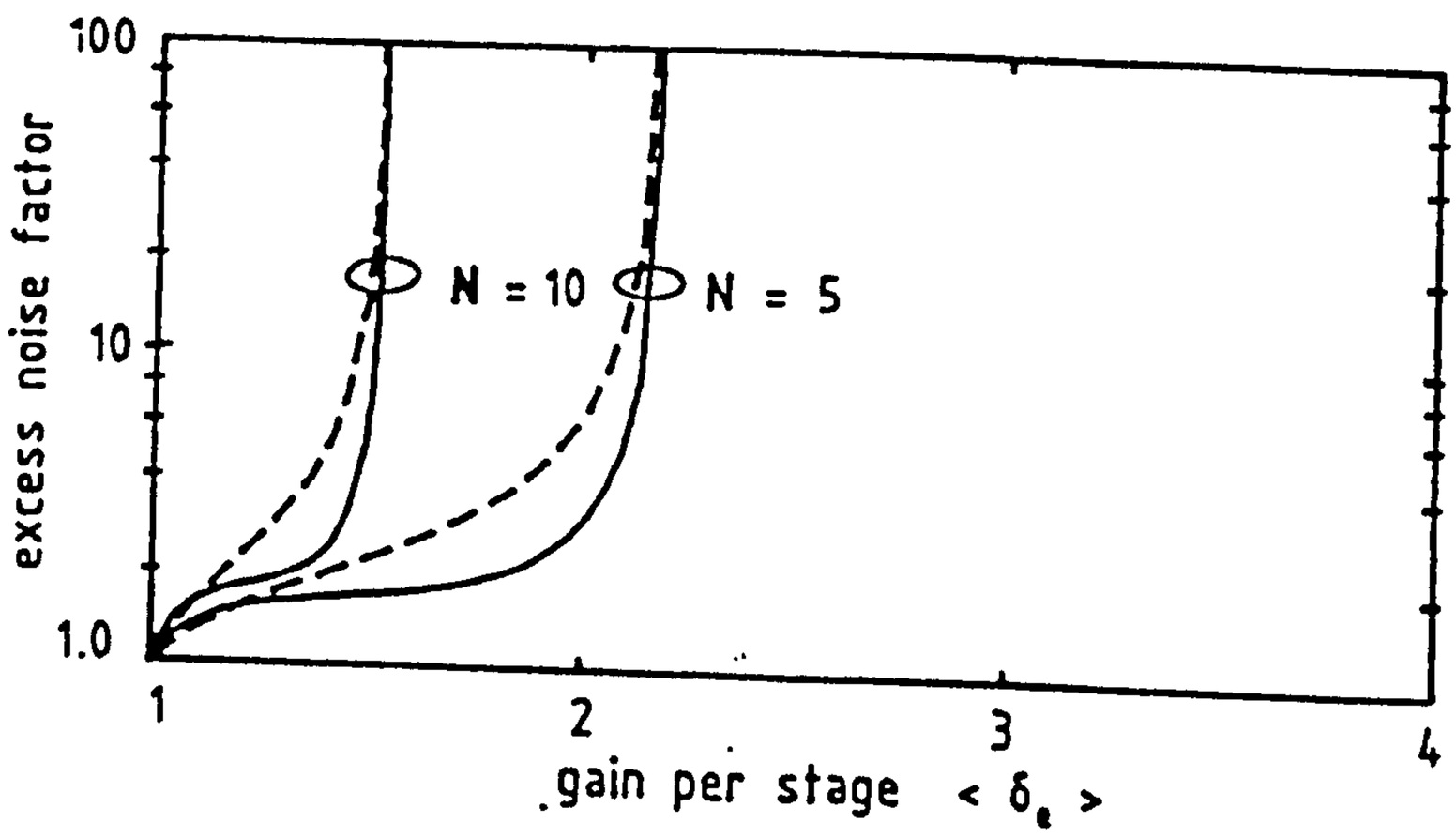

Fig. 6.6 Effect of residual hole ionisation on excess noise factor of SSPM with $A_e = A_h = 1$. (a) k=0.0 (b) k=0.01 (c) k=0.01

——— F_e — — — F_{eff}

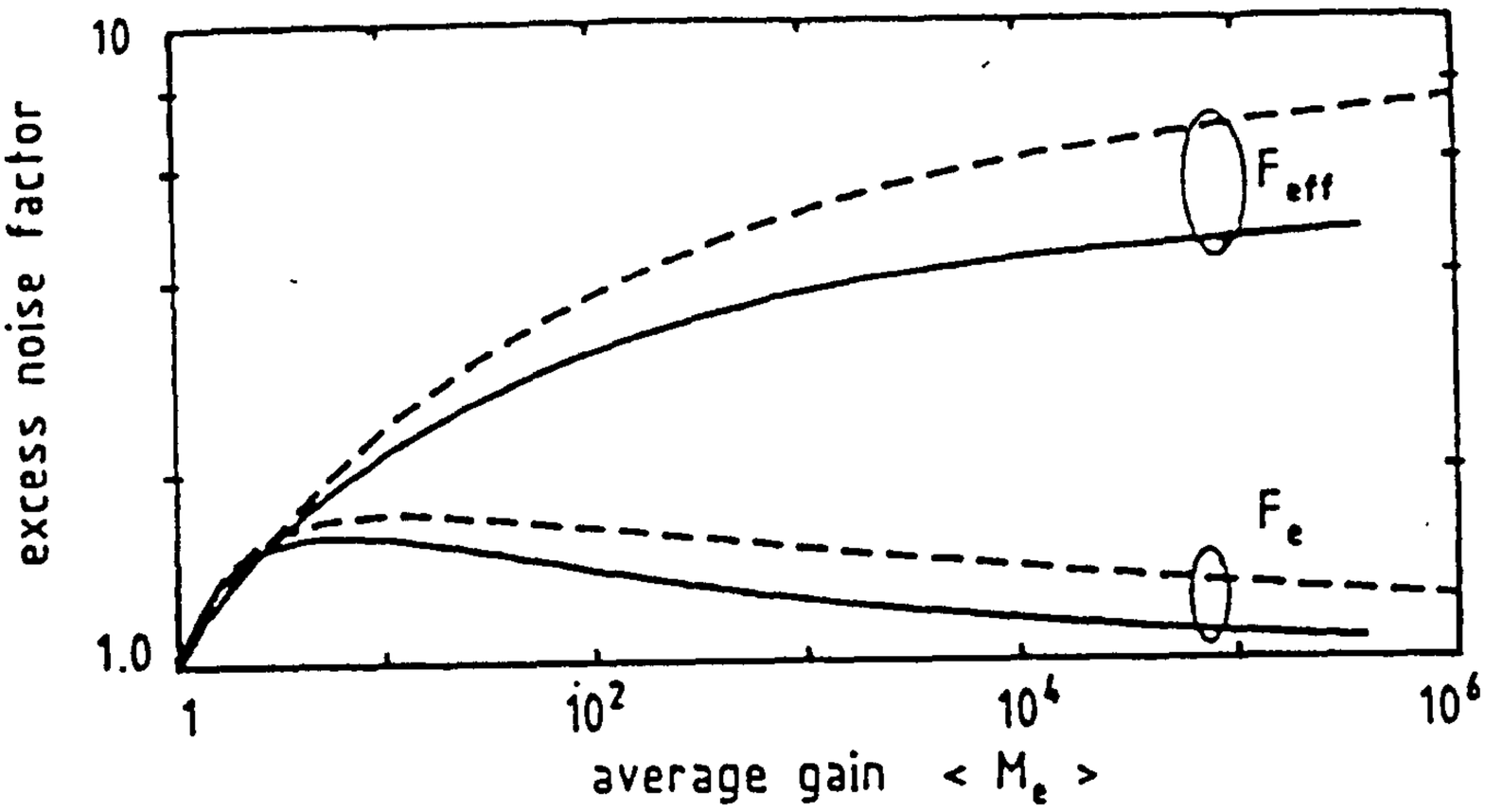

(a)

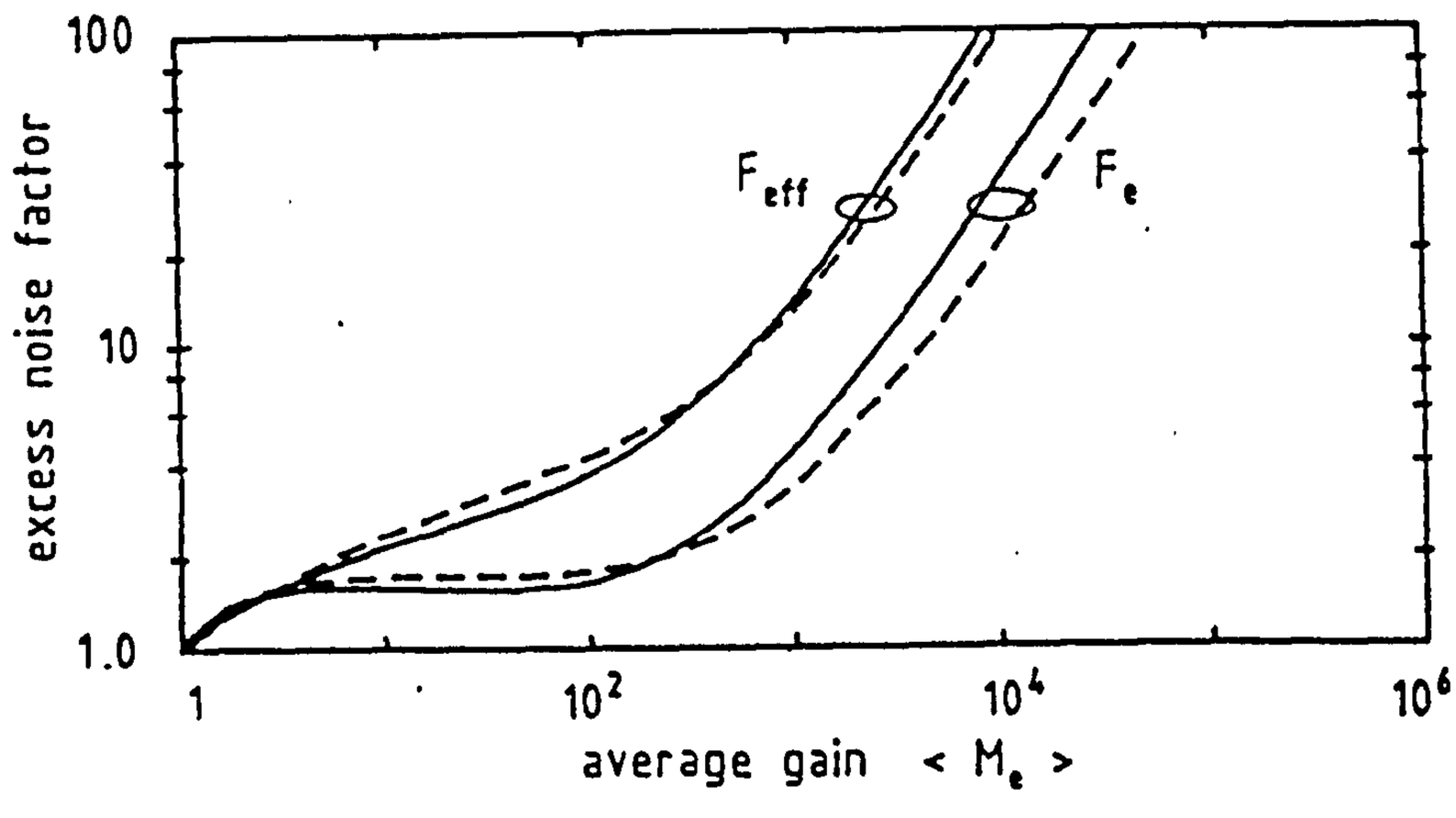

(b)

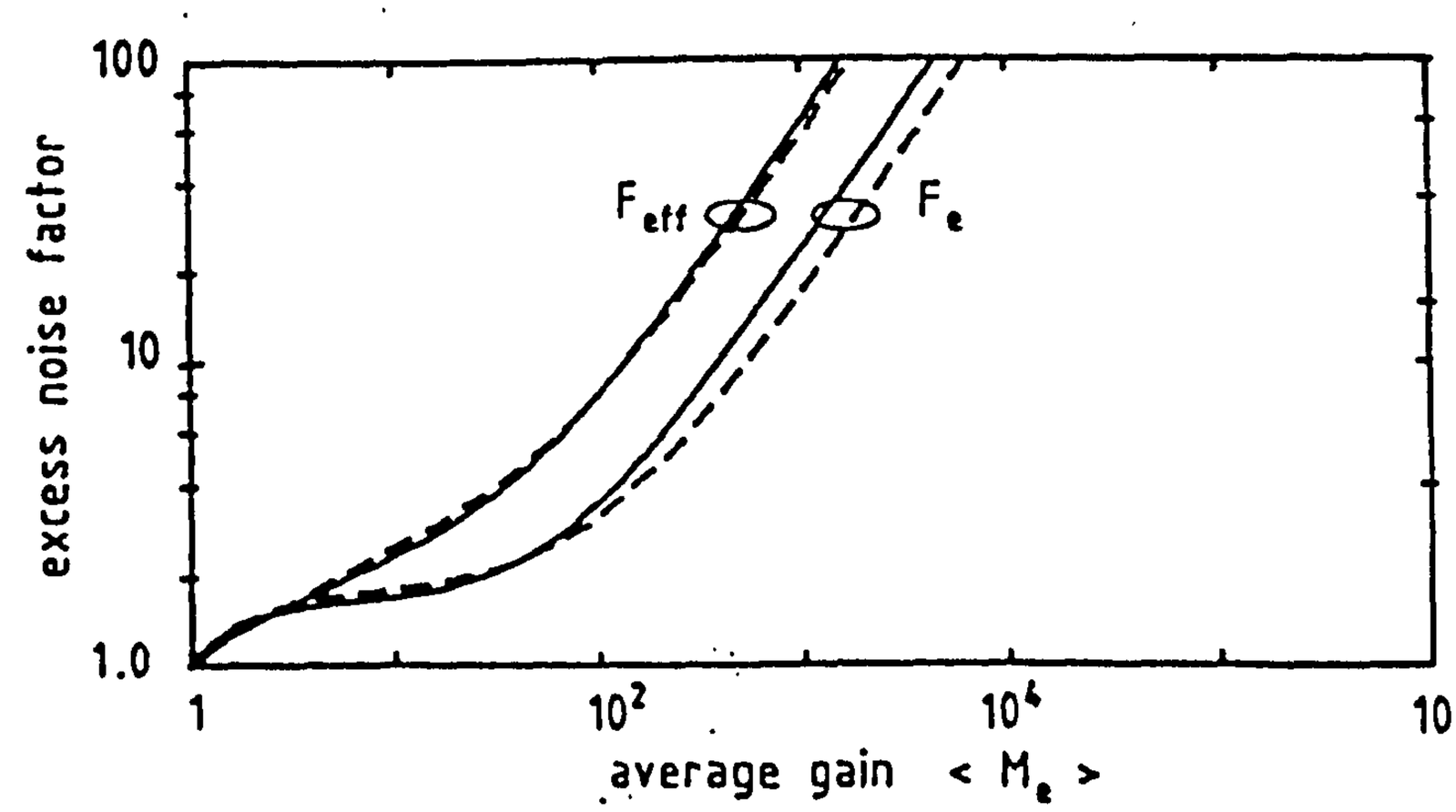

(c)

Fig. 6.7 Excess noise factor as a function of device gain $<M_e>$ assuming $A_e=A_h=1$. (a) k=0.0 (b) k=0.001 (c) k=0.01

—— N=5 – – – N=10

Fig. 6.8 illustrates the effect of A_e on the excess noise factor of a 10-stage device with $A_h=1$. As expected, higher values of A_e lead to an increase in the multiplication noise, but this effect is less pronounced for $k>0$ due to the excess noise associated with the feedback process. Note that for a given k, the curves correspond to lower values of A_e extending over a small range of $<\delta_e>$ due to the restrictions imposed by keeping ϕ'_e, ϕ''_e, ϕ'_h and ϕ''_h always non-negative. The effect of A_h on the excess noise factor is given in Fig. 6.9 assuming $A_e=1$. No results are shown for $k=0$ since this refers to the case of no residual hole ionisation. Also, it is impossible to adopt lower values of A_h (i.e. $A_h<1$) for the values of k indicated and at the same time keep the above four parameters non-negative.

6.5 Receiver Performance

In this section the sensitivity $\eta\bar{P}$ of an optical receiver employing a SSPM will be evaluated for bit error rate (BER) of 10^{-9}, using Personick's approach [Personick, 1973] based on a Gaussian noise approximation. Further we shall assume in the subsequent analysis that the gain-bandwidth product of the diode is extremely high, such that it is not a limiting factor for receiver performance.

For the purpose of illustration we consider the 2 Gbit/s receiver described earlier, with parameters as in Table 3.1. Figs. 6.10a and 6.10b show the receiver sensitivity $\eta\bar{P}$ as a function of $<\delta_e>$ for N=5 and N=10, respectively. In each figure two values of k are considered, 0 and 0.001, in addition to two values of dark current 0 and 50 nA, this being assumed to be generated equally among the various stages. For k=0 both receivers give better sensitivity as the

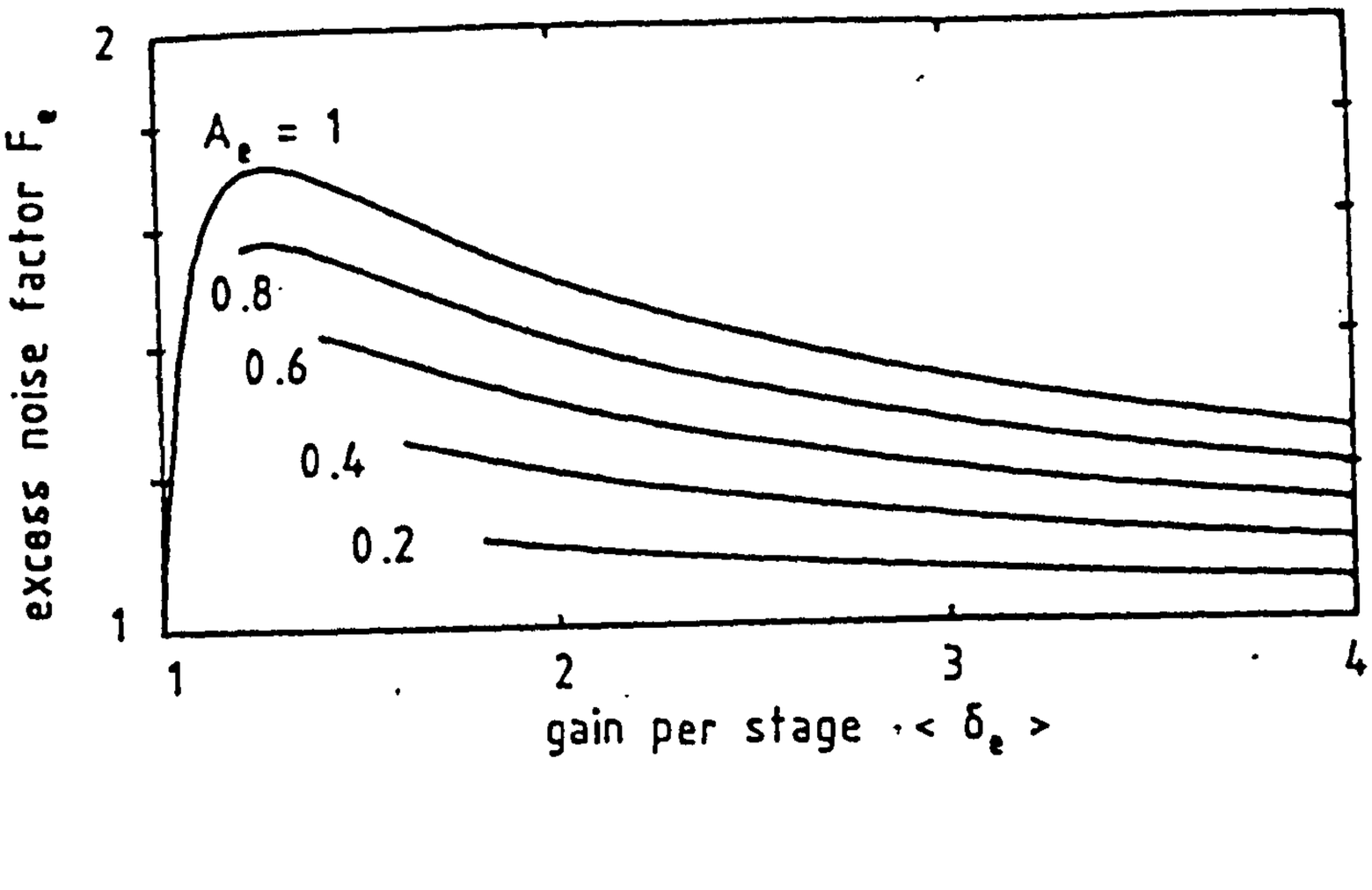

(a)

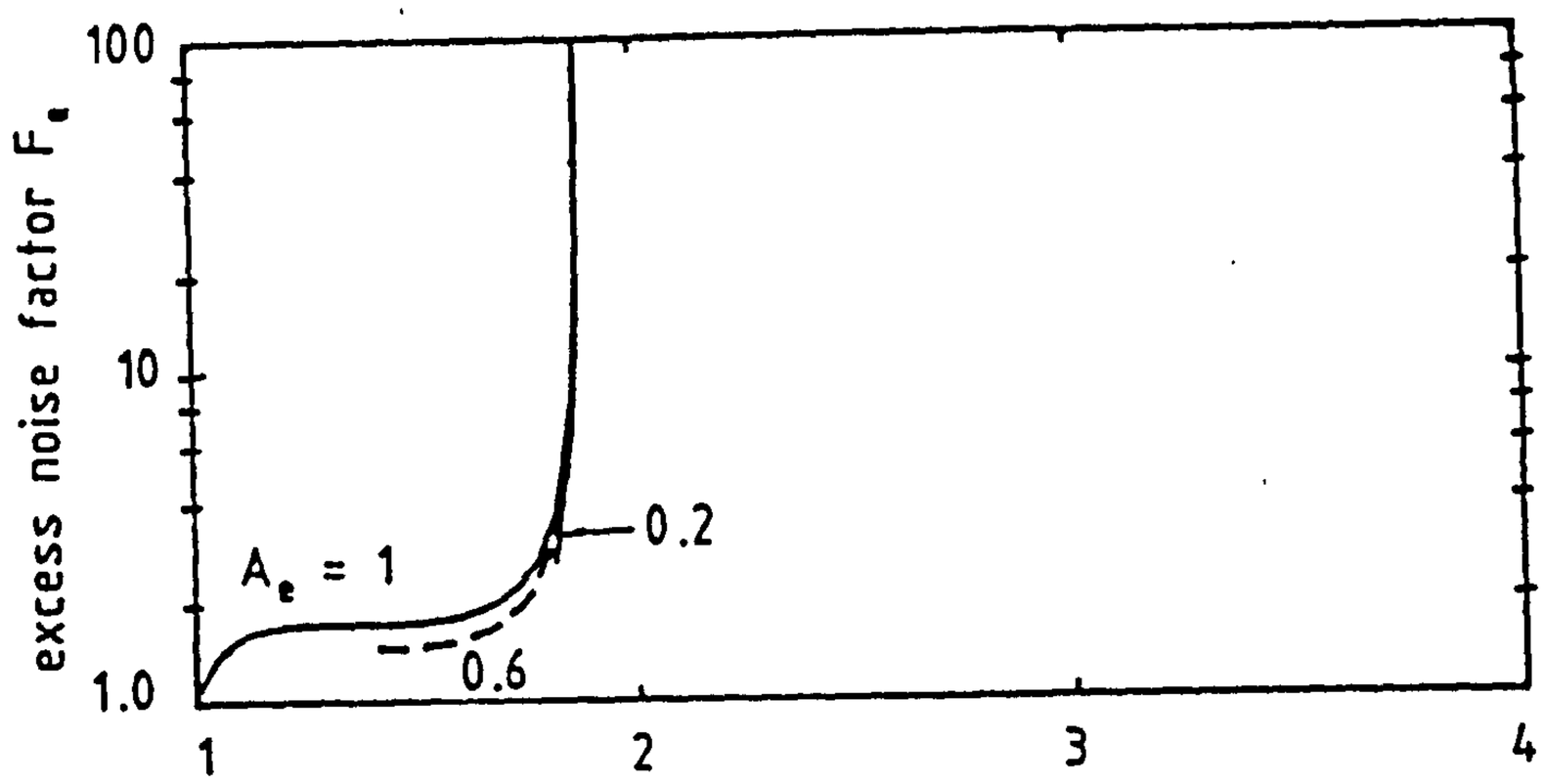

(b)

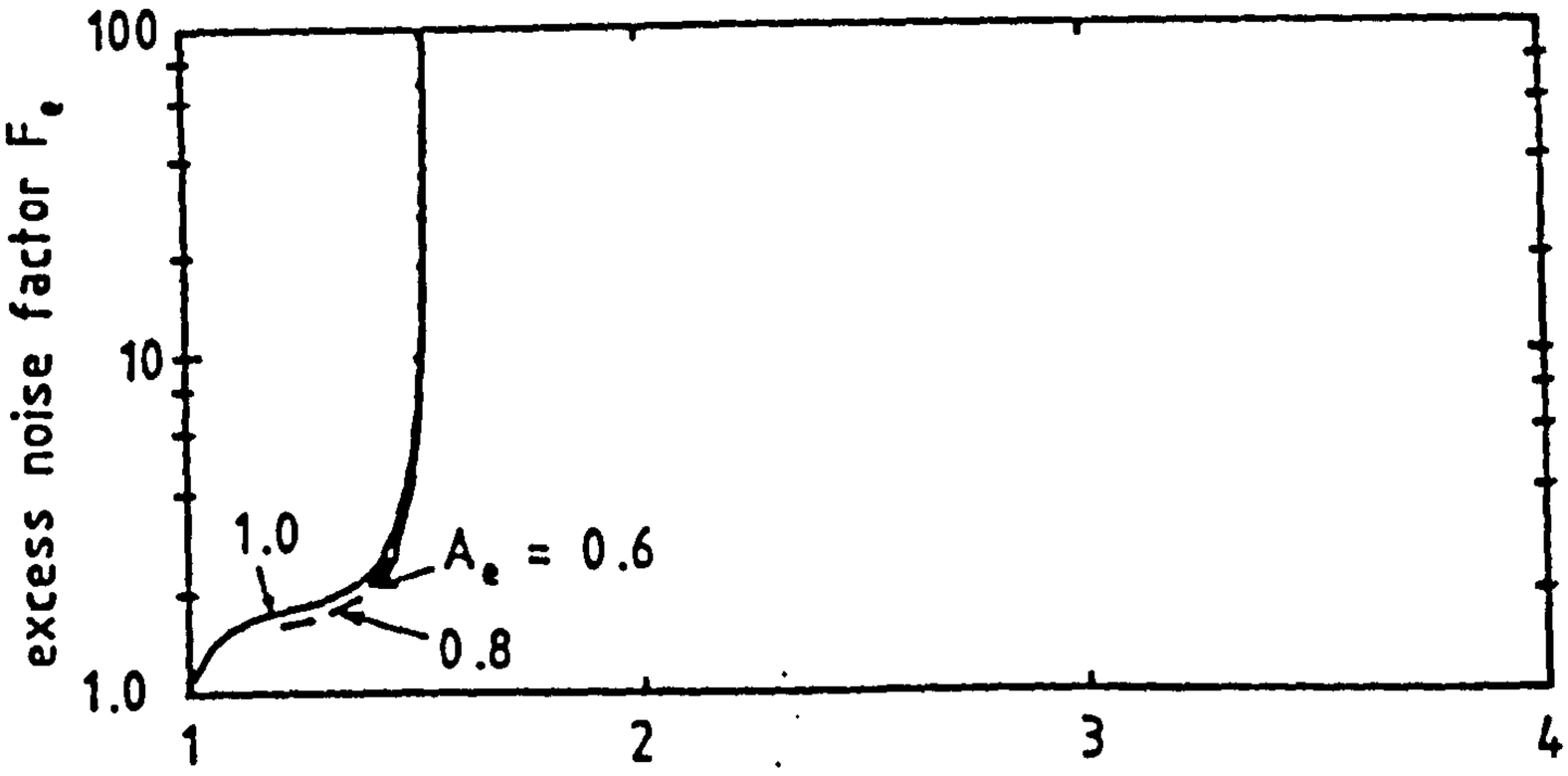

(c)

Fig. 6.8 Effect of parameter A_e on excess noise factor of 10-stage SSPM with A_h=1. (a) k=0.0 (b) k=0.001 (c) k=0.01

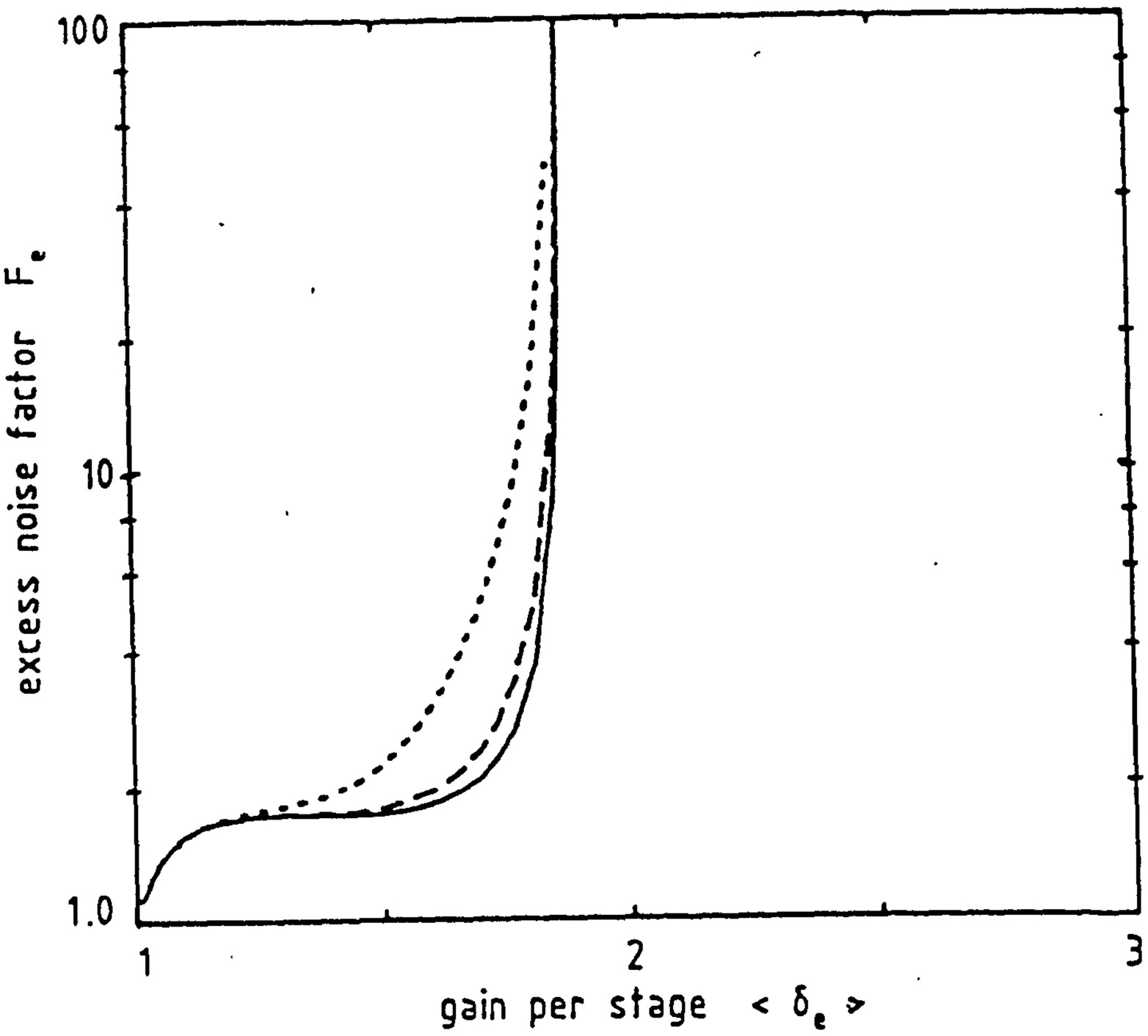

(a)

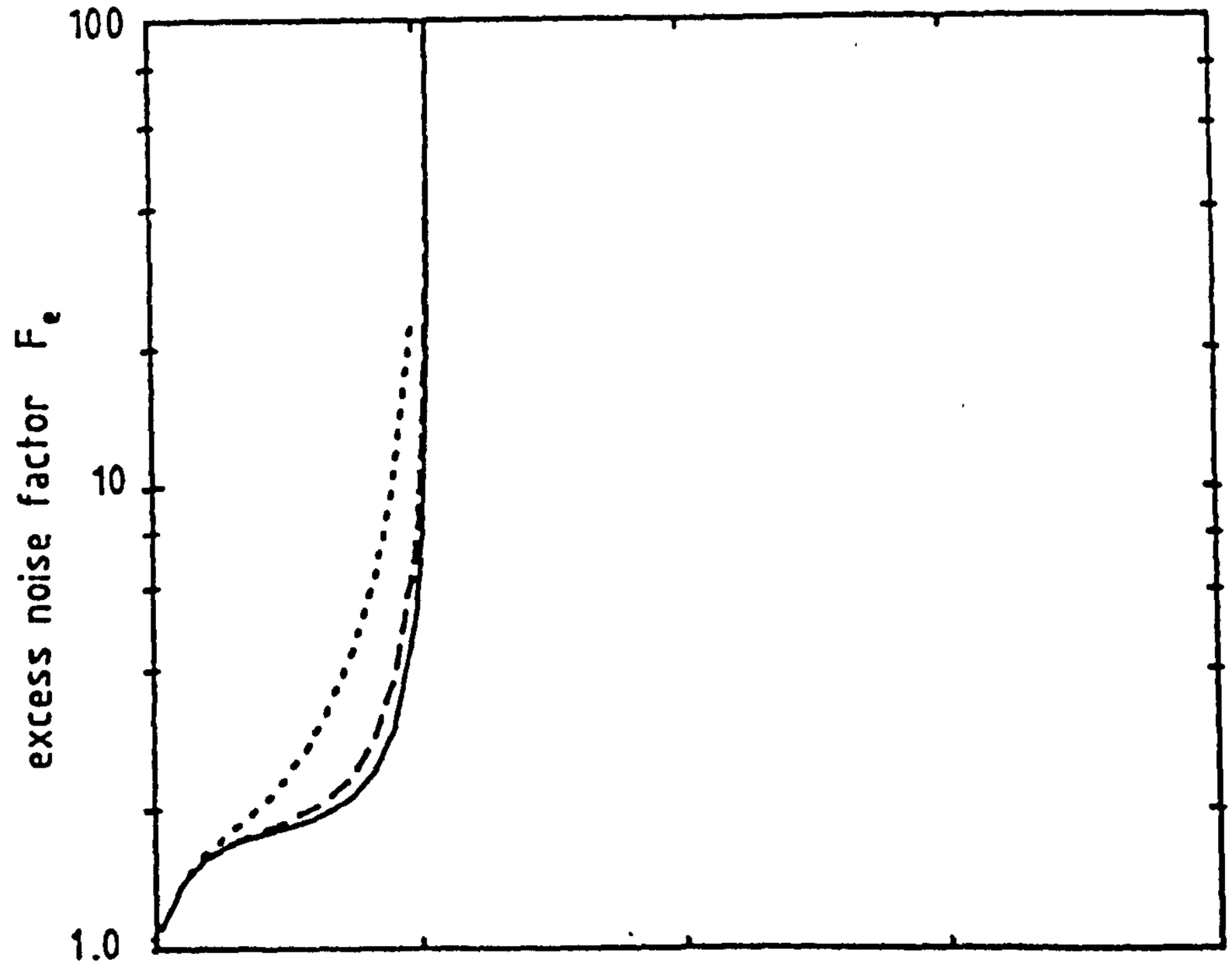

(b)

Fig. 6.9 Effect of parameter A_h on excess noise factor of 10-stage SSPM with A_e=1. (a) k=0.001 (b) k=0.01

——— A_h=1 - - - A_h=2 ····· A_h=10

gain per stage $<\delta_e>$ increases until a saturation limit is achieved which for N=5 and N=10 with zero dark current is approximately 3.2dB and 3.13dB, respectively worse than the quantum limit. Note than for N=10 the saturation in sensitivity occurs at a lower value of $<\delta_e>$ compared with that for N=5. The difficulty in achieving the quantum limit is primarily due to the equalisation stage used in the receiver, and partly due to noise associated with the detector and amplifier. The existence of dark current degrades the sensitivity of both receivers, especially at higher values of $<\delta_e>$.

The system performance in the presence of residual hole ionisation is significantly impaired. In this case there is an optimum gain at which the detectable optical power is minimum (maximum sensitivity). Beyond this optimum gain a strong reduction in receiver sensitivity occurs due to high excess noise factor associated with the detector since the device is then operating almost in the avalanche breakdown region. Note that for N=10 the optimum gain occurs at a lower value of $<\delta_e>$ compared with that for N=5. It is clear from the above discussion that there is no advantage to be gained from adopting multiple ionisations per stage unless the residual hole ionisation can be made vanishingly small. Even if this condition is satisfied, there is a limit to the gain per stage beyond which the receiver performance is unaffected unless the receiver is based on a photon counting approach.

To proceed further, we calculate the optimum sensitivity achieved by the receiver as a function of k taking $<I_d>$ and N as parameters, as shown in Fig. 6.11. In this calculation, both $<\delta_e>$ and the decision threshold are adjusted to obtain minimum detectable power for each set of parameters. The important conclusion drawn from this figure is

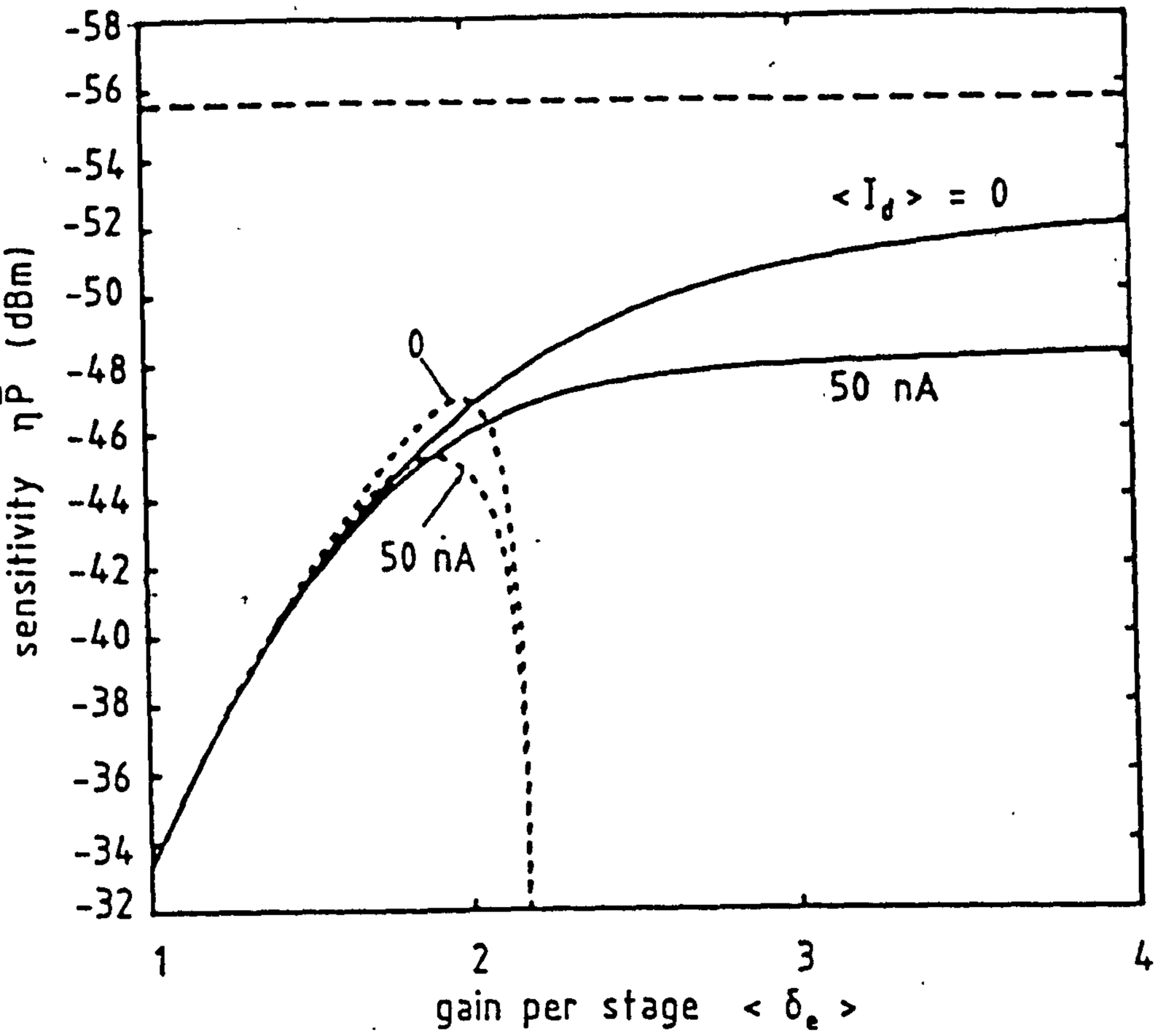

(a)

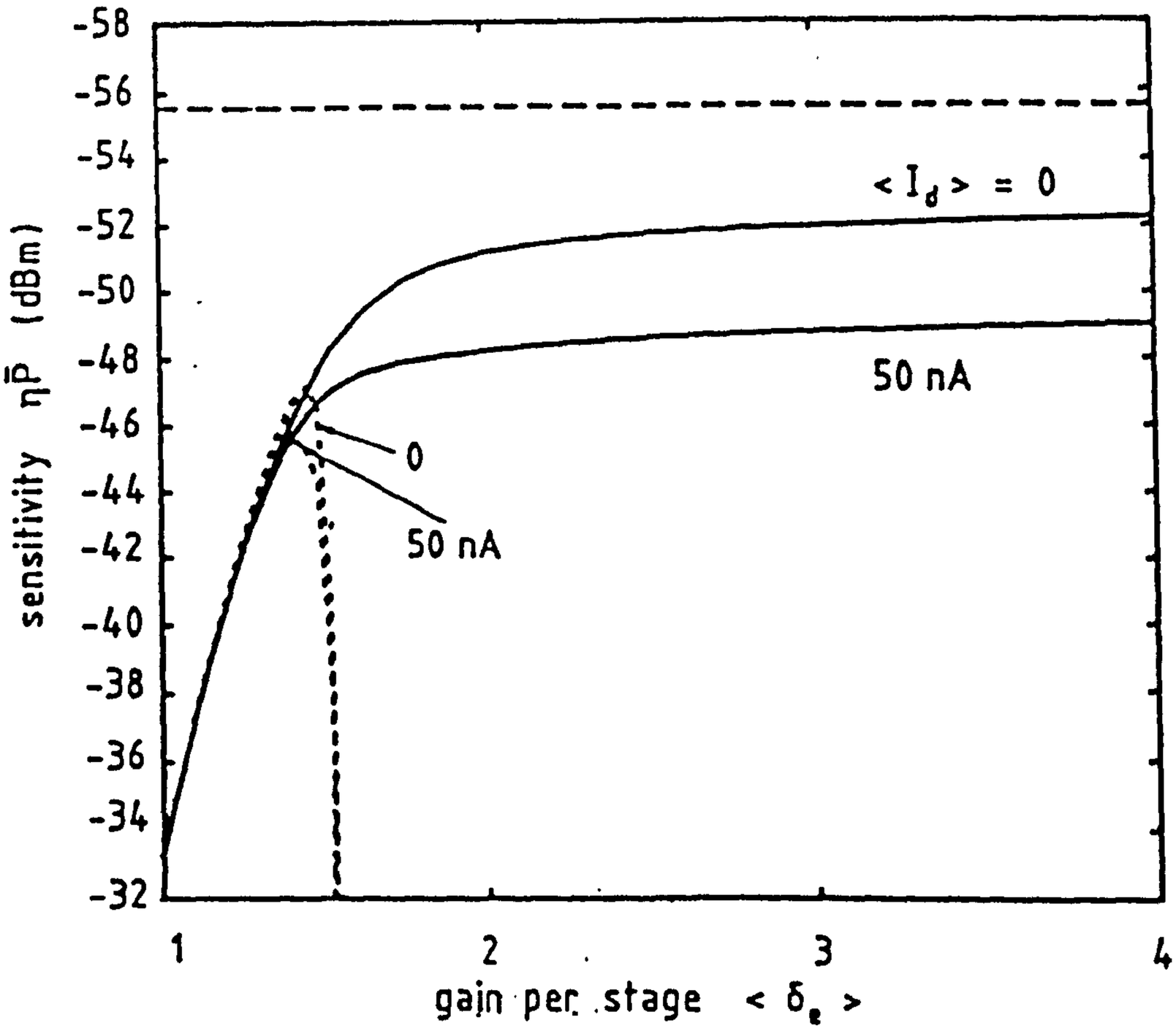

(b)

Fig. 6.10 Sensitivity of 2 Gbit/s optical receiver employing SSPM as a function of gain per stage $\langle \delta_e \rangle$ for various values of ionisation rate ratio k and dark currents $\langle I_d \rangle$.

(a) N=5 (b) N=10

——— k=0.0 ····· k=0.01 — — — quantum limit

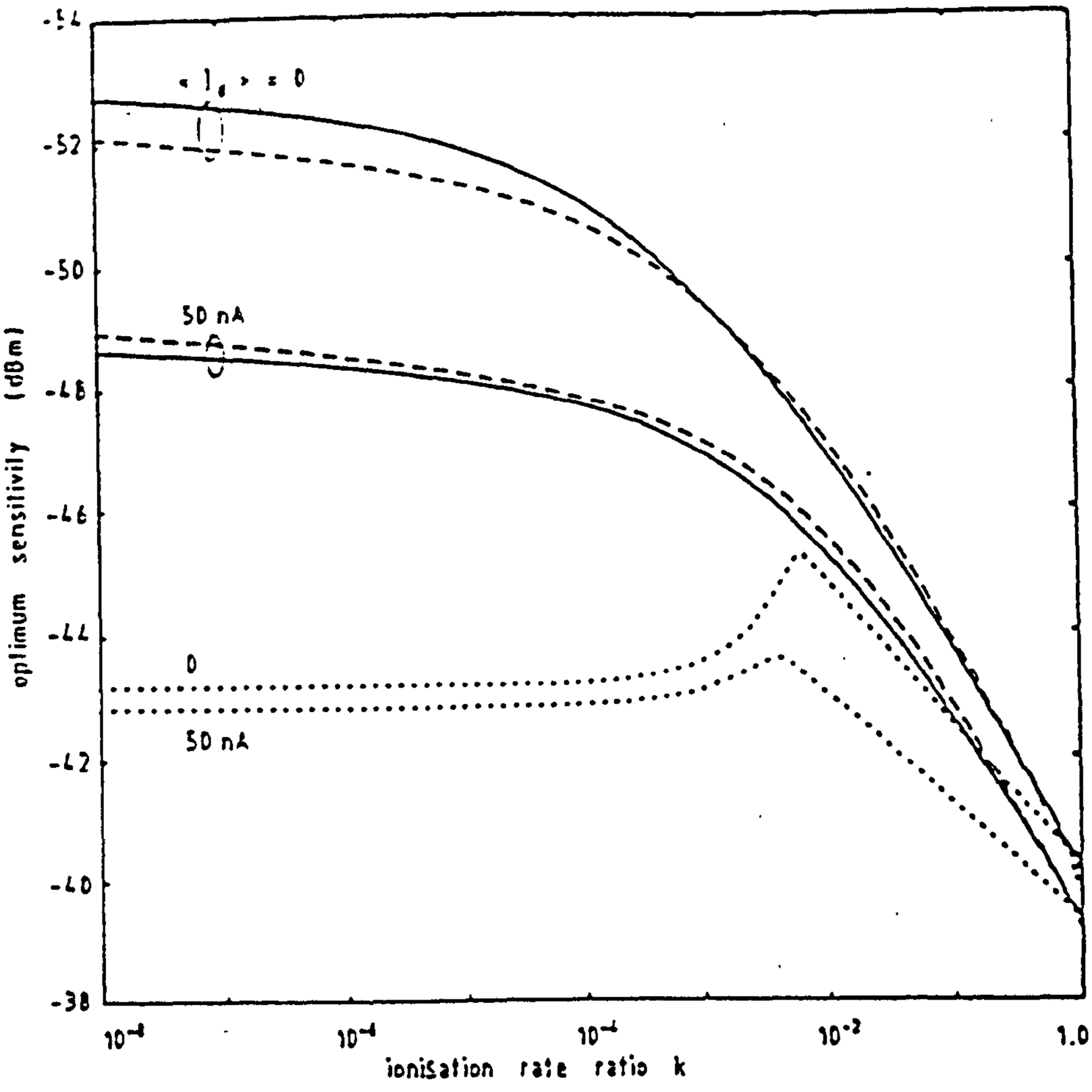

Fig. 6.11 Minimum detectable power required for SSPM receiver to achieve BER=10^{-9} as a function of ionisation rate ratio k.

····· N=1 ——— N=5 — — — N=10

that even for k as low as 10^{-8}, the 5 stage device is capable of giving better sensitivity than the N=10 device, assuming zero dark current. As k increases the difference between the sensitivity of the two receivers decreases, and the N=10 case leads to slightly improved performance when $k > 10^{-3}$. The penalty incurred due to 50nA dark current is lower for the 10 stage receiver leading to slightly improved sensitivity compared with N=5 for the entire range of k considered. Fig. 6.11 also shows some results for a single stage device which has attracted attention recently in the literature as a promising structure for a high speed APD. Here there is a well defined

value of k at which the sensitivity is optimum. This result may be qualitatively interpreted as follows. Neglecting the dark current for a moment, we can claim that as k increases both the gain $<M_o>$ and the excess noise factor F_o increase and this increment will be larger if the device operates near avalanche breakdown. Thus, the sensitivity is improved or degraded as a result of the relative magnitudes of the two effects. At lower values of k, no avalanche breakdown occurs in this device leading to improved sensitivity as $<\delta_o>$ increases. Under these circumstances, as k increases, F_o increases only slightly compared with the gain $<M_o>$, leading to the observed improved performance. At higher values of k, where avalanche breakdown occurs, the excess noise factor increases strongly as k increases which results in sensitivity degradation.

The optimum values of $<\delta_o>$ and average gain used in the calculation of Fig. 6.11 are displayed in Figs. 6.12 and 6.13, respectively. For N=1 we limit our calculations to $<\delta_o>$ <11 since no breakdown occurs at lower values of k. Fig. 6.12 indicates that lower values of $<\delta_o>_{opt}$ are required for higher values of N, all other parameters being kept the same. Note that $<\delta_o>_{opt}$ is less than two for $k>10^{-4}$ for the case of N=10 and $k>10^{-2}$ for N=5. Fig. 6.13 predicts a reduction in the optimum gain $<M_o>_{opt}$ as k increases for both N=5 and N=10 devices, with higher values for the latter receiver. For N=1, $<M_o>_{opt}$ is nearly constant at lower values of k since, no avalanche breakdown occurs, while $<\delta_o>$ is limited to <11 in our calculations.

It is appropriate to mention that the above discussion is limited to receiver sensitivity. For optical receivers other figures of merit may also be relevant such as speed of operation, which requires a

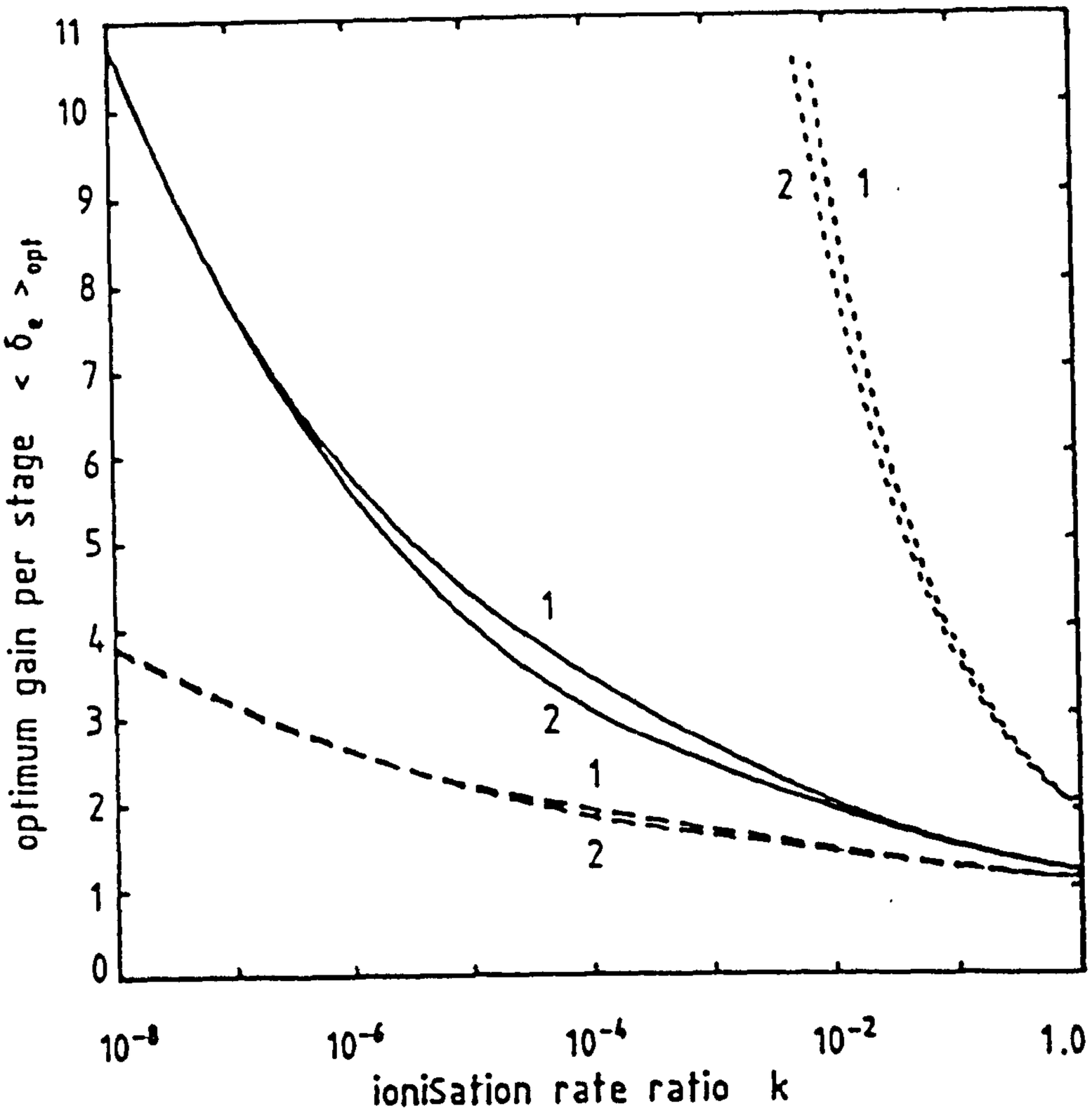

Fig. 6.12 Optimum gain per stage $<\delta_e>_{opt}$ against ionisation rate ratio.

1: zero dark current 2: 50 nA dark current

····· N=1 —— N=5 – – – N=10

complete description for the structure of the device. In general, though, we can say that high speed operation may be achieved by using lower values of N, assuming all other parameters including the structure of the individual stages to be the same.

6.6 Summary

General expressions have been obtained for the average gain and excess noise factor associated with photocurrent and dark current in superlattice APDs where multiple ionisations per stage, similar to secondary emission in a photomultiplier tube, may occur. It has been found that the multiplication noise characteristics of these devices

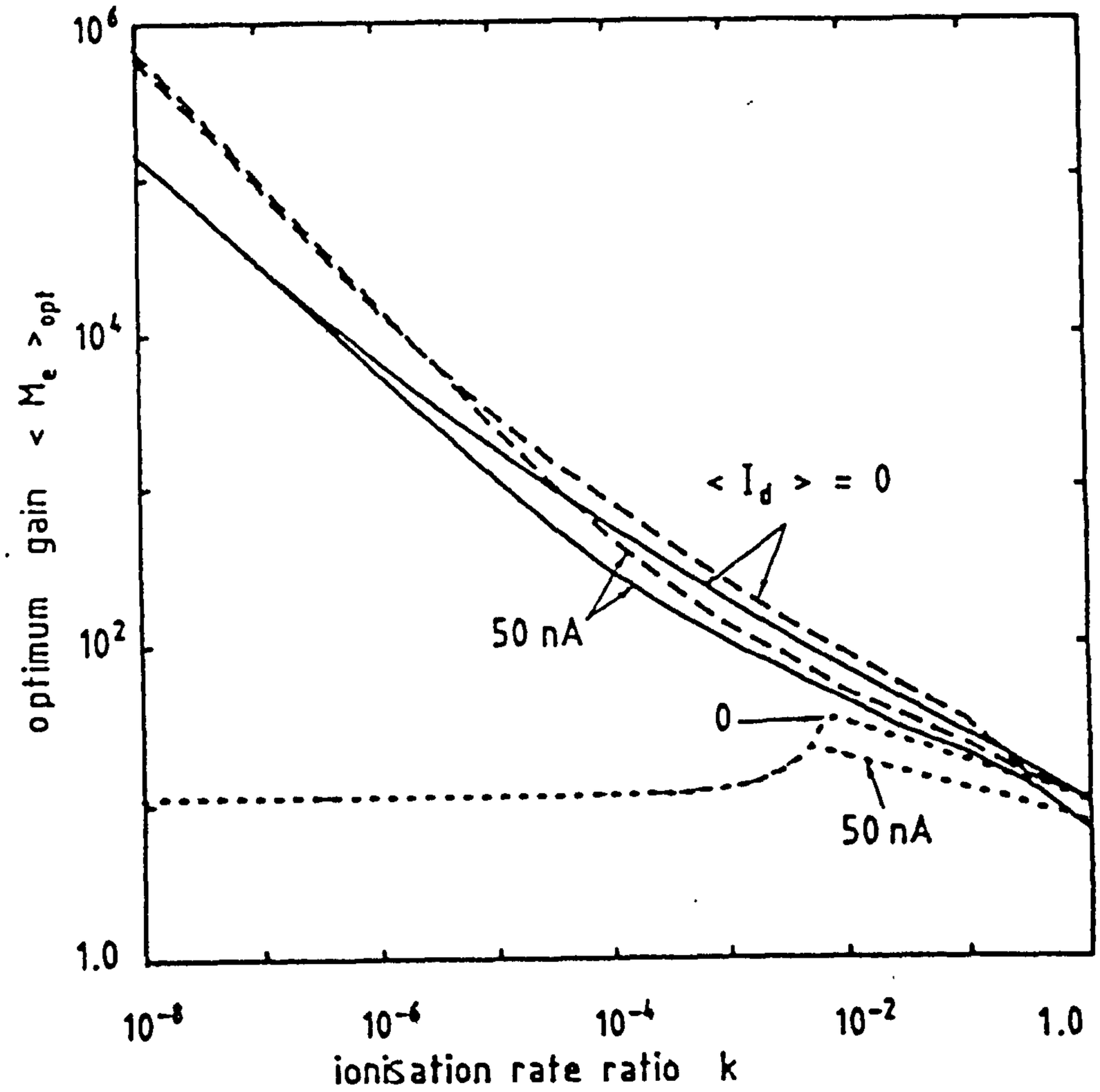

Fig. 6.13 Optimum gain $<M_e>_{opt}$ against ionisation rate ratio.

..... N=1 ——— N=5 - - - N=10

can be expressed as a function of the mean and variance of the number of ionisations per stage initiated by electrons and holes, respectively. An indication has been provided of how these parameters may be deduced experimentally from measurements of the gain and the variance for both pure hole injection and pure electron injection. The performance of a 2 Gbit/s optical receiver incorporating a SSPM has been evaluated allowing for both dark current and residual hole ionisation. The analysis shows that hole ionisation may be a severe limiting factor for these advanced receivers unless it can be reduced to an extremely low value. The existence of hole ionisation restricts the gain per stage $<\delta_e>$ to a relatively low value, both for stable operation and to obtain optimum sensitivity.

CHAPTER 7

GAIN MOMENT GENERATING FUNCTION OF SAPDS

A Gaussian approximation (GA) is commonly used to predict the performance of optical receivers. This technique is based on the excess noise factor, representing first and second order statistical properties of the gain fluctuations introduced by the multiplication process. A more precise measure for the performance of these systems requires a comprehensive statistical description for the random gain associated with the APD and thus complete knowledge of the probability distribution or the moment generating function (MGF) is required for exact evaluation. Various techniques based on MGF (or other related functions have been previously reported for optical receivers based on conventional avalanche photodiodes (CAPDs) [e.g. Personick et al., 1977; da Rocha and O'Reilly, 1982; Helstrom, 1988]. For superlattice avalanche photodiodes (SAPDs) characterisation in these terms has been limited to single-carrier multiplication devices, that is with no residual hole ionisation, since the MGF of the random gain has been reported only for these idealised detectors. Within these limitations Teich et al. [1986b] have evaluated the bit error rate (BER) of "integrater and dump" receivers employing SAPDs with zero dark current, assuming maximum likelihood detection.

The purposes of this chapter are twofold. First we present a numerical technique with which to determine and evaluate the MGF associated with the multiplication process of nonideal SAPDs, allowing for nonnegligible hole ionisation, based on a discrete ionisation model. Secondly, we use the MGF together with a modified Chernoff

bound (MCB) [Prabhu, 1982; da Rocha and O'Reilly, 1982] to predict the performance of optical receivers incorporating these advanced detectors, allowing for residual hole ionisation, detector dark current generated in the various stages, and circuit noise. The MCB technique has a sound fundamental basis in employing the MGF, encapsulating the entire signal and noise process statistics and is known to provide very accurate error probability predictions. Consequently the MCB can be used to effect for SAPDs a comparison with - and in the eventuality a validation of - the widely adopted but much less soundly based Gaussian approximation. The latter aspect is an important feature of the work reported here since the possible inadmissibility of the GA in these circumstances has been an uncertainty underlying - and to some extent undermining - performance analyses presented to date for SAPD receivers. We shall see that the assumed applicability of the GA is indeed justified, in fact even more so than for conventional APDs. The results indicate clearly that the GA, whilst slightly overestimating the receiver sensitivity (by less than 0.3dB) and also overestimating the optimum gain, provides a generally good prediction of the optimum threshold and represents a useful basis for initial comparison of the performance of alternative receiver strategies.

There is a wealth of evidence in the literature demonstrating the accuracy and flexibility of the MCB technique for optical communication [O'Reilly, 1984; O'Reilly and da Rocha, 1987]. In addition, it has been found that a very wide range of system impairments may be readily incorporated into the formulation both for performance assessment and receiver optimisation [O'Reilly, et al., 1985; da Rocha and O'Reilly, 1986; O'Reilly et al., 1986]. However,

it should be noted that much of the analyses given here allow also for the use of other performance evaluation techniques based on the MGF such as the Gram-Charlier series [Mansuripur, 1980; Cartledge and Coathup, 1986], maximum entropy methods [Cartledge, 1987], and Edgeworth series expansion [Wu et al., 1988].

In the following sections the analysis is given for a SAPD in which the initiating carrier can impact a single ionisation per stage. Extension for more than one ionisation per stage is also possible but will not be considered here.

7.1 Optical Receiver Model

An outline block diagram for an optical receiver used in binary direct detection systems is illustrated in Fig. 7.1. The optical signal incident on the photodetector may be expressed as:

$$P_i(t) = \sum_{j=-\infty}^{\infty} a_j h_p(t-jT) \qquad (7.1)$$

where $h_p(t)$ is the elemental optical pulse and $1/T$ is the signalling rate. The sequence $\{a_j\}$ denotes the transmitted, independent, identically distributed data amplitudes. We assume that a_j equals one or zero depending on whether a binary "1" or binary "0" is transmitted during the j^{th} signalling interval. In the receiver the optical power is first converted into an electrical signal. After amplification and equalisation the electrical signal is sampled at regular intervals T and a decision whether a_j is "1" or "0" is made in accordance with the sampled value being above or below a fixed threshold d. The output of the receiver filter can be considered as a linear combination of three statistically independent processes

$$i_t(t) = i_s(t) + i_d(t) + i_n(t) \qquad (7.2)$$

where $i_s(t)$ is the filtered output signal current of the detector, $i_d(t)$ is due to the dark current of the detector, and $i_n(t)$ is independent zero-mean Gaussian filtered thermal noise generated in the front-end amplifier. Note that the mathematical model of $i_s(t)$ is that of a filtered doubly stochastic process [Snyder, 1975; O'Reilly, 1984]. Let the decision to be made about data bit a_0 be based on a sampled value of $i_t(t)$ at time t_s. Since $i_t(t_s)$ is the sum of three

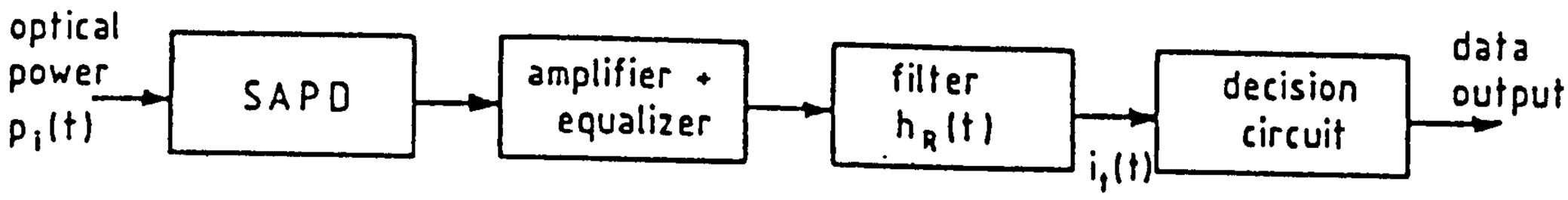

Fig. 7.1 Schematic diagram of direct detection optical receiver.

statistically independent random variables, the MGF of the composite variable corresponds to the product of the MGFs of the constituents [Cattermole, 1984].

$$M_t(s) = M_s(s).M_d(s).M_n(s) \qquad (7.3)$$

Note that the output MGF, $M_t(s)$ is sequence conditioned: a different MGF results for each sequence $\{a_j\}$ of the transmitted symbols. It is more appropriate to make use of symbol-conditioned MGFs obtained by averaging eqn. 7.3 over all possible sequence realisations with a_0 kept fixed. For binary communications, two symbol-conditioned MGFs are obtained [O'Reilly and da Rocha, 1987].

$$M_{t_k}(s) = M_{s_k}(s).M_d(s).M_n(s) \qquad k=0,1 \qquad (7.4)$$

where $M_{t_k}(s)$ and $M_{s_k}(s)$ are the symbol-conditioned MGFs for the total output and filtered signal current, respectively, corresponding to $a_0=k$, and

$$M_{s_0}(s) = \frac{1}{2^{2n1}} \prod_{\substack{i=-n1 \\ i\neq 0}}^{n1} \left[1+\exp(H_i(s)) \right] \qquad (7.5a)$$

$$M_{s_1}(s) = M_{s_0}(s).\exp(H_0(s)) \qquad (7.5b)$$

where a finite sequence $(a_{-n1}, \ldots, a_{-1}, a_0, a_1, \ldots, a_{n1})$ with $(2n_1+1)$ elements is assumed and

$$H_i(s) = \mathscr{R} \int_{-\infty}^{\infty} h_p(\tau-iT) \left[M_{g_N}(sqh_R(t_s-\tau))-1 \right] d\tau \qquad (7.6)$$

Here $M_{g_N}(s)$ is the MGF of the avalanche gain of the SAPD, $h_R(t)$ is the impulse response of the receiver filter, q is the electronic charge, and $\mathscr{R} \equiv \eta/h\upsilon$, with η the detector quantum efficiency, h Planck's constant and υ the optical frequency.

The error probability for a binary communication system is given by

$$p_e = p_0 Pr[1|0] + p_1 Pr[0|1] \tag{7.7}$$

where p_0, p_1 are *apriori* element probabilities and Pr[1|0], Pr[0|1] are conditional error probabilities for "0" or "1" being transmitted. The MCB on p_e is given by

$$p_e \leq MCB = \frac{1}{\sqrt{2\pi}\, s\sigma_n} \left[p_0 M_{t_0}(s).\exp(-ds) + p_1 M_{t_1}(-s).\exp(ds) \right] \tag{7.8}$$

where σ_n^2 is the variance of the filtered Gaussian additive noise.

The optimum threshold d_{opt} which minimises the bound on error probability can be obtained by setting to zero the derivative of eqn. 7.8 with regard to d

$$d_{opt} = (1/2s) \ln \left[\frac{p_0 M_d(s).M_{s_0}(s)}{p_1 M_d(-s) \,.\, M_{s1}(-s)} \right] \tag{7.9}$$

which leads to

$$p_e \leq \text{MCB} = \frac{2}{\sqrt{2\pi}\, s\sigma_n} \left[p_0 M_{t_0}(s).p_1 M_{t_1}(-s) \right]^{1/2} \qquad (7.10)$$

To obtain the tightest form of the bound, we seek an optimum value of s which minimises the MCB in eqn. 7.10.

Complete descriptions of the signal and noise at the decision times in terms of MGFs are required in order to estimate from eqn. 7.10 the error probability for the system. The MGFs associated with Gaussian additive noise $M_n(s)$ and with detector dark current $M_d(s)$ will first be described in the following sections.

7.1.1 Additive Gaussian Noise

Additive Gaussian noise introduced by the receiver front-end is generally not white but often has a power spectral density of the form

$$N(f) = N_0 f + N_2 f^2 \qquad (7.11)$$

where N_0, N_2 are constants associated with the receiver. For an APD/FET front-end we have

$$N_0 = (4K\Theta/R_L)\left[1 + \Gamma/(g_m R_L) \right] + 2qI_g \qquad (7.12a)$$

$$N_2 = 16\pi^2 K\Theta\Gamma C_t^2/g_m \qquad (7.12b)$$

where

K = Boltzmann's constant

Θ = absolute temperature

Γ = FET noise factor

C_t = amplifier input capacitance

R_L = amplifier input load

I_g = FET gate leakage current

g_m = FET transconductance

Here the 1/f FET noise is neglected, which is certainly appropriate for high bit rate systems, and so is any additional noise introduced by subsequent amplification stages. After filtering, this noise has variance σ_n^2 given by [O'Reilly and da Rocha, 1987].

$$\sigma_n^2 = 0.5 \int_{-\infty}^{\infty} \left[N_0 h_R^2(t) + N_2 h_R'^2(t) \right] dt \qquad (7.13)$$

with MGF

$$M_n(s) = \exp(\sigma_n^2 s^2/2) \qquad (7.14)$$

The prime in eqn. 7.13 denotes the derivative with respect to t. Eqn. 7.13 can be rewritten in the simpler form

$$\sigma_n^2 = N_0 I_2 B + N_2 I_3 B^3 \qquad (7.15)$$

where $B \equiv 1/T$ is the bit rate and I_2, I_3 are Personick intergrals [Personick, 1973]

$$I_m = \int_0^{\infty} y^{m-2} |H_R(y)|^2 \, dy \qquad m=2,3 \qquad (7.16)$$

where $y=f/B$ is the normalised frequency and $H_R(f)$ is the Fourier transform of $h_R(t)$. Because of the normalisation the values of these integrals depend only on the relative shapes of the input and output pulses.

7.1.2 Dark Current

In the following, we direct our attention to determining the MGF of the dark current components generated within the multiplication region (i.e. in different stages) since it contributes predominantly to the multiplied dark current. The effect of diffusion dark current will be considered later.

We consider a SAPD having a p-i-n structure in which the intrinsic region, fully depleted by the external electric field, consists of N identical stages. Let g_j denote the total number of hole-electron pairs generated due to a single hole-electron pair initiated at position A(j), including the original pair, where j denotes the number of stages crossed by the initiating electron while moving to the n^+ contact. It is safe to assume that the dark current components generated within the various stages are statistically independent and hence the MGF of the filtered dark current at the input of the decision circuit is given by

$$M_d(s) = \prod_{j=1}^{N} M_{d_j}(s) \qquad (7.17)$$

where

$$M_{d_j}(s) = \exp\left[\int_{-\infty}^{\infty} r_j \left[M_{g_j}(sqh_R(t_s-\tau))-1 \right] d\tau \right] \qquad (7.18)$$

Here r_j is the rate of generation of dark current in the $(N-j+1)^{th}$ stage, $M_{g_j}(s)$ is the MGF of the random gain g_j and $M_{d_j}(s)$ is the MGF associated with the filtered dark current component arising from r_j only. Under the assumption that the rate of generation of dark current carriers is the same in the various stages, we have

$$M_d(s) = \exp\left[(Nr_o) \int_{-\infty}^{\infty} (1/N) \sum_{j=1}^{N} \left[M_{g_j}(sqh_R(t_s-\tau))-1 \right] d\tau \right] \qquad (7.19)$$

where

$$r_o = r_j \qquad j=1,2,\ldots,N \qquad (7.20)$$

Comparing eqn. 7.19 and eqn. 7.6 we note that dark current generated within the multiplication region can be treated as if it were photocurrent generated (with the same rate) in the p^+ region, but with an effective random gain g_{eff} differing from that for photocarriers (g_N). The MGF of g_{eff} can be expressed as

$$M_{eff}(s) = (1/N) \sum_{j=1}^{N} M_{g_j}(s) \qquad (7.21)$$

Here eqn. 7.19 can be put in the following form

$$M_d(s) = \exp\left[(Nr_o) \int_{-\infty}^{\infty} \left[M_{eff}(sqh_R(t_s-\tau))-1 \right] d\tau \right] \qquad (7.22)$$

Hence Nr_o is the rate of generation of dark current carriers in all stages.

It is worth noting here that in calculating receiver sensitivity using a GA, only the first and second moments of the effective gain g_{eff} are required. These can be calculated from eqn. 7.21 using the fact that the n^{th} derivative of the MGF at s=0 is the n^{th} moment of the random variable [Cattermole, 1984]. Thus

$$\langle g_{eff}^n \rangle = \frac{d^n}{ds^n} M_{eff}(s)\Big|_{s=0}$$

$$= (1/N) \sum_{j=1}^{N} \langle g_j^n \rangle \qquad (7.23)$$

where the angular brackets $\langle . \rangle$ denote ensemble average. The effective average gain and effective excess noise factor associated with dark current are given by

$$\langle g_{eff} \rangle = (1/N) \sum_{j=1}^{N} \langle g_j \rangle \qquad (7.24)$$

$$F_{eff} = \frac{\langle g_{eff}^2 \rangle}{\langle g_{eff} \rangle^2} = \frac{N \sum_{j=1}^{N} F_j \langle g_j \rangle^2}{\left[\sum_{j=1}^{N} \langle g_j \rangle \right]^2} \qquad (7.25)$$

where $\langle g_j \rangle$, F_j are, respectively, the gain and excess noise factor

associated with a hole-electron pair initiated at position A(j), and they are related to $<g_N>$ and F_N (for pure electron injection) according to eqns. 3.1 and 3.2, respectively. Note also that eqns. 7.24 and 7.25 are in accord with our previous results reported in section 3.3.

The effect of nonnegligible diffusion dark current can also be included in the above analysis. The MGF associated with this component is given by

$$M_{d_{diff}}(s) = \exp\left[r_{diff} \int_{-\infty}^{\infty} \left[M_{g_N}(sqh_R(t_s-\tau))-1 \right] d\tau \right] \qquad (7.26)$$

where r_{diff} is the rate of diffusion into the depletion region of dark current carriers. The average gain and excess noise factor associated with this dark current component are, respectively, $<g_N>$ and F_N.

The MGF of the total output dark current can be evaulated by multiplying $M_d(s)$ by $M_{d_{diff}}(s)$, assuming both dark current components are statistically independent.

7.2 Moment Generating Function of the Gain

It is clear from the previous analysis that to perform MCB calculations, a complete description is required for the MGFs of the individual gains g_j. The evaluation of these MGFs will be considered here.

Our starting point is the same as that of van Vliet et al. [1979a; 1979b] who treated the noise characteristics of small avalanche region-devices using a discrete ionisation model. Here the MGF of the random gain g_j can be related to the MGFs of other

individual gains according to*

$$M_{g_j}(s) = \exp(s) \prod_{i=0}^{j-1} \left[pM_{g_i}(s) + 1-p \right] \cdot \prod_{i=j+1}^{N} \left[uM_{g_i}(s) + 1-u \right] \tag{7.27}$$

where u (p) is the probability of hole (electron) impact ionisation per stage. Eqn. 7.27 will lead to the following recurrence relation

$$M_{g_j}(s).\left[uM_{g_j}(s) + 1-u\right] = M_{g_{j-1}}(s).\left[pM_{g_{j-1}}(s) + 1-p\right] \tag{7.28}$$

For pure electron injection we set j=N in eqn. 7.27.

$$M_{g_N}(s) = \exp(s) \prod_{i=0}^{N-1} \left[pM_{g_i}(s) + 1-p \right] \tag{7.29}$$

Also for pure hole injection

$$M_{g_0}(s) = \exp(s) \prod_{i=1}^{N} \left[uM_{g_1}(s) + 1-u \right] \tag{7.30}$$

Eqn. 7.29 can be solved for $M_{g_N}(s)$ under the constraints imposed by eqn. 7.28. The solution can be achieved analytically for special cases, or numerically as will be shown later.

Let us examine eqns. 7.27-7.29 for the following extreme cases

---

** Eqn. 7.27 is obtained from the probability generating function given by van Vliet et al. [1979b] by replacing z by exp(s) to obtain a MGF-based formulation. For simplicity, we avoid the use of two indices (j,N-j) to be associated with the position of injection of the primary hole-electron pair as adopted in that reference.*

(i) No residual hole ionisation (i.e. u=0), which represents to a very low noise device, then

$$M_{g_j}(s) = \begin{cases} (1-p)M_{g_{j-1}}(s) + pM^2_{g_{j-1}}(s) & 1 \le j \le N \\ \exp(s) & j = 0 \end{cases} \quad (7.31)$$

as previously reported by Teich et al. [1986b].

(ii) For u=p, a very noisy device,

$$M_{g_j}(s) = M_{g_N}(s) \qquad 0 \le j \le N \quad (7.32)$$

independent of the position of injection. Also

$$M_{g_N}(s) = \exp(s)\left[pM_{g_N}(s) + 1-p \right]^N \quad (7.33)$$

Eqn. 7.33 may be viewed as a nonlinear equation in the single variable $M_{g_N}(s)$.

(iii) For a single stage device, N=1, we have

$$M_{g_1}(s) = \frac{(1-p).\exp(s) + (1-u)p.\exp(2s)}{[1-u\,p\,.\exp(2s)]} \quad (7.34)$$

For the more general case the MGF of the SAPD gain can be determined numerically as a function of s using the following five-step simulation flow, based on eqns. 7.28, 7.29.

Step (i)

Set an initial value for $M_{g_0}(s)$ to start the minimisation procedure adopted here. It has been found that to achieve rapid

convergence it is appropriate to approximate g_0, for pure hole injection, as a random variable with Gaussian distribution:

$$M_{g_0}(s) = \exp\left[\langle g_0 \rangle s + \mathrm{Var}(g_0)s^2/2 \right] \qquad (7.35)$$

Here $\langle g_0 \rangle$ and $\mathrm{Var}(g_0 \rangle$ denote, respectively, the average and the variance of the random gain g_0, and they are related to p, k ($\equiv$u/p), and N according to

$$\langle g_0 \rangle = \frac{(1-k)(1+k\ p)^N}{(1+kp)^{N+1} - k\ (1+p)^{N+1}} \qquad (7.36)$$

$$\mathrm{Var}(g_0) = \langle g_0 \rangle^2 (F_0 - 1) \qquad (7.37)$$

were F_0 is the excess noise factor for pure hole injection

$$F_0 = 1 + \frac{[1-1/\langle g_0 \rangle](k-1)}{k\ [2+p\,(1+k)]} \left\{ -kp + \frac{2(1-kp)^2}{1+kp} \left[\langle g_0 \rangle (1+kp)/(k-1) + 1/(1+kp) \right] \right\} \qquad (7.38)$$

Eqns. 7.36 and 7.38 are identical to those for pure electron injection except that the roles of u and p are interchanged.

Step (ii)

Calculate with the aid of eqn. 7.38 the MGFs $M_{g_1}(s),\ldots, M_{g_N}(s)$ corresponding the value evaluated for $M_{g_0}(s)$:

$$M_{g_j}(s) = \frac{-(1-u)+[(1-u)^2+4uc_o]^{1/2}}{2u} \qquad (7.39a)$$

with

$$c_o = M_{g_{j-1}}(s) \cdot \left[pM_{g_{j-1}}(s) + 1-p \right] \qquad (7.39b)$$

Starting with $M_{g_0}(s)$, $M_{g_1}(s)$ can be estimated via eqns. 7.39 then $M_{g_1}(s)$ is used to estimate $M_{g_2}(s)$ using the same formula and so on.

Step (iii)

Evaluate $M_{g_N}(s)$ using eqn. 7.29. This calculation is based on the values of $M_{g_j}(s)$, j=0,1,...,N-1 determined in the previous step.

Step (iv)

Search for the optimum value of $M_{g_0}(s)$ which minimises the absolute value of the difference between the two values of $M_{g_N}(s)$ calculated in steps (ii) and (iii).

Step (v)

Use the optimum value of $M_{g_0}(s)$ to evaulate the other individual MGFs via eqns. 7.39.

Figs. 7.2 and 7.3 illustrate the behaviour of the MGF, $M_{g_N}(s)$, for N=1 and N=10 stage devices, respectively. The results in Fig. 7.2 are obtained using eqn. 7.34 for p=1 and taking k as a parameter, while the curves of Fig. 7.3 are obtained numerically using the minimisation procedure outlined above and assuming p=0.4. As we

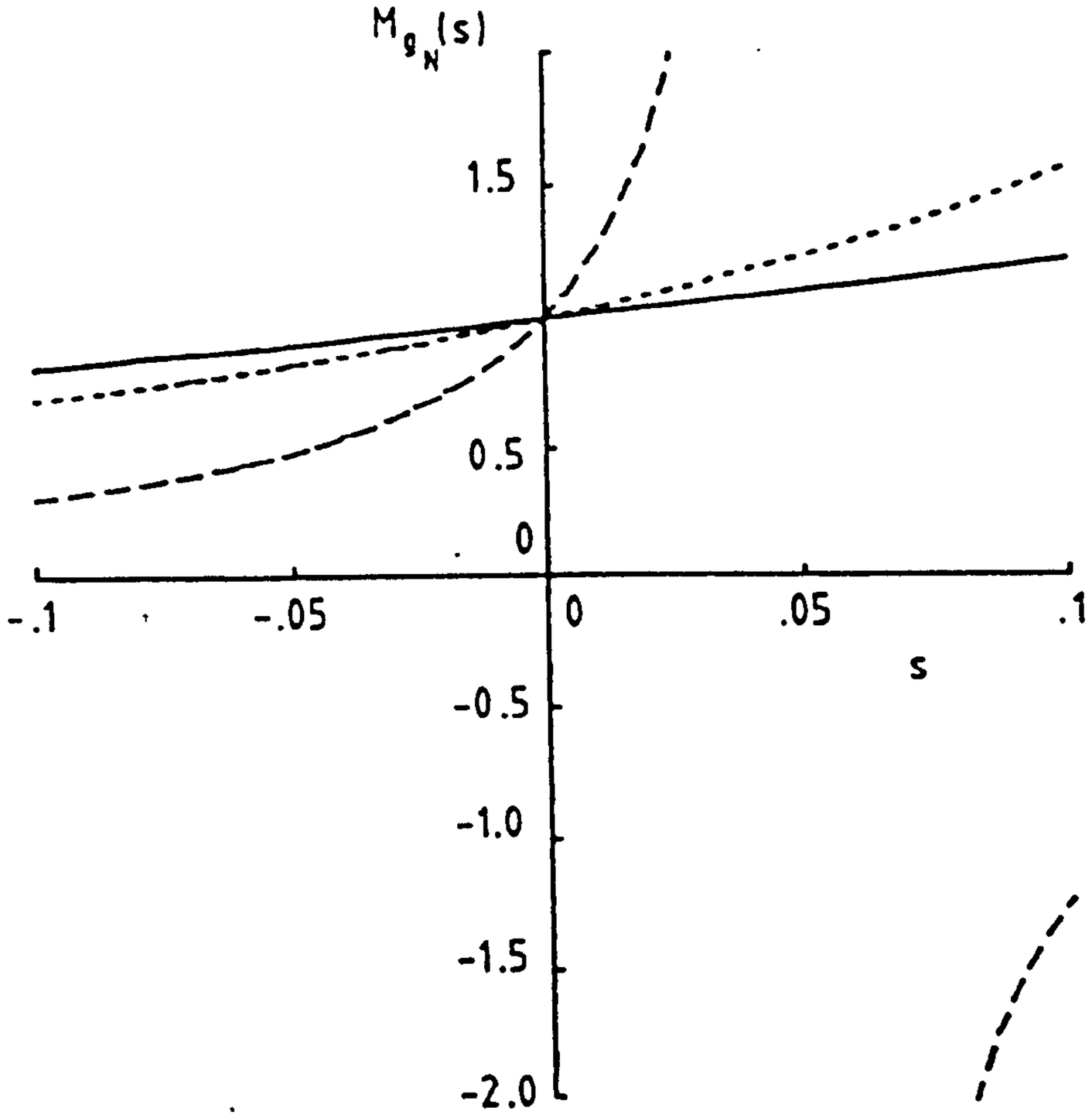

Fig. 7.2 Gain moment generating function of single stage SAPD with p=1.

—— k=0.0 ····· k=0.5 – – – k=0.9

expect, the slope of these curves at s=0, which represents the average gain $<g_N>$, is always positive and increases as residual hole ionisation increases. Note that $M_g(0)$ is always equal to 1; a necessary property for a MGF. It is apparent from Fig. 7.3 that even small deviations of k from zero result in substantial increase in the gain of the device. For this reason our calculations are limited to lower values of k to ensure stable operation without avalanche breakdown. To check the accuracy of our numerical approach we compare the $M_{g_N}(s)$ at k=0 in Fig. 7.3 with that obtained analytically from eqn. 7.31. The two results are essentially identical. It is

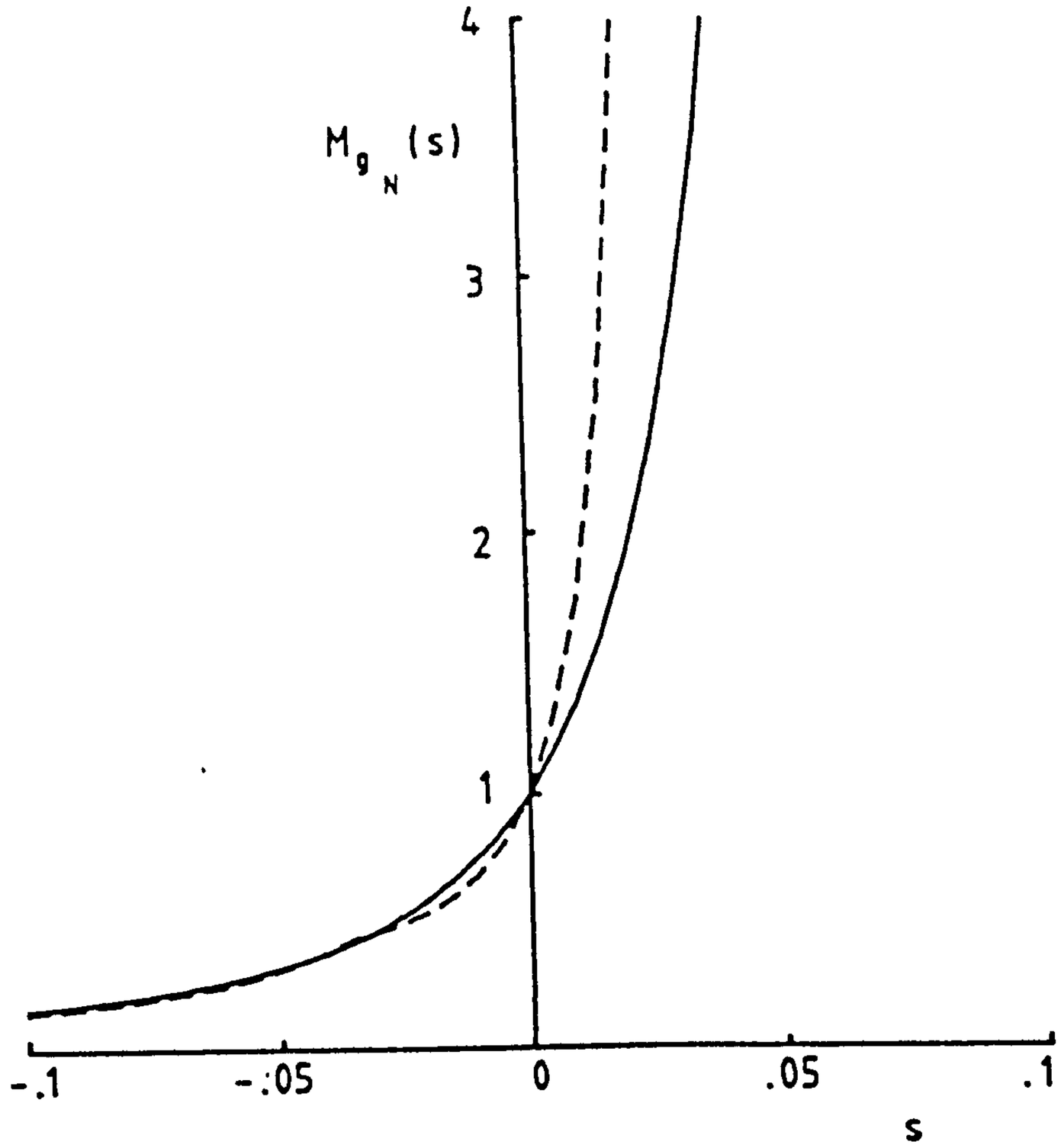

Fig. 7.3 Gain moment generating function for 10-stage SAPD with p=0.5.

——— k=0.0 – – – k=0.01

interesting to observe that the starting point for the minimisation technique is $M_{g_0}(s)=\exp(s)$ (see eqn. 7.35) which is the required optimum value as can be seen from eqn. 7.31. In addition, the average gain and the excess noise factor for a 10-stage SAPD with k=0.01 and p=0.4 have been calculated numerically from the first and second derivatives of the corresponding $M_{g_N}(s)$ evaluated at s=0; they are found to be in excellent agreement with those obtained analytically. The same procedure has been repeated for other cases and similar results are obtained.

7.3 Optical Receiver Performance

In this section we evaluate the performance of SAPD-based optical receivers using the complete statistics of the detection process as outlined previously. The results are compared with those obtained utilizing the conventional Gaussian approximation which is based on the mean and variance of the detection process. Illustrative results are presented for a SAPD/FET front-end optical receiver operating at $\lambda=1.5\mu$m and a bit rate of 2Gbit/s. Return to zero (RZ) signal format with 50% duty cycle is assumed for the input optical pulses while the shape of the signal at the decision circuit is taken to correspond to a full raised-cosine element spectrum to ensure zero intersymbol interference. Unless otherwise stated, the following parameters have been used to obtain the numerical results: $I_g=2$nA, $g_m=40$ mS, $\Gamma=1.78$, $C_t=1$ pF, $R_L=22$ kΩ, $\eta=1$, $\Theta=300$K, and $p_o=p_1=0.5$ (equal *apriori* binary element probabilities). We note also that in these calculations the gain bandwidth product of the detector is assumed to be very high.

7.3.1 Ideal SAPD (k=0)

Here illustrative results are presented for a single carrier multiplication-SAPD (i.e. k=0). Figs. 7.4a and 7.4b show the BER characteristics for N=5 and N=10 respectively as a function of the average number of detected photons per bit. These calculations are performed for p=0.5 and assuming zero dark current. The broken line corresponds to an accurate performance evaulation based on use of the modified Chernoff bound (MCB) making use of the full avalanche gain MGF characterisation while the solid line refers to a Gaussian approximation (GA). It is clear from these figures that the GA is in good agreement with the more precise and soundly based MCB

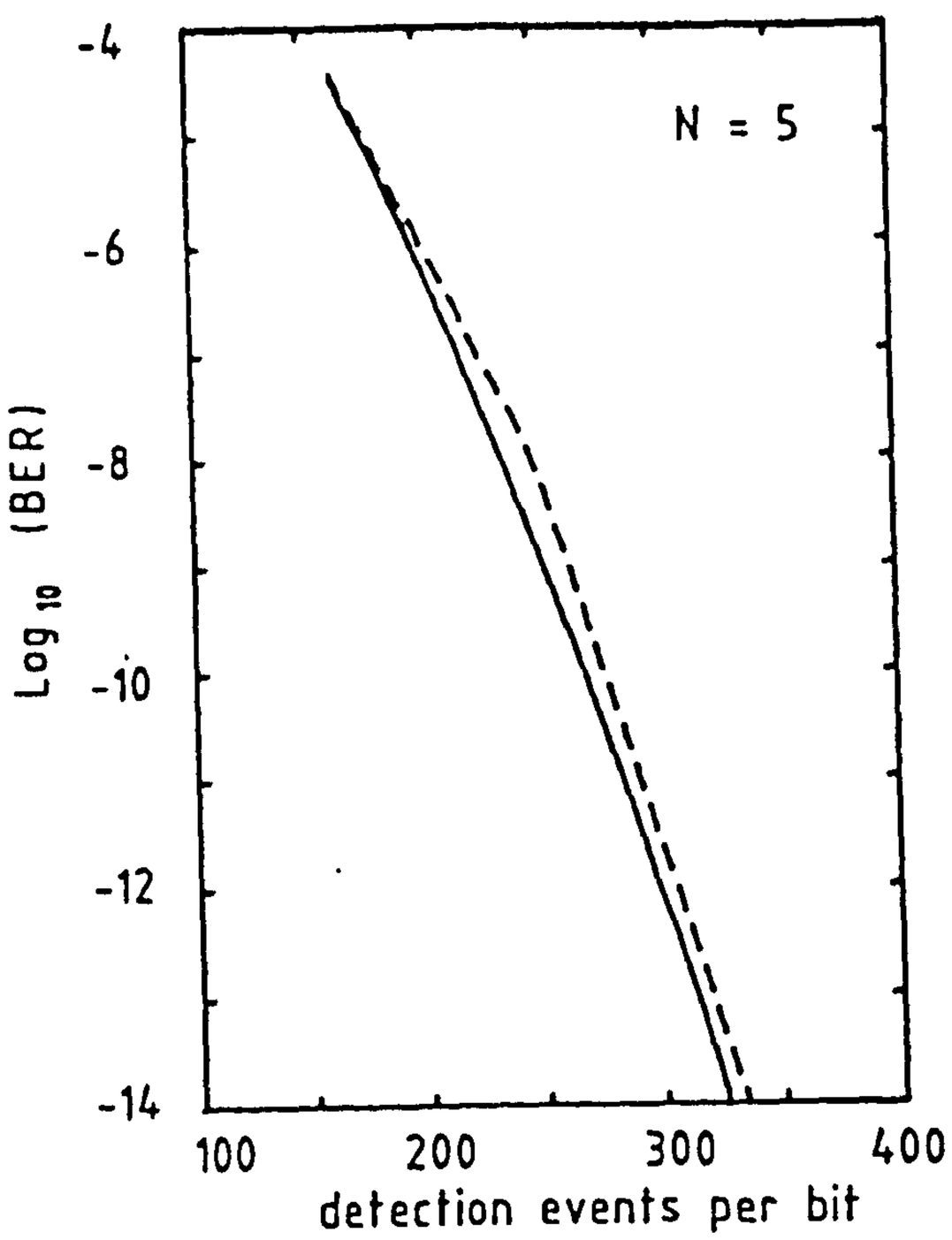

(a)

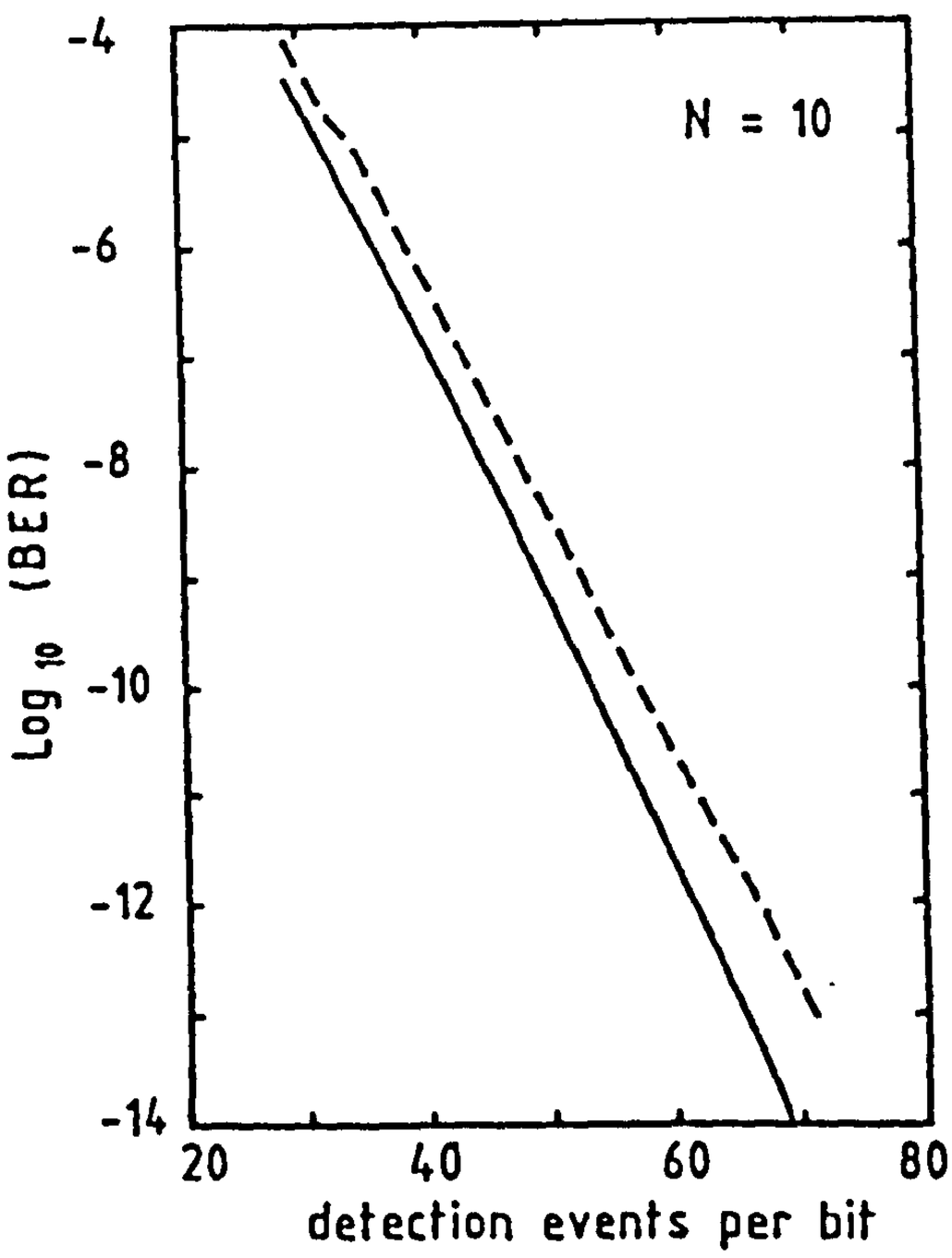

(b)

Fig. 7.4 Bit error rate (BER) characteristics of optical receiver employing ideal SAPD. p=0.5, k=0 and dark current=zero.
(a) N=5 (b) N=10 ——— GA - - - MCB

formulation. The small discrepancy between the two approaches is slightly greater for the N=10 case. This can be explained as follows. Both ideal devices will behave as low noise APDs. The sensitivity of a N=5 receiver is less than that for the N=10 case due to the lower gain associated with the 5-stage device. This corresponds to higher optical power incident on the detector and hence the density of detected events is larger. In this case the Poisson shot noise process tends to approach more closely a Gaussian process.

To carry this calculation further, we plot in Fig. 7.5 the receiver sensitivity as a function of electron ionisation probability p, assuming an ideal SAPD with 5 stages. The results are displayed for BER=10^{-9} and assuming two values of dark current: zero dark current (Fig. 7.5a) and 100nA dark current, taken to be generated uniformly among the various stages (Fig. 7.5b). The optimum threshold levels used in these calculations, obtained from eqn. 7.9 are also shown in the figures. For comparison purposes both MCB and GA techniques are used to estimate the receiver performance. Note that the detectable optical power required to achieve BER=10^{-9} decreases (i.e. the sensitivity improves) as p increases, with optimum sensitivity being obtained at p=1. This occurs because as p increases the average gain of the detector increases dramatically ($<g_N>=(1+p)^N$) while the device still behaves as a low noise detector. It is worth noting here that the GA can estimate quite accurately the receiver sensitivity for all values of p. Similar conclusions may be drawn for the threshold level for $p<0.7$, as shown in Fig. 7.5b.

To proceed further, we now repeat the same calculations for the 10-stage device, as shown in Fig. 7.6. Again sensitivity calculations estimated by the MCB and by a GA are found to be in good agreement.

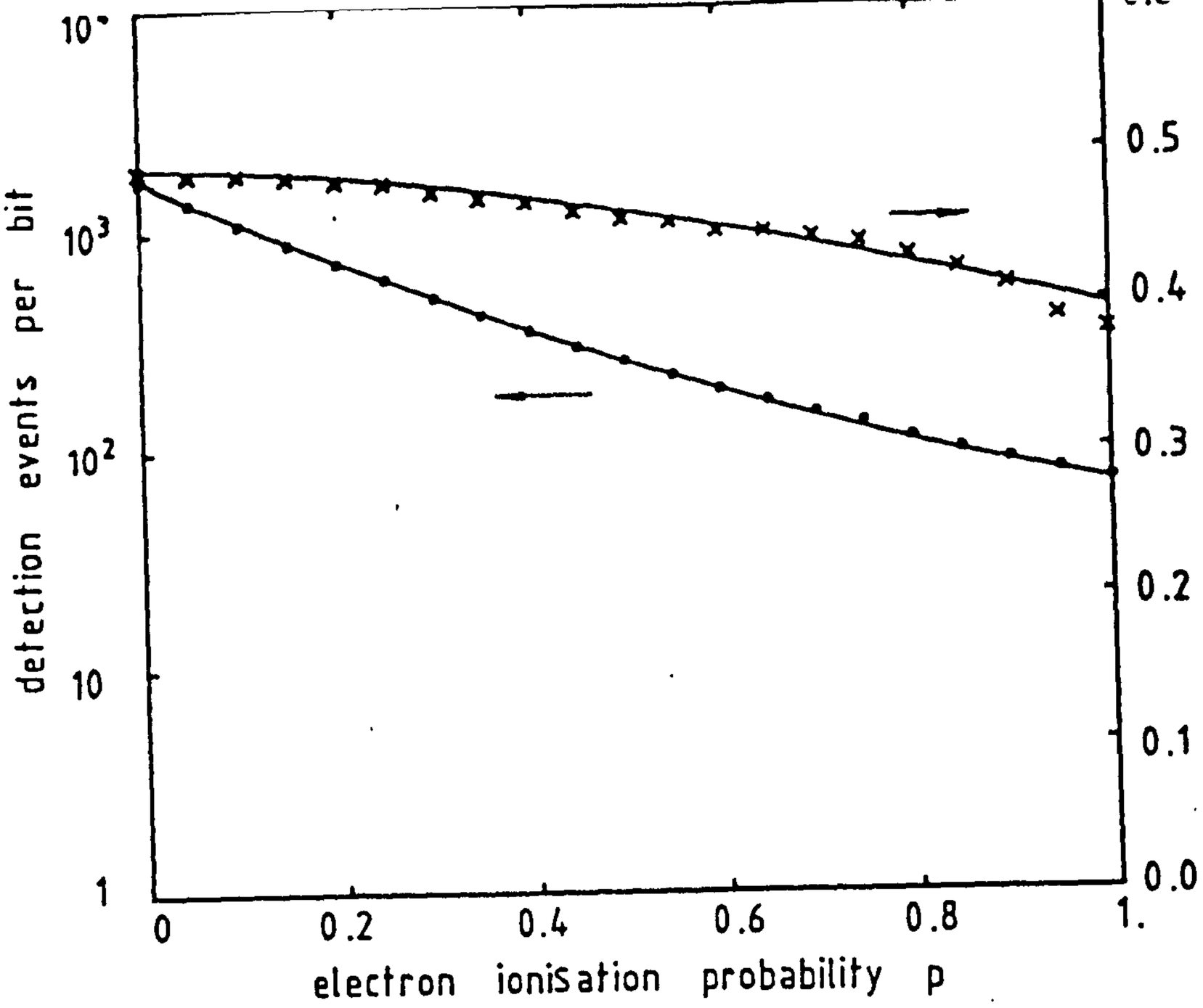

(a)

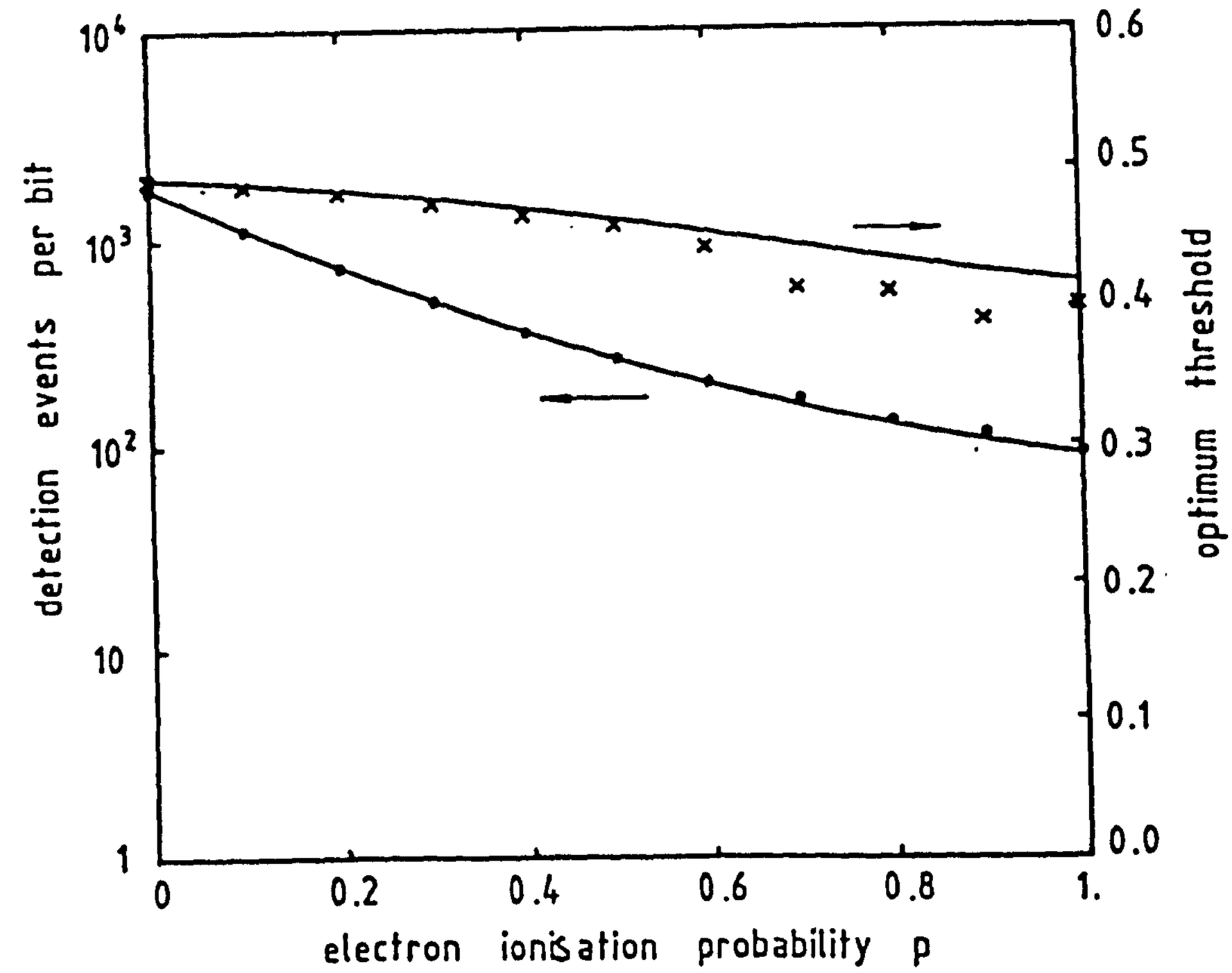

(b)

Fig. 7.5 Performance of optical receivers employing 5-stage SAPD as a function of electron ionisation probability. k=0, BER=10^{-9}.

(a) zero dark current (b) 100 nA dark current

—— GA marks: MCB

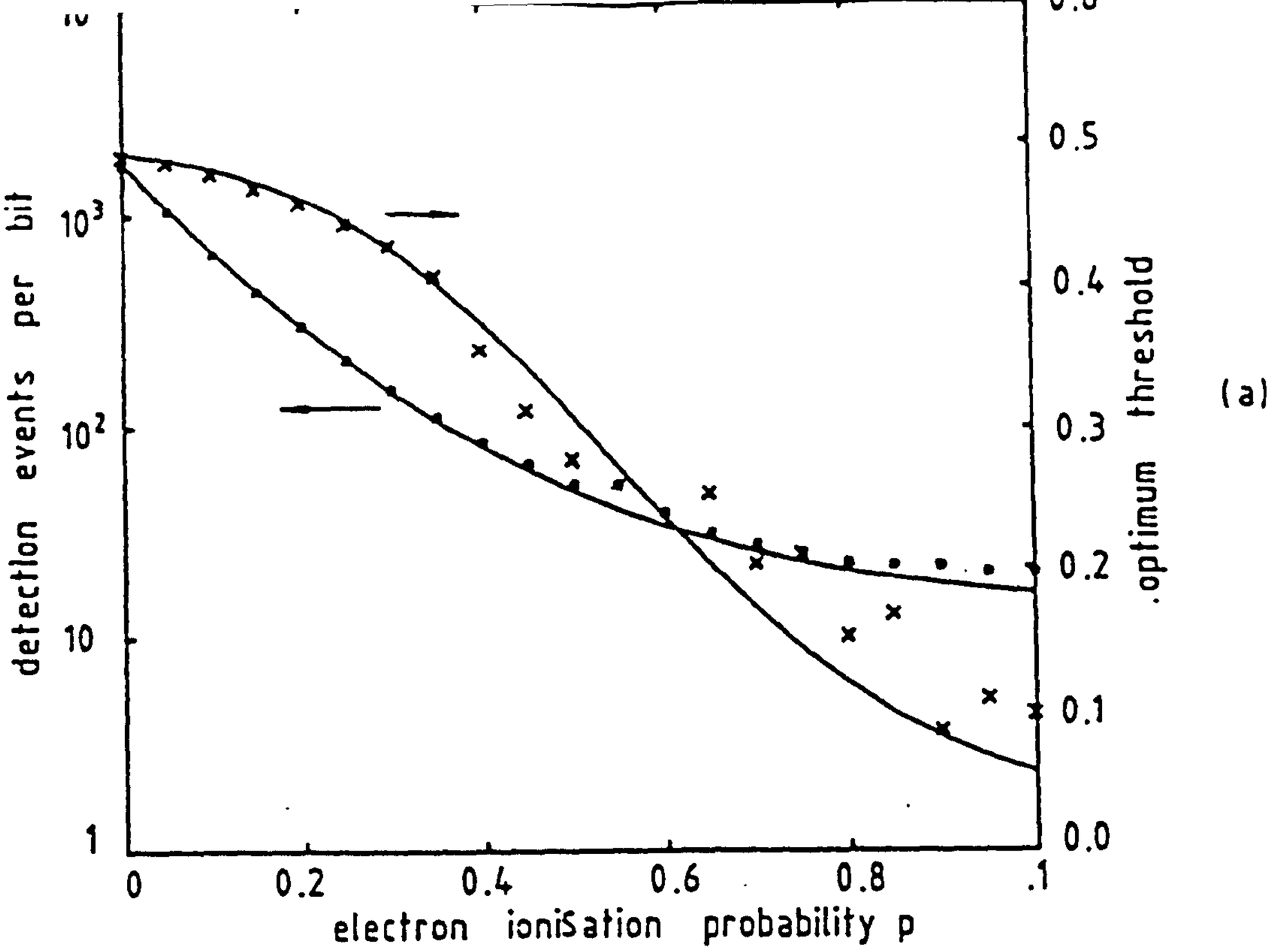

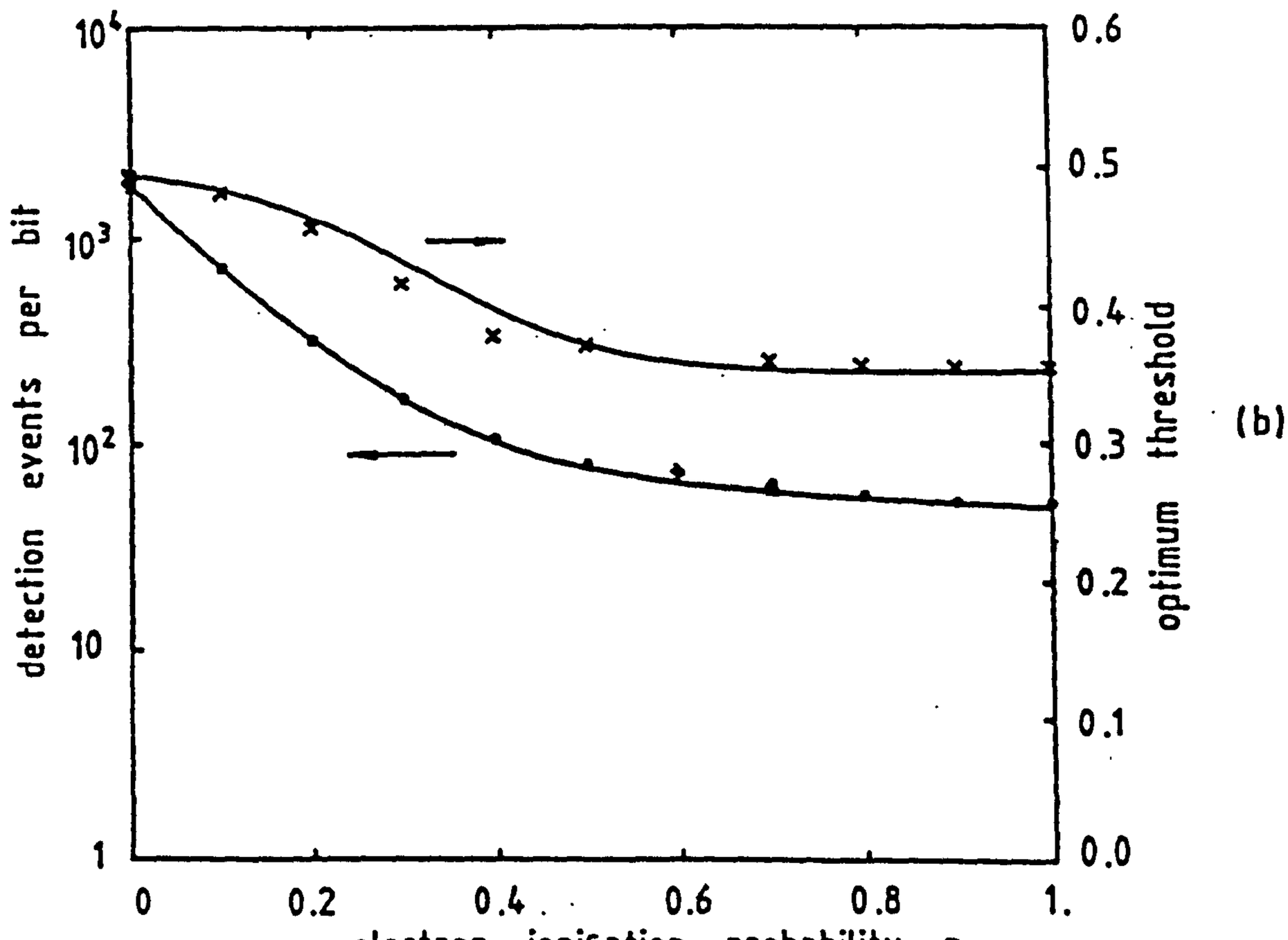

Fig. 7.6 As in Fig. 7.5, but with N=10 stages.

However, the GA fails to predict accurately the threshold level at higher values of p when dark current is negligible (Fig. 7.6a). Note that a 10-stage device can offer improved sensitivity compared with a 5-stage detector, assuming negligible dark current. However the existence of just 100nA dark current degrades significantly the performance of the former receiver. This is attributable mainly to the higher gain associated with N=10. On the other hand, the average number of detected photons per bit required to achieve BER=10^{-9} for N=10, p=1 is 16 (based on a GA) which is greater than the 10.5 photons per bit representing the quantum limit. This difference is attributable mainly to the equalisation stage used in the receiver to ensure zero intersymbol interference and in part also to circuit and multiplication noise.

Comparing the threshold curves plotted in Fig. 7.5 and 7.6 we may note the following: When p=0 (where $<g_N>=1$) so that both devices behave as a PIN detector) the threshold is set at 0.5 since the noise associated with a detected binary "0" is for practical purposes equal to that associated with a binary "1". This corresponds to an additive Gaussian noise-limited receiver. As p increases, lower values of threshold are expected due to higher noise associated with a binary "1" in view of the multiplication process. The presence of dark current tends to restore the balance in the noise associated with both symbols, hence the optimum threshold increases towards 0.5 again.

7.3.2 Nonideal SAPD (k > 0)

Single carrier multiplication is an obvious goal in designing high performance SAPDs. Unfortunately, practical results and theoretical simulations indicate that residual hole ionisation is

still a problem in these devices. Here we present some results related to these nonideal detectors (that is $k>0$). We start with a single stage device, $N=1$. This case has attracted attention recently as a high speed photodetector with a low ratio of excess noise to gain. Fig. 7.7a shows the number of detected photons per bit required to achieve BER$=10^{-9}$, as a function of ionisation rate ratio, taking p as a parameter and with zero dark current being assumed. Fig. 7.7b is a plot of the optimum threshold level used in these calculations. It is clear that the results obtained by the GA approach are in excellent agreement with those predicted by the fundamentally more sound MCB, both for receiver sensitivity and threshold evaluation. This may be attributed mainly to the low noise operation - even with the existence of residual hole ionisation - of a single stage device. Inspection of Fig. 7.7a shows that substantial improvement in receiver sensitivity occurs when $p=1$ and k tends to 1. This is illustrated further in Table 7.1 which shows the required number of photons per bit for four different values of k, assuming $p=1$. Here the GA slightly underestimates the required number of detected photons.

TABLE 7.1

Performance of an optical receiver incorporating a single stage SAPD BER$=10^{-9}$.

k	number of detected photons per bit	
	GA	MCB
0.01	895.2	900.2
0.1	816.5	821.5
0.8	209	213
0.9977	31.7	27.6

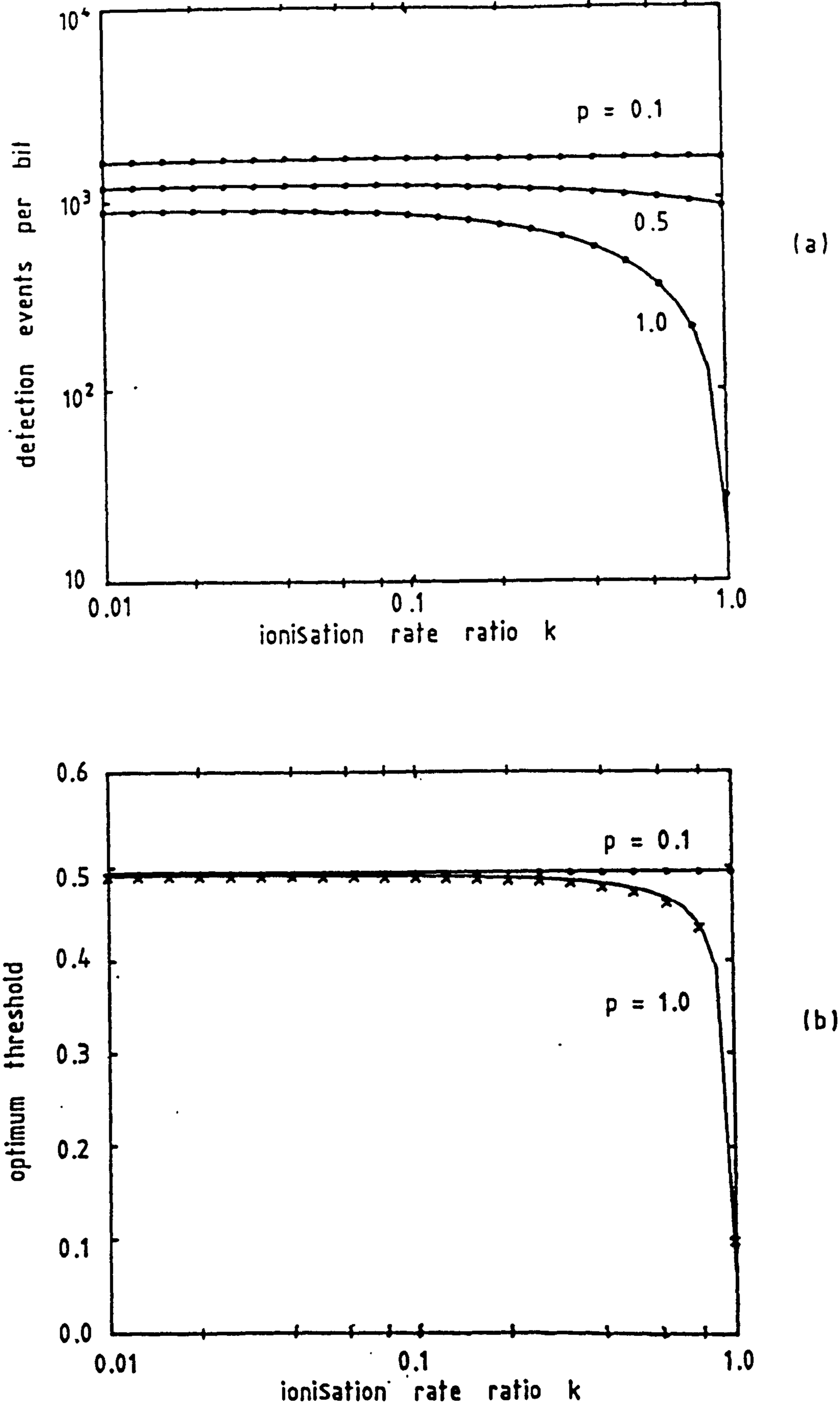

Fig. 7.7 Performance of optical receiver incorporating single stage SAPD as a function of ionisation rate ratio.

——— GA marks: MCB

Typical BER characteristics for an optical receiver using a nonideal 5-stage SAPD are shown in Fig. 7.8, together with the corresponding optimum threshold. Results are presented for zero dark current and assuming p=0.8, k=0.01 (Fig. 7.8a) and p=0.4, k=0.1 (Fig. 7.8b). Solid lines and closed circles refer to the GA and MCB respectively. The steps indicated in the MCB threshold derive from numerical imprecision and do not have specific practical significance. Although the GA overestimates slightly the receiver sensitivity, it is still in close agreement with the MCB. Similar remarks may be made in relation to Fig. 7.9, where a 10-stage detector is considered. A brief summary of the characteristics of both receivers for BER=10^{-9} is presented in Table 7.2. Note that the GA can predict the receiver

TABLE 7.2

Summary of results for 5-stage and 10-stage SAPD-receivers. BER=10^{-9}.

N	p k	gain $\langle g_N \rangle$	photons/bit		sensitivity (dBm)		threshold	
			GA	MCB	GA	MCB	GA	MCB
5	0.8 0.01	26.39	88	93.60	-46.3	-46.05	.383	.396
	0.4 0.1	9.44	220.6	236.8	-42.33	-42.02	.426	.437
10	0.4 0.01	44.74	67.56	71	-47.47	-47.25	.294	.308
	0.2 0.1	11.137	197.4	210.6	-42.8	-42.53	.404	.417

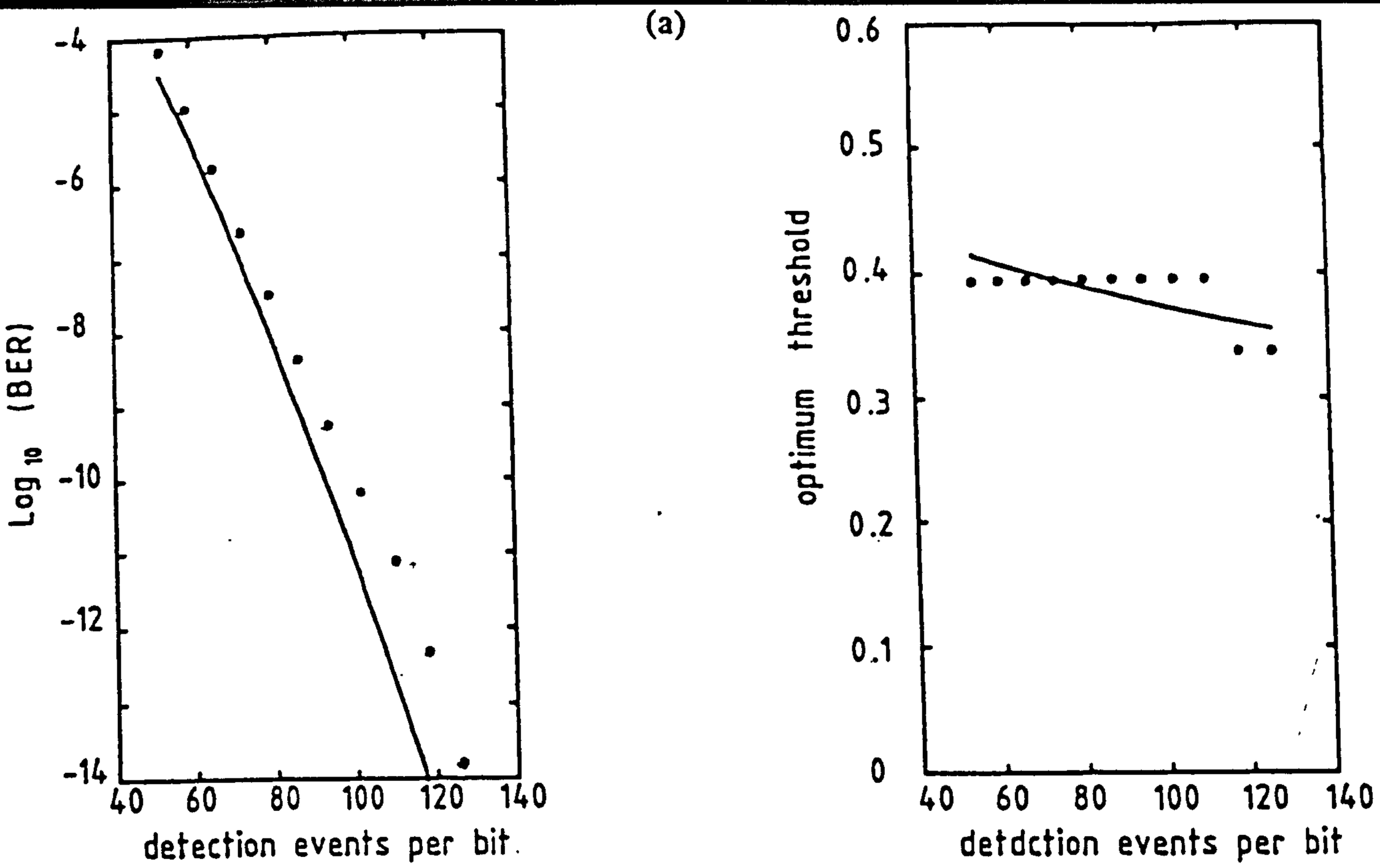

Fig. 7.8 BER characteristics and optimum threshold level for optical receiver employing nonideal 5-stage SAPD.

(a) p=0.8, k=0.01 (b) p=0.4, k=0.1

——— GA • • • MCB

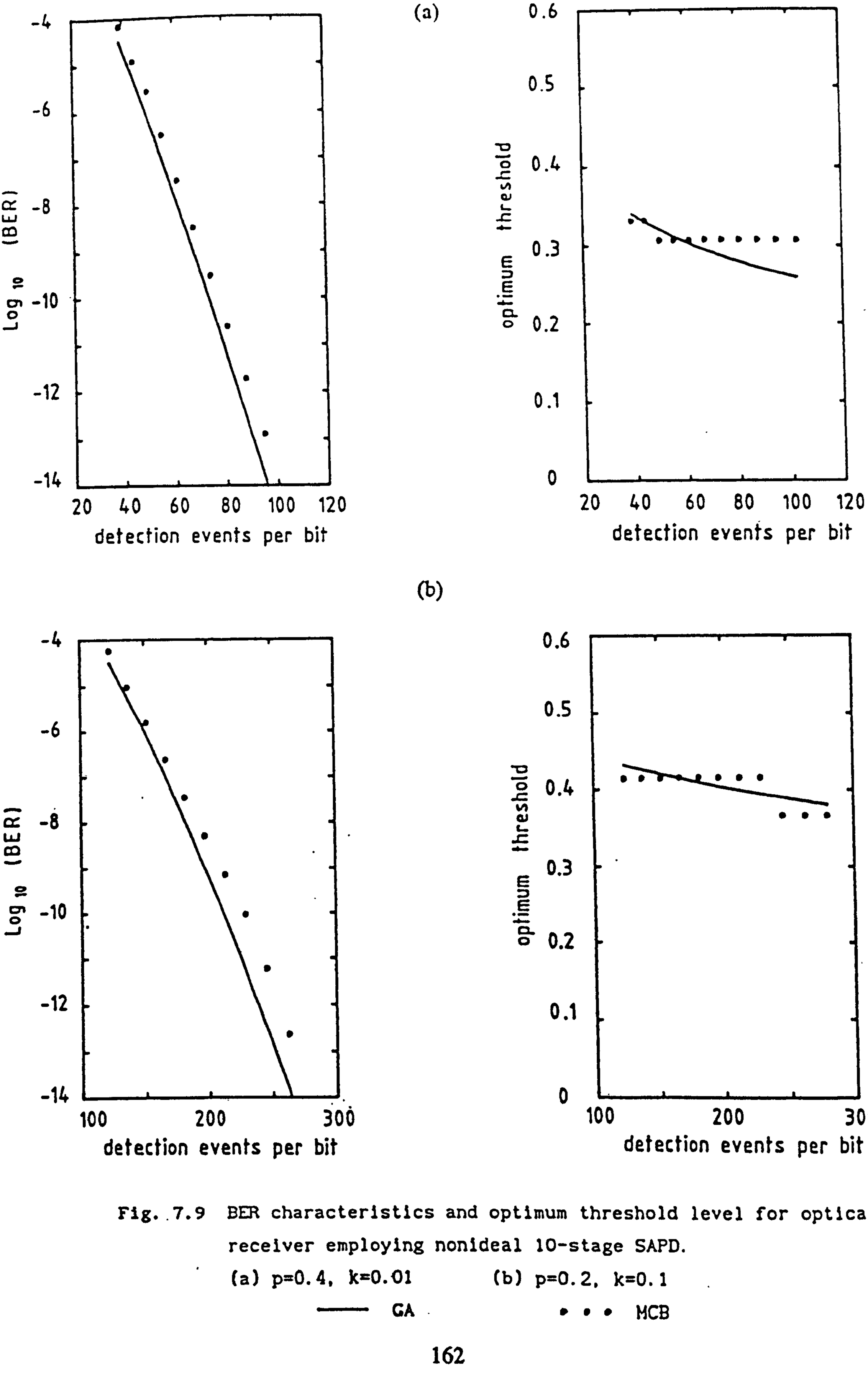

Fig. 7.9 BER characteristics and optimum threshold level for optical receiver employing nonideal 10-stage SAPD.
(a) p=0.4, k=0.01 (b) p=0.2, k=0.1
—— GA • • • MCB

sensitivity within 0.3 dB compared with the MCB. We note also that it slightly underestimates the optimum threshold.

To investigate the optimum SAPD gain required to achieve minimum detectable optical power we plot in Figs. 7.10 and 7.11 the variation of BER as a function of SAPD gain under constant optical power for N=5 and N=10, respectively. Figs. 10a and 11a correspond to an average incident optical power level of 100 photons/bit and k=0.01, while Figs. 10b and 11b correspond to 200 photons/bit and k=0.1. In addition, the optimum threshold levels used in these calculations are also shown in these figures. Note that there is a well-defined optimum gain at which BER is minimum, although the GA overestimates the optimum gain, as ilustrated in Table 7.3. While the difference between the minimum values of BER estimated by the MCB and the GA may seem to be relatively high it should be noted that this corresponds to only a

TABLE 7.3

Optimum electron ionisation probability p_{opt} and optimum gain $\langle g_N \rangle_{opt}$ required to achieve minimum detectable optical power

no. of stages	ionisation rate ratio	optimum probability p_{opt}		optimum gain $\langle g_N \rangle_{opt}$	
N	k	GA	MCB	GA	MCB
5	0.01	1.0	0.97	75.1	61.82
	0.1	0.493	0.477	29.38	22.38
10	0.01	0.4485	0.43	87.23	76.295
	0.1	0.236	0.23	28.9	23.06

(a)

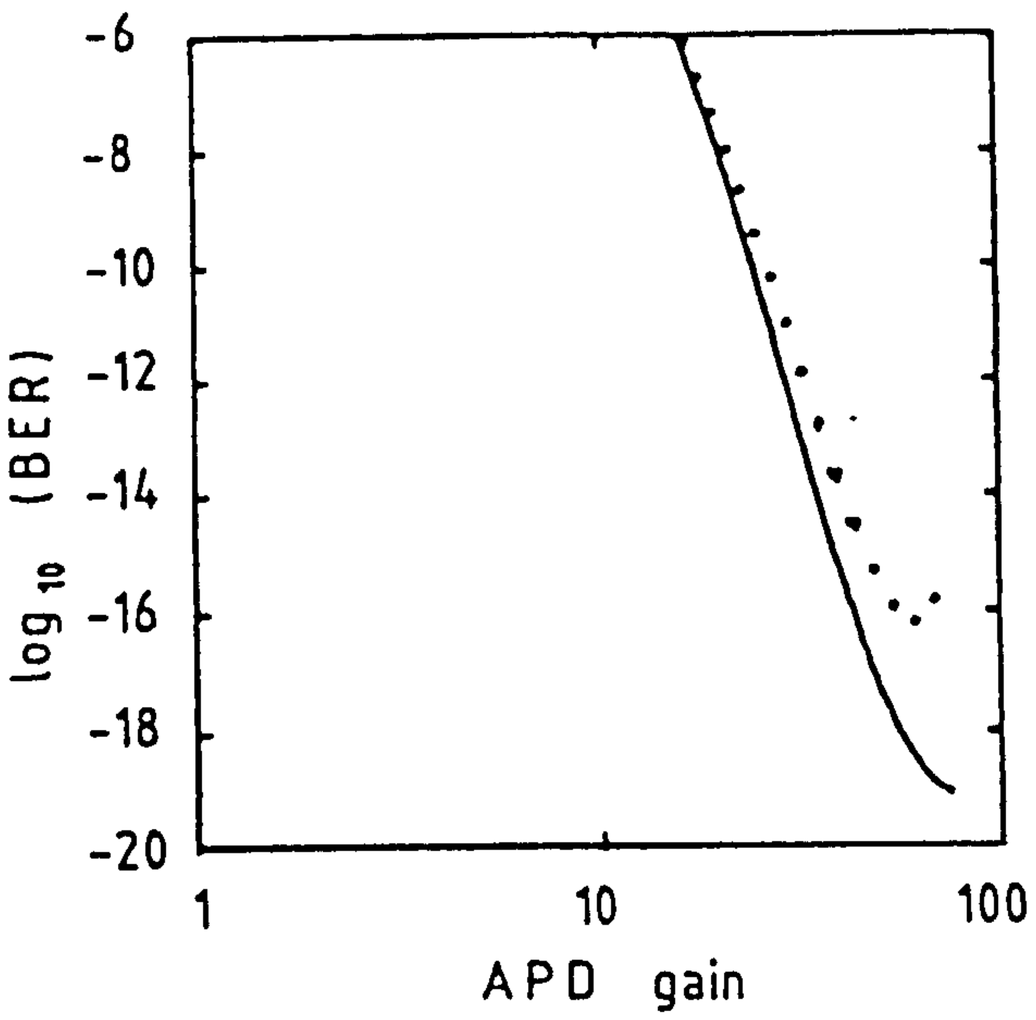

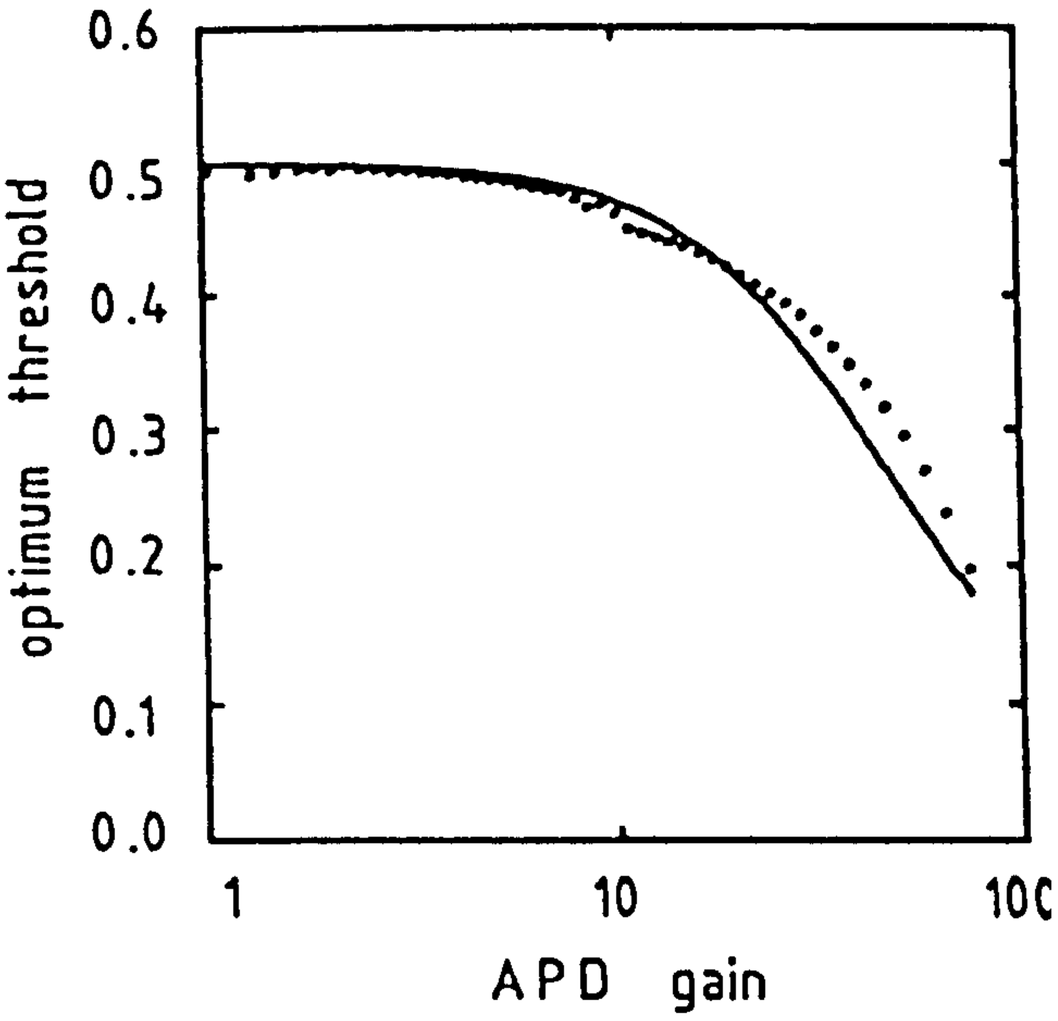

(b)

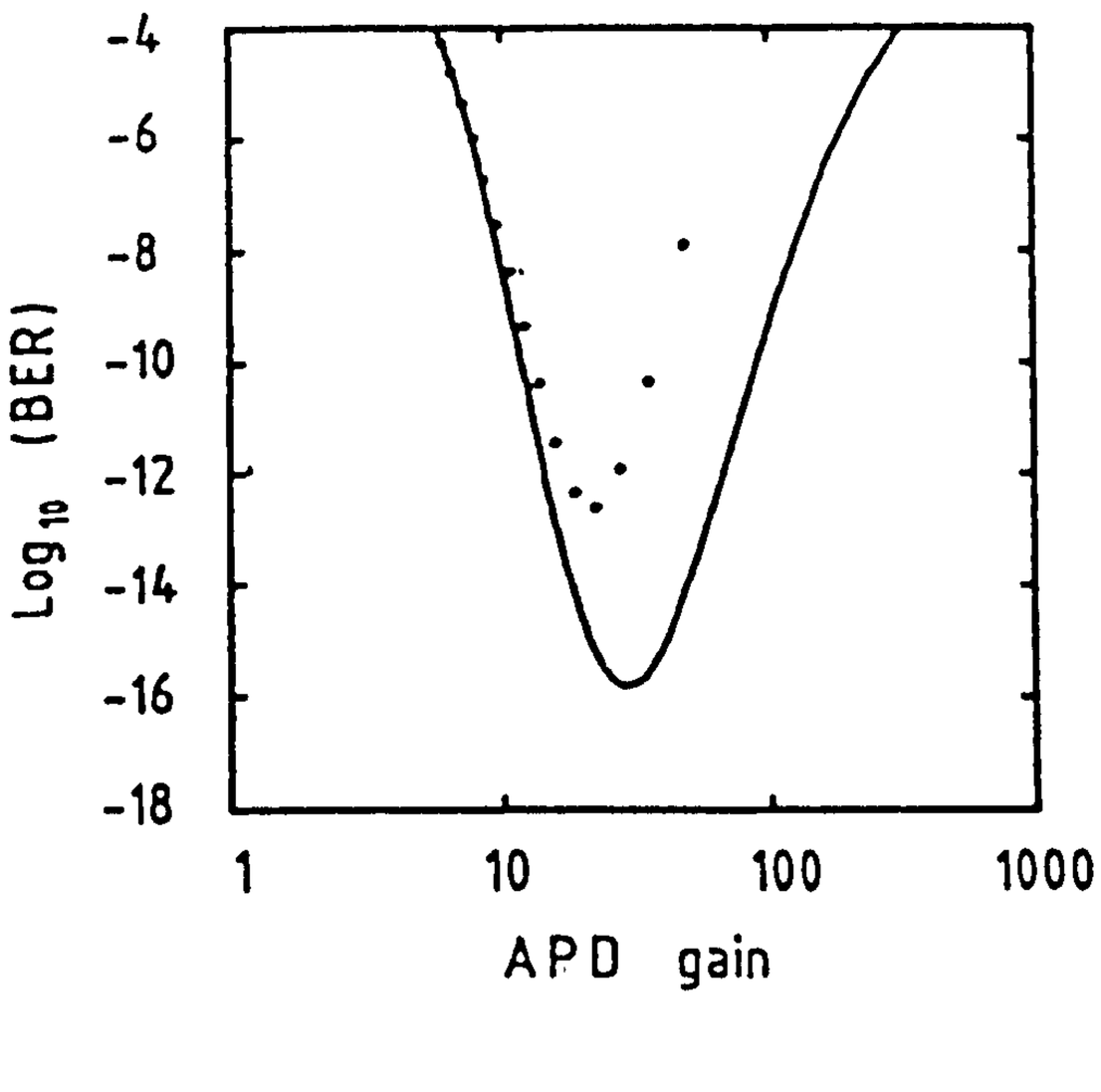

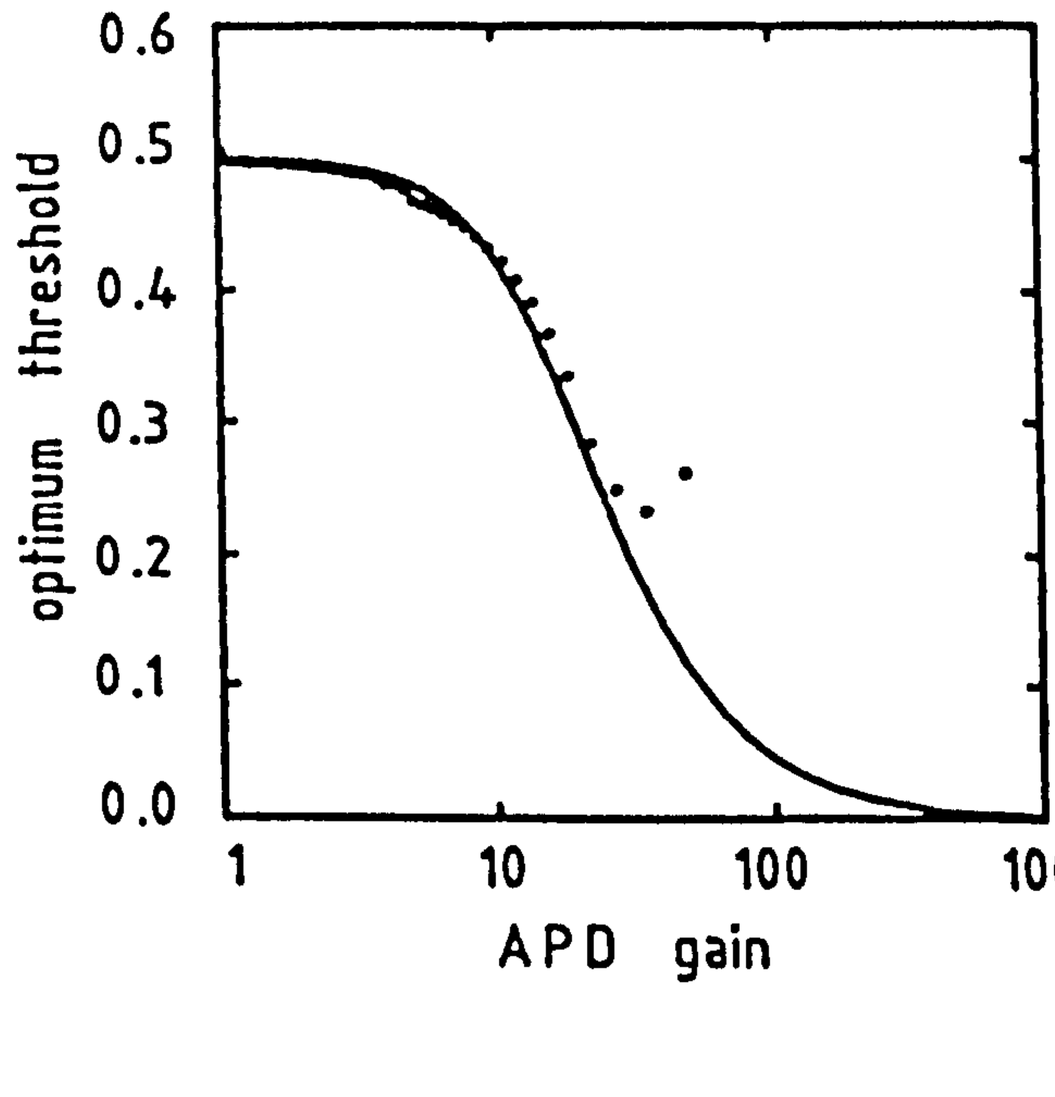

Fig. 7.10 Variation of BER and optimum threshold as a function of SAPD gain, assuming N=5.

(a) average detection events/bit =100, k=0.01

(b) average detection events/bit =200, k=0.1

——— GA • • • MCB

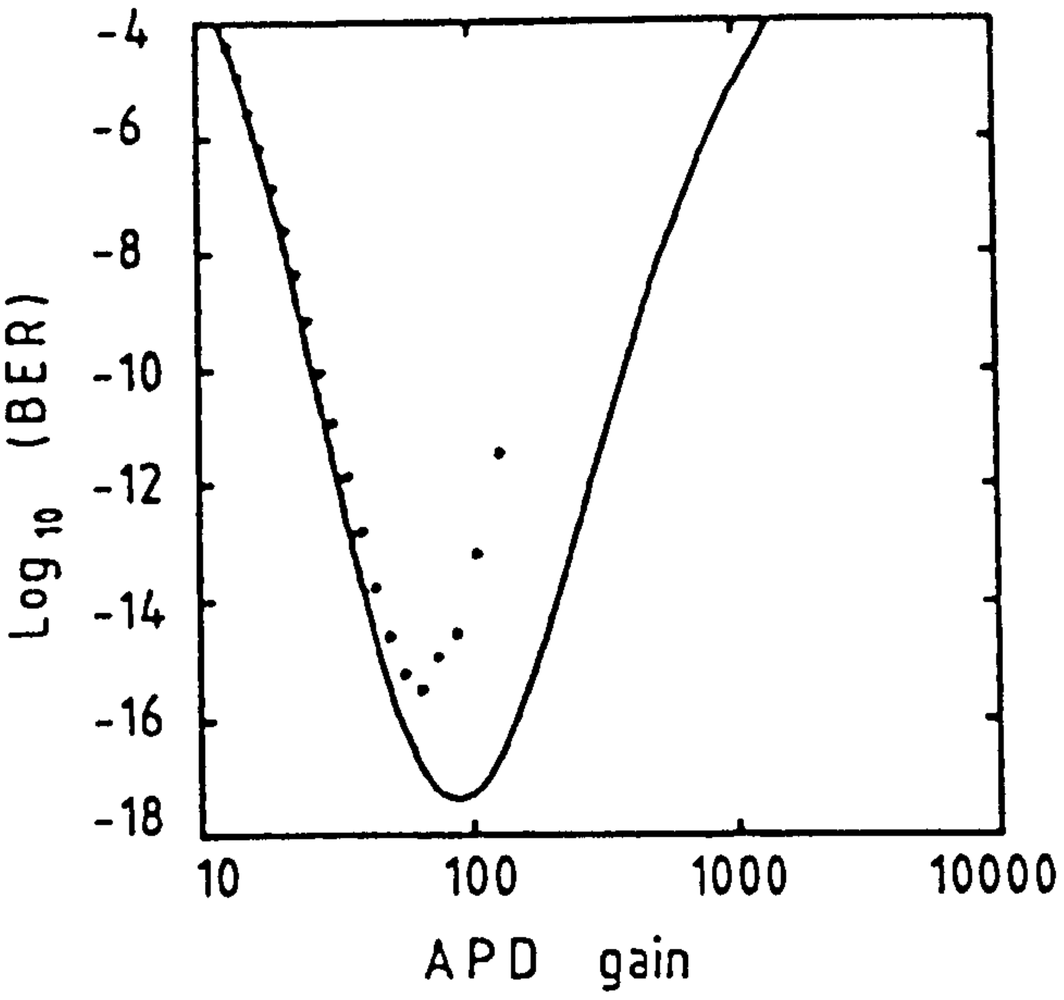

Fig. 7.11 As in Fig. 7.10, but with N=10 stages.

small change in receiver sensitivity since BER varies rapidly with signal power in this region. We also emphasise that for most cases the predection of optimum threshold based on a GA is in good agreement with that obtained using the MCB.

7.4 Summary

A gain moment generating function formulation for SAPDs has been developed and evaluated numerically taking into account the effect of residual hole ionisation. This has been used as a basis for a rigorous analysis of optical receivers utilising these advanced detectors. We have described a statistical model for the detection process using the modified Chernoff bound (MCB) and the moment generating function (MGF) of the signal at the input to the decision circuit. This model has enabled us to assess accurately receiver performance in the presence of hole ionisation and dark current generated in the various stages of the detector. The Gaussian approximation (GA) was also investigated and compared with more precise and formally based calculations using the complete statistics of the detection process. The results indicate that for SAPD receivers the GA can predict quite accurately receiver sensitivity whilst overestimating slightly the optimum gain. The optimum threshold predicted by the GA has also been found to be in good agreement with that predicted using the MCB for most cases considered here.

The development presented here has provided precise performance evaluation tools. These are based soundly on a moment generating function formulation encapsulating the entire statistics of the underlying stochastic processes associated with the signal and noise components. This has enabled a detailed analytic investigation of the

performance of advanced SAPD optical receivers to be undertaken and a comparison effected with performance predictions based on the widely adopted Gaussian approximation which uses only first and second order statistics. The results of the study clearly validate the simple GA approach enabling it to be adopted henceforth with complete confidence for practical system studies and comparison. The simplicity and ease of calculation of the GA justifies this approach as an efficient tool for system design engineers to use as the basis for rapid prediction of the performance of optical receivers.

In this and previous chapters, the performance of optical receivers has been estimated under the assumption that the gain bandwidth product of the APD is extremely large so as not to impose any limitation on system performance. In practice, this parameter could prove to be a limiting factor for the performance of gigabit per second systems. Accordingly, the next chapter, we discuss the speed of response of SAPDs, and the effect on performance of high bit rate lightwave receivers.

CHAPTER 8

FREQUENCY RESPONSE CHARACTERISATION OF SAPDS

In this chapter we will discuss the speed of response of superlattice avalanche photodiodes (SAPDs) and the effect on the performance of multigigabit-per-second lightwave receivers. An expression for the frequency response of single carrier multiplication SAPDs is presented, providing an estimate for the maximum gain bandwidth (GB) product which can be achieved with ideal devices. The existence of residual hole ionisation degrades GB product mainly due to avalanche build-up time, arising from the regenerative nature of the avalanche process. In this case the GB product is found to be inversely proportion al to the width of the multiplication region W and directly proportional to the number of stages N, especially when N is large. Sensitivity calculations for equalised GB-limited SAPD receivers are presented which take into account the effects of both residual hole ionisation and the width of the avalanche region. The analyses should provide useful guidelines for the design of high bit rate optical receivers employing SAPDs.

8.1 General Remarks

The speed of response of APDs can be an important factor in determining the performance of high bit rate optical receivers. In general, heterojunction conventional APDs (CAPDs) and superlattice APDs (SAPDs) have response speeds which are limited by various physical processes [Forrest, 1984; Kasper and Campbell, 1987; Mattera et al., 1986]. The most common sources of speed degradation are: RC

time constant resulting from the finite capacitance of the diode C together with load resistance R, charge accumulation at the heterointerfaces, the transit time of carriers through the depletion region, and the gain bandwidth (GB) product due to avalanche build-up time arising from the regenerative nature of the avalanche process. Proper device design enables the effect of the RC time constant to be reduced by choosing small values for R and C (a well-designed APD can have a time constant of the order of 10ps). Response speed limitations due to charge trapping at the interfaces can be lessened by grading the interface [Capasso et al., 1983; Campbell et al., 1988; 1989b] or by using higher electric fields there [Osaka and Mikawa, 1986; Brennan and Wang, 1988]. The latter solution may lead to higher tunnelling dark current but this has little influence on the sensitivity of optical receivers operating at high bit rates [Smith and Forrest, 1982]. Thus the speed of these detectors is intrinsically limited by the total time for both the primary and secondary carriers to be swept out of the depletion region.

It should be noted that while the results developed in the following sections are based on considerations of staircase APDs, they are also applicable to other SAPDs in which carrier transport is perpendicular to the superlattice planes.

8.2 Frequency Response of Ideal SAPDs

The target in designing SAPDs is that only one species of carrier (electrons or holes) should impact ionise, thereby eliminating the feedback noise associated with two-carrier CAPDs. Such ideal devices can provide low noise and high speed detection for the optical signal. In this section we shall discuss the time response and frequency

response of such ideal SAPDs.

Matsuo et al. [1985] have analysed the time response of a staircase APD due to a single photon absorbed in the p^+ region. In their treatment they assumed the width of the p^+ region to be negligible. The current pulse i(t) arising from a single photon absorbed at t=0 is the superposition of contributions from the initial electron and from the secondary electrons and holes created at the steps. It is given by

$$i(t) = a_0(t) + p\sum_{k=1}^{N}(1+p)^{k-1}\left[a_k(t) + b_k(t)\right] \qquad (8.1)$$

where p is the probability for the electron to impact ionise at the step and N is the total number of stages. Further, $a_0(t)$, $a_k(t)$ and $b_k(t)$ are respectively the current pulses arising from the primary electron, secondary electron and secondary hole created at the k^{th} step, given by*

$$a_k(t) = \frac{q}{N\tau_e}\left[\,U(t-k\tau_e) - U(t-N\tau_e)\,\right] \qquad 0\leq k\leq N \qquad (8.2)$$

$$b_k(t) = \frac{q}{N\tau_h}\left[\,U(t-k\tau_e) - U(t-k(\tau_e+\tau_h))\,\right] \qquad 1\leq k\leq N \qquad (8.3)$$

where q is the electronic charge, U(.) denotes a unit step function and $\tau_e(\tau_h)$ is the time it takes the electron (hole) to drift across a single stage. Note that eqns. 8.1-8.3 employ a deterministic

---

* *Note that for the structure considered here (see Fig. 2.2), the total transit time for the electron to dirft across the entire device is equal to $N\tau_e$ in contrast to $(N+1)\tau_e$ adopted by Matsuo et al. [1985].*

$$\tau_e = W/(Nv_e) \tag{8.4a}$$

$$\tau_h = W/(Nv_h) \tag{8.4b}$$

where W is the width of the depletion region and $v_e(v_h)$ is the average speed of electrons (holes) in the device. We note here that while the above expressions for i(t) are derived assuming short circuit operation, the effect of a finite RC time constant is readily included simply by considering each current pulse arising from a hole or electron to charge the capacitance C through load resistance R.

The frequency response of an ideal staircase APD can be obtained by taking the Fourier transform of the impulse response given in eqn. 8.1. Thus

$$I(j\omega) = \frac{q}{j\omega N\tau_e}\left[1-\exp(-j\omega N\tau_e)\right] + p\sum_{k=1}^{N}(1+p)^{k-1}\left[\frac{q}{j\omega N\tau_e}\left[\exp(-j\omega k\tau_e) - \exp(-j\omega N\tau_e)\right] + \frac{q}{j\omega N\tau_h}\left[\exp(-j\omega k\tau_e) - \exp\left[-j\omega k(\tau_e+\tau_h)\right]\right]\right] \tag{8.5}$$

where ω is the angular frequency. Eqn. 8.5 can be simplified further by recognising the summation as a geometric series, giving:

$$I(j\omega) = \frac{q}{j\omega N\tau_e}\left[1-\exp(-j\omega N\tau_e)\right] + \frac{pq}{j\omega N\tau_e}\left[\frac{(1+p)^N\exp(-j\omega N\tau_e)-1}{(1+p)-\exp(j\omega\tau_e)} - \left[\frac{(1+p)^N-1}{p}\right]\exp(j\omega N\tau_e)\right] + \frac{pq}{j\omega N\tau_h}\left[\frac{(1+p)^N\exp(-j\omega N\tau_e)-1}{(1+p)-\exp(j\omega\tau_e)}\right.$$

$$- \frac{(1+p)^N \exp[-j\omega N(\tau_e+\tau_h)]}{(1+p)-\exp[j\omega(\tau_e+\tau_h)]} \Bigg] \tag{8.6}$$

Note that $I(0)=q(1+p)^N$, where $(1+p)^N$ is the dc gain of the diode. The real and imaginary parts of the transfer function can be expressed as

$$\begin{aligned}\mathrm{Re}[I(j\omega)] &= A_1\sin(\omega N\tau_e) + A_2(1+\tau_e/\tau_h)\sin(\omega\tau_e)\Big[(1+p)^N\cos(\omega N\tau_e)-1\Big] \\ &- A_2(1+\tau_e/\tau_h)\Big[(1+p)^N\sin(\omega N\tau_e)\Big[(1+p)-\cos(\omega\tau_e)\Big]\Big] \\ &+ A_3\sin(\omega N\tau_e) - A_4\sin(\omega(\tau_e+\tau_h))\Big[(1+p)^N\cos(\omega N(\tau_e+\tau_h))-1\Big] \\ &+ A_4(1+p)^N\sin(\omega N(\tau_e+\tau_h))\Big[(1+p)-\cos(\omega(\tau_e+\tau_h))\Big] \end{aligned} \tag{8.7}$$

$$\begin{aligned}\mathrm{Im}[I(j\omega)] &= -A_1\Big[1-\cos(\omega N\tau_e)\Big] - A_2(1+\tau_e/\tau_h)\Big[(1+p)^N\cos(\omega N\tau_e)-1\Big] \\ &\cdot\Big[(1+p)-\cos(\omega\tau_e)\Big] - A_2(1+\tau_e/\tau_h)(1+p)^N\sin(\omega N\tau_e)\sin(\omega\tau_e) \\ &+ A_3\cos(\omega N\tau_e) + A_4\Big[(1+p)^N\cos(\omega N(\tau_e+\tau_h))-1\Big]\Big[(1+p)-\cos(\omega(\tau_e+t_h))\Big] \\ &+ A_4\sin(\omega(\tau_e+\tau_h))(1+p)^N\sin(\omega N(\tau_e+\tau_h)) \end{aligned} \tag{8.8}$$

where

$$A_1 = q/(\omega N\tau_e) \tag{8.9a}$$

$$A_2 = \frac{pq}{\omega N\tau_e\left[[(1+p)-\cos(\omega\tau_e)]^2 + \sin^2(\omega\tau_e)\right]} \tag{8.9b}$$

$$A_3 = \frac{q[(1+p)^N-1]}{\omega N\tau_e} \tag{8.9c}$$

$$A_4 = \frac{pq}{\omega N\tau_h\left[[(1+p)-\cos(\omega(\tau_e+\tau_h))]^2 + \sin^2(\omega(\tau_e+\tau_h))\right]} \tag{8.9d}$$

It is appropriate to note that the above equations can be used to describe the frequency response of ideal CAPDs by letting the number of stages N tend to infinity with the width of each stage approaching zero. With such a procedure we recover eqn. 13 of ref. [Teich et al., 1986c].

In Fig. 8.1 we present the impulse response and the frequency response (both magnitude and phase) for a device with N=5, p=0.5. The results are calculated from eqns. 8.1, 8.7 and 8.8 assuming $\tau_e=\tau_h$. Similar results relating to N=10 are shown in Fig. 8.2 for comparison. In Figs. 8.1a and 8.2a the ordinate represents current (in units of q/τ_e) whereas the abscissa represents normalised time (in units of t/τ_e). In Figs. 8.1b and 8.2b the lower abscissa represents normalised frequency (in units of $\tau_e f$) and the upper abscissa denotes illustrative actual frequency values (in GHz) assuming $v_e=v_h=10^7$ cm/s and 0.2μm for the stage width. Note that the total area underneath the impulse response function corresponds to the average dc gain of the device, $(1+p)^N$. Randomness of the carrier transit time [Matsuo et al., 1985] and the finite RC time constant will have the effect of smoothing and extending the impulse response. The duration of the

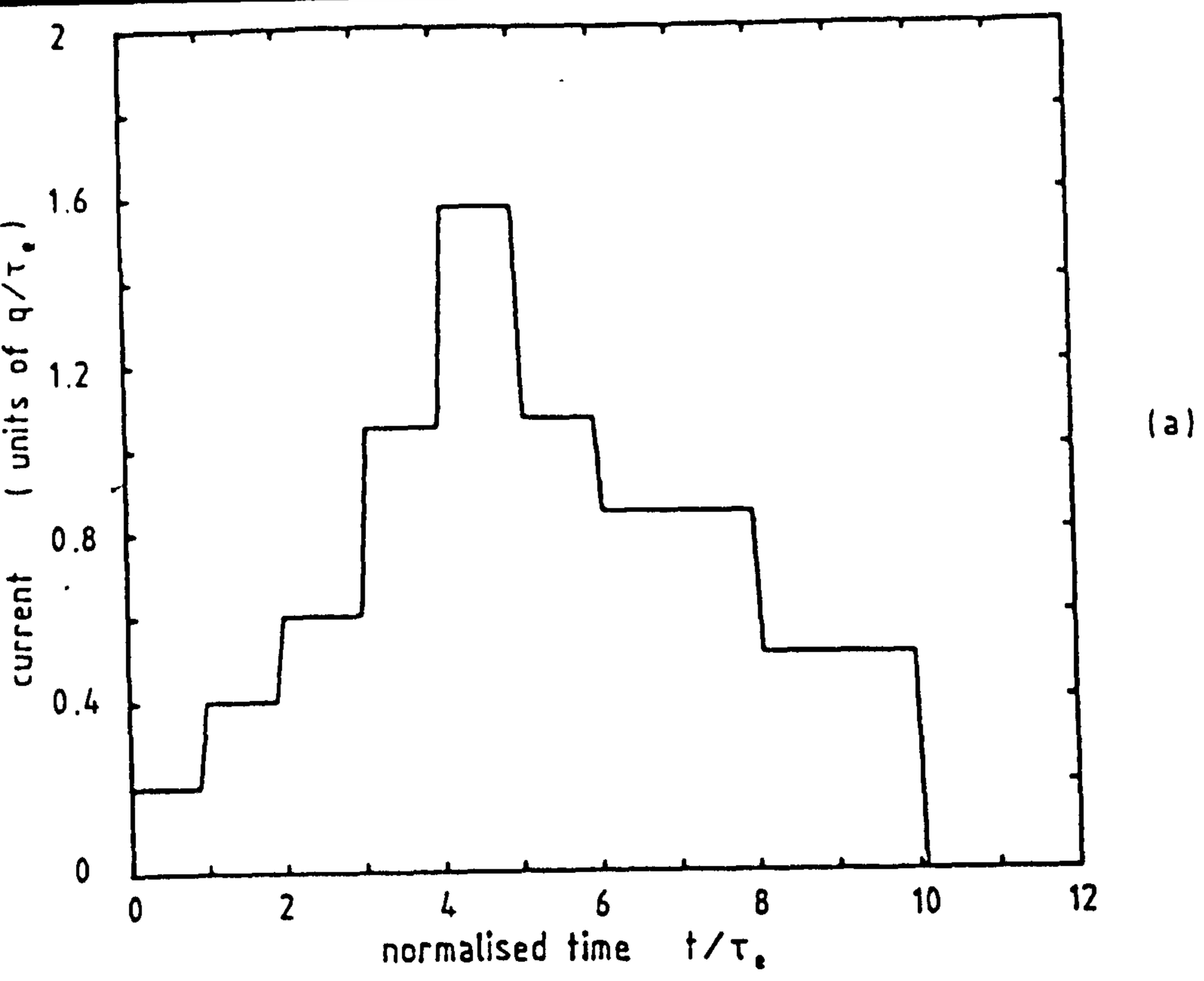

(a)

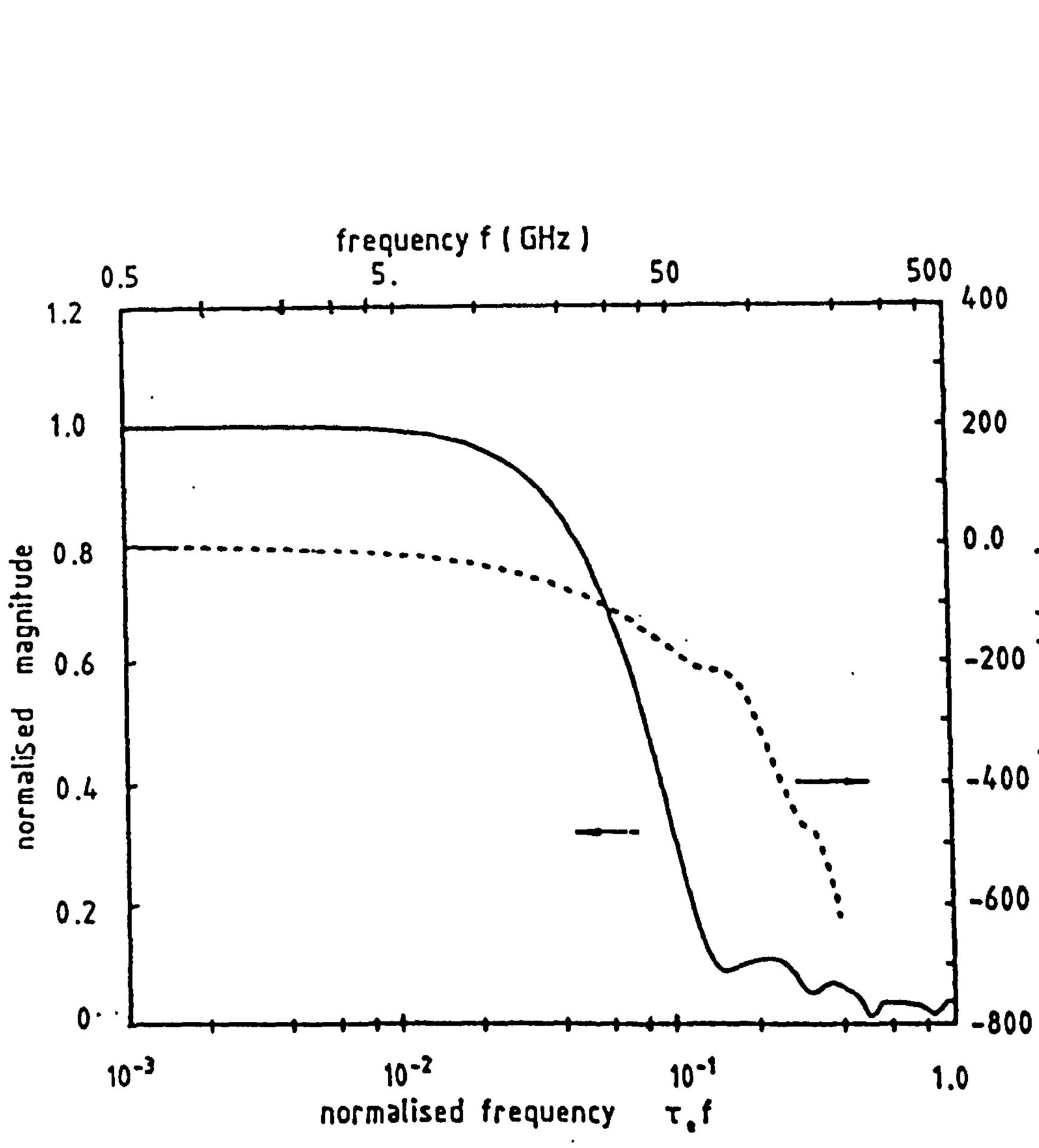

(b)

Fig. 8.1 (a) Impulse response function for an ideal 5-stage SAPD with deterministic transit time $\tau_e=\tau_h$ and p=0.5.

(b) Frequency response for the SAPD described above.

——— magnitude ..... phase

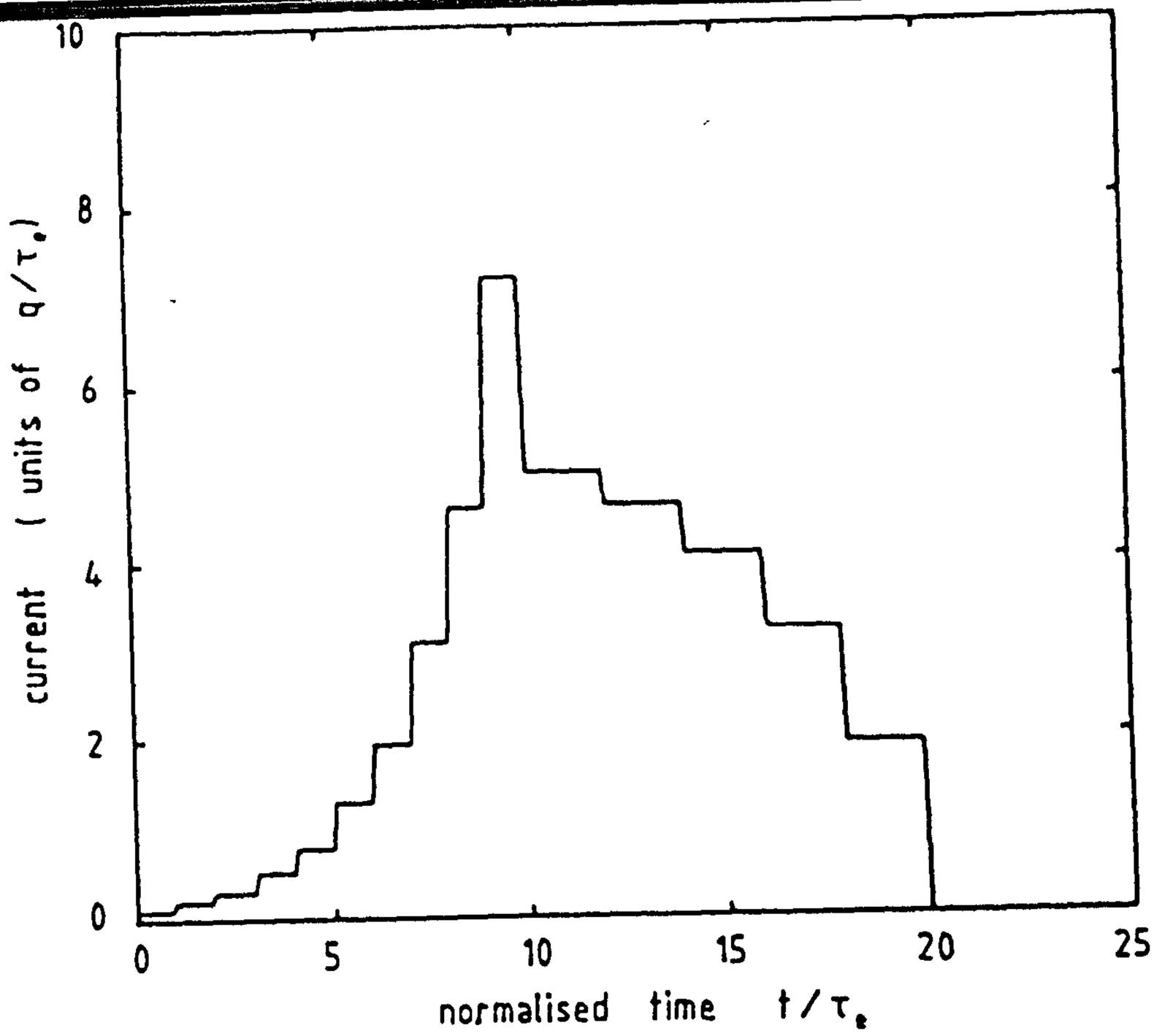

(a)

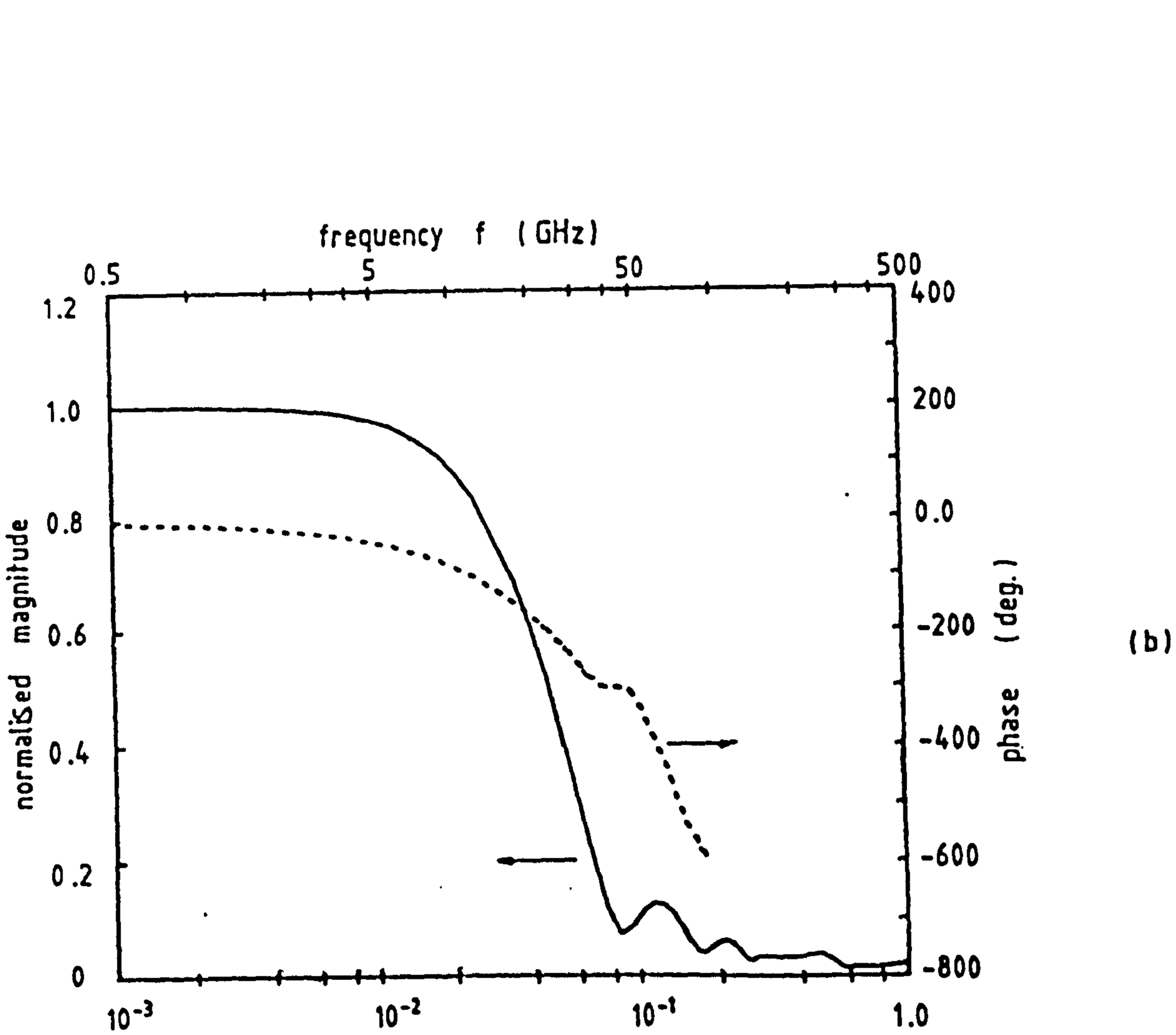

(b)

Fig. 8.2 (a) Impulse response function for an ideal 10-stage SAPD with deterministic transit time $\tau_e = \tau_h$ and p=0.5.

(b) Frequency response for the device described above.

——— magnitude ..... phase

current pulse is equal to $N(\tau_e+\tau_h)$ leading to higher bandwidth for the 5-stage device compared with N=10, assuming τ_e is the same. The bandwidth is approximately 28.53 GHz and 16.74 GHz for N=5 and N=10 respectively. This is less than that predicted by Matsuo et al. [1985] using the approximate formula $1/[N(\tau_e+\tau_h)]$.

Fig. 8.3 shows the effect of the electron ionisation probability at the step, p, on both the GB product and the bandwidth of these devices. The dotted line corresponds to a 5-stage device of width 1μm (i.e. W/N=0.2μm); the solid and dashed lines correspond to N=10 assuming W=2μm and 1μm respectively. Once again these calculations assume $v_e=v_h=10^7$cm/s. For all three cases the GB product increases as p increases, with higher values achieved with N=10 and W=1μm. Note that the 5-stage device has a higher GB product at lower values of p. Summarising qualitatively, at lower values of p the 10-stage device offers slightly higher gain than does the 5-stage device but the bandwidth of the latter is much wider, as seen from Fig. 8.3b.

The variation of the bandwidth with p is plotted in Fig. 8.3b for the three cases discussed above. Note that there is a certain value of p for which the bandwidth is minimum. With stage width of 0.2μm, the N=5 device offers higher bandwidth than does the N=10 device since the impulse current response is of shorter duration. If the total width of the two devices is the same (1μm) the higher bandwidth will be achieved with N=10, particularly for p>0.2. Note that the bandwidth and GB product is the same for both devices when p=0, and W=1μm, as one would expect since then no impact ionisation occurs and both cases yield the same impulse time response function.

The main conclusion to be drawn from the foregoing discussion is that very high GB products may be achieved in ideal SAPDs, with GB an

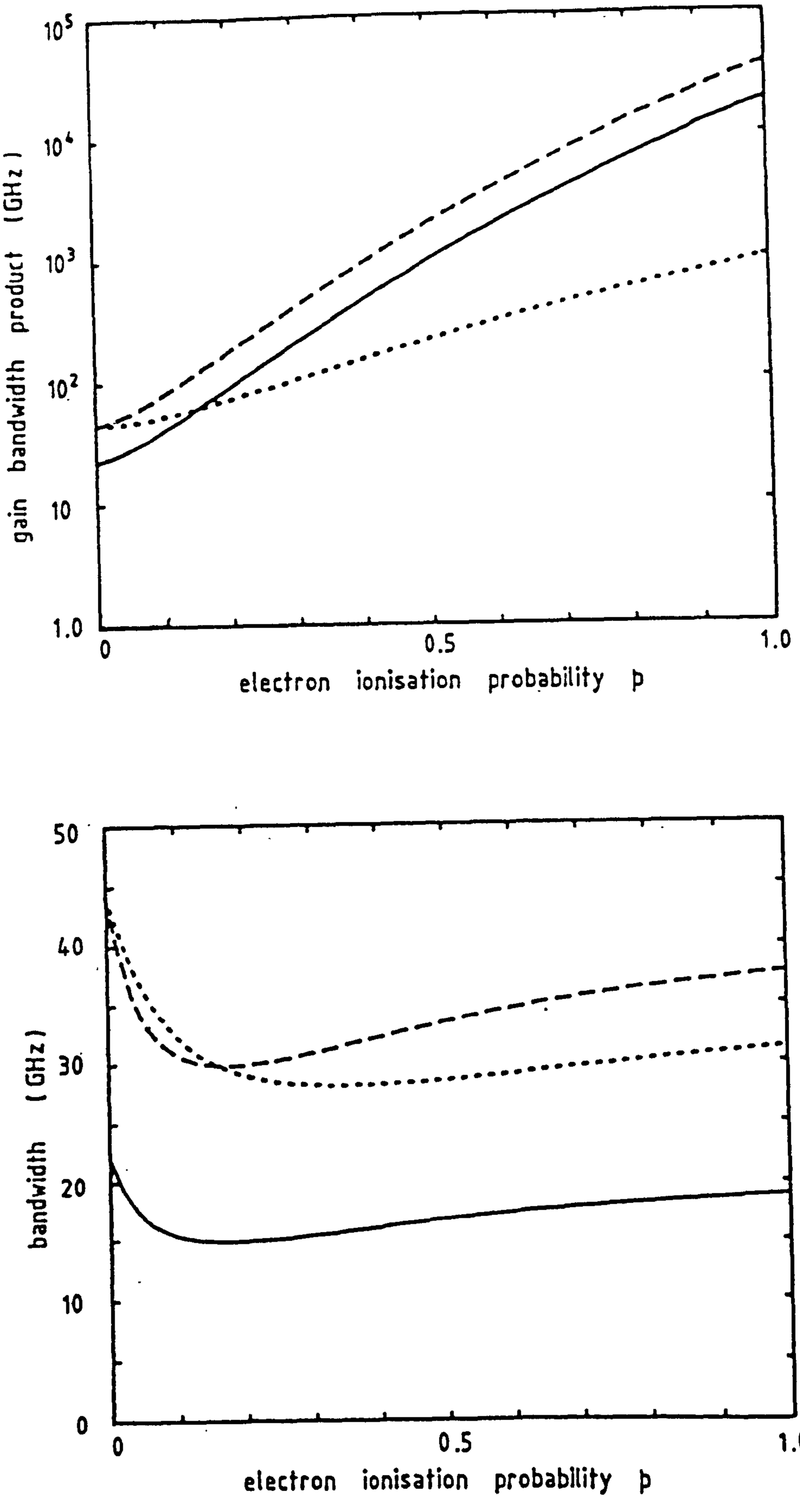

(a)

(b)

Fig. 8.3 Effect of electron ionisation probability p on the frequency response characteristics of an ideal SAPD. The drift velocity is taken to be 10^7 cm/s for both carriers.

(a) GB product vs. p (b) bandwidth vs. p

····· N=5, W=1 μm —— N=10, W=2 μm – – – N=10, W=1 μm

increasing function of N assuming p and W are the same. In particular the analysis predicts GB products of 10^3 GHz and $5x10^4$ GHz for the 5-stage and 10-stage devices respectively, assuming W=1μm and $v_e = v_h = 10^7$ cm/s.

8.3 Effect of Avalanche Build-up Time

The high bandwidths calculated in the previous section cannot be achieved in practical devices due to the influence of residual hole ionisation. Owing to the regenerative nature of the avalanche process, the higher the gain the longer it takes the avalanche process to build up. This gives rise to a constant GB product which is the most restrictive limitation to the speed of response of these detectors. The avalanche build-up time and hence the GB product are strong functions of the hole to electron ionisation ratio. For very low ionisation ratio the avalanche build-up time is relatively small and hence the bandwidth is limited by other effects. The existence of higher residual hole ionisation rates leads to increased avalanche build-up time which degrades the speed of operation of the detectors. Most SAPDs, fabricated using various techniques, have ionisation rate ratios of more than 0.1 [Mohammed et al., 1985; Juang et al., 1985; Yu et al., 1987] and hence their bandwidth is expected to be strongly affected by avalanche build-up time. We shall now examine this problem in some detail.

The theory of avalanche build-up time in CAPDs has been extensively studied and reported [Lee et al., 1967; Kuvas and Lee, 1970a and 1970b]. In order to be able to apply these results to SAPDs we shall show how the latter may be modelled as CAPDs. This modelling approach will also enable us to predict other gain characteristics of

SAPDs based on information previously published for CAPDs.

8.3.1 A New SAPD Model

Consider a SAPD having a depletion region of width W distributed equally among the N stages as shown in Fig. 8.4. Such a structure is usually analysed using a discrete ionisation model, each carrier having a given probability to impact a single ionisation per stage. Hence the gain and noise characteristics of these devices are different from CAPDs where a continuous ionisation process is assumed. Here we shall examine SAPDs in an alternative manner. We shall treat these advanced devices as if they were CAPDs in which the electron and hole ionisation rates α and β are not constant throughout the depletion region extending from x=0 to x=W. In order to model the discrete ionisation process $\alpha(x)$ is represented as a series of N impulses, one impulse per stage. A similar presentation may also be employed for holes, even though for some devices - such as a staircase APD - continuous ionisation is more realistic. In the latter case the low ionisation rate and small width of the individual graded regions make a discrete approximation appropriate. Hence we have

$$\alpha(x) = \alpha_o \sum_{i=1}^{N} \delta(x-x_i-iW/N) \qquad 0 \le x_i \le W/N \tag{8.10}$$

$$\beta(x) = \beta_o \sum_{i=1}^{N} \delta(x-x'_i-iW/N) \qquad 0 \le x'_i \le W/N \tag{8.11}$$

where $\delta(.)$ denotes the dirac delta function and $x_i(x'_i)$ corresponds to the position where the initiated electron (hole) impact ionises at the

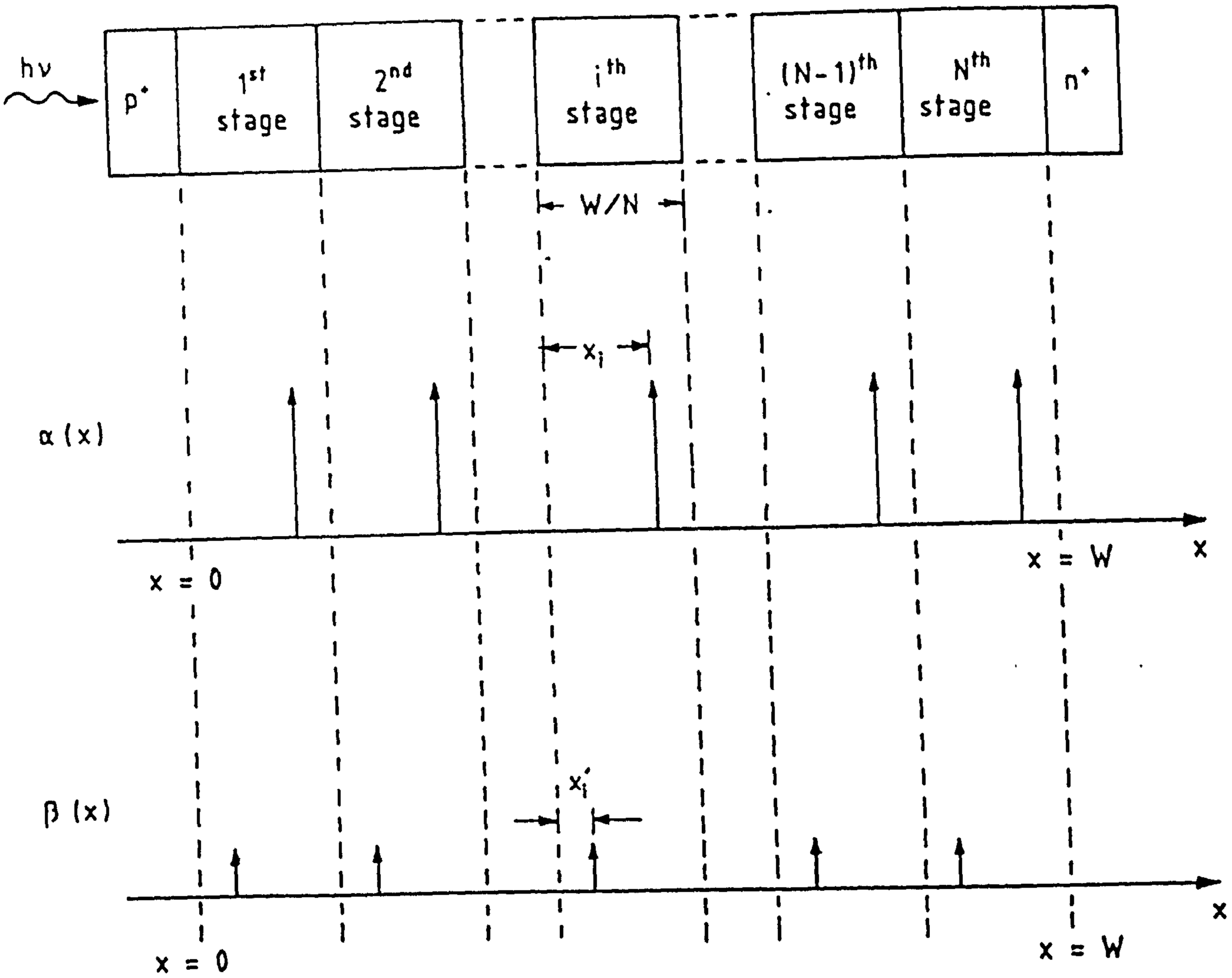

Fig. 8.4 New mathematical model to predict the gain characteristics of SAPD. The device is modelled as a PIN avalanche diode in which the electron and hole ionisation rates $\alpha(x)$ and $\beta(x)$ have delta-function spatial dependence.

i^{th} stage. The weights α_o and β_o of the impulses are related to p and u, the probabilities for the electron and hole respectively to cause a single ionisation per stage according to,

$$1+p \equiv \int_{(i-1)W/N}^{iW/N} \exp(\alpha x).dx = \exp(\alpha_o) \qquad (8.12)$$

$$1+u \equiv \int_{(i-1)W/N}^{iW/N} \exp(\beta x).dx = \exp(\beta_o) \qquad (8.13)$$

or

$$\alpha_o = \ln(1+p) \qquad (8.14)$$

$$\beta_o = \ln(1+u) \qquad (8.15)$$

While the above equations are written for the special case of the ionisation probabilities p and u being the same for the various stages, they can be readily extended to the general case by allowing α_o and β_o to vary from one stage to another according to the values of the individual parameters p and u.

The average gain for pure electron injection $<M_o>$ can be calculated for a CAPD using the following expression [Lee et al., 1967]

$$<M_e> = \frac{\exp\left[\int_0^W (\alpha-\beta).dx\right]}{1-\int_0^W \beta.\exp\left[\int_x^W (\alpha-\beta).dx'\right] dx} \qquad (8.16)$$

where α and β are functions of x. If eqns. 8.10 and 8.11 are used to replace α and β respectively, then we can simply show that

$$\langle g_N \rangle \equiv \langle M_e \rangle = \frac{Q^N}{1-\ln(1+u)\left[\frac{Q^N-1}{Q-1}\right]} \qquad (8.17)$$

which is independent of x_i and x_i' and

$$Q = (1+p)/(1+u) \qquad (8.18)$$

Comparing eqn. 8.17 with the exact formula given in the literature for the gain of a SAPD [Teich et al., 1986a]

$$\langle g_N \rangle \equiv \langle M_e \rangle = \frac{Q^N}{1-u\left[\frac{Q^N-1}{Q-1}\right]} \qquad (8.19)$$

shows that the new model is able to predict accurately the gain of these advanced detectors when the residual hole ionisation is small since $\ln(1+u) \cong u$ for $u \ll 1$. In fact we find that the model gives a good estimate for the gain when $u < 0.1$ as shown in Fig. 8.5. Here eqns. 8.17 and 8.19 are compared graphically for two values of N, 5 and 10, taking $k \equiv u/p$ as a parameter. It is clear that there is a good agreement between the two expressions for all values of k for $N=10$ and for k less than 0.1 for $N=5$. We can reasonably assert that the new model can be used to estimate the gain characteristics of SAPDs for all values of k when $N \leq 10$ since the maximum value of u required to avoid avalanche breakdown is limited to 1/N when $k=1$. For simplicity in the following analysis we shall take $x_i = W/N$ and $x_i' = 0$ for $1 \leq i \leq N$.

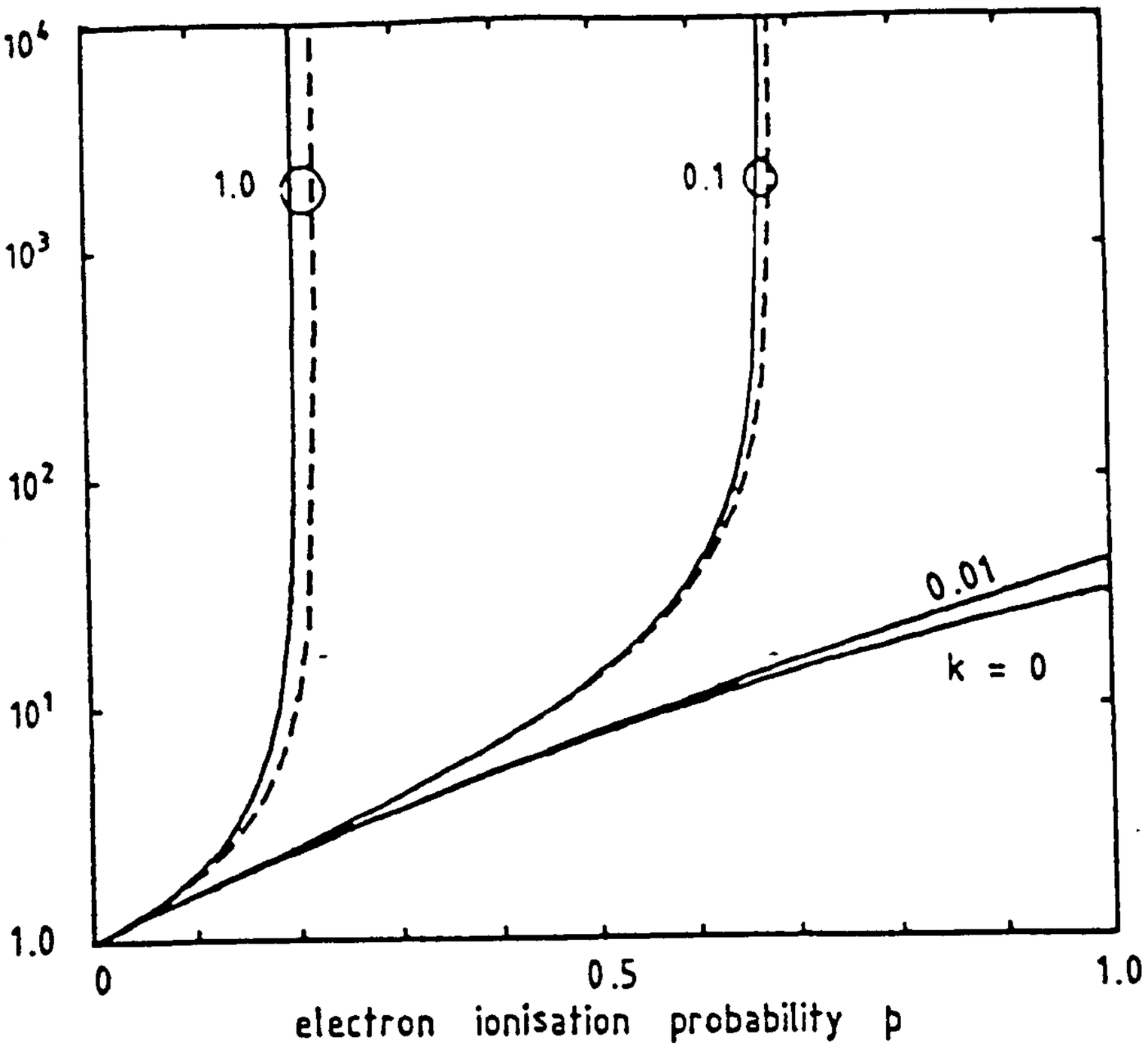

(a)

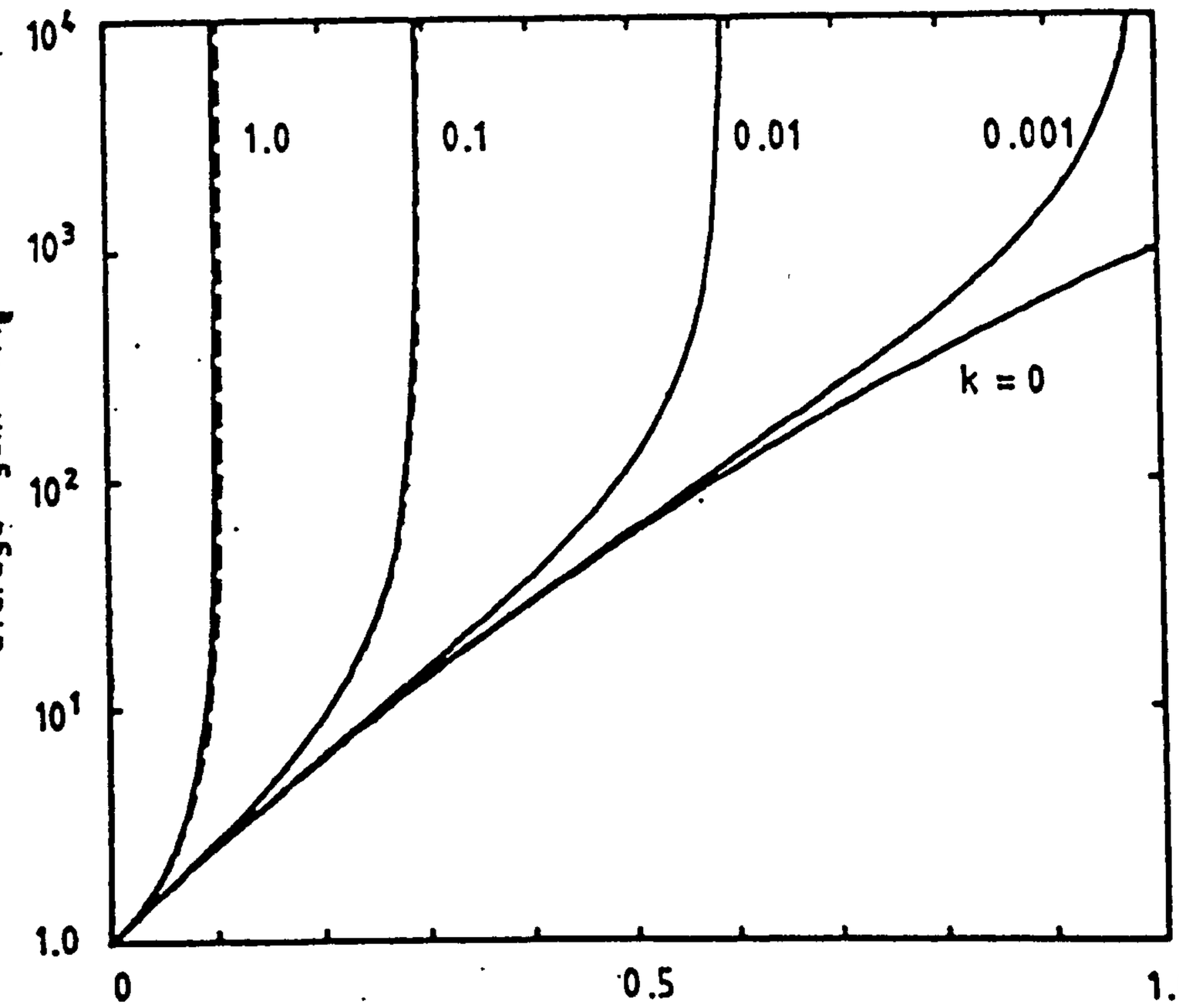

(b)

Fig. 8.5 Average gain of a SAPD as a function of electron ionisation probability. (a) N=5 (b) N=10

——— exact (eqn. 8.17) — — — approximate (eqn. 8.19)

This assumption may affect slightly the calculation of the speed of response, but the effect is very small when N is large.

The average gain $M_i \equiv \langle g_{N-i} \rangle$ associated with a hole-electron pair initiated at the entry of the $(i+1)^{th}$ stage can be estimated according to the new model as follows. The average gain for a CAPD as a function of position x can be expressed as

$$M(x) = M(0).\exp\left[-\int_0^x (\alpha-\beta).dx' \right] \tag{8.20}$$

where $M(0) \equiv \langle M_e \rangle$. Using eqns. 8.10 and 8.11 with eqn. 8.20 yields

$$M_i = M_0 Q^{-i} \tag{8.21}$$

where $M_0 \equiv \langle M_e \rangle$ for pure electron injection. Eqn. 8.21 is in accord with previously reported results for SAPDs (eqn. 3.1).

8.3.2 Determination of Avalanche Build-up Time

For a CAPD the frequency variation of the multiplication can be represented by an equation of the form [Naqavi, 1973].

$$M(x,\omega) = \frac{M(x)}{1+j\omega M(x)\tau(x)} \tag{8.22}$$

where $\langle M_e \rangle > \alpha/\beta$ is assumed. Here $M(x) \equiv M(x,0)$ is the dc gain given in eqn. 8.21 and $\tau(x)$ is the effective transit time which is dependent on the ionisation rate ratio $k \equiv \beta/\alpha$ and the mean transit time of the carriers across the avalanche region

$$\tau(x) = \tau(0).\exp\left[\int_0^x (\alpha-\beta).dx'\right] \tag{8.23}$$

where $\tau(0)$ is the effective transit time for pure electron injection

$$\tau(0) = \frac{k_o}{(v_e+v_h)} \int_0^w \exp\left[-\int_0^x (\alpha-\beta).dx'\right]dx \tag{8.24}$$

Here k_o is a correction factor introduced by Kuvås et al. [1970a] to include the effects of carrier induced displacement current which depends on the ionisation rate ratio, the velocity of charge carriers and the diode structure. Eqn. 8.22 indicates the existence of a gain bandwidth product (GB):

$$GB = 1/[2\pi\tau(0)] \tag{8.25}$$

assuming that avalanche is electron initiated with avalanche build-up time given by $\tau(0)M(0)$.

We shall now apply the above results to SAPDs using our model. The effective transit time for pure electron injection τ_o can be obtained from eqn. 8.25 with the aid of eqns. 8.10 and 8.11.

$$\tau_o = \frac{k_o}{(v_e+v_h)} \sum_{i=1}^{N} \int_{(i-1)W/N}^{iW/N} \exp\left[-\int_0^x (\alpha-\beta).dx'\right]dx$$

$$= \frac{k_o W}{N(v_e+v_h)} \sum_{i=1}^{N} \exp\left[-\alpha_o(i-1)+\beta_o i\right] \tag{8.26}$$

where $x_i = W/N$ and $x_i' = 0$ are assumed. Eqn. 8.26 can be simplified further using eqns. 8.14 and 8.16.

$$\tau_o = \frac{k_o W(1+u)}{N(v_e + v_h)} \left[\frac{1-Q^{-N}}{1-Q^{-1}} \right] \qquad (8.27)$$

The interesting feature of eqn. 8.27 is that the effective transit time for SAPDs is directly proportional to the width of the multiplication region. Moreover, as the number of stages increases, τ_o will increase or decrease according to the net effect of $[1-Q^{-N}]/N$. Generally, when N is large and $Q>1$ then $Q^{-N} \to 0$ leaving the GB product directly proportional to N. For very high noise APDs (i.e. $k \equiv u/p = 1$) eqn. 8.27 reads

$$\tau_o = 2k_o W/(v_e + v_h) \qquad (8.28)$$

which for given W is independent of the number of stages. In this case the GB product degrades severely.

The correction factor k_o may be calculated approximately using an expression reported in the literature for uniform CAPDs [Kuvas, 1970a] and assuming effective ionisation rates $\alpha_{eff} = N.\ln(1+p)/W$ and $\beta_{eff} = N.\ln(1+u)/W$,

$$k_o \cong \frac{(v_e + v_h)^2}{v_e v_h} \frac{a}{(a-1)^2} \left[\frac{a+1}{a-1} \ln(a) - 2 \right] \qquad (8.29)$$

where

$$a = \ln(1+p)/\ln(1+u) \qquad (8.30)$$

This approximation is used here in the interest of simplicity, the expression for the correction factor k_o for nonuniform CAPDs being quite complicated.

Before we proceed further let us check the validity of eqns. 8.27 and 8.29. To apply these equations to a uniform PIN avalanche diode we let $N\rightarrow\infty$, and $p=\alpha.\Delta x$, $u=\beta.\Delta x$ where Δx is the width of a single stage. When $\Delta x\rightarrow 0$, eqns. 8.27 and 8.29 reduce to the following expressions.

$$\tau_o = \frac{k_o}{v_e + v_h}\left[\, 1-\exp[-(\alpha-\beta)W] \,\right] \tag{8.31}$$

$$k_o = \frac{(v_e + v_h)}{v_e v_h}\,\frac{k}{(1-k)^2}\left[\, \frac{1+k}{1-k}\ \ln(1/k)-2 \,\right] \tag{8.32}$$

where $k\equiv\beta/\alpha$ is the ionisation rate ratio for a CAPD and we make use of the following relation [van Vliet et al., 1979b].

$$\lim_{N\rightarrow\infty} Q^N \cong \exp[\alpha-\beta)W] \tag{8.33}$$

Equations 8.31 and 8.32 are identical to those given in the literature for uniform PIN avalanche diodes.

The effective transit time τ_i associated with a hole-electron pair initiated at the entry of the $(i+1)^{th}$ stage can be determined with the aid of eqn. 8.23

$$\tau_i = \tau_0 Q^i \tag{8.34}$$

Thus $\tau_i M_i=\tau_0 M_0$ independent of the position of injection. Here M_0 and

M_i represent the dc gain defined in eqns. 8.17 and 8.21 respectively.

Figs. 8.6a and 8.6b present the GB product and the bandwidth of a SAPD due to avalanche build-up time as a function of the electron ionisation probability p for two values of N, 5 and 10. In these examples the ionisation rate ratio $k \equiv u/p$ is taken up as a parameter, the width of the stage is assumed to be $0.2\mu m$ for both devices and the speed of both carrier species to be $10^7 cm/s$. Note that existence of residual hole ionisation will limit the range of p over which the device can be operated without avalanche breakdown occurring. Comparing the various curves we make the following observations:

(i) As p increases a high GB product can be achieved in both devices. This is true for all values of k except when $k=1$. In this case the figure suggests that GB product decreases as p increases and according to eqn. 8.29 the correction factor k_o still depends on p even for $k=1$. This apparent contrast with uniform PIN avalanche diodes - for which k_o is independent of α and β when the ionisation rate ratio is equal one [Kuvas, 1970a] - is in fact due to the approximation used in the calculation of k_o. An exact expression for k_o for superlattice devices is expected to be independent of p for $k=1$. This is not a serious limitation since SAPDs are usually realised with k different from one.

(ii) The bandwidth for both devices degrades as p increases, tending to a very low value in the vicinity of avalanche breakdown since the gain becomes extremely large.

(iii) As k increases lower values for GB product and bandwidth are to be expected for both devices.

(iv) The 5-stage device offers wider bandwidth and higher GB product at a given value of p compared with the 10-stage device. For

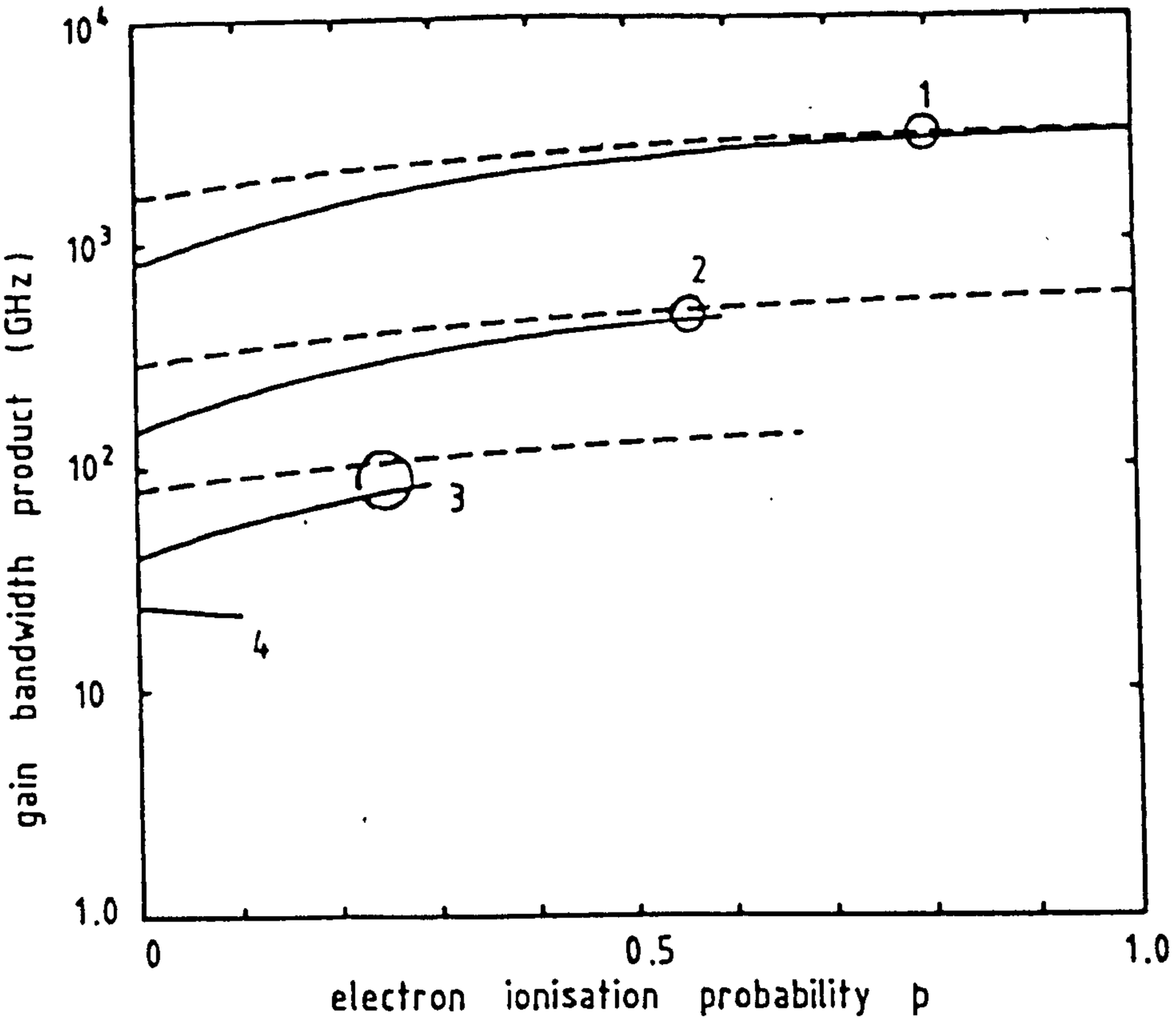

(a)

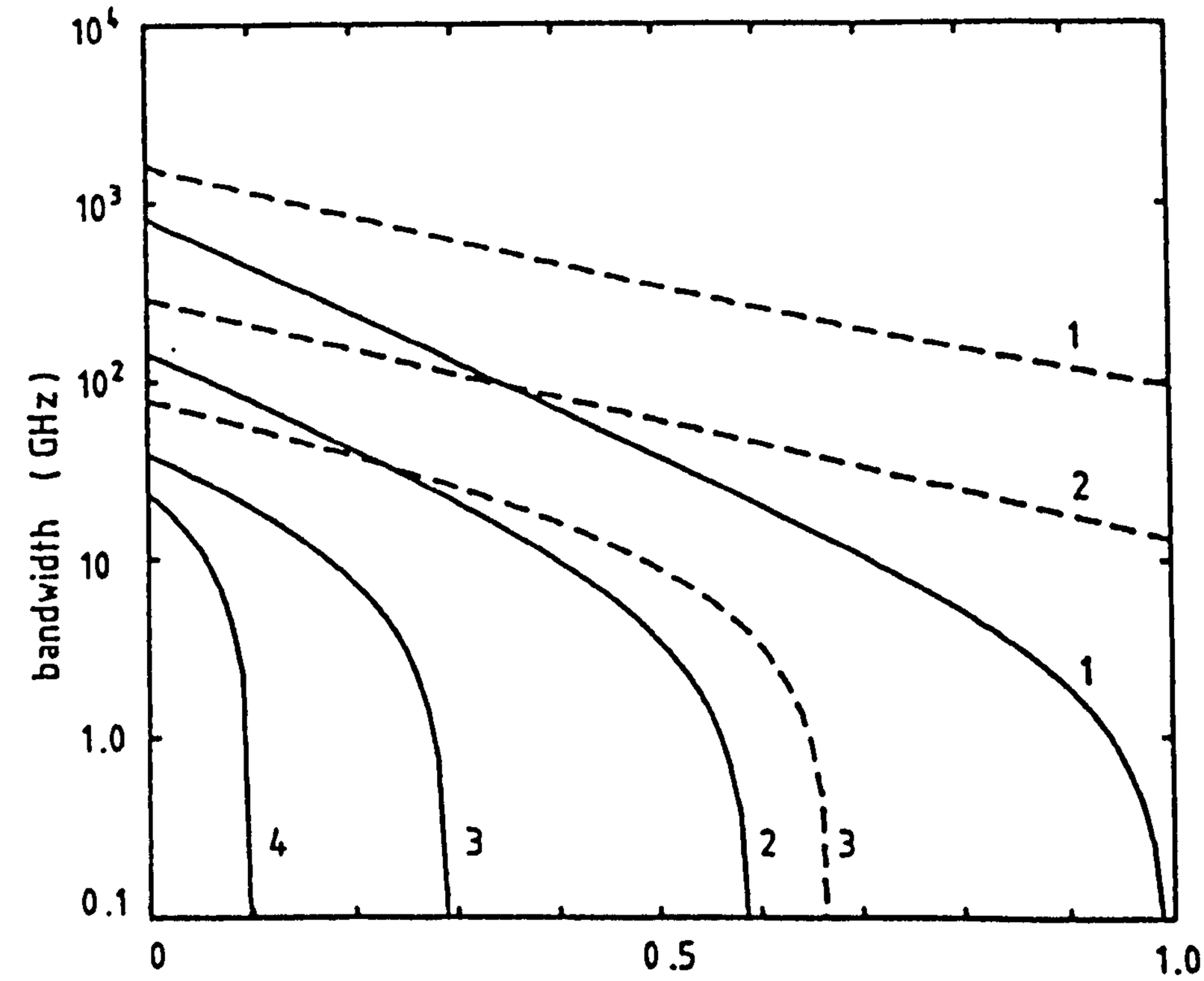

(b)

Fig. 8.6 Variation of GB product and bandwidth of a SAPD, arising from the avalanche build-up time, with electron ionisation probability. The drift velocity of both carriers is taken to be 10^7 cm/s and 0.2 μm is assumed for the width of a single stage. ——— N=10 --- N=5

1: k=0.001 2: k=0.01 3: k=0.1 4: k=1.0

large values of p the GB products of both devices tend to the same value since W/N, the dominant parameter in determining τ_o, is the same for both devices.

In Fig. 8.7 similar results are presented but with the width of the depletion region of the 10-stage device reduced to 1μm to be the same as that of the 5-stage device. Similar conclusions may be drawn here except that the GB product for N=10 is higher than that for the 5-stage device. Note that for N=10 the GB product of Fig. 8.7a is twice that of Fig. 8.6a, since for Fig. 8.7a W is reduced to one half of its former value.

From the above discussions it is clear that for given p, k and W higher GB products and lower bandwidths are expected as the number of stages increases. In addition, the avalanche build-up time imposes limitations on the speed of these devices when k>0.1. For example for N=10 the GB product is limited to 100 GHz assuming W=2μm and k=0.1. This is much less than the value of 10^4 GHz which can in principle be obtained for an ideal device (see Fig. 8.3a).

8.4 Sensitivity Degradation due to Avalanche Build-up Time

For gigabit-per-second systems, the APD GB product is a very important factor, which affects receiver sensitivity since it limits the APD gain to less than the optimum value in order to maintain the required signal bandwidth. In this section the performance degradation of optical receivers due to limited GB product arising from avalanche build-up time is assessed. This analysis can readily be extended to include the effect of other factors limiting the speed of these superlattice devices.

In order to reduce the effect of limited GB product of APDs at

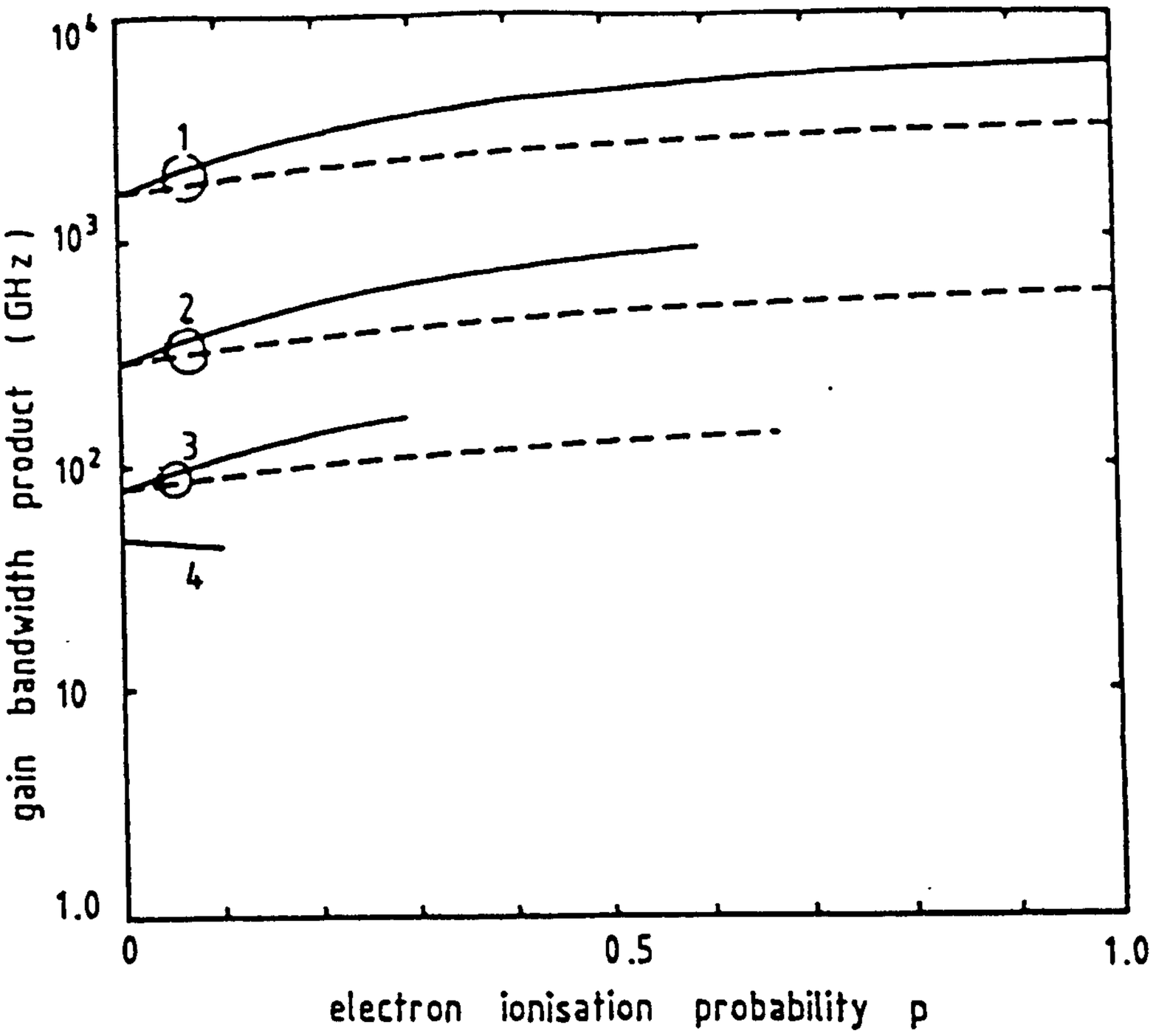

(a)

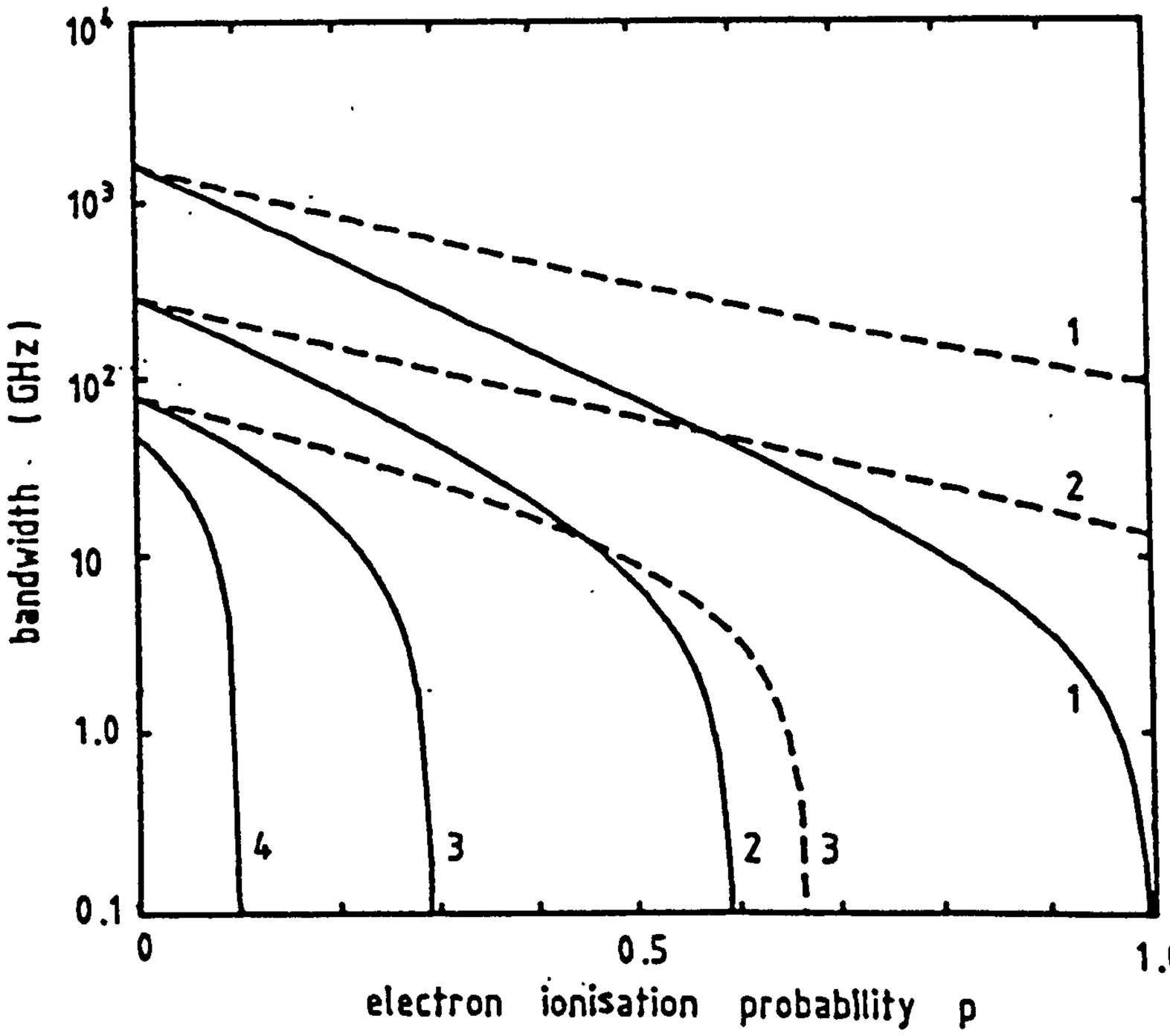

(b)

Fig. 8.7 As in Fig. 8.6 except the width of the avalanche region is taken to be 1 μm for both devices.

very high bit rate, the receiver may be operated either at sufficiently low avalanche gain that the bandwidth ensures that no intersymbol interference (ISI) is produce [Forrest, 1984; Shikada et al., 1987], or at a larger APD gain with equalization of the APD response to remove the ISI introduced by limited bandwidth. The latter involves a penalty due to increased high frequency receiver noise [Ando and Kanbe, 1985; Kasper and Campbell, 1987], but leads to higher sensitivity. Accordingly, this approach is adopted here. In calculating the sensitivity we follow Personick (1973) in adopting a Gaussian approximation. We note also that the equalised APD noise spectrum may be taken as uniform since the equalised APD response is flat.

To illustrate our analysis we will assume an APD/FET receiver operating at wavelength $\lambda=1.5\mu$m. The equivalent noise current of the amplifier can be estimated from eqn. 3.26 by replacing Personick integrals I_2 and I_3 by new weighting functions I_2' and I_3', respectively [Kasper and Campbell, 1987]:

$$I_n' = I_n + \frac{<M_o>^2 B^2}{(GB)^2} I_{n+1} \qquad \text{for } n=2,3 \qquad (8.35)$$

Where I_n (n=1, ..., 4) are Personick integrals [Personick, 1973] with values related to the input and output pulse shapes. Further, $<M_o>$ is the dc avalanche gain, assuming electrons initiate the avalanche, and B is the bit rate. In the calculation which follows, we assume 50Ω load resistance, 0.5pF input capacitance and $v_e=v_h=10^7$cm/s. Other receiver parameters are given in Table 3.1. We note that while the 25ps RC time constant will affect the response speed of the diode, our analysis will be directed towards estimating the influence of finite

GB product arising from avalanche build-up time.

Eqn. 8.35 implies that the excess amplifier noise power arising from equalisation of the APD response is proportional to the square of the ratio of bit rate to unequalised APD bandwidth. Thus the amplifier noise is now a function of the APD gain $<M_e>$ because the corner frequency of the equaliser must be adjusted to match the bandwidth of the diode, which depends in turn on $<M_e>$. This dependence has been previously predicted by Kasper et al. [1987] and it is illustrated in Fig. 8.8, which shows the bit rate dependency of the amplifier input noise current spectral density $[<i_{na}^2>/B]^{1/2}$ for different values of GB product and assuming $<M_e>=10$. The solid line, which corresponds to infinite GB product, shows only a slow increase with B since Johnson noise associated with the 50Ω load resistance dominates other amplifier noise sources.

Figures 8.9a and 8.9b present, for N=10 and N=5 respectively, the variation with ionisation rate ratio k of the sensitivity $\eta\bar{P}$ of a 10Gbit/s receiver. The width of the avalanche region W, which leads to a finite GB product, is taken as a parameter. In these calculations the APD gain $<M_e>$ (and hence p) is adjusted for each set of parameters to obtain the minimum detectable optical power required to achieve BER=10^{-9}. Results corresponding to k>0.1 when N=5 are also plotted in Fig. 8.9b - even though our model predicts less accurately the GB product in this region - for comparison with N=10. Figure 8.9 indicates clearly that sensitivity penalty due to finite GB product increases with k for a given W. This arises from the degradation of GB product when k increases as explained in the previous section. It is worth mentioning here that for the 5-stage device there is a certain value of k for which $\eta\bar{P}$ is minimum due to the net effects of

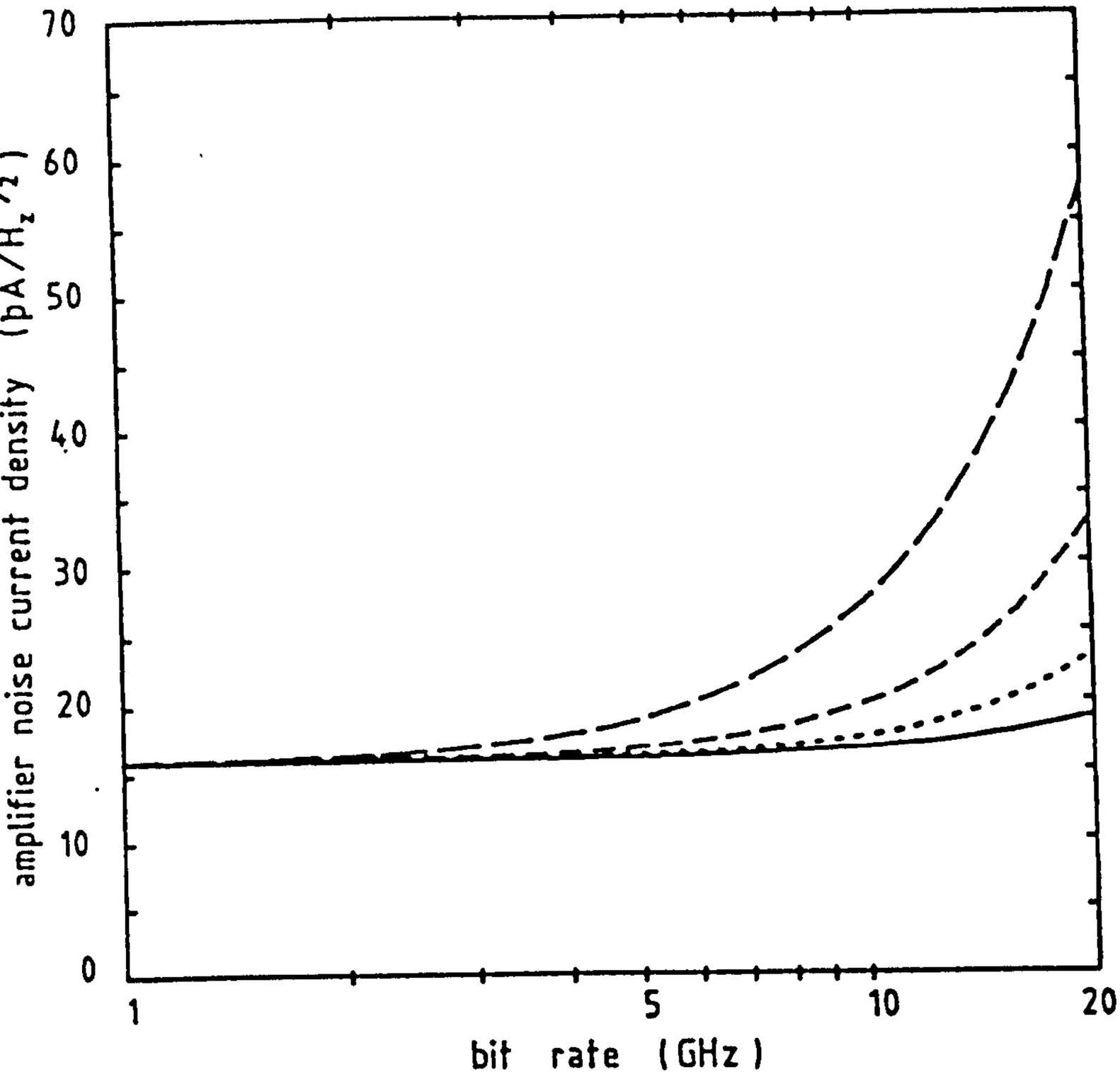

Fig. 8.8 Effect of limited GB product on the amplifier equivalent noise current spectral density, assuming APD gain $\langle M_e \rangle = 10$.
——— GB=∞ ···· GB=100 GHz – – – GB=50 GHz — — GB=25 GHz

both $\langle M_e \rangle$ and F_e which are strong functions of k. This is particularly marked when W is small.

Figures 8.10a and 8.10b show the variation of receiver sensitivity with bit rate for a 10-stage device assuming k=0.01 and 0.1 respectively. We note from these curves that for B<10 Gbit/s and k<0.1 the penalty incurred due to avalanche build-up time is predicted as less than 1dB when the device is fabricated with W=1μm or less. In contrast, a higher penalty is incurred when W>3μm even at bit rates as low as 2 Gbit/s, as may be seen from Fig. 8.10b.

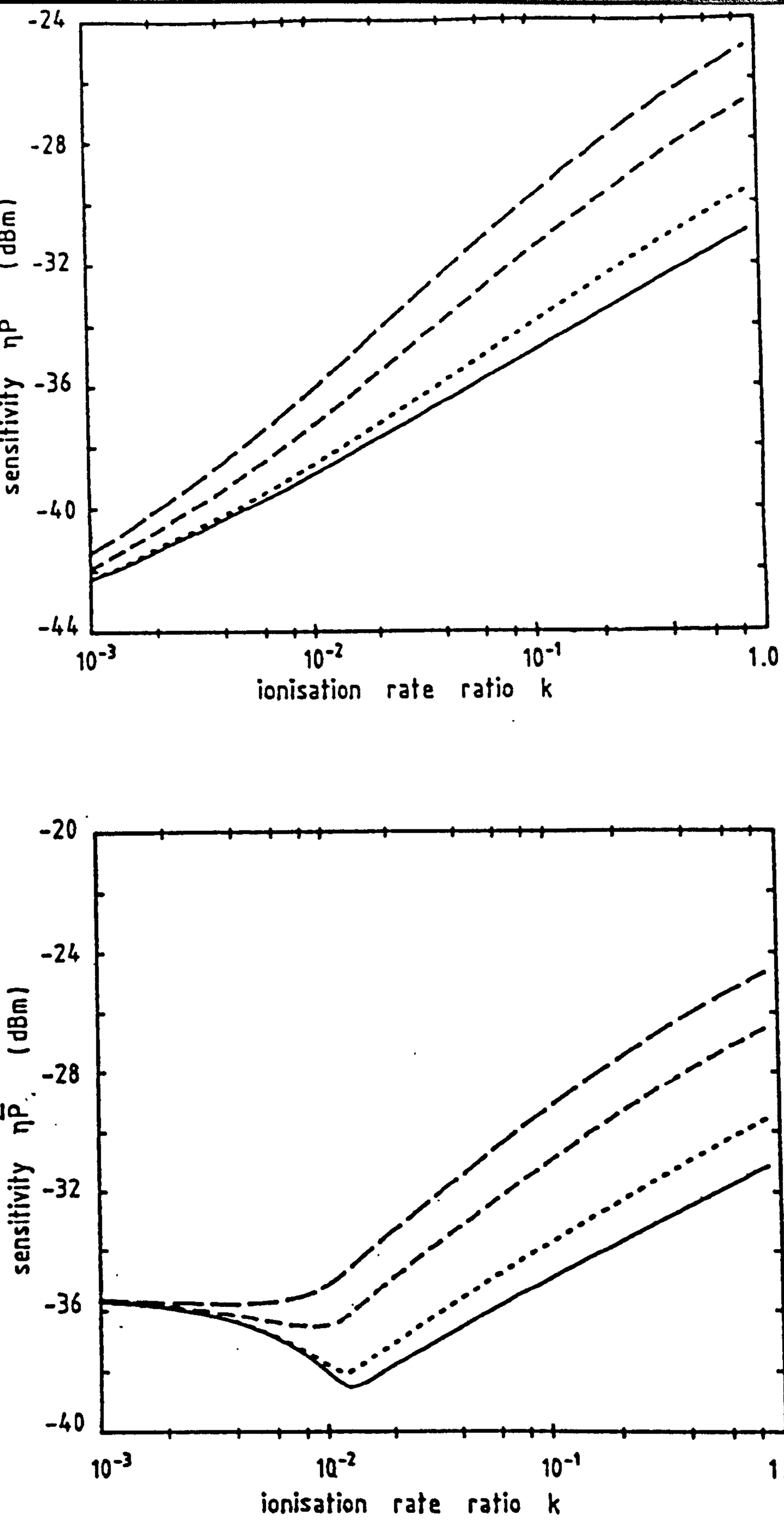

Fig. 8.9 Sensitivity of 10 Gbit/s optical receiver employing a SAPD, as a function of ionisation rate ratio k taking the width of the avalanche region W as a parameter. (a) N=10 (b) N=5

—— W→0 ···· W=1 μm — — — W=3 μm — — W=5 μm

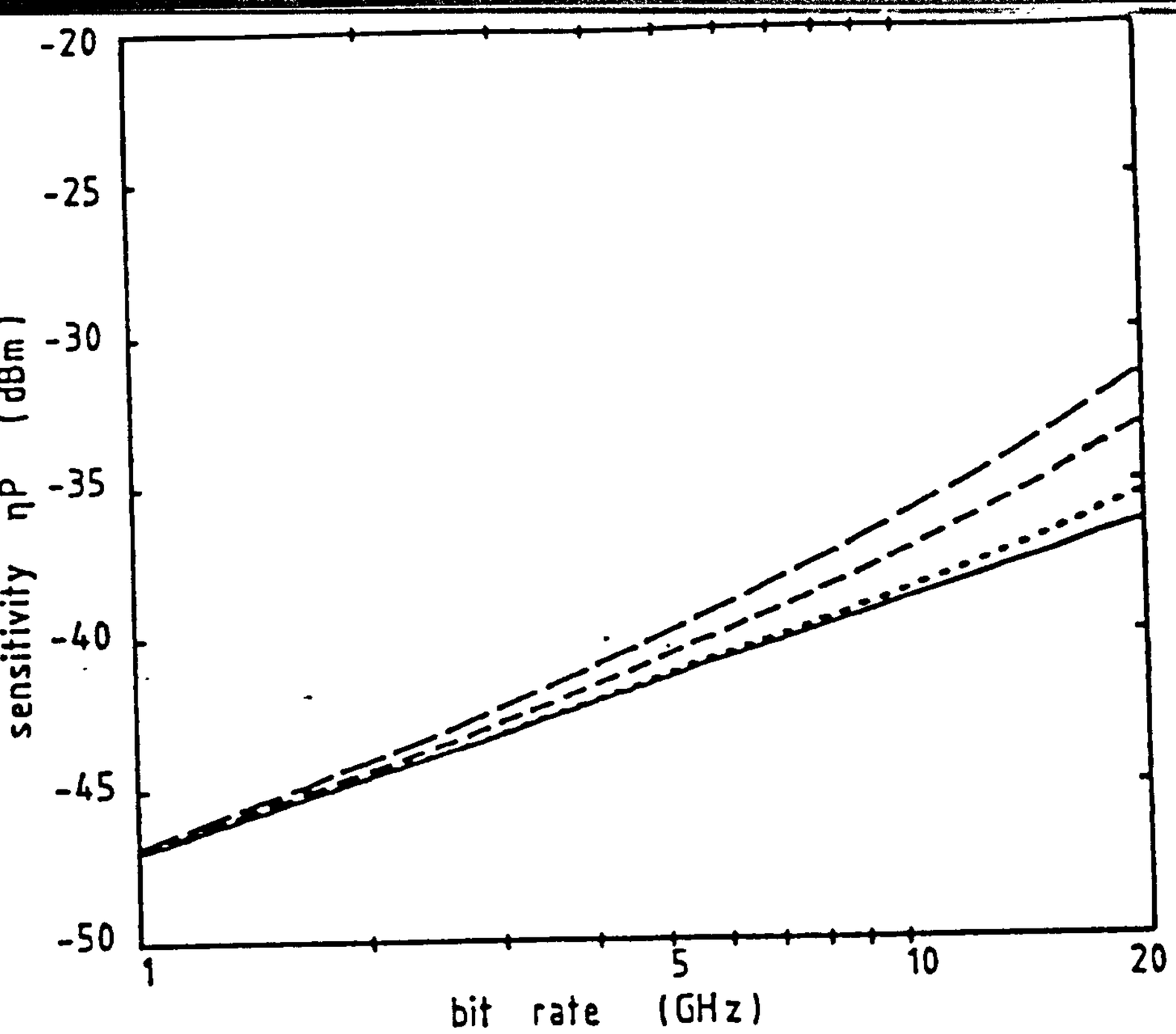

(a)

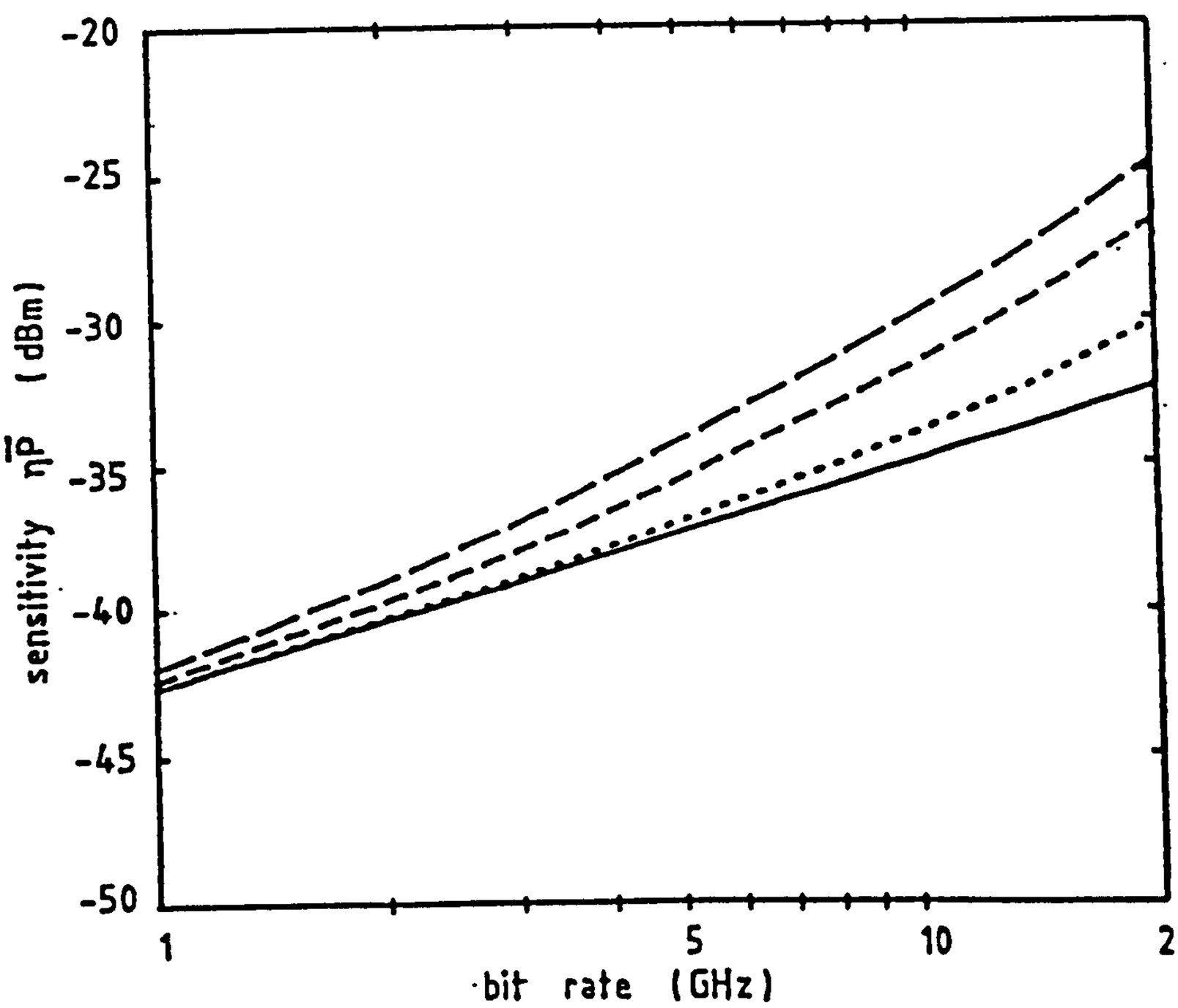

(b)

Fig. 8.10 Effect of bit rate B on the sensitivity of a 10-stage SAPD receiver for different values of W. (a) k=0.01 (b) k=0.1
——— W→0 ·---· W=1 μm – – – W=3 μm —— —— W=5 μm

The primary conclusion to be drawn here is that SAPDs should be fabricated with a short avalanche region ($1<\mu$m) and low residual hole ionisation ($k<0.1$) to ensure high speed, high sensitivity optical receivers for future multigigabit-per-second lightwave transmission systems.

Recently Moseley and co-workers [1988] have succeeded in fabricating a high speed quantum well APD using the GaInAs/InP material system. They were able to achieve GB=25 GHz, with N=50 and W=0.7μm, which is the highest GB product to date for a SAPD made from this material system. No information was reported concerning the ionisation rate ratio, but we believe that a value of $k>0.1$ was primarily responsible for the lower value of GB product reported by them, consistent with the theory presented here.

8.5 Summary

High gain bandwidth products may be achieved with ideal SAPDs. The existence of residual hole ionisation impairs the speed of response of these devices, primarily due to avalanche build-up time. To estimate the GB product in this case we have shown that the SAPD may be modelled as a CAPD in which hole and electron ionisation rates β and α exhibit position dependency corresponding to a series of impulses - one per stage. This has enabled us to apply the theory of CAPDs directly to predict the gain characteristics of SAPDs. The results show that the GB product of SAPDs is inversely proportional to the width of the avalanche region W and directly proportional to the number of stages N, for $N\gg1$. Analysis of the sensitivity of optical receivers incorporating GB-limited SAPDs indicates clearly that these advanced detectors should be fabricated with $W<1\mu$m and low residual

hole ionisation ($k < 0.1$) to ensure negligible penalty for gigabit-per-second operation.

In the next chapter we compare the performance of SAPD receivers, with that for CAPDs and then introduce a new receiver signal processing scheme which leads to signal element waveforms satisfying Nyquist's first and second criteria with respect to the depressed optimum decision threshold encountered with high performance APD receivers These new signal design targets offer improved tolerance to alignment jitter when used in conventional fully retimed optical receivers.

CHAPTER 9

OVERALL RECEIVER CONSIDERATIONS

In previous chapters, the performance of optical receivers incorporating superlattice avalanche photodiodes (SAPDs) has been evaluated allowing for the influence of both residual hole ionisation and dark current. In this chapter we compare these results with those for conventional APDs to indicate the number of stages required for superlattice devices to provide improved sensitivity. Later we describe new signal designs for optical communications based on APD receivers. This new receiver signal processing strategy leads to signal element waveforms satisfying Nyquist's first and second criteria with respect to the depressed optimum decision threshold enountered with high performance APD receivers. This results in an eye pattern for binary optical communications which is well disposed around the depressed threshold. The new signal design targets are thus well suited to untimed transmission whilst also offering improved tolerance to alignment jitter when used in conventional fully retimed optical receivers. The practical realisation is considered to consist of signal shaping networks with responses closely approximating these new designs.

9.1 Performance of CAPD and SAPD Receivers

In this section the sensitivity degradation of optical receivers due to residual hole ionisation and dark current is presented for both SAPD and CAPD detectors. Illustrative results will be presented for two values of N, namely 5 and 10, since the behaviour of the SAPD receiver performance differs according to N in some cases. We note

also that in these calculations the gain-bandwidth product of the APD is assumed high enough to be considered as not a limiting factor for the performance of the receiver at high bit rate.

We consider as an example a 2 Gbit/s receiver operating at $\lambda=1.5\mu$m. The sensitivity is estimated for BER=10^{-9} assuming 22kΩ load resistance. Other parameters used in the calculation are given in Table 3.1. Fig. 9.1 shows the receiver sensitivity $\eta\bar{P}$ as a function of APD gain for different values of ionisation rate ratio k, assuming zero dark current. The solid lines correspond to a SAPD and the broken lines to a CAPD. Note that for relatively high values of k there is a well-defined optimum gain at which the detected optical power is minimum (the sensitivity is optimum) for a SAPD receiver, a behaviour similar to that of a CAPD. For lower values of k the SAPD receiver continues to give improved sensitivity as p (electron ionisation probability per stage) increases with optimum performance occuring at p=1 since no avalanche breakdown occurs in the detector under these circumstances. The optimum sensitivity of the 10-stage SAPD is higher than that of the CAPD at lower values of k. It is also evident from Figs. 9.1a and 9.1b that the receivers have the same performance for k > 0.1. The optimum gain has been calculated as a function of ionisation rate ratio for these detectors and the results are displayed in Fig. 9.2. The optimum gain is almost the same for both the 10-stage SAPD and the CAPD, at fixed values of k. However the 5-stage SAPD exhibits a lower optimum gain at lower values of k.

Figs. 9.3a and 9.3b show the variation of the optimum sensitivity as a function of k for N=5 and N=10 respectively. Results for a CAPD are also shown for comparison. Two types of dark current component are considered: I_{da} generated uniformly in the avalanche region and

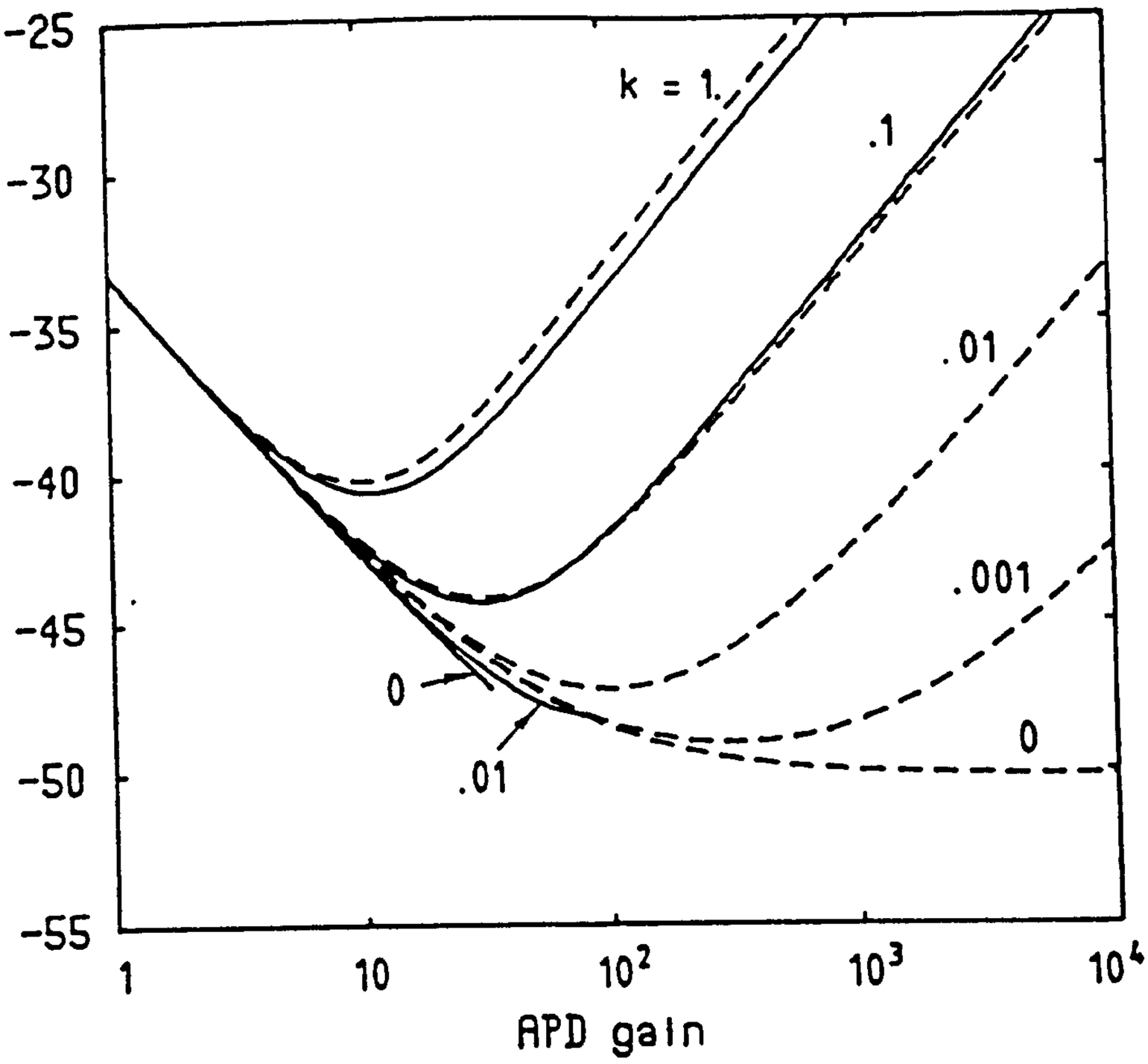

(a)

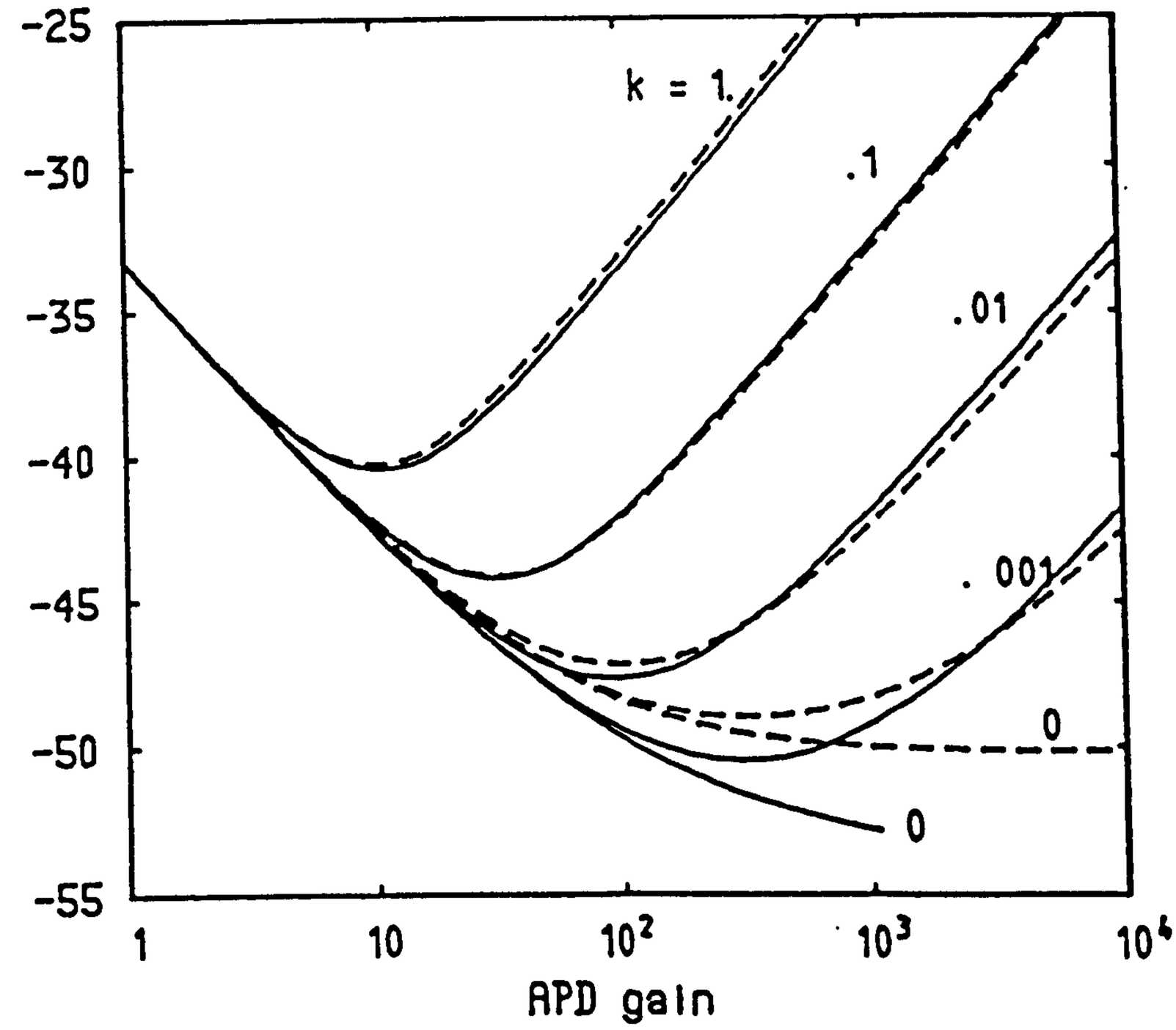

(b)

Fig. 9.1 Receiver sensitivity versus APD gain.
(a) N=5 (b) N=10
——— SAPD - - - CAPD

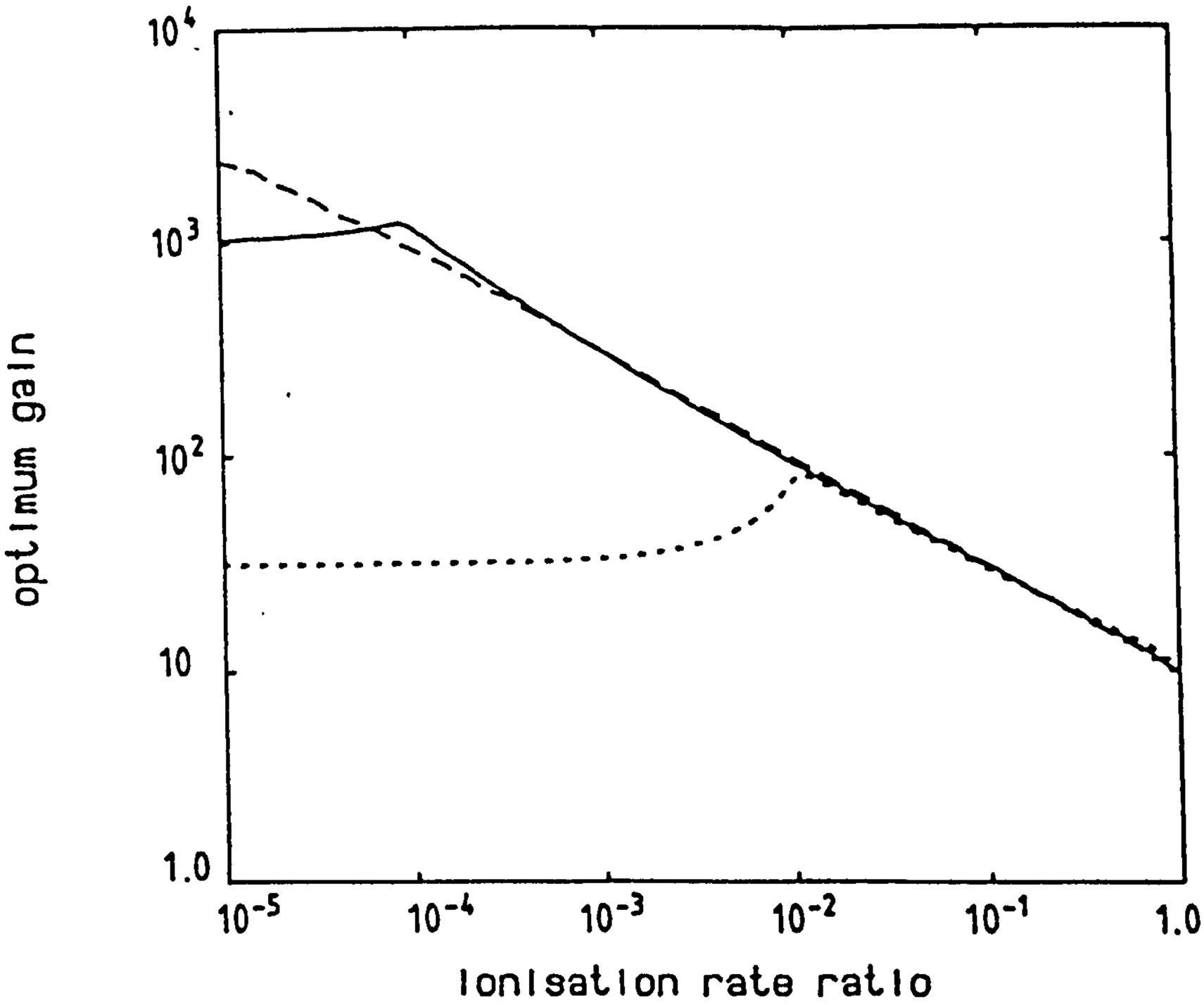

Fig. 9.2 Optimum gain as a function of ionisation rate ratio k.
..... N=5 —— N=10 - - - CAPD

I_{dd} due to minority carriers diffusing from the p^+ region. Fig. 9.3a illustrates that at zero dark current the CAPD offers better sensitivity than the 5-stage SAPD at lower values of k. Also there is an optimum value of k at which the sensitivity of the SAPD receiver is maximised, in contrast to the CAPD receiver for which the sensitivity degrades as k increases. The existence of 100 nA dark current degrades the performance of both receivers, but the influence is greater for CAPD, especially due to the diffusion dark current component. Note that for I_{dd}=100 nA the SAPD receiver gives improved sensitivity compared with a CAPD receiver over the entire range of k.

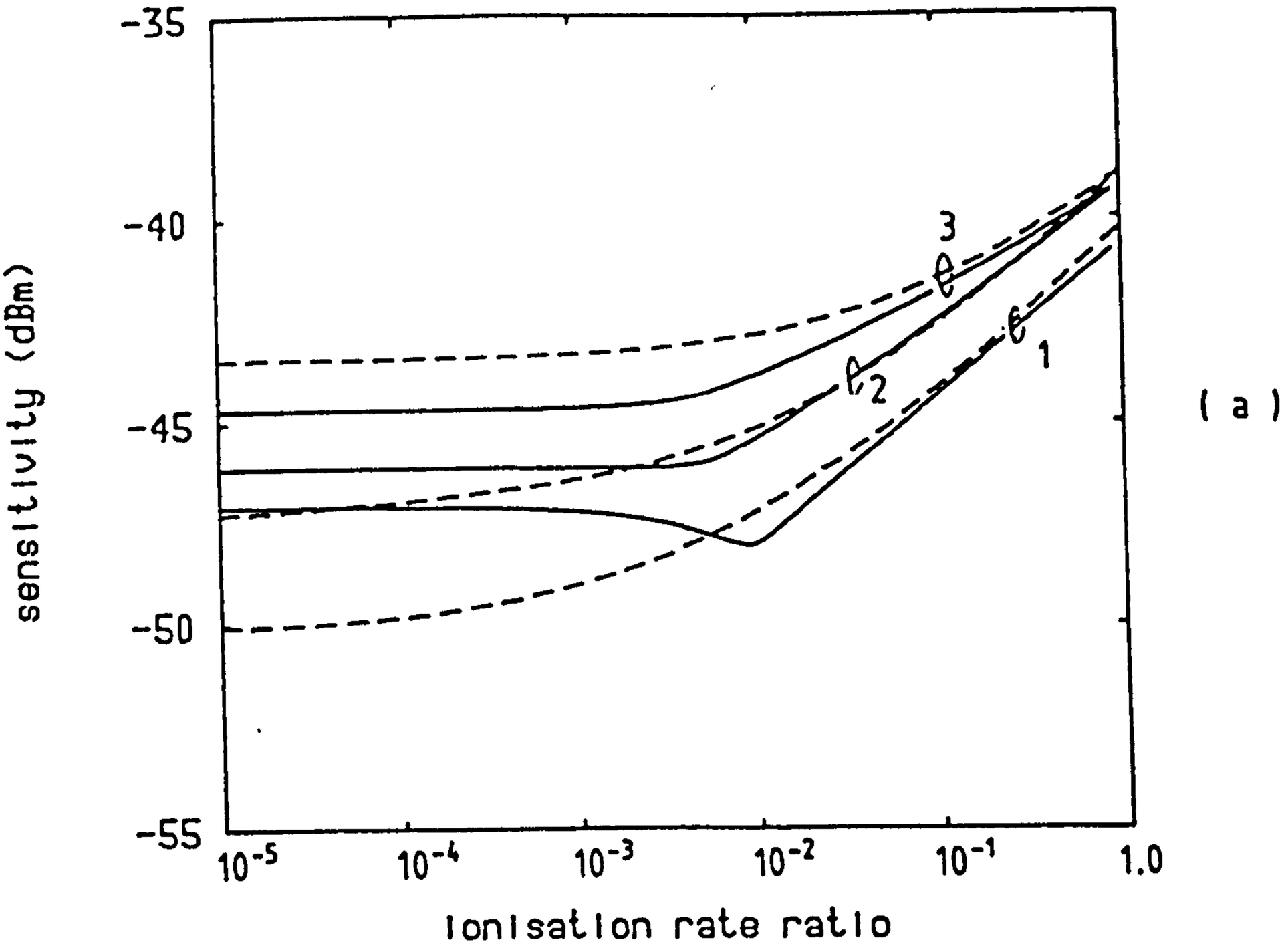

(a)

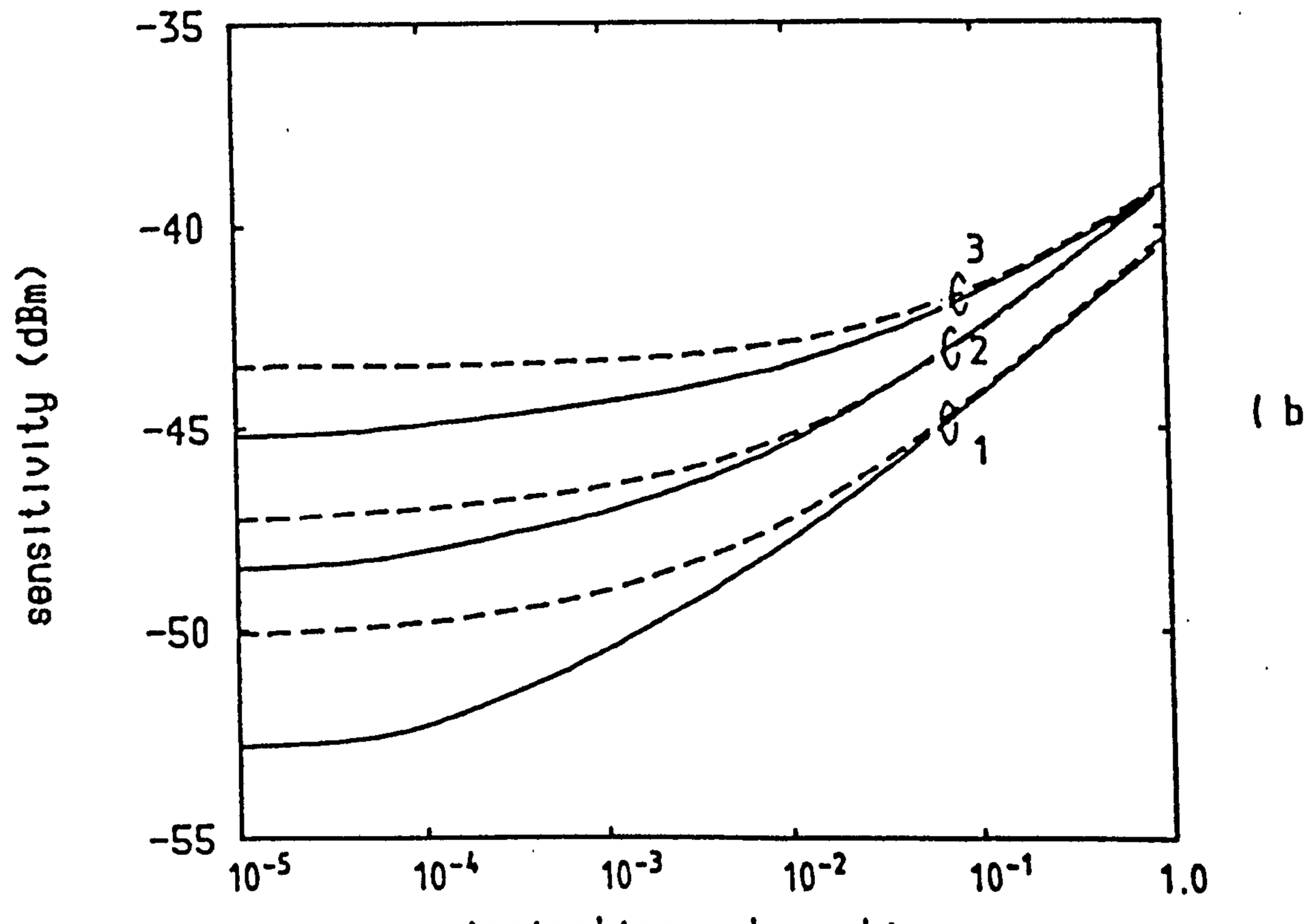

(b)

Fig. 9.3 Optimum sensitivity versus ionisation rate ratio.

(a) N=5 (b) N=10 SAPD CAPD

1: $I_{da}=I_{dd}=0$ 2: $I_{da}=100$ nA 3: $I_{dd}=100$ nA

Fig. 9.3b indicates clearly that sensitivity improvement can be attained by a 10-stage SAPD compared with a CAPD receiver when k is small, but it is more severely affected by dark current. Since long wavelength CAPDs have k between 0.1 and 1, Figs.9.3a and 9.3b indicate that a SAPD can offer about 5dB sensitivity improvement if k is kept less than 0.01. However, the sensitivity improvement will be larger at higher bit rate when the effect of finit gain-bandwidth product is taken into account [MacBean, 1990a]. Note that for $k>0.1$ the optimum sensitivity is almost the same for $N=5$ and $N=10$. In this case $N=5$ is preferred for high speed operation. Our previous results in Section 3.5 show that a single stage SAPD can provide better performance if k is close to 1. Figs. 9.4a and 9.4b summarise the sensitivity penalty due to $I_{dd}=100nA$ and $I_{dd}=100nA$ respectively for the three types of receiver. As expected, the penalty due to I_{dd} is higher than that due to I_{da} for all receivers.

9.2 Signal Design for APD Receivers

9.2.1 Introduction

Receivers for digital direct detection optical communications generally employ a signal element waveform providing a close approximation to a full raised-cosine Fourier spectrum. For conventional digital electrical communications this signal satisfies Nyquist's first and second criteria for distortionless transmission [Nyquist, 1928; Bennett and Davey, 1965]; it provides both zero intersymbol interference (ISI) and zero telegraph distortion (TD) so the system eye pattern is wide-open both vertically and horizontally. For optical communications based on direct detection receivers employing APDs, the optimum decision threshold may be depressed

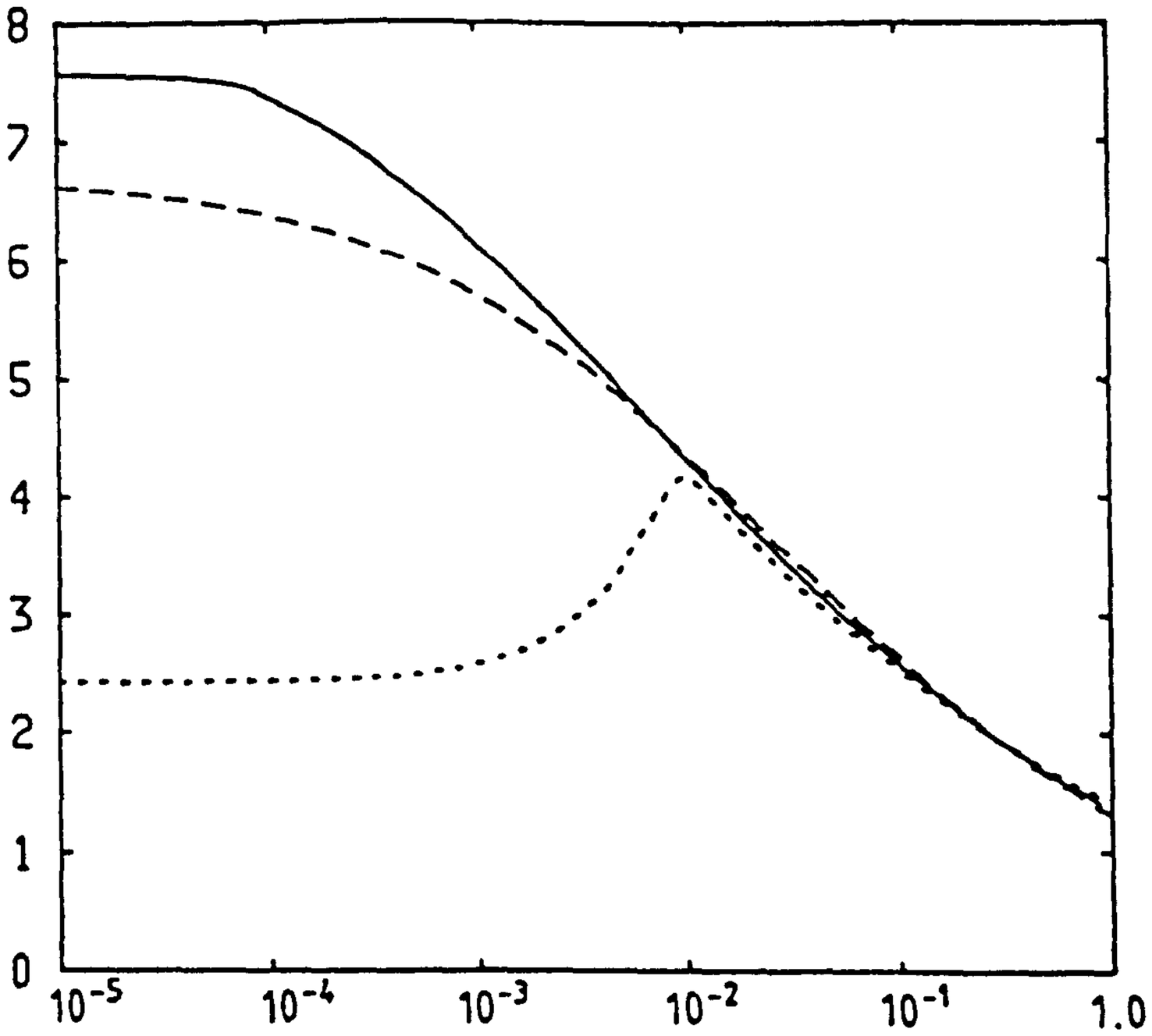

(a)

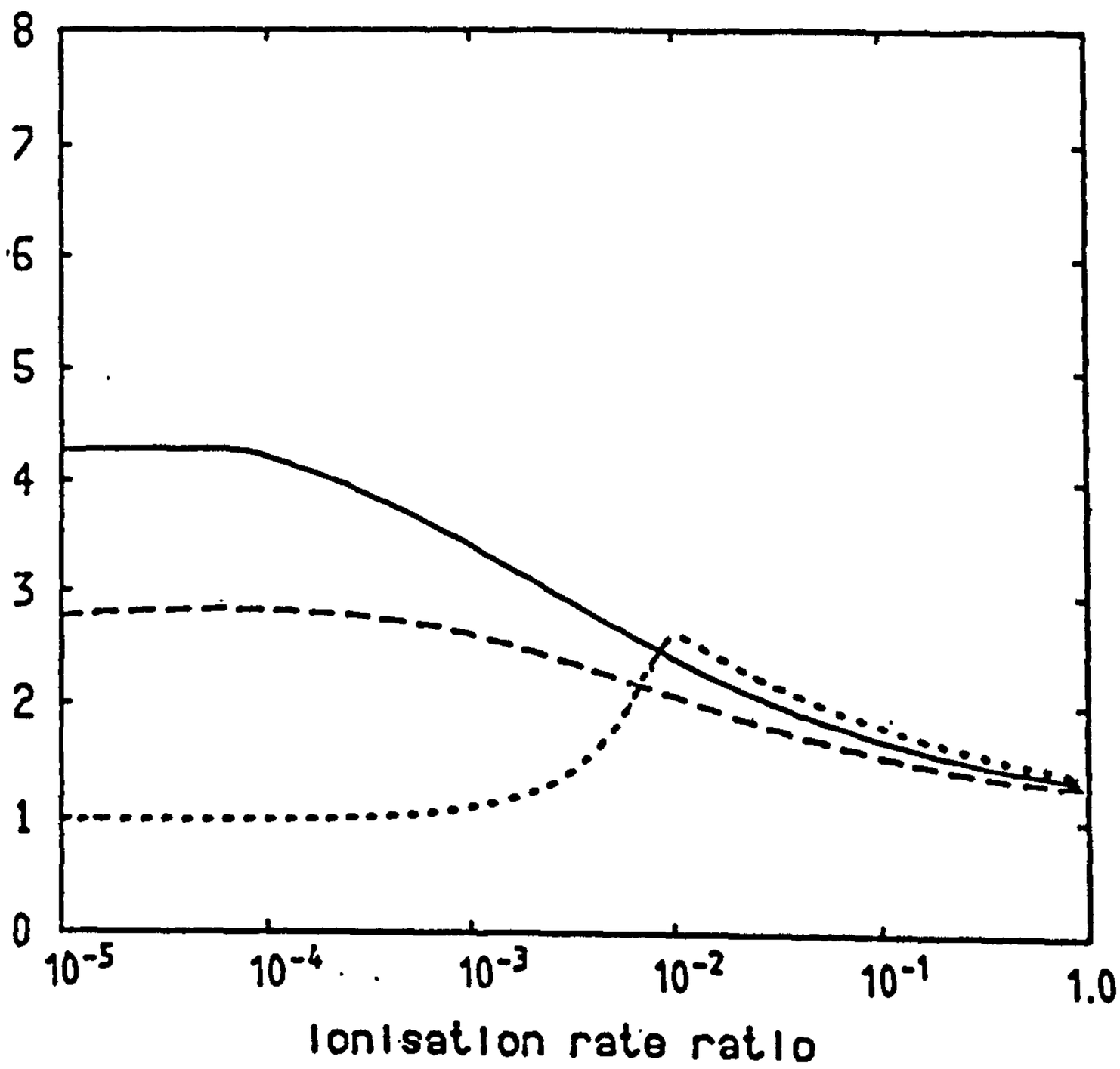

(b)

Fig. 9.4 Sensitivity penalty due to dark current.

(a) I_{dd}=100 nA (b) I_{da}=100 nA

..... N=5 —— N=10 --- CAPD

significantly below the mid-range of the vertical eye opening. This is true for both CAPD receivers [Personick, 1973] and SAPD receivers [Fyath and O'Reilly, 1989b; 1989d], as illustrated previously in Chapter 7. In these circumstances, a full raised-cosine signal does not actually provide zero TD, since signal transmissions, while crossing the half-amplitude level mid-way between sampling instants, give rise to threshold crossings which are displaced from these times. There are two important consequences for practical application:

(a) For untimed or 2R repeaters, providing signal reshaping and regeneration but not retiming, a non-optimum midway decision threshold must be adopted if severe telegraph distortion is not to occur [O'Reilly and Cochrane, 1980].

(b) For retimed or 3R repeaters (reshaping, regeneration and retiming) the eye closes assymmetrically for "ones" and "zeros" in the presence of sampling time offset or sampling alignment jitter.

In the rest of this chapter we address the problem of identifying and evaluating signal processing strategies which provide signal element waveforms offering both zero ISI and TD for APD-based optical receivers with depressed threshold. In the absence of timing errors, the sensitivity of receivers based on these new signal designs is found to be marginally better than that obtained for full raised-cosine receivers. Most significantly, though, the sensitivity penalty due to sampling alignment jitter is much reduced.

9.2.2 New Signal Design

Let $h_o(t)$ be the equalised pulse shape at the input to the decision circuit, so that

$$h_o(t) = \begin{cases} 1;\ t=0 \\ 0;\ t=KT,\ K\neq 0 \end{cases} \Big\} \text{zero ISI}$$
$$\qquad\qquad \begin{cases} 0;\ t=(K+\frac{1}{2})T,\ K\neq 0,-1 \\ d;\ t=\pm T/2 \end{cases} \Big\} \text{zero TD} \qquad (9.1)$$

where T is the signalling interval and d is the normalised decision threshold ($0 < d \leq 0.5$). These constraints on $h_o(t)$ can be expressed concisely as

$$h_o(t) \sum_{K=-\infty}^{\infty} \delta(t-KT/2) = \delta(t) + d.\delta(t \pm T/2) \qquad (9.2)$$

where $\delta(.)$ is the Dirac delta function. This implies constraints in the frequency domain on $H_o(f)$, the Fourier transform of $h_o(t)$, as follows

$$H_o(f) * \frac{2}{T} \sum_{K=-\infty}^{\infty} \delta(f-2K/T) = 1+2d\ \cos(\pi fT) \qquad (9.3)$$

or

$$\frac{2}{T} \sum_{K=-\infty}^{\infty} H_o(f-2K/T) = 1+2d\ \cos(\pi fT) \qquad (9.4)$$

where * denotes convolution. For eqn. 9.4 to be satisfied $H_o(f) \Leftrightarrow h_o(t)$ must occupy a bandwidth of at least 1/T, and for this minimum bandwidth case $H_o(f)$ can be expressed, amplitude normalised to T/2, as

$$H_o(f) = \begin{cases} 1 + 2d\cos(\pi fT);\ |f| < 1/T \\ 0 \qquad\qquad \text{elsewhere} \end{cases} \qquad (9.5)$$

The corresponding time-domain signal element waveform is given by

$$h_o(t) = \frac{\sin(2\pi t/T)}{2\pi t/T}\left\{\frac{1-4(t/T)^2(1-2d)}{1-4(t/T)^2}\right\} \qquad (9.6)$$

for d=0.5 the full raised-cosine response is obtained. This latter case is appropriate for optical receivers using PIN photodiode in which the signal dependent noise is negligible so that a threshold value corresponding to one half of the vertical eye aperture is appropriate. For APD receivers the optimum value of d is generally less than 0.5, often significantly so. Figs. 9.5a and 9.5b illustrate in the time and frequency domains, respectively, the required response for d=0.3

We note that although the responses specified by eqns. 9.5 and 9.6 are ideal minimum bandwidth solutions for the problem posed, there are significant practical difficulties which render them inappropriate as target functions for signal element waveform design. Specifically, for $d<0.5$ the spectrum falls abruptly to zero at $f=1/T$, necessitating a very sharp cut-off filter which is difficult to realise, while the not unrelated oscillatory nature of $h_o(t)$ requires precisely synchronised sampling. Slight deviations in pulse rate, decision sampling time or filter cut-off frequency can lead to significant impairment.

It is appropriate therefore to modify the initial target frequency response to provide a gradual roll-off whilst retaining the property indicated in eqn. 9.4, and thereby ensuring that the conditions specified in eqn. 9.1 remain satisfied. We begin by noting that the response $H_o(f)$ can be considered as the sum of two

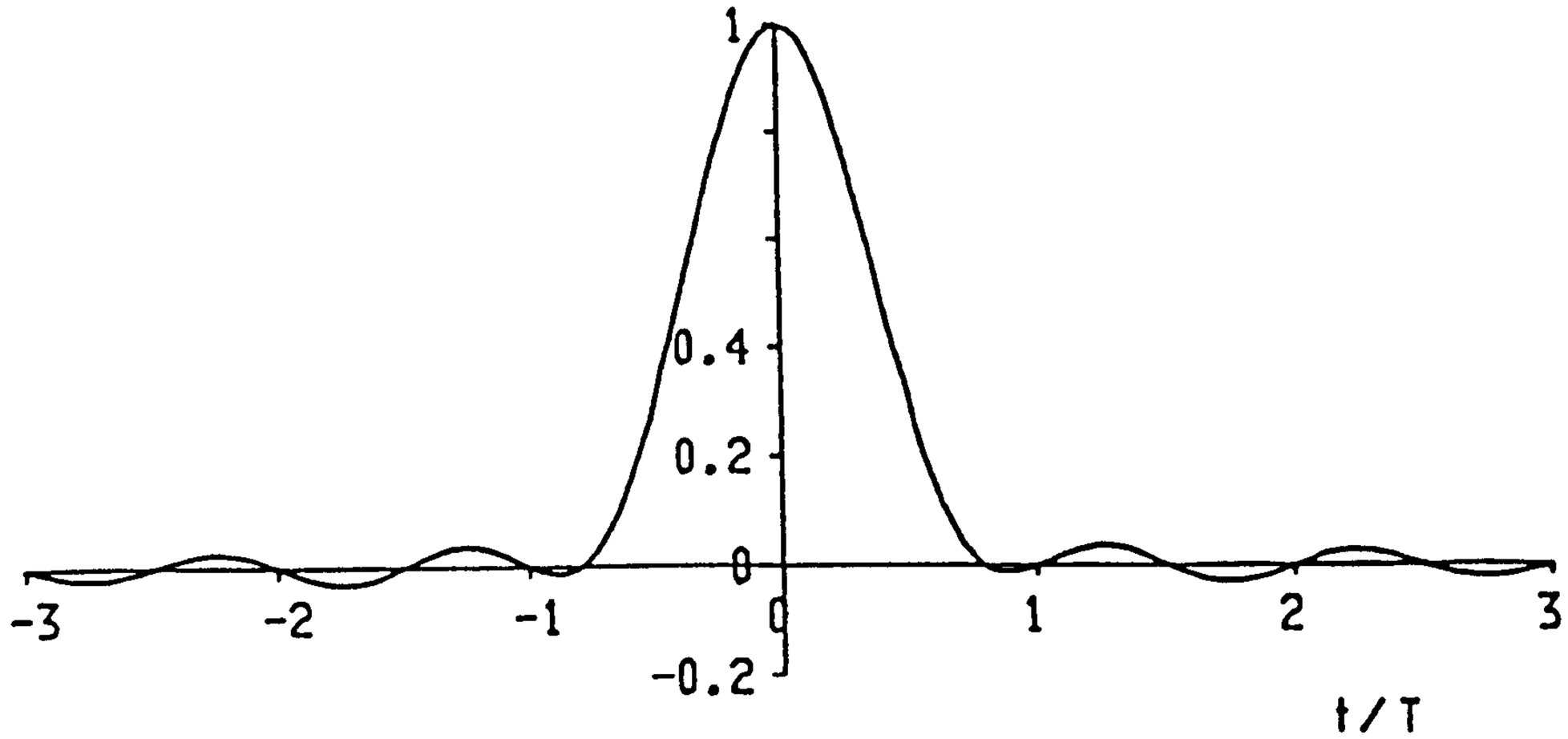

(a)

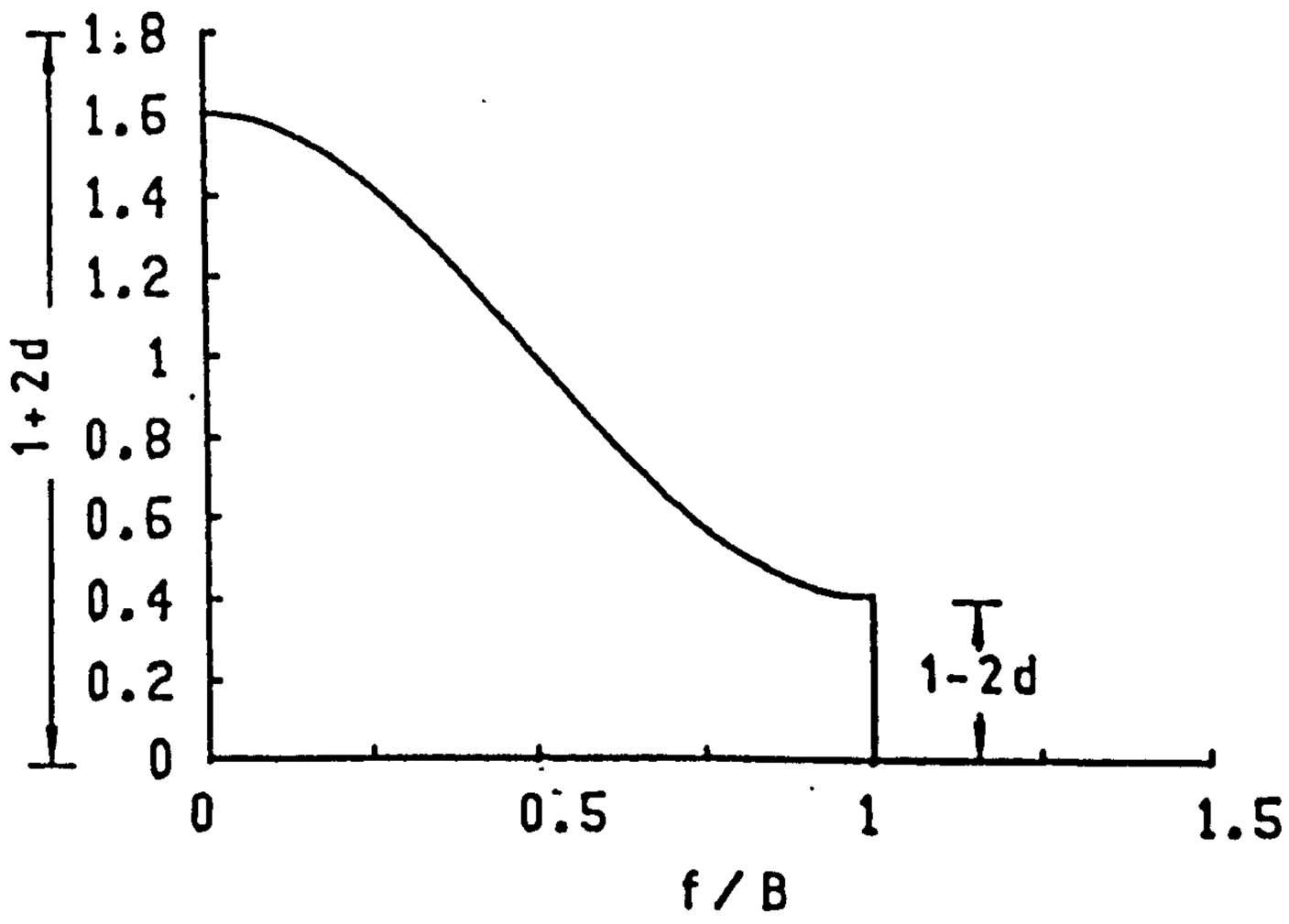

(b)

Fig. 9.5 Signal designs achieving zero ISI and zero TD for d=0.3 in the minimum bandwidth of 1/T.

(a) time domain response (b) frequency response

components: a full raised-cosine function $H_1(f)$ and a rectangular function $H_2(f)$

$$H_o(f) = H_1(f) + H_2(f) \tag{9.7}$$

where

$$H_1(f) = \begin{cases} 2d[1+\cos(\pi ft)] & ; \quad |f| < 1/T \\ 0 & \text{elsewhere} \end{cases} \tag{9.8}$$

$$H_2(f) = \begin{cases} 1-2d & ; \quad |f| < 1/T \\ 0 & \text{elsewhere} \end{cases} \tag{9.9}$$

The corresponding time domain responses for the individual components of eqns. 9.8 and 9.9 satisfy the following conditions

$$h_1(t) = \begin{cases} 2d; & t=0 \\ d; & t=\pm T/2 \\ 0; & t=KT/2,\ K\neq 0,\ \pm\ 1 \end{cases} \tag{9.10}$$

$$h_2(t) = \begin{cases} 1-2d; & t=0 \\ 0; & t=KT/2,\ K\neq 0 \end{cases} \tag{9.11}$$

Note that $h_2(t)$ = zero when $h_1(t)$ is equal to either zero or d. Hence $H_2(f)$ can be modified in accordance with Nyquist's first criterion by adding a transmission function which has skew symmetry about the cut-off frequency of 1/T [Nyquist, 1928], and the resultant time response will satisfy the conditions summarised by the right hand side of eqn. 9.11. The modified characteristic $\hat{H}_2(f)$ can conveniently be chosen to have a sinusoidal roll-off. It then has the form

$$\tilde{H}_2(f) = \begin{cases} 1\text{-}2d & \text{for } 0 < |f| < (1-\alpha)B \\ \frac{1}{2}\text{-}2d \left[1\text{-}\sin\left[\frac{\pi(f-B)}{2\alpha B}\right]\right] & \text{for } (1-\alpha)B < |f| (1+\alpha)B \\ 0 & \text{for } |f| > (1+\alpha)B \end{cases} \quad (9.12)$$

where $B \equiv 1/T$ is the signalling rate, and α is the roll-off factor ($0 \leq \alpha \leq 1$). Hence the overall modified frequency response $\tilde{H}_0(f)$ is given by

$$\tilde{H}_o(f) = H_1(f) + \tilde{H}_2(f) \quad (9.13)$$

with time domain response

$$\tilde{h}_o(t) = \frac{\sin(2\pi t/T)}{(2\pi t/T)} \left[\frac{2d}{1-4(t/T)^2} + \frac{(1-2d)\cos(2\pi\alpha t/T)}{1-(4\alpha t/T)^2} \right] \quad (9.14)$$

Eqn. 9.14 represents a family of signals satisfying the conditions of eqn. 9.1, which reduces to the response for a full raised-cosine for d=0.5 and α=0. Figs. 9.6a and 9.6b illustrate the corresponding time and frequency domain responses for the case d=0.3 and α=0.25. Note that $\tilde{h}_o(t)$ exhibits only slight oscillations, and consequently is not unduly sensitive to sample time errors or variations in the signalling rate.

The modified signals are strictly bandlimited to $(1+\alpha)$ times the signalling rate. Investigation has shown that values of α between 0 and 0.3 provide a suitably smooth roll-off for values of d in the range 0.5 to 0.2.

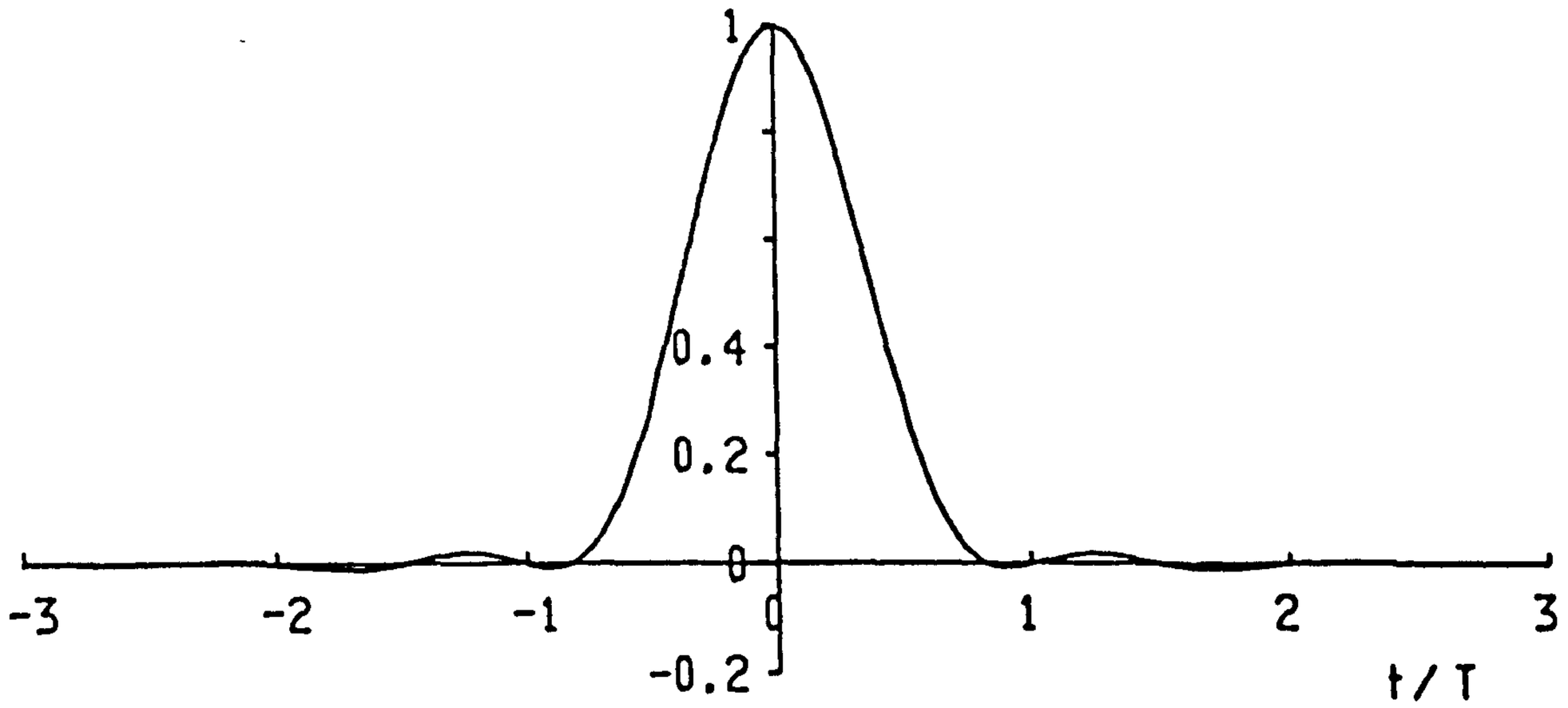

(a)

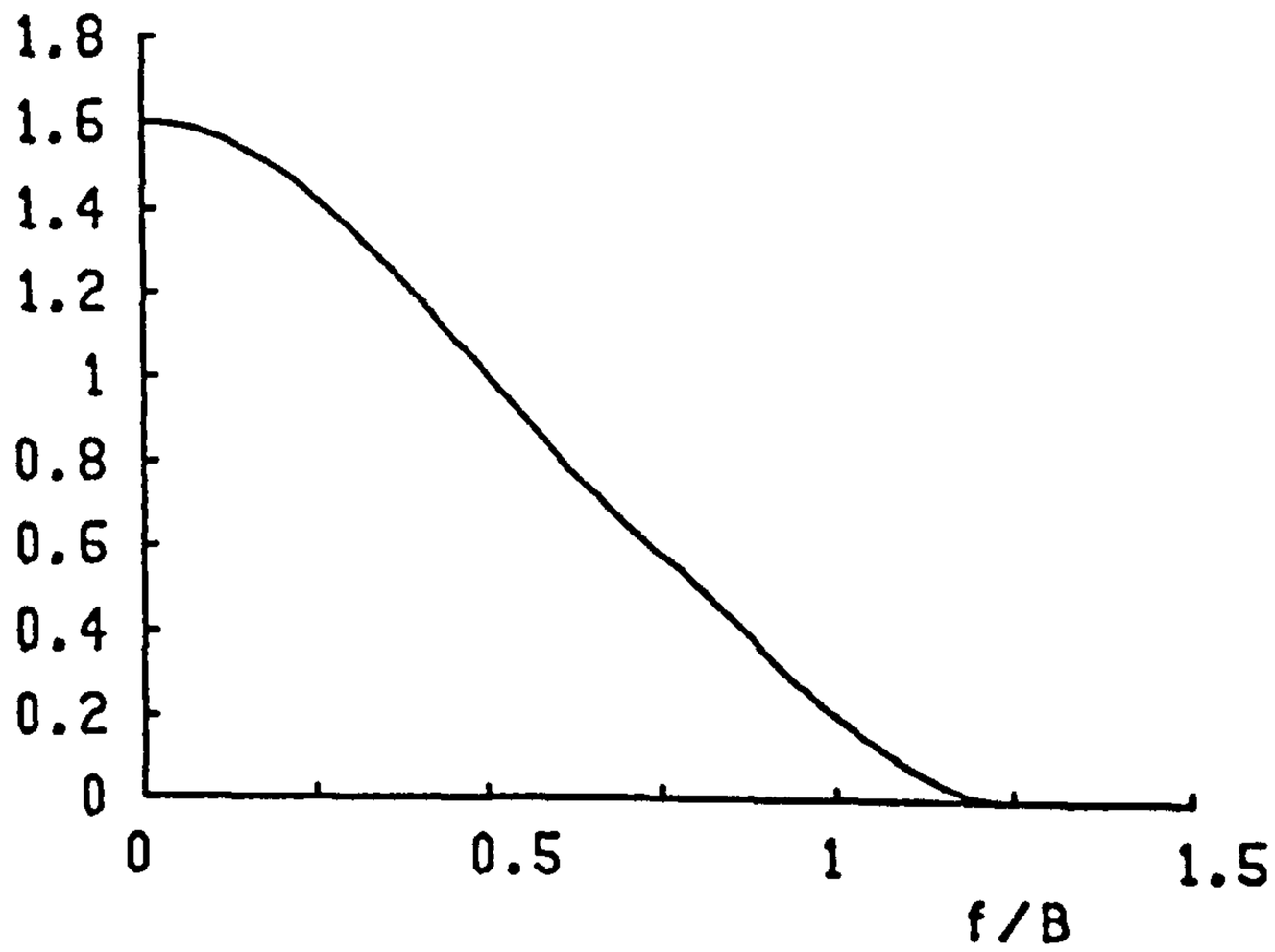

(b)

Fig. 9.6 Modified signal designs achieving zero ISI and zero TD for d=0.3 with α=0.25 giving an extended bandwidth of (1+α)/T.

(a) time response (b) frequency response

9.3 Practical Filter Realisation

The procedure outlined in Section 9.2.2 has identified desired signal pulse waveforms and spectra at the output of the receiver. The actual characteristic required for the filter $H_f(f)$, will depend, of course, on the signal element waveform $h_i(t)$, and hence spectrum $H_i(f)$, at the input to the filter:

$$H_f(f) = \hat{H}_o(f)/H_i(f) \tag{9.15}$$

For most practical applications the input will be essentially an approximately rectangular pulse of width either T, corresponding to non-return to zero (NRZ) signalling, or T/2, corresponding to return to zero (RZ) signalling. The signal designs we are concerned with here are applicable to RZ and we shall adopt this format when presenting illustrative examples. We find that $H_f(f)$ can be reasonably approximated by a fourth order lowpass ladder filter, as shown in Fig. 9.7, with pole locations chosen to minimise a frequency domain mean squared error function given by

$$E = \sum_{i=1}^{n} |H_f(f_i) - H_p(f_i)|^2 \tag{9.16}$$

where $H_p(f)$ is the transfer function of the practical filter and n is the number of evaluation points selected in the frequency range $0<f<2B$. In our studies $n=80$ was employed. For a particular case of $d=0.3$, $\alpha=0.25$ the normalised ($B=1Hz$) pole locations obtained were $-1.63\pm j5.02$ and $-2.1\pm j1.53$ rad/s. The computed equalised pulse shape and corresponding filter frequency responses are compared in Fig. 9.8

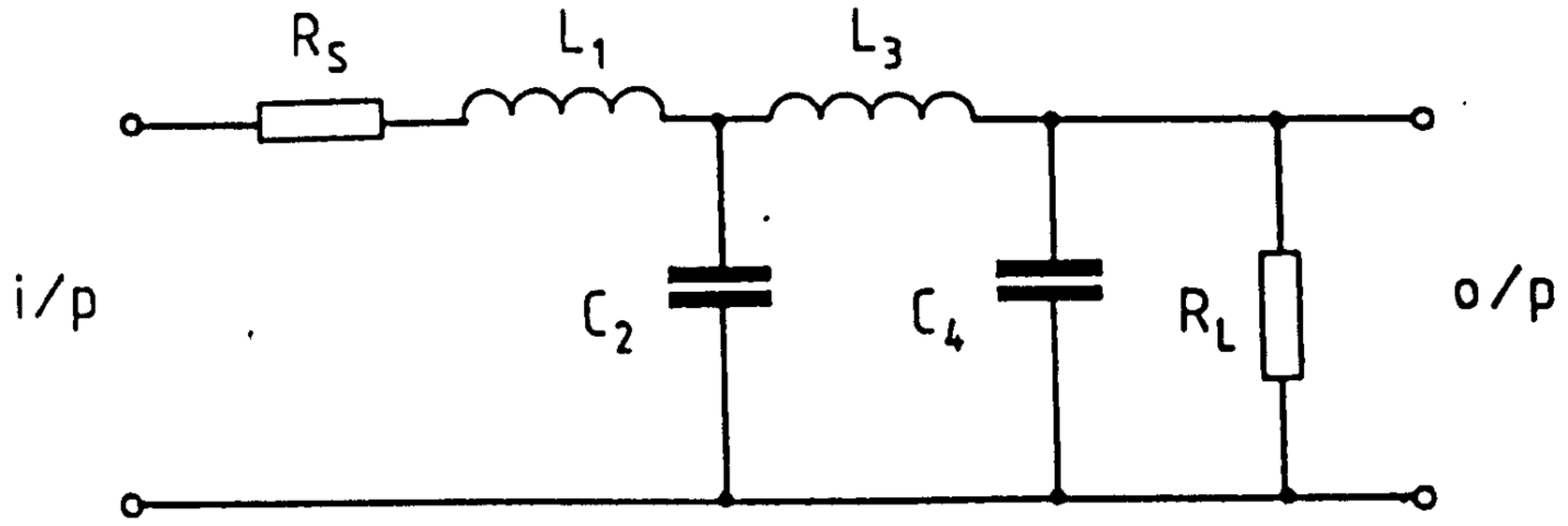

Fig. 9.7 Fourth order ladder filter network providing the basis for approximate realisation of the signal designs of eqns. 9.13 and 9.14.

with the idealised target functions. The practical filter is seen to provide a good approximation to the ideal response, both in the time and frequency domains. The summed square ISI and TD have been calculated as 6.02×10^{-4} and 2.76×10^{-3}, respectively.

The performance of the design may be further illustrated with reference to the system eye-diagram. Computed results for both the ideal target and practical filter are shown in Fig. 9.9 while Fig. 9.10 illustrates the impulse response, pulse response and eye pattern obtained in the laboratory with an experimental system.

Whilst it is possible to design a specific filter for a given threshold value, there are clear operational advantages in being able to tune a given design to cover a range of values; This can be achieved by varying the filter element values, the influence of each on the near-zero-TD threshold is illustrated in Fig. 9.11. Our

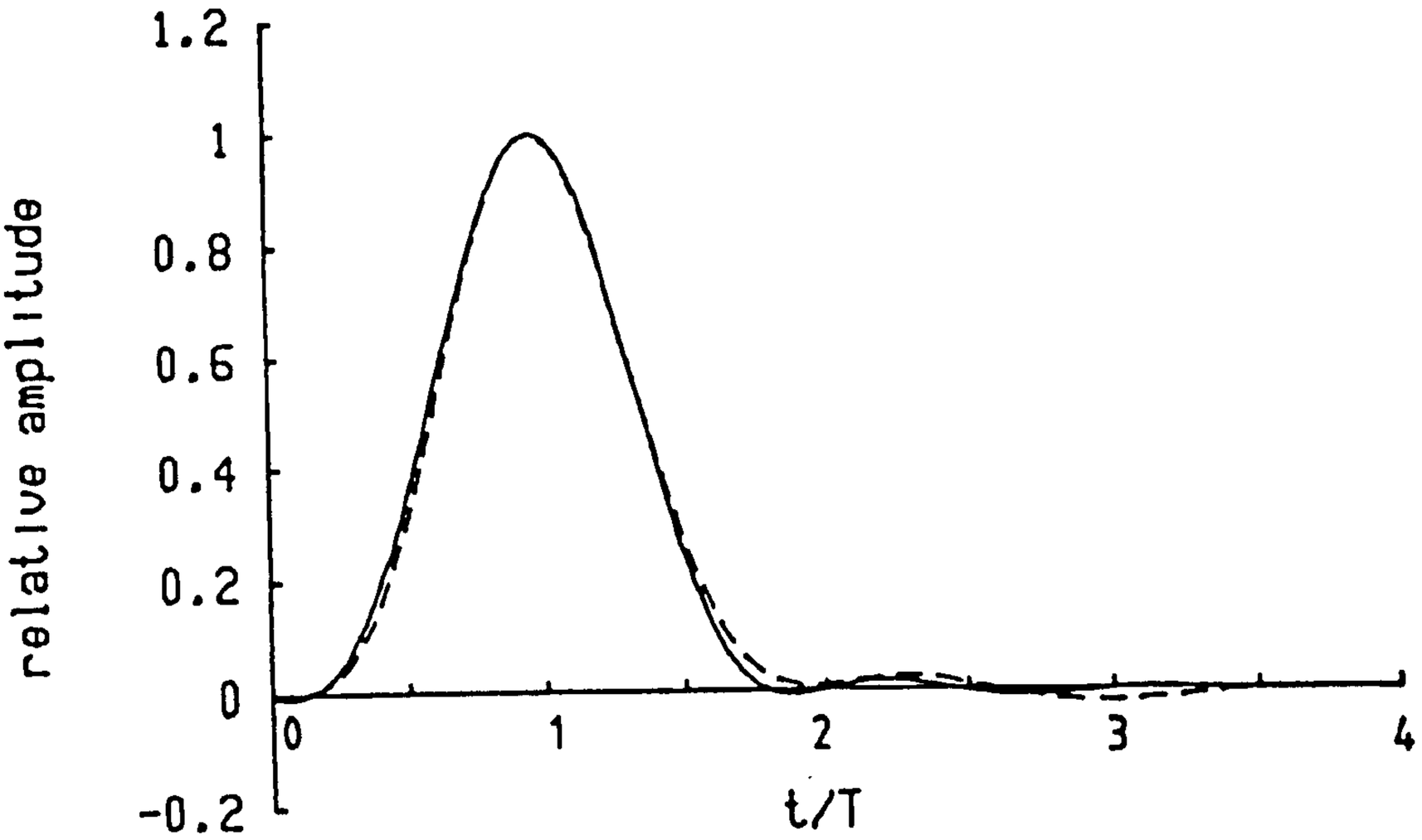

(a)

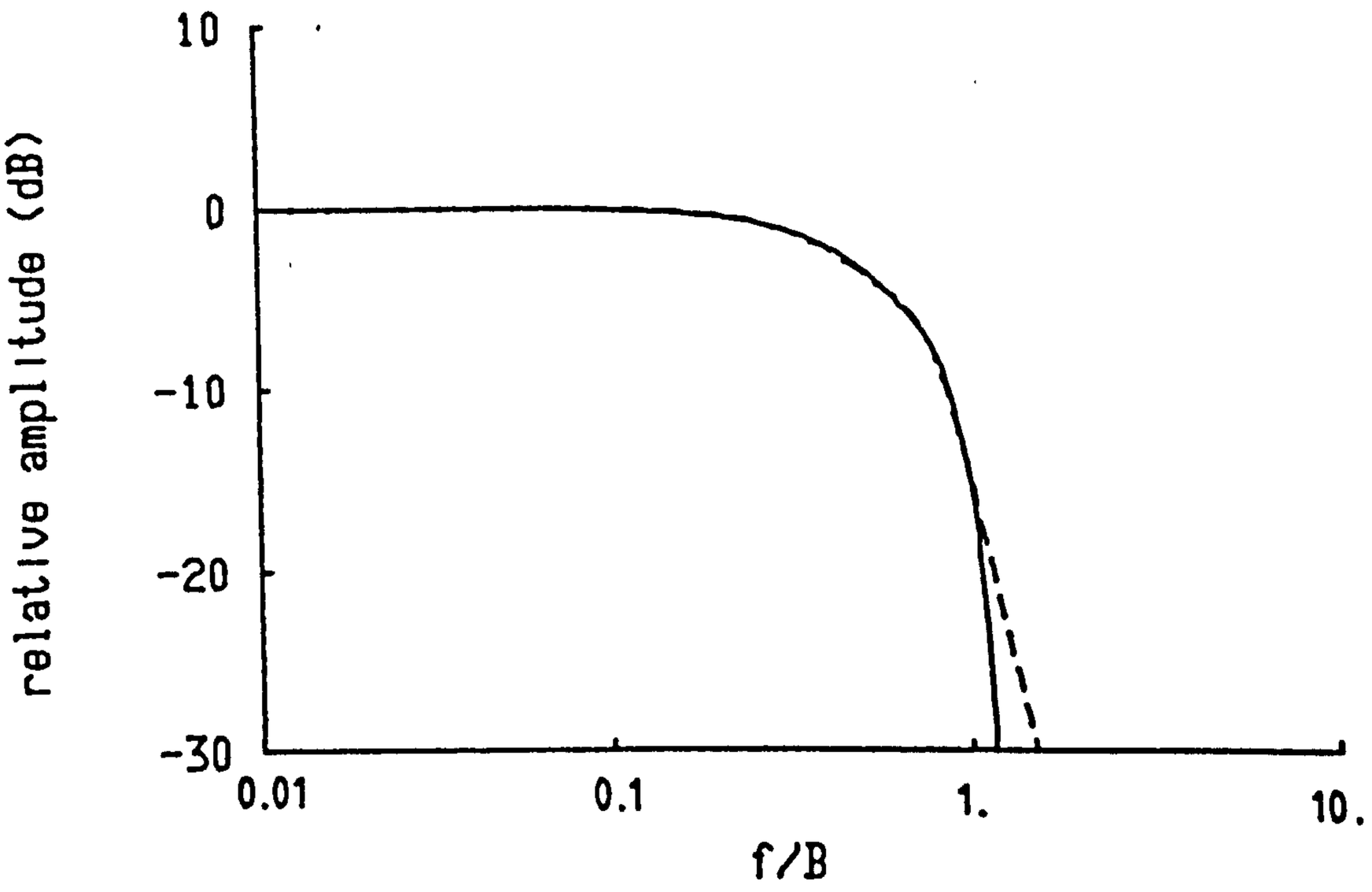

(b)

Fig. 9.8 Comparison of idealised and practical responses achieved by optimising pole locations for the network of Fig. 9.7 with d=0.3 and α=0.25. (a) pulse shapes (b) frequency response functions

——— ideal — — — practical

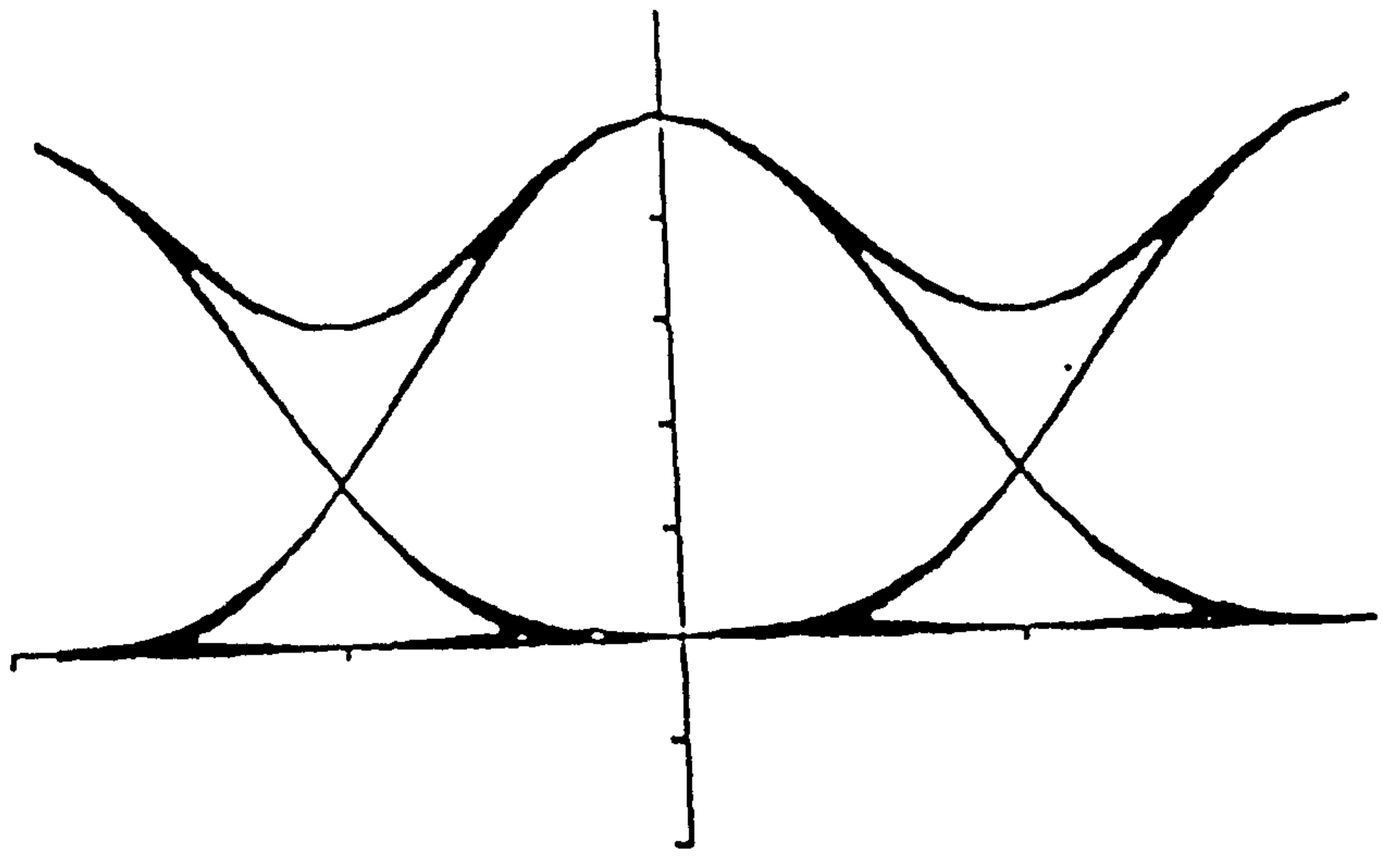

(a)

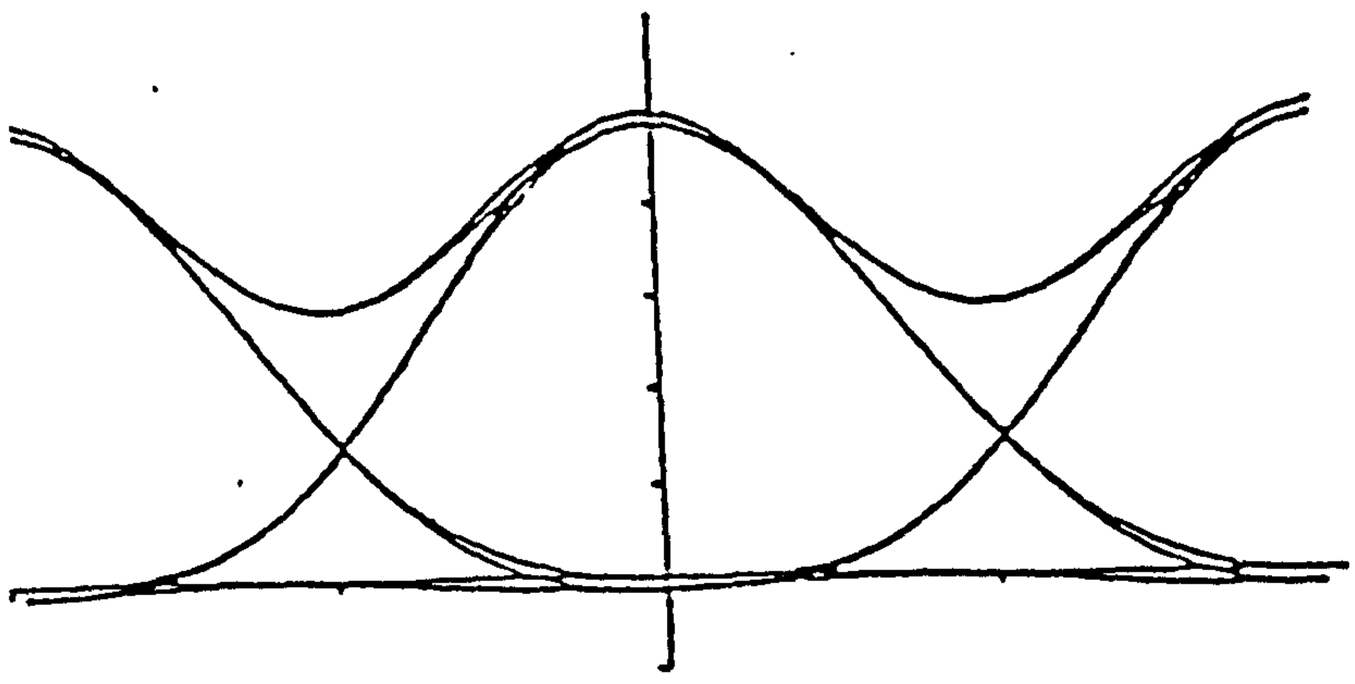

(b)

Fig. 9.9 Computed eye-diagrams at the input to the decision circuit for d=0.3, α=0.25.
(a) ideal signal of eqn. 9.14 (b) practical filter

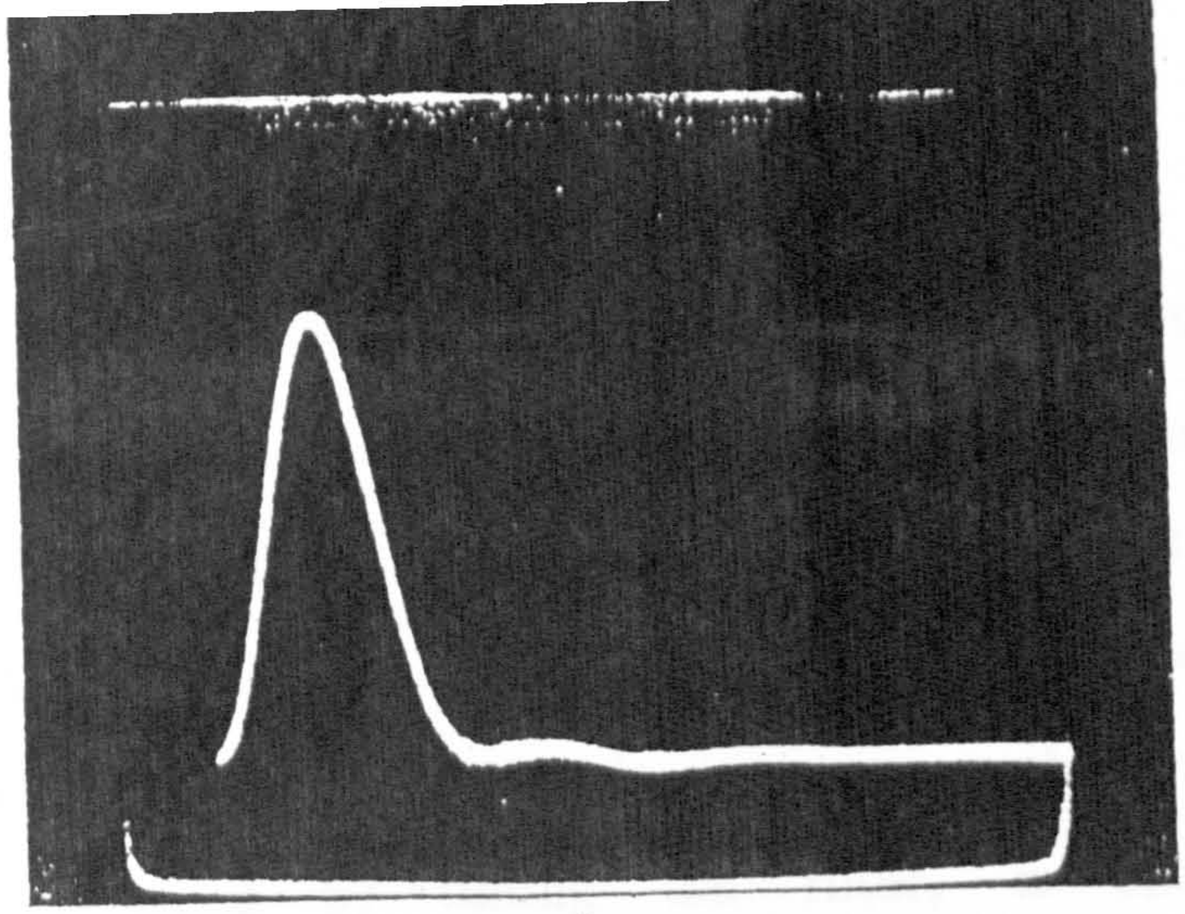

c

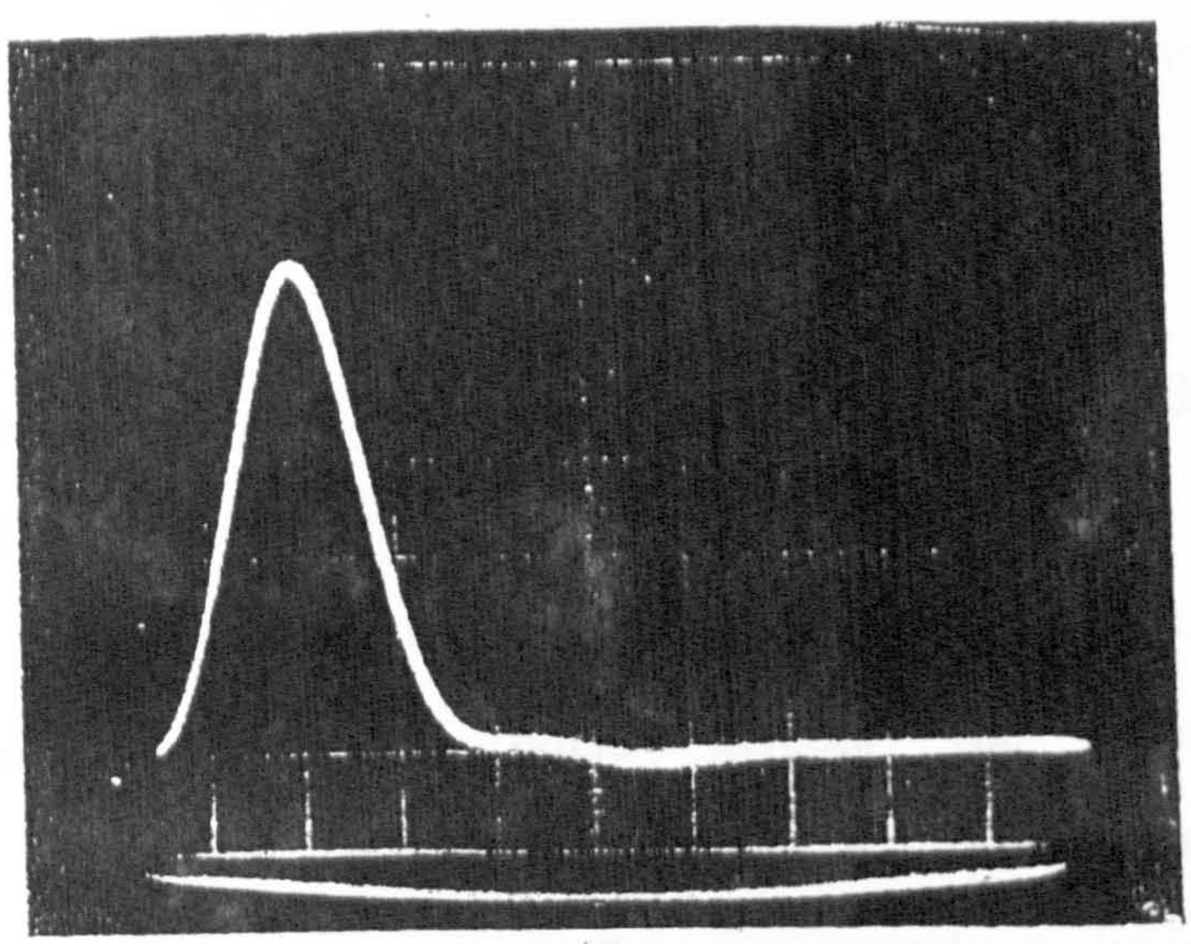

b

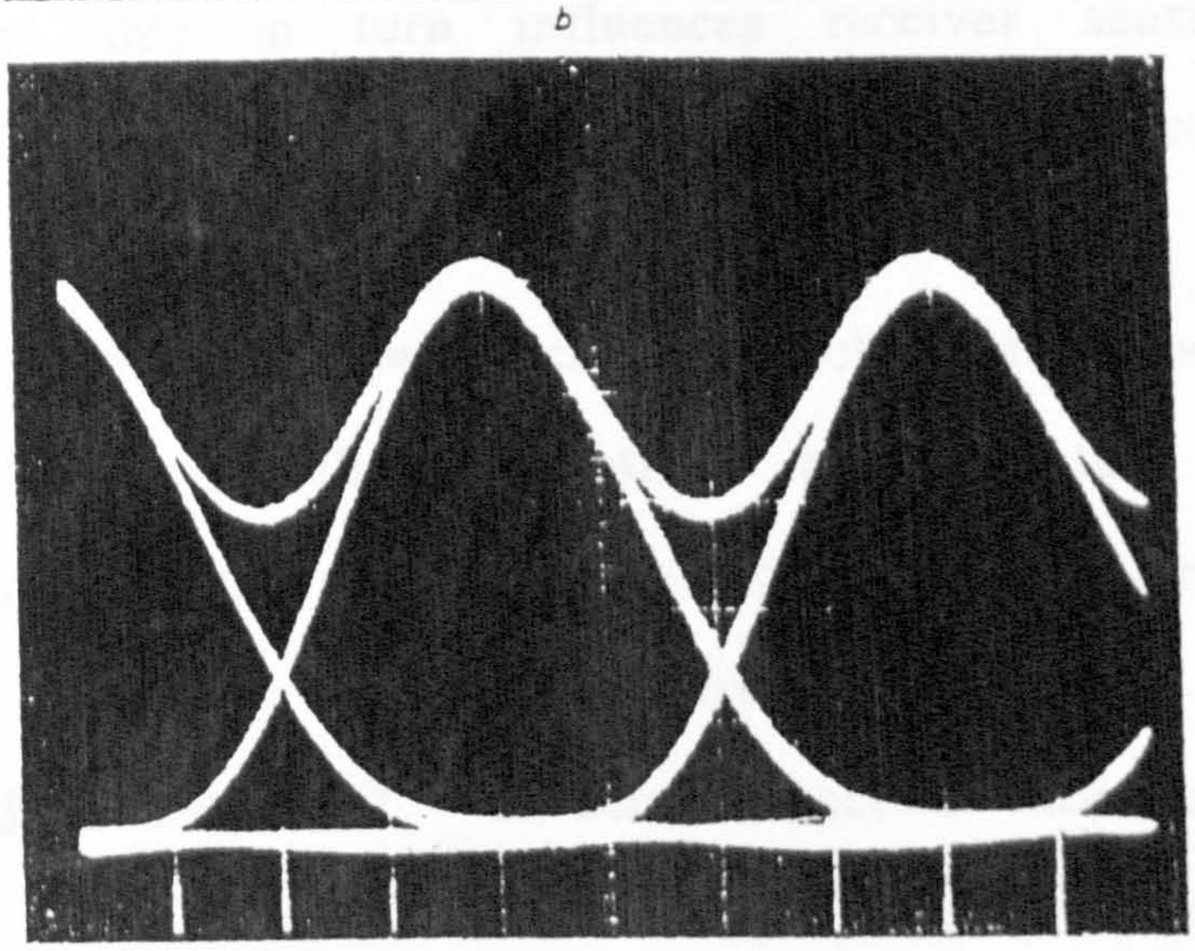

Fig. 9.10 Illustrative results for an experimental system with d=0.3, α=0.25. (a) filter impulse response (b) response to rectangular pulse of width T/2 (c) observed eye pattern

studies indicate that it is practicable to tune a single design over the entire threshold range shown, $0.2<d<0.4$, using just a single variable element and yet maintain a system eye pattern with low ISI and TD. We have found it most appropriate to adopt just L_3 or C_4 as the variable element for this purpose; the relative error in eqn. 9.16, produced by tuning the filter, is shown in Fig. 9.12. Illustrative eye patterns with different threshold values obtained in this way are shown in Fig. 9.13.

9.4 Performance of Optical Receivers using the New Signal Designs

In this section we will discuss the influence of the new signal designs on the performance of fully-retimed receivers. The new shape of the equalised signal pulse affects the value of the noise equivalent bandwidth integrals (denoted as I_1, I_2 and I_3 by Personick [1973]), and this in turn influences receiver sensitivity. For the purposes of illustration we consider a CAPD-FET receiver operating at 2Gbit/s. However, our conclusions are also valid for optical receivers employing superlattice avalanche photodiodes. The APD parameters used in the calculations are: quantum efficiency $\eta=0.7$, ionisation rate ratio $k=0.35$, and diffusion dark current $I_d=10nA$. The front-end amplifier is characterised by the parameter values summarised in Table 3.1. If zero extinction ratio and equiprobable RZ signalling is assumed, then the usual Gaussian approximation [Personick; 1973] indicates an optimum decision threshold level of 0.3. The sensitivity of the receiver for a bit error rate (BER) of 10^{-9} is shown as a function of APD gain $<g>$ in Fig. 9.14 for two equalised signal shapes: the conventional full raised-cosine and the new modified design for $d=0.3$, $\alpha=0.25$. An appropriate threshold is

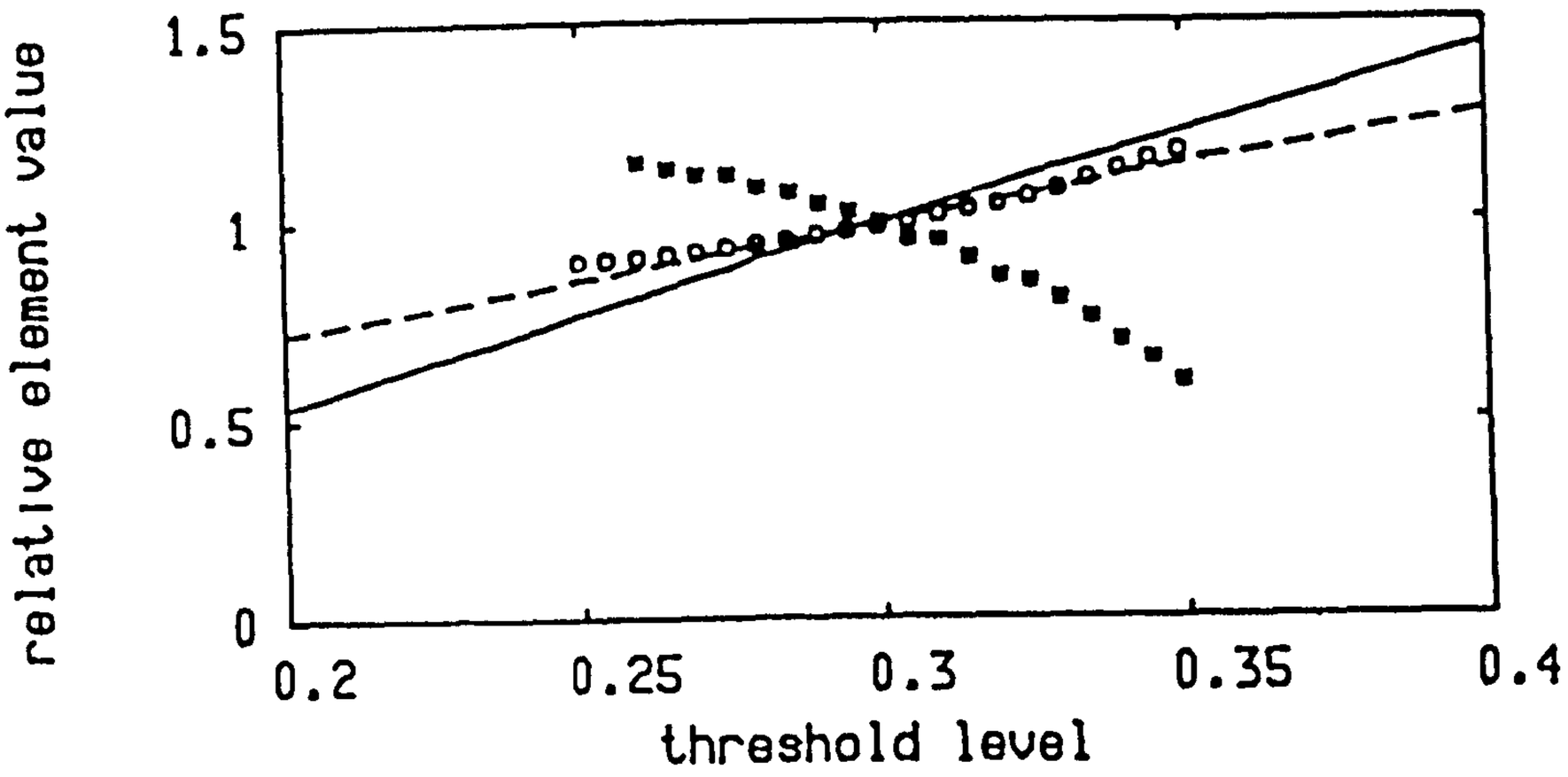

Fig. 9.11 Tuning characteristic of the filter of Fig. 9.7 with respect to each relative element for a nominal d=0.3, α=0.25.

ooo L_1 *** C_2 --- L_3 ——— C_4

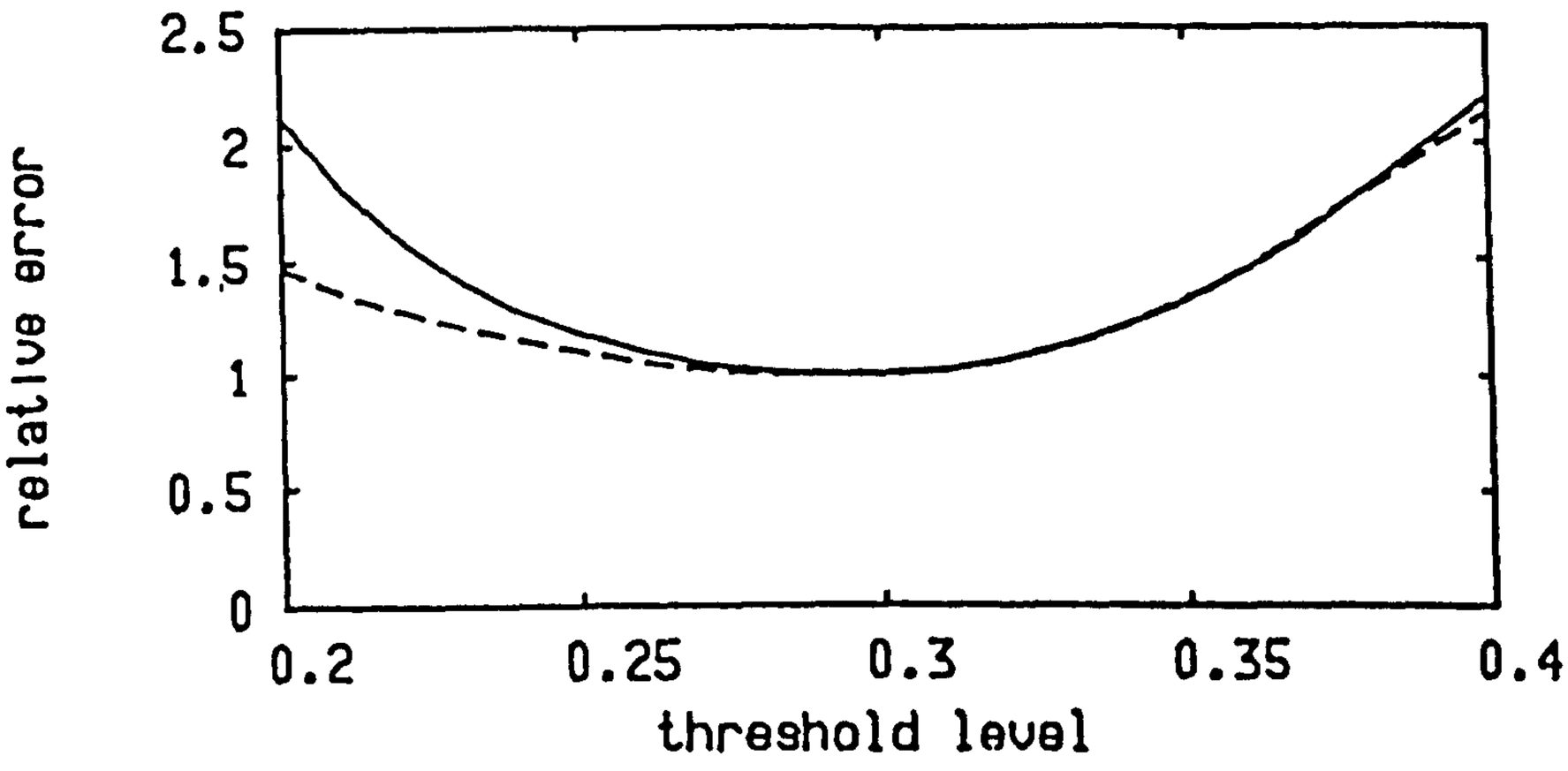

Fig. 9.12 Relative variation in the mean square approximation error of eqn. 9.16 resulting from tuning the filter of Fig. 9.7 by varying L_3 (— — — —) or C_4 (———) to achieve different threshold levels.

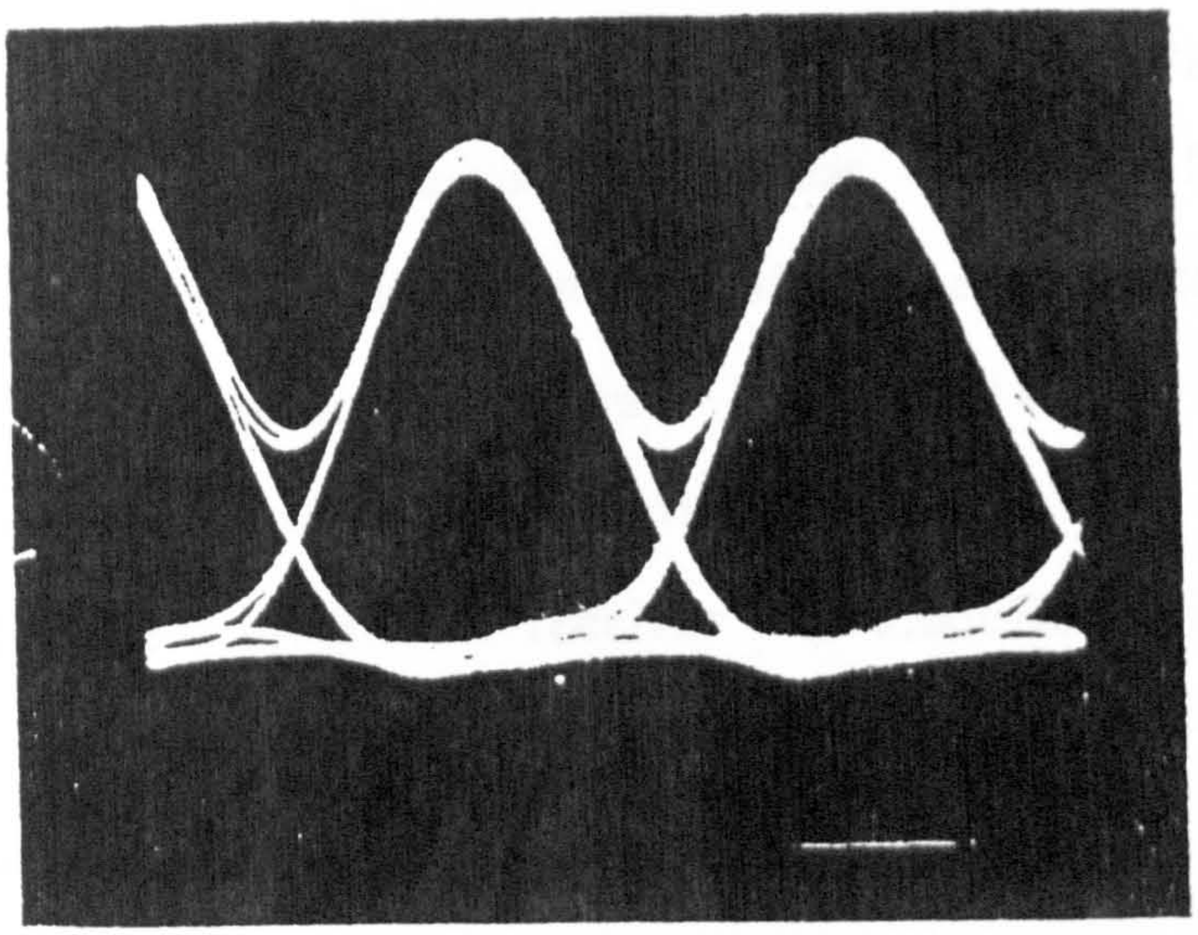

c = 0.2

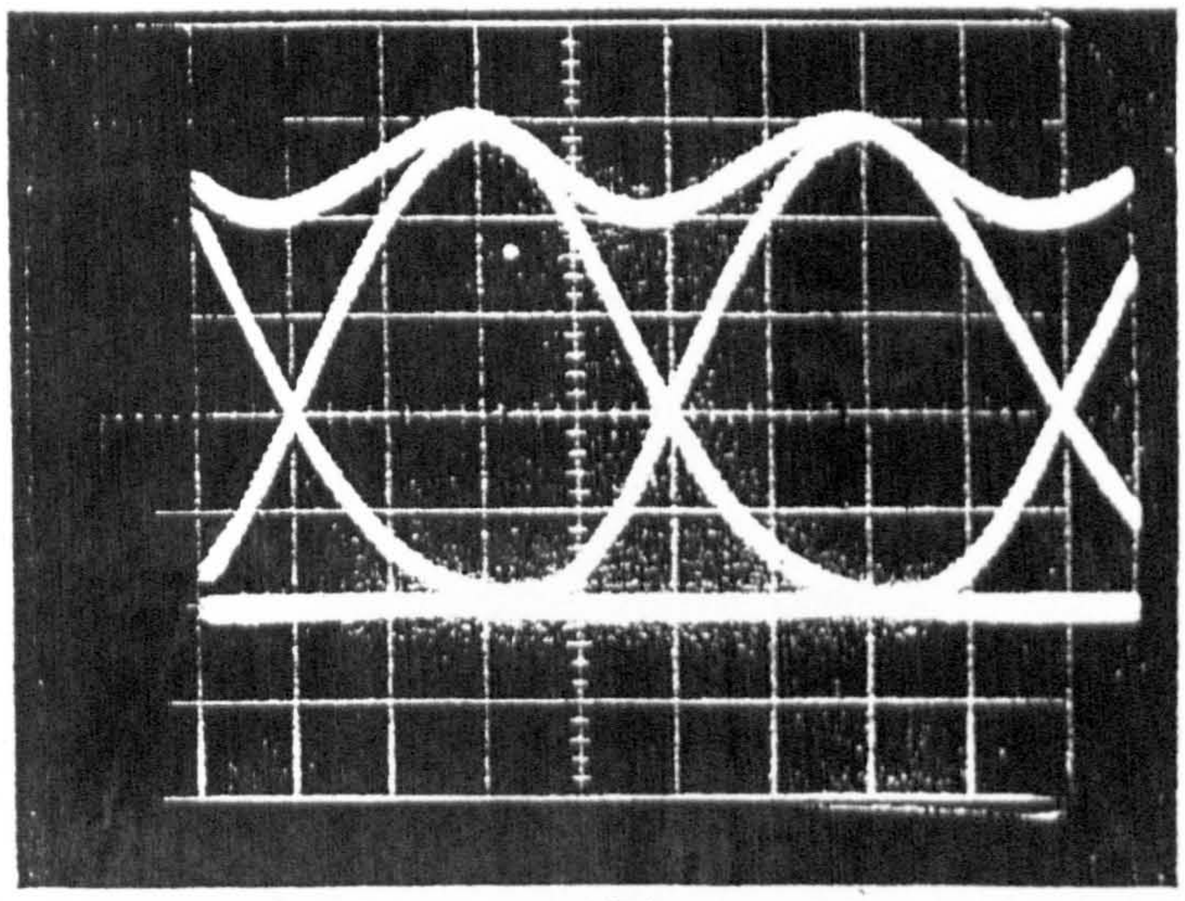

c = 0.4

Fig. 9.13 Experimental eye patterns obtained by varying L_3 to tune the filter of Fig. 9.7 for different decision threshold values.

selected for each gain value without adjusting the filter characteristic. It is to be observed that the modification of the signal design to improve the symmetry of the eye pattern with respect to the depressed threshold has not resulted in a degradation in sensitivity compared with aconventional design. The maximum sensitivity of the modified receiver (-40.65dBm) is a marginal improvement on that for the raised-cosine receiver (-40.5dBm) albeit with a slightly higher value of APD gain (18.48 compared with 15.38).

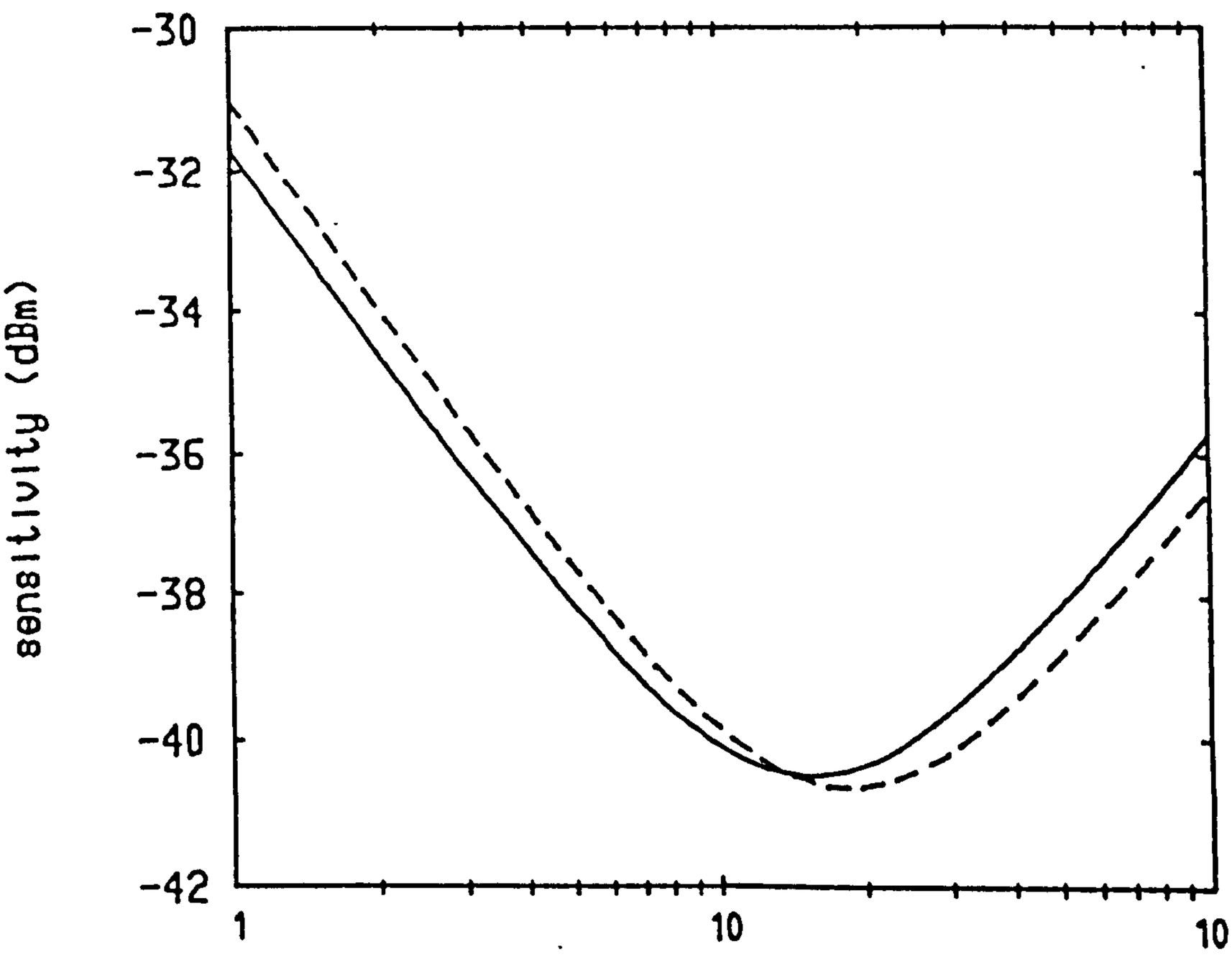

Fig. 9.14 Comparison of sensitivity of full raised cosine (solid) and modified receivers (broken) assuming zero timing error.

The implications of decision time alignment errors on system performance may be appreciated with reference to Fig. 9.15. The normalised root mean square (rms) ISI is plotted as a function of time offset τ for full raised-cosine receiver and for a modified response with d=0.3, α=0.25. In both cases the rms ISI increases with τ, but markedly less so for the signal design. We may determine the mean error probability by averaging, for a given data block size, the sequence conditioned error probabilities. This enables graphs of the receiver sensitivity penalty as a function of time offset to be

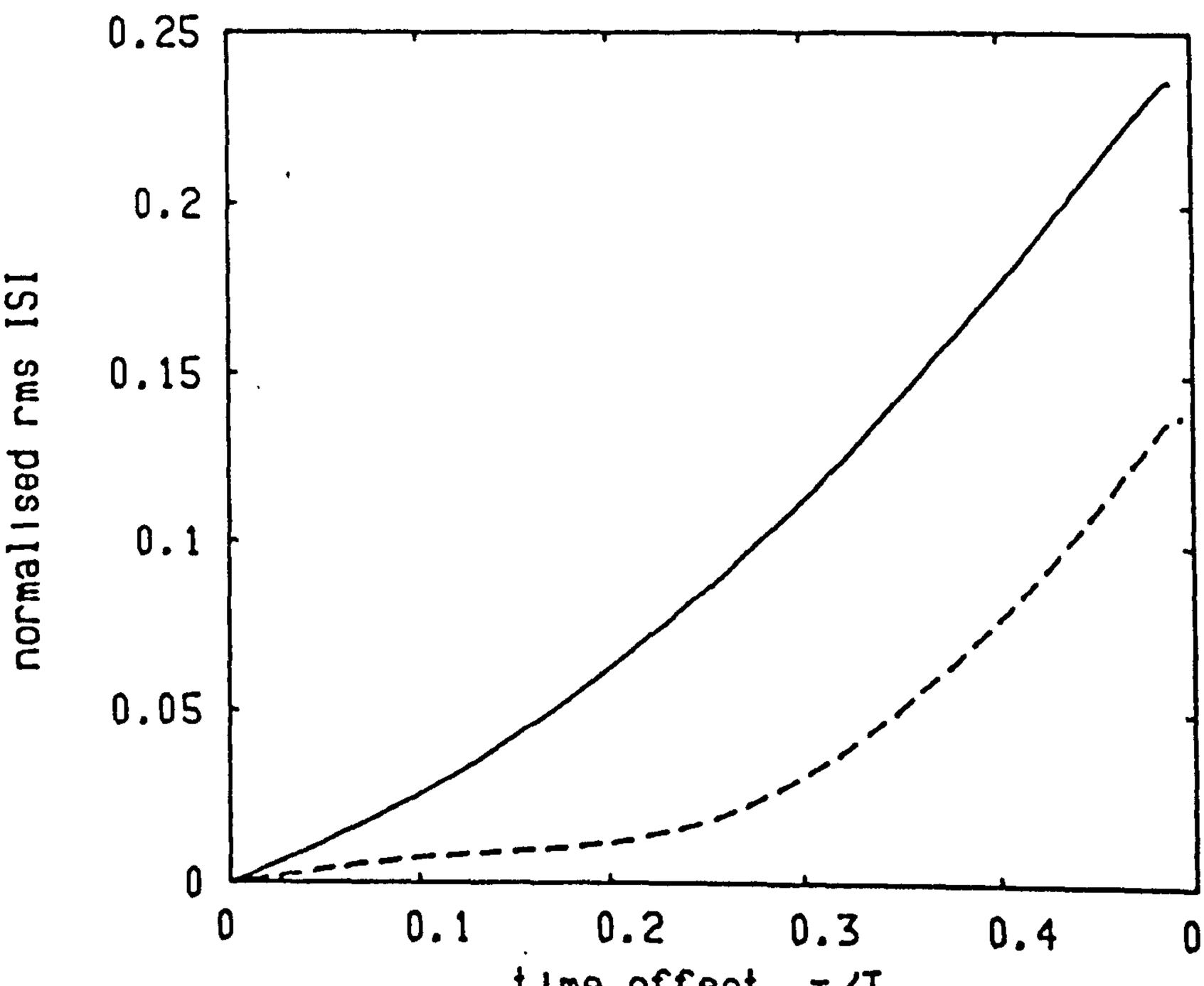

Fig. 9.15 Normalised rms ISI as a function of time offset τ/T.
——— raised cosine - - - modified (d=0.3, α=0.25)

obtained as shown in Fig. 9.16. It is clear that the full raised-cosine receiver incurs the greater penalty owing to alignment jitter and that this penalty increases rapidly with τ. In contrast, the modified receiver is remarkably tolerant to timing errors with the penalty being less than 2dB even for alignment errors as large as 25% of a signal element time slot.

To illustrate further the performance of the modified signal, we consider decision times displaced to 0.15T. For a full raised-cosine

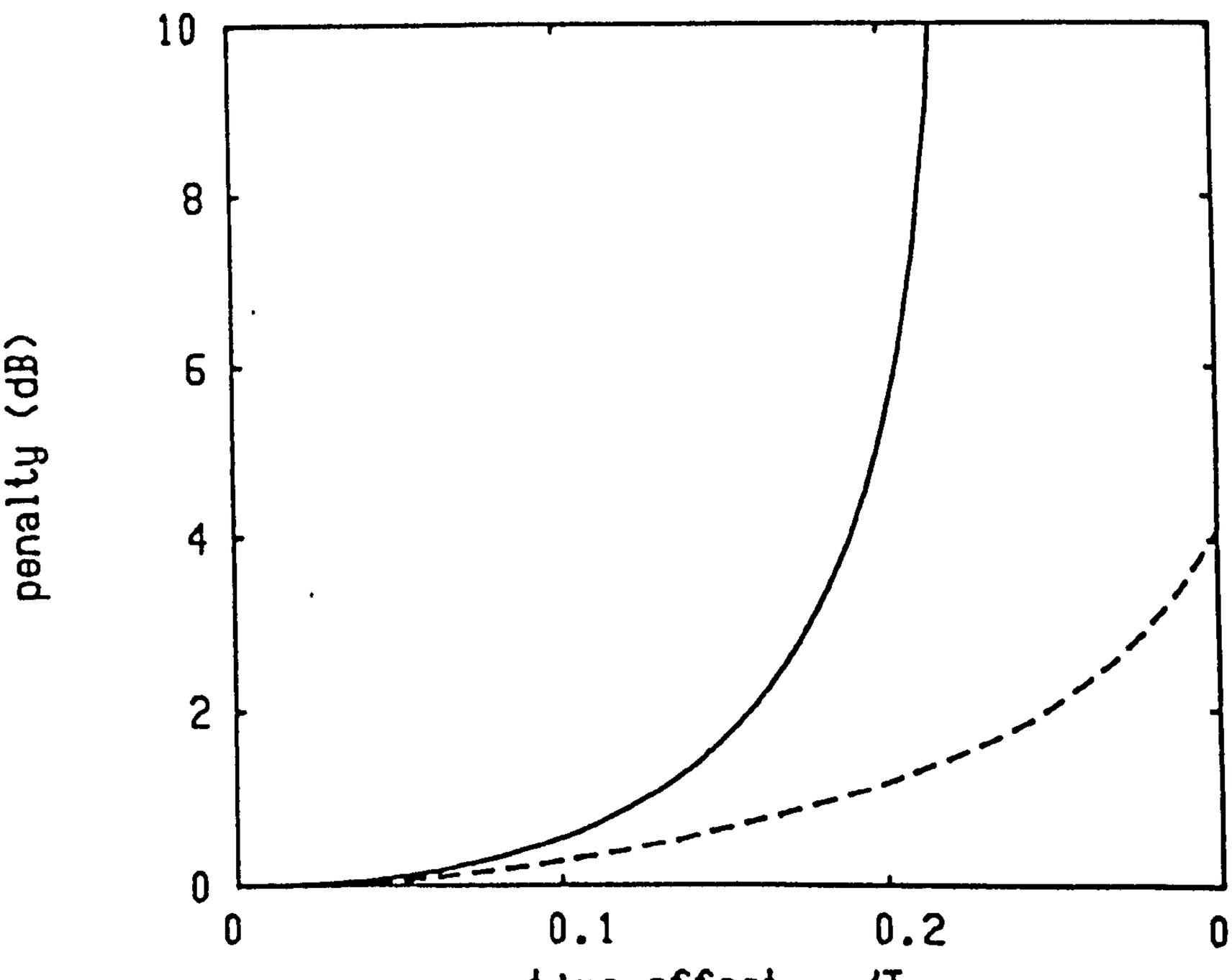

Fig. 9.16 Receiver sensitivity penalty versus time offset τ/T for raised cosine and modified (d=0.3, α=0.25) receiver designs.
——— raised cosine – – – modified

receiver the nominal signal value is then reduced to 0.943 and the rms ISI is 0.04237 while the corresponding values for the modified signal design are 0.907 and 0.00962, respectively. The influence on BER is shown in Fig. 9.17 where curves for the two receivers are presented for τ=0 and τ=0.15T. The new signal design is seen to offer a clear performance advantage. The sensitivity of the two receivers for this time offset as a function of APD gain is shown in Fig. 9.18. The conventional raised-cosine receiver has an optimum sensitivity of

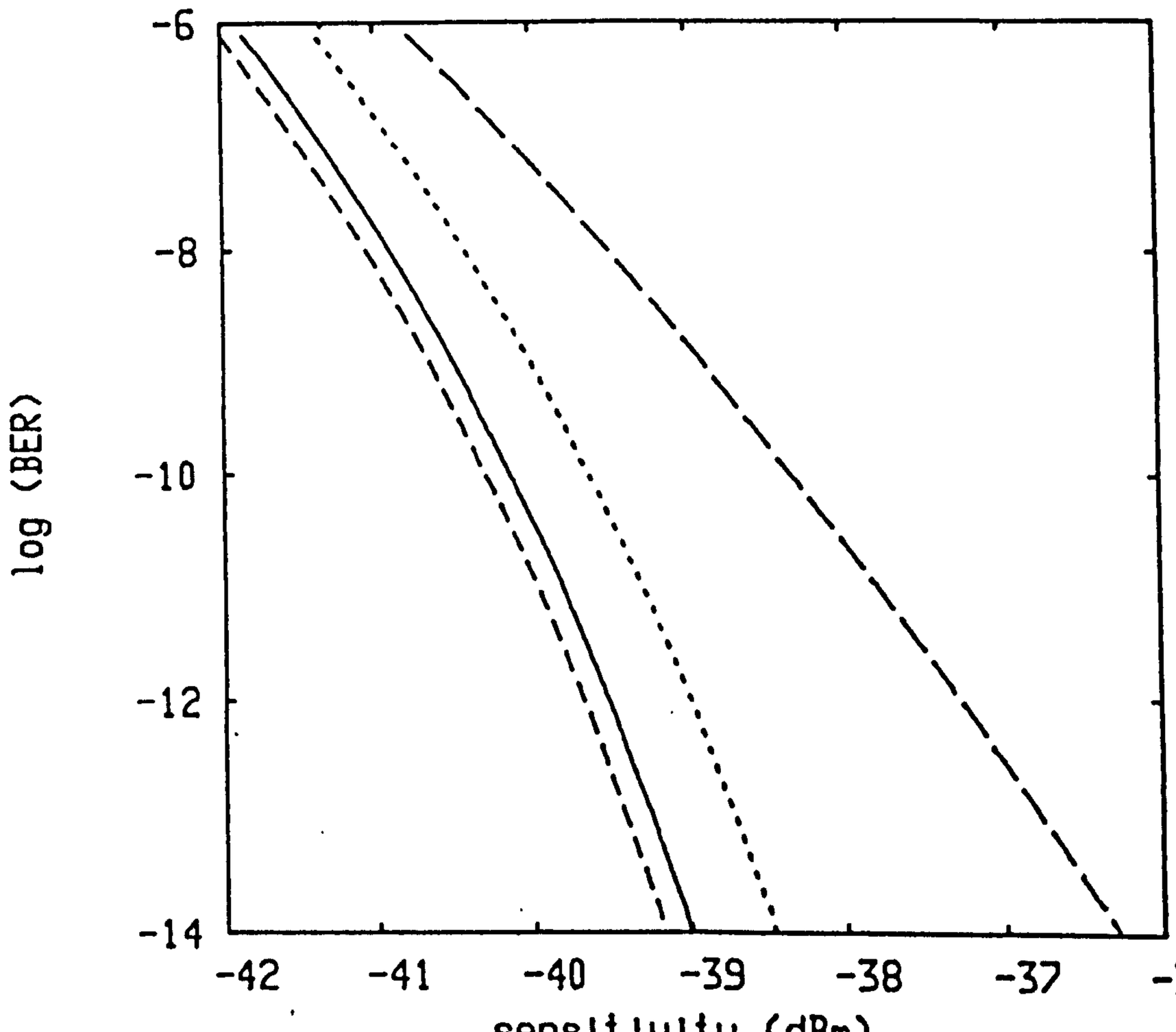

Fig. 9.17 Error probability comparison for full raised cosine and modified receivers for zero and 15% time offset.
raised cosine (—— τ=0 — — τ=0.15T)
modified (--- τ=0 ..... τ=0.15T)

-38.9dBm at an APD gain $<g>=12.8$ while the modified receiver has an optimum sensitivity of -40dBm at $<g>=17.85$. Fig. 9.19 shows the sensitivity penalty for $\tau=0.15T$ for both cases as a function of APD gain.

Here we note that the penalty increases with gain but much less so for the new design. The lowest value of the penalty for both cases occurs at $<g>=1$, indicating that, as noted elsewhere [O'Reilly et al. 1985], PIN receivers are generally more tolerant to time offset than are receivers making use of APDs.

9.5 Summary

We have presented a comparison in the performance of optical receivers incorporating SAPDs with those for CAPD receivers. This is necessary to indicate upper bounds on superlattice device non-idealities, which are strongly dependent on the number of stages, below which these advanced APDs can offer improved performance compared with existing long wavelength CAPDs. The results indicate that SAPDs should be designed with a large number of stages to ensure better sensitivity when residual hole ionisation vanishes. However, for high values of k a smaller number of stages is required to achieve better performance. For $k=1$ a single-stage is the optimum case.

New signal designs have been presented which are appropriate for direct detection optical receivers employing APDs. These signals achieve simultaneously both zero ISI and zero TD with respect to a depressed optimum threshold and can thus be used for both 2R and 3R repeaters. A fourth order low pass ladder network filter has been shown to provide a suitable basis for a practicable realisation approximation. This network can be tuned over a wide range of

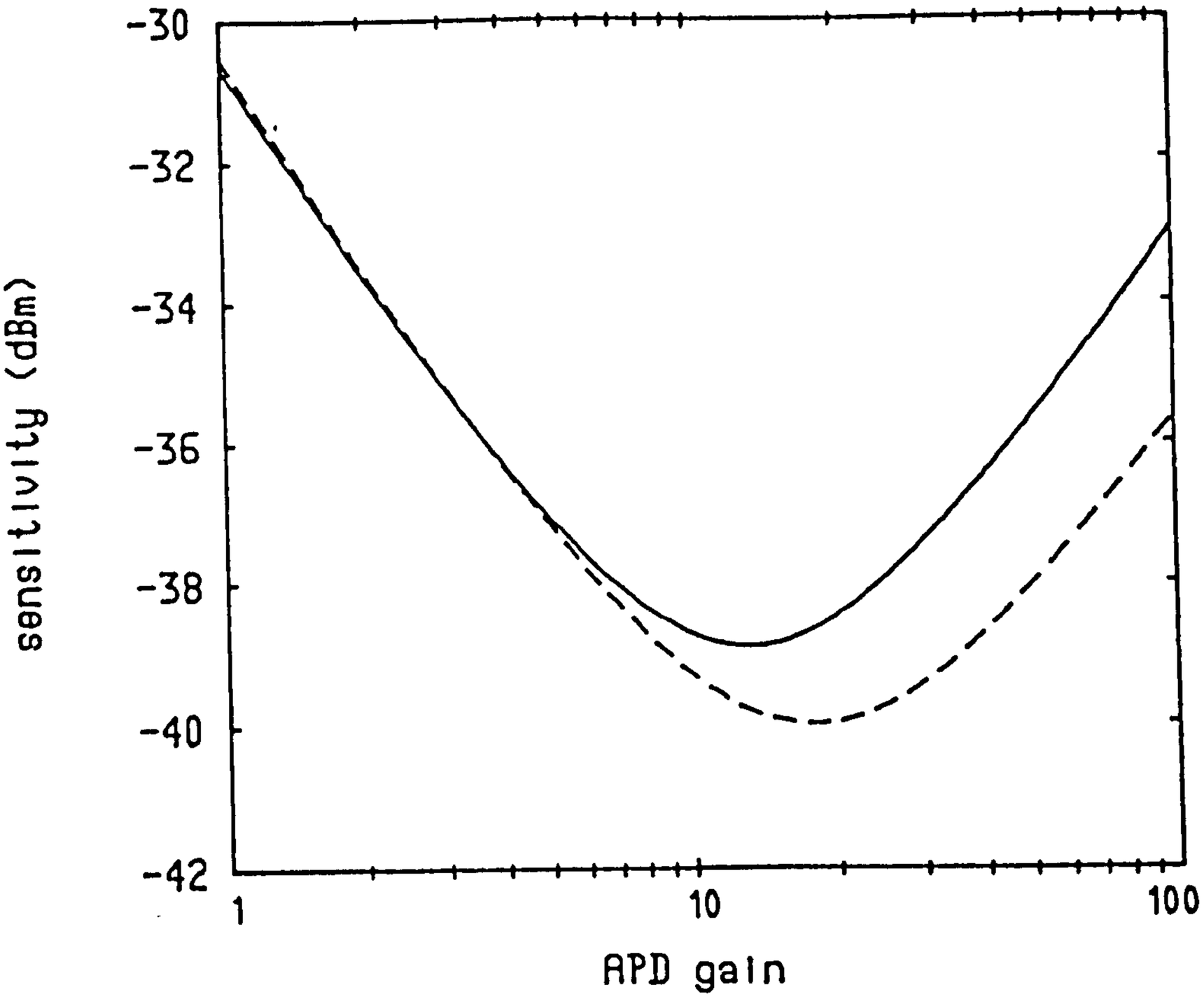

Fig. 9.18 Comparison of receiver sensitivities in the presence of 15% time offset for full raised cosine and modified (d=.3, α=.25) receivers. ——— raised cosine - - - modified

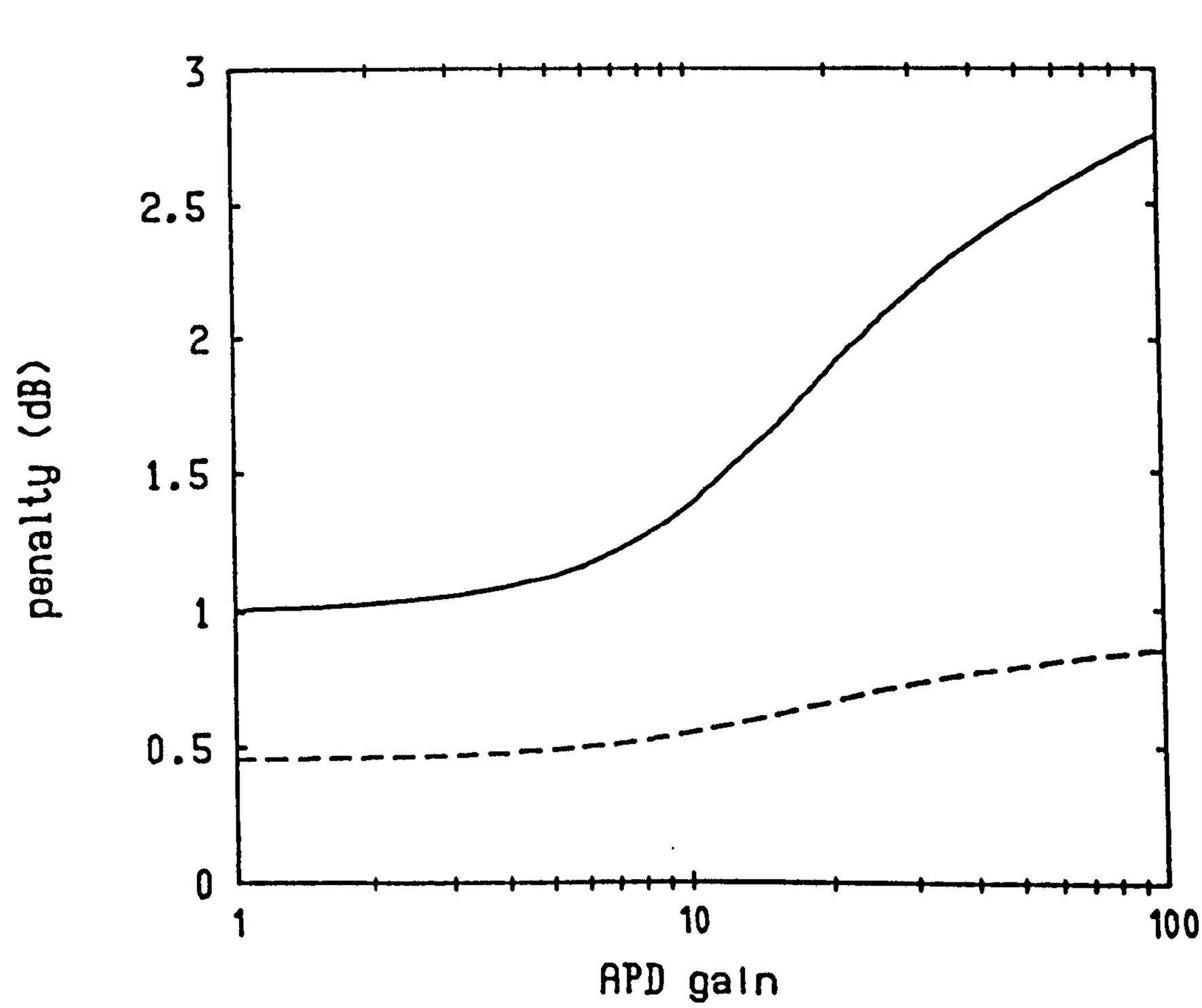

Fig. 9.19 Sensitivity penalty versus APD gain for raised cosine (solid) and modified (broken) receivers.

threshold values using just a single element.

The effect of timing jitter on the performance of fully retimed (3R) receivers has been considered and the new designs have been shown to offer reduced power penalties. We have noted, in agreement with previous studiés, that PIN receivers are more tolerant to alignment jitter than are receivers based on APDs. However, if the new signal element waveforms identified in this chapter are employed then practical APD receivers can be designed which are remarkably tolerant to decision time errors.

CHAPTER 10

CONCLUSIONS

The performance of superlattice avalanche photodiodes (SAPDs) has been investigated in this thesis as a means of realising high-sensitivity, high-speed direct-detection receivers. The various potential impairments which may constrain the design and dimensioning of such systems have been detailed and quantified. The aim throughout has been to provide appropriate analytical models together with quantitative results encompassing a wide range of parameter values, thereby ensuring a sound, comprehensive platform for the design and realisation of practical receivers matched to specific application requirements.

The analysis presented here is based upon the "discrete ionisation model" which has its origins in the work of van Vliet et al. [1979a, 1979b], Capasso et al. [1983] and Teich et al. [1986a, 1986b]. Van Vliet et al. have developed a comprehensive analysis for the gain and excess noise in short avalanche region devices, assuming a discrete statistical process whereby a limited number of ionisations can occur per carrier transit in the avalanche region. Capasso et al. have shown that the noise characteristics of staircase APDs cannot be calculated using the conventional McIntyre analysis [1966] which assumes carrier ionisation to be a continuous process, as is appropriate for conventional avalanche photodiodes (CAPDs). Later Teich et al. found that the theory of discrete ionisation processes developed by van Vliet et al. is applicable to staircase APDs and other SAPD structures, assuming a single ionisation per initiating

carrier per stage. The work presented here is a continuation of this line of research covering the following principal aspects.

(i) Extension of the discrete ionisation model to investigate the noise performance of advanced SAPDs where the injected carrier can impact more than one ionisation per stage.

(ii) Performance evaluation of optical receivers incorporating SAPDs; emphasis being placed on the effect of residual hole ionisation, dark current generated within the multiplication region, and the frequency response of the detector.

(iii) Development of acomprehensive moment generating function characterisation of SAPD gain and its application as a basis for accurate receiver performance evaluation.

(iv) Application of certain SAPD results to CAPDs, as a limiting case where the number of stages tends to ∞.

In Chapter 3 we extended the discrete ionisation model to include the position of the injected carrier in the multiplication region. This allows us to derive expressions for the gain and excess noise factor associated with dark current components generated in various stages, assuming a single ionisation per initiated carrier per stage. The performance of optical receivers incorporating SAPDs was then examined using a Gaussian approximation and taking into account the influence of the number of stages N, various dark current components and residual hole ionisation. The results show that as the ionisation rate ratio k increases the best receiver performance can be achieved

with a small number of stages. The expressions derived here can be used as guidelines for designing high performance SAPD receivers. The analyses were also extended to CAPDs to examine the influence of dark current generated within the avalanche region. The results indicate clearly that this component of dark current has less effect on receiver performance than does the diffusion current, especially when hole and electron ionisation rates are very different.

Chapter 4 concerns the performance of staircase APDs. These SAPDs are usually analysed assuming the electrons ionise at the steps only while the holes ionise within the graded-gap region [Capasso et al. 1983]. We carry the analysis further in order to consider the effect of carrier (electron and hole) impact ionisation both in the graded regions and at these steps. The modelling procedure adopted represents an expedient simplification, selected to render tractable a complex subject, and tailoring this to potential physical device model leads to consideration of three extreme cases. The expressions derived for the gain and excess noise factor allow us to predict the performance of optical receivers employing these detectors. The results indicate clearly that electron ionisation in the graded region can lead to improved sensitivity when residual hole ionisation in both regions is kept to a minimum.

One of the cases examined in Chapter 4 shows that staircase APD can be modelled under certain conditions as a SAPD where the injected carrier can impact upto two ionisations per stage. Further, recently interest has also been expressed in SAPDs in which multiple ionisations per initiating carrier per stage can occur, similar to secondary emission in photomultiplier tubes, thereby greatly enhancing the gain of the device [Capasso, 1984;1985; Brennan et al. 1987a]. The

performance of these devices was examined in Chapter 5 and Chapter 6. In Chapter 5 we extended the existing analysis of SAPDs to allow for the production of upto two impact ionisations per initiating carrier per stage. Extension for more than two ionisations was considered in Chapter 6 where a new discrete ionisation model for a solid-state photomultiplier (SSPM) was presented and used to derive expressions for gain and excess noise factors associated with both photocurrent and dark current generated in various stages. These expressions are quite general and can be applied to photomultiplier tubes, single ionisation or two-ionisation SAPDs, and CAPDs. We established that the noise characteristic of a SSPM can be expressed using four parameters: the means and the variances of both the hole and electron ionisation rate per stage, and these may in principle be determined experimentally from measurement of the average and the variance of the gain for both pure hole and pure electron injection currents. The performance of optical receivers employing SSPM was examined and the results indicate that when hole ionisation exists the gain per stage must be limited to a low value to prevent avalanche breakdown and to attain optimum sensitivity.

In Chapter 7 the gain moment generating function formulation for SAPDs was developed using a discrete ionisation model and allowing for nonnegligible residual hole ionisation. This was used with the modified Chernoff bound (MCB) as a basis for a rigorous analysis of optical receivers utilising these advanced detectors, allowing for residual hole ionisation, detector dark current generated in the various stages, and circuit noise. The development presented has provided precise performance evaluation tools encapsulating the entire statistics of the underlying stochastic processes associated with the

signal and noise components. This has enabled a comparison to be effecfted with performance predictions based on the widely adopted Gaussian Approximation (GA) which uses only first and second order statistics. The results indicate that for a SAPD receiver the GA can predict quite accurately receiver sensitivity while overestimating slightly the optimum gain. The optimum threshold predicted by the GA has also been found to be in good agreement with that predicted using MCB for most cases considered. The optimum decision threshold may be depressed significantly below the mid-range of the vertical eye opening.

Attention was directed in Chapter 8 to the speed of response of SAPDs and the effect on the performance of multigigabit-per-second lightwave receivers. An expression for the frequency response of single carrier multiplication SAPDs (no residual hole ionisation) was presented, providing an estimate for the maximum gain bandwidth (GB) product which can be achieved with ideal devices. The existence of residual hole ionisation degrades GB product mainly due to avalanche build-up time, arising from the regenerative nature of the avalanche process. To estimate the GB product in this case we established that the SAPD can be modelled as a CAPD in which hole and electron ionisation rates exhibit position dependency corresponding to one impulse per stage. This enabled us to apply the theory of CAPDs directly to predict the gain characteristics of SAPDs. The GB product was found to be inversely proportional to the width of the multiplication region W, and directly proportional to the number of stages N, especially when N is large. Sensitivity calculations for equalised GB-limited SAPD receivers indicated clearly that these advanced detectors should be fabricated with $W < 1\mu m$ and low residual

hole ionisation · ($k < 0.1$) to ensure negligible penalty for gigabit-per-second operation.

Chapter 9 was devoted to overall receiver considerations. A comparison was presented of the performance of optical receivers employing SAPDs with those for CAPD receivers. This was necessary to indicate upper bounds on superlattice device non-idealities, which are strongly dependent on the number of stages, below which these advanced APDs can offer improved performance compared with existing long wavelength CAPDs. The results indicate that SAPDs should be designed with a large number of stages to ensure better sensitivity when residual hole ionisation vanishes. However for high values of k a smaller number of stages is equired to achieve better performance. For $k=1$ a single stage is the optimum case. We then described new signal designs for optical communications based on APD receivers. This new receiver signal processing strategy leads to signal element waveforms satisfying Nyquist's first and second criteria with respect to a depressed optimum decision threshold, as encountered with high performance APD receivers. These signals achieve simultaneously both zero intersymbol interference and zero telegraph distortion with respect to a depressed optimum threshold and can thus be used for both 2R and 3R repeaters. A fourth order low pass ladder network filter was shown to provide a suitable basis for a practical realisation approximation. The effect of timing jitter on the performance of fully retimed (3R) receivers was considered and the new designs were shown to offer reduced power penalties.

The research summarised above indicates several possible directions for future investigation. Among these, the following deserve specific mention.

(i) The discrete ionisation model provides a powerful means of analysing the noise of SAPDs. There is however a need to relate the parameters of this model with more practical aspects such as material properties, physical device structure and measured data. Some work in this direction has been already started in the School [Burns et al. 1990a, 1990b] where the performance of a specific SAPD structure, reported by Capasso et al. [1982] has been investigated.

(ii) A more detailed theoretical analysis of the design considerations and operating characteristics of various SAPD structures is required. This would allow us to calculate the impact ionisation rate, different dark current components, carrier thermalisation distance and for examine the effect of different geometries, doping concentrations and electric field on the device gain and excess noise factor. The validity of this analysis should be checked against practical results or Monte Carlo simulation.

(iii) The gain moment generating function (MGF) of a nonideal SAPD has been evaluated here numerically. This requires a relatively long computation time especially when the MGF associated with dark current is considered. A more efficient technique is to obtain analytic (even approximate) expressions for the gain MGF as a function of the number of stages and carrier ionisation probabilities. In addition, other performance evaluation techniques based on the MGF such as Gram-Charlier series, maximum entropy methods and Edgeworth series expansion can be used to assess the performance of these advanced receivers.

(iv) Recently there is interest in superlattice phototransistors

with controlled avalanche gain [Chin and Bhattacharya, 1989]. In these devices a large current output over significant bias region is achieved by incorporating a staircase multiplication region at the base-collector junction to enhance the ionisation rate ratio and enabling the avalanche gain to be controlled easily. The noise performance of these high gain phototransistors could be investigated using a discrete ionisation model. This would allow us to predict the performance of optical receivers employing these new devices.

(v) The performance of PIN and CAPD receivers have been examined extensively in the literature under various system impairments such as chirp, jitter and intersymbol interference. Extending this work to SAPD receivers is essential to assess the robustness of these advanced receivers and to compare the result with the performance of other types of receiver. The lower values of ionisation rate ratio associated with SAPDs can play an important role in determining the response of these advanced receivers to different system impairments.

APPENDIX A

Expression for the Gain $<g_j>$

The derivation of eqn. 3.1 is based on equations given by van Vliet et al. [1979b].

Let $\phi_j(z)$ be the probability generating function of the gain g_j. From eqn. 46 in [van Vliet et al., 1979b], and assuming u and p are identical for each stage, we have

$$\phi_j'(1) = \phi_0'(1)\ [(1+p)/(1+u)]^j \qquad \text{(A1)}$$

where $\phi_j'(1)$ is the derivative with respect to z of $\phi_j(z)$ evaulated at z=1. For simplicity, $\phi_j'(1)$ will be denoted by ϕ_j'. For j=N, eqn. A1 becomes

$$\phi_N' = \phi_0'[(1+p)/(1+u)]^N \qquad \text{(A2)}$$

From eqn. A1 and A2 we have

$$\phi_j' = \phi_N'\ [(1+p)/(1+u)]^{j-N} \qquad \text{(A3)}$$

Since $\phi_j' = <g_j>$ [Cattermole, 1984] then

$$<g_j> = <g_N>[(1+p)/(1+u)]^{j-N} \qquad \text{(A4)}$$

or

$$<g_j> = <g_N> Q^{j-N} \qquad \text{(A5)}$$

where $Q = (1+p)/(1+u)$.

APPENDIX B

Expression for the Excess Noise Factor F_j

Consider eqn. 65a in [van Vliet et al., 1979b].

$$\phi_j'' = Q^j \phi_o'' + \frac{2(1-up)\ <g_N>^2}{(1+u)^2 Q^{2N}} Q^{j-1}\ (Q^j-1) \qquad \text{(B1)}$$

where ϕ_j'' stands for the second derivative with respect to z of $\phi_j(z)$ evaluated at z=1, and $Q = (1+p)/(1+u)$. For j=N, eqn. B1 reduces to

$$\phi_N'' = Q^N \phi_0'' + \frac{2(1-up)\ <g_N>^2}{(1+u)^2 Q^{N+1}} (Q^N-1) \qquad \text{(B2)}$$

Let $B_1 = Q^N - Q^j$ (B3)

then eqn. B1 reduces to

$$\phi_j'' = Q^j \phi_0'' + \frac{2(1-up)\ <g_N>^2}{(1+u)^2 Q^{2N-j+1}} (Q^N-B_1-1) \qquad \text{(B4)}$$

From eqns. B2 and B4

$$\phi_j'' = Q^{j-N}\ \phi_N'' - \frac{2B_1(1-up)<g_N>^2}{(1+u)^2 Q^{2N-j+1}} \qquad \text{(B5)}$$

The variance of g_j is related to ϕ_j' and ϕ_j'' by [Cattermole, 1984].

$$\mathrm{Var}(g_j) = \phi''_j - \phi'^2_j + \phi'_j \qquad \text{(B6)}$$

Substituting eqns. A5 and B5 into eqn. B6 yields

$$\mathrm{Var}(g_j) = \frac{\phi''_N + \langle g_N \rangle + (B_2 - 1)\langle g_N \rangle^2}{Q^{N-j}} - \frac{2B_1 (1-up)\langle g_N \rangle^2}{(1+u)^2 Q^{2N-j+1}} \qquad \text{(B7)}$$

where $B_2 = 1 - Q^{j-N}$ (B8)

For $j=N$

$$\mathrm{Var}(g_N) = \phi''_N + \langle g_N \rangle - \langle g_N \rangle^2 \qquad \text{(B9)}$$

From eqns. B7 and B9 we have

$$\mathrm{Var}(g_j) = Q^{j-N} [\mathrm{Var}(g_N) + B_2 \langle g_N \rangle^2] - \frac{2B_1 (1-up)\langle g_N \rangle^2}{(1+u) Q^{2N-j+1}} \qquad \text{(B10)}$$

The excess noise factor F_j can be expressed as [Teich et al., 1986a; van der Ziel, 1986].

$$F_j = 1 + \frac{\mathrm{Var}(g_j)}{\langle g_j \rangle^2} \qquad \text{(B11)}$$

Substituting eqns. A5 and B10 into eqn. B11 yields

$$F_j = 1 + \frac{Q^{N-j}\ \mathrm{Var}(g_N)}{\langle g_N \rangle^2} + B_2 Q^{N-j} - \frac{2B_1 (1-up)}{(1+u)^2 Q^{j+1}} \qquad \text{(B12)}$$

but

$$F_N = 1 + \frac{Var(g_N)}{\langle g_N \rangle^2}$$

then

$$F_j = 1+Q^{N-j}\,(F_N-1) + B_2 Q^{N-j} + \frac{2B_1\,(1-up)}{(1+u)^2 Q^{j+1}} \qquad \text{(B13)}$$

and since $B_2 = 1-Q^{j-N}$, then

$$F_j = Q^{N-j}\,F_N - \frac{2B_1\,(1-up)}{(1+u)^2 Q^{j+1}} \qquad \text{(B14)}$$

or

$$F_j = Q^{N-j}\,F_N - \frac{2(1-up)}{(1+u)^2 Q}\,[\,Q^{N-j} - 1] \qquad \text{(B15)}$$

where eqn. B3 has been used.

APPENDIX C

Average Gain for Two-Ionisation SAPD

Let $\phi_j(z)$ be the probability generating function of the gain g_j. Then [van Vliet et al., 1979b]:

$$\phi_j(z) = z \prod_{i=1}^{j} [1-p+p_1\phi_{j-i}(z) + p_2\phi^2_{j-1}(z)] \cdot \prod_{i=1}^{N-j} [1-u+u\phi_{j+i}(z)] \qquad \text{(C1)}$$

Applying eqn. C1 for j=0 we have

$$\phi_0(z) = z \prod_{i=1}^{N} [1-u+u\ \phi_i(z)] \qquad \text{(C2)}$$

Eqn. C1 can be put in the form of recurrence relation

$$\phi_j(z)\ [1-p+p_1\phi_j(z)+p_2\phi^2_j(z)] = \phi_{j+1}(z)\ [1-u+u\phi_{j+1}(z)] \qquad \text{(C3)}$$

Differentiating eqn. C3 with respect to z yields

$$\phi'_j(z)\ [1-p+p_1\phi_j(z)+p_2\phi^2_j(z)] + p_1\phi_j(z).\phi'_j(z) + 2p_2\phi^2_j(z).\phi'_j(z) = \phi'_{j+1}(z)\ [1-u+u\phi_{j+1}(z)] + u\ \phi_{j+1}(z).\phi'_{j+1}(z) \qquad \text{(C4)}$$

where $\phi'_j(z)$ is the first derivative with respect to z of $\phi_j(z)$. Evaluating eqn. C4 at z=1 (and denoting $\phi'_j(1)$ by ϕ'_j for simplicity) yields

$$\phi'_j.(1+p_1+2p_2) = \phi'_{j+1}.(1+u) \qquad \text{(C5)}$$

where $\phi_j(1) = 1$. Starting with j=0, we find

$$\phi'_j = Q^j\phi'_0 \qquad \text{(C6)}$$

$$\phi'_N = Q^N\phi'_0 \qquad \text{(C7)}$$

where $Q = [(1+p_1+2p_2)/(1+u)]$. Differentiating eqn. C2 with respect to z and evaluating the result at z=1 yields:

$$\phi'_0 = 1+u\sum_{j=1}^{N}\phi'_j \qquad \text{(C8)}$$

Substituting eqn. C6 into eqn. C8 gives

$$\phi'_0 = \left[\, 1-u\sum_{j=1}^{N}\phi'_j \,\right]^{-1}$$

$$= \frac{p_1+2p_2-u}{(p_1+2p_2)(1-u)-u(1+p_1+p_2)Q^N} \qquad \text{(C9)}$$

Substituting eqn. C9 into eqn. C7 and noting that Φ'_N is equal to the average gain $<g_N>$ gives

$$<g_N> = \frac{(p_1+2p_2-u)Q^N}{(p_1+2p_2)(1+u) - u(1+p_1+2p_2)Q^N} \qquad \text{(C10)}$$

Hence from eqns. C6, C7 and C10 we find

$$<g_j> = \phi_j' = <g_N>Q^{j-N} \qquad \text{(C11)}$$

APPENDIX D

Excess Noise Factor for Two-Ionization SAPD

Differentiating eqn. C4 with respect to z yields

$$\phi''_j(z)[1-p+p_1\phi_j(z)+p_2\phi_j^2(z)] + \phi'_j(z)[2p_1\phi_j(z) + 6p_2\phi_j(z).\phi'_j(z)]$$

$$+p_1\phi_j(z).\phi''_j(z) + 2p_2\phi_j^2(z).\phi''_j(z) = \phi''_{j+1}(z)[1-u+u\phi_{j+1}(z)]+2u\phi'^2_{j+1}(z)$$

$$+ u\phi_{j+1}(z).\phi''_{j+1}(z) \qquad \text{(D1)}$$

where $\phi''_j(z)$ represents the second derivative of $\phi_j(z)$ with respect to z and $p=p_1+p_2$. Evaluating eqn. D1 at $z=1$ gives

$$\phi''_{j+1} = Q\phi''_j + 2SQ^{2j}\phi'^2_0 \qquad \text{(D2)}$$

where $S=(p_1+3p_2-uQ)/(1+u)$. Again ϕ''_j denotes $\phi''_j(1)$. Starting with $j=0$, eqn. D2 can be put in the following form

$$\phi''_j = Q^j\,\phi''_0 + \frac{2S<g_N>^2\ Q^{j-1}\ (Q^j-1)}{(Q-1)\,Q^{2N}} \qquad \text{(D3)}$$

For $j=N$

$$\phi''_N = Q^N\phi''_0 + \frac{2S<g_N>\ \ (Q^N-1)}{(Q-1)\,Q^{N+1}} \qquad \text{(D4)}$$

Differentiating eqn. C4 with respect to z and evaluating the result at $z=1$, we have [van Vliet et al., 1979b].

$$\phi_0'' = 2u \sum_{j=1}^{N} \phi_j' + u \sum_{j=1}^{N} \phi_j'' + u^2 \left[\sum_{j=1}^{N} \phi_j' \right]^2 - u^2 \sum_{j=1}^{N} \phi_j^2 \qquad \text{(D5)}$$

Substituting for ϕ_j'' from eqns. D3 and ϕ_j' from eqn. C6 we have

$$\phi_0'' = \frac{\langle g_N \rangle}{Q^N} \left[\frac{2u(Q^N-1)\ \langle g_N \rangle}{(Q-1)Q^{N-1}} + \frac{u^2(Q^N-1)\langle g_N \rangle^2}{(Q-1)^2 Q^{2N-2}} \right.$$

$$+ \left[\frac{2uS}{Q-1} - u^2 Q \right] \frac{(Q^{2N}-1)\ \langle g_N \rangle^2}{(Q^2-1)Q^{2N-1}}$$

$$\left. - \frac{2uS(Q^N-1)\ \langle g_N \rangle^2}{(Q-1)^2 Q^{2N}} \right] \qquad \text{(D6)}$$

Substituting eqn. D6 into eqn. D4 yields

$$\phi_N'' = \langle g_N \rangle \left[\frac{2u(Q^N-1)\ \langle g_N \rangle}{(Q-1)Q^{N-1}} + \frac{u^2(Q^N-1)\langle g_N \rangle^2}{(Q-1)^2 Q^{2N-2}} \right.$$

$$+ \left[\frac{2uS}{Q-1} - u^2 Q \right] \frac{(Q^{2N}-1)\ \langle g_N \rangle^2}{(Q^2-1)Q^{2N-1}}$$

$$\left. - \frac{2uS(Q^N-1)\langle g_N \rangle^2}{(Q-1)^2 Q^{2N}} + \frac{2S(Q^N-1)\ \langle g_N \rangle}{(Q-1)Q^{N+1}} \right]$$

The variance of g_N can be expressed as [Cattermole, 1984].

$$\text{Var}(g_N) = \phi_N'' - \phi_N'^2 + \phi_N' \qquad \text{(D8)}$$

The excess noise factor is defined as [van der Ziel et al., 1986]:

$$F_N = \frac{\langle g_N^2 \rangle}{\langle g_N \rangle^2} = 1 + \frac{Var(g_N)}{\langle g_N \rangle^2} \qquad \text{(D9)}$$

Substituting eqn. D8 into eqn. D9 yields

$$F_N = \phi_N'' / \langle g_N \rangle^2 + 1/\langle g_N \rangle \qquad \text{(D10)}$$

Hence the expression of F_N given by eqn. 5.4 can be obtained by substituting eqns. C10 and D7 into eqn. D10.

In similar manner F_j can be expressed as

$$F_j = \frac{\langle g_j^2 \rangle}{\langle g_j \rangle^2} = \frac{\phi_j''}{\phi_j'^2} + \frac{1}{\phi_j'} \qquad \text{(D11)}$$

Using eqns. C11 and D3 in eqn. D11 yields

$$F_j = Q^{N-j} F_N - \frac{2S}{Q(Q-1)} \left[Q^{N-j} - 1 \right] \qquad \text{(D12)}$$

APPENDIX E

Expressions for ϕ''_N and F_j for a SSPM

The second derivative of eqn. 6.5 with respect to z can be expressed as

$$\phi''_j(z).\phi_\circ(\phi_j(z)) + \phi'^2_j(z)\left[\frac{d\phi_\circ(\phi_j(z))}{d\phi_j(z)}\right]$$

$$+ \phi'^2_j(z)\left[\frac{d\phi_\circ(\phi_j(z))}{d\phi_j(z)}\right]$$

$$+ \phi_j(z)\left[\frac{d\phi_\circ(\phi_j(z))}{d\phi_j(z)}\ \phi''_j(z) + \frac{d^2\phi_\circ(\phi_j(z))}{d\phi_j^2(z)}\ \phi'^2_j(z)\right]$$

$$= \phi''_{j+1}(z).\ \phi_h(\phi_{j+1}(z)) + \phi'^2_{j+1}(z)\left[\frac{d\phi_h(\phi_{j+1}(z))}{d\phi_{j+1}(z)}\right]$$

$$+ \phi'^2_{j+1}(z)\left[\frac{d\phi_h(\phi_{j+1}(z))}{d\phi_{j+1}(z)}\right]$$

$$+ \phi_{j+1}(z)\left[\frac{d\phi_h(\phi_{j+1}(z))}{d\phi_{j+1}(z)}\ \phi''_{j+1}\right.$$

$$\left.+ \frac{d^2\phi_h(\phi_{j+1}(z))}{d\phi_{j+1}^2(z)}\ \phi'^2_{j+1}(z)\right] \qquad \text{(E1)}$$

where

$$\phi'_j(z) \equiv \frac{d\phi_j(z)}{dz} \quad \text{and} \quad \phi''_j(z) \equiv \frac{d^2\phi_j(z)}{dz^2}$$

At z = 1 eqn. E1 reads:

$$\phi''_{j+1} = \frac{(1+\phi'_e)\phi''_j + (2\phi'_e+\phi''_e)\phi'^2_j - (2\phi'_h+\phi''_h)\phi'^2_{j+1}}{1 + \phi'_h} \qquad \text{(E2)}$$

Recalling that $\phi'_j = Q^j\phi'_0$

$$\phi''_j = Q\phi''_j + 2SQ^{2j}.\ \phi'^2_0 \qquad \text{(E3)}$$

where S is defined in eqn. 6.21. Starting with j=0, eqn. E3 can be written as

$$\phi''_j = Q^j\phi''_0 + \frac{2S<M_e>^2}{(Q-1)Q^{2N}} Q^{j-1}(Q^j-1) \qquad \text{(E4)}$$

For j = N we have

$$\phi''_N = Q^N\phi''_0 + \frac{2S<M_e>^2}{(Q-1)Q^{N+1}} (Q^N-1) \qquad \text{(E5)}$$

From eqn. 6.3, the second derivative of ϕ_0 with respect to z can be expressed as follows:

$$\phi''_0(z) = 2\sum_{m=1}^{N}\phi'_m(z)\left[\frac{d\phi_h(\phi_m(z))}{d\phi_m(z)}\right]\prod_{\substack{i=1\\ i\neq m}}^{N}\phi_h(\phi_i(z))$$

$$+ z\sum_{m=1}^{N}\left[\phi''_m(z)\left[\frac{d\phi_h(\phi_m(z))}{d\phi_m(z)}\right]\prod_{\substack{i=1\\ i\neq m}}^{N}\phi_h(\phi_i(z))\right.$$

$$\left. + \phi'^2_m(z)\left[\frac{d^2\phi_h(\phi_m(z))}{d\phi^2_m(z)}\right]\prod_{\substack{i=1\\ i\neq m}}^{N}\phi_h(\phi_i(z))\right.$$

$$+ \quad \phi_m'(z) \left[\frac{d\phi_h(\phi_m(z))}{d\phi_m(z)} \right]$$

$$\cdot \sum_{\substack{i=1 \\ i \neq m}}^{N} \phi_i'(z) \left[\frac{d\phi_h(\phi_i(z))}{d\phi_i(z)} \right] \prod_{\substack{q=1 \\ q \neq i,m}}^{N} \phi_h(\phi_q(z)) \Bigg] \qquad \text{(E6)}$$

For $z = 1$ eqn. E6 gives

$$\phi_0'' = 2\phi_h' \sum_{m=1}^{N} \phi_m' + \phi_h' \sum_{m=1}^{N} \phi_m'' + \phi_h'' \sum_{m=1}^{N} \phi'^2_m$$

$$+ \phi'^2_h \sum_{m=1}^{N} \left[\phi'_m \sum_{\substack{i=1 \\ i \neq m}}^{N} \phi_i' \right] \qquad \text{(E7)}$$

Making use of eqns. 6.7, 6.8 and E4, the above equation can be simplified to

$$\phi_0'' = \frac{<M_e>}{Q^N} \left[\frac{2\phi_h'(Q^N-1)}{(Q-1)Q^{N-1}} <M_e> + \frac{\phi_h'^2(Q^N-1)^2}{(Q-1)^2 Q^{2N-2}} <M_e>^2 \right.$$

$$+ \left[\frac{2S\phi_h'}{(Q-1)} + Q[\phi_h'' - \phi_h'^2] \right] \frac{(Q^{2N}-1)}{(Q^2-1)Q^{2N-1}} <M_e>^2$$

$$\left. - \frac{2S\phi_h'(Q^N-1)<M_e>^2}{(Q-1)^2 Q^{2N}} \right] \qquad \text{(E8)}$$

Substituting eqn. E8 into eqn. E5 yields

$$\phi_N'' = <M_e> \left[\frac{2\phi_h'(Q^N-1)}{(Q-1)Q^{N-1}} <M_e> + \frac{\phi_h'^2(Q^N-1)^2}{(Q-1)^2 Q^{2N-2}} <M_e>^2 \right.$$

$$+\left[\frac{2S\phi_h'}{(Q-1)}+Q[\phi_h''-\phi_h'^2]\right]\frac{(Q^{2N}-1)}{(Q^2-1)Q^{2N-1}}<M_o>^2$$

$$-\frac{2S\phi_h'(Q^N-1)}{(Q-1)^2Q^{2N}}<M_o>^2+\frac{2S(Q^N-1)}{(Q-1)Q^{N+1}}<M_o>\Bigg] \qquad \text{(E9)}$$

At this stage the expression for F_j given in eqn. 6.23 can be obtained by recalling that

$$F_j \equiv 1+\frac{Var(g_j)}{<g_j>^2}=\frac{\phi_j''}{<g_j>^2}+\frac{1}{<g_j>} \qquad \text{(E10)}$$

Where $<g_j>$ and ϕ_j'' are defined in eqns. 6.13 and E4, respectively

$$F_j=\frac{Q^{2N-j}\phi_0''+2S(Q^j-1)(Q-1)^{-1}Q^{-(1+j)}<M_o>^2}{<M_o>^2}+\frac{Q^{N-j}}{<M_o>} \qquad \text{(E11)}$$

From eqns. E5 and E11 we obtain

$$F_j=Q^{N-j}\left[\frac{\phi_N''}{<M_o>^2}\right]-\frac{2S}{Q(Q-1)}[Q^{N-j}-1]+\frac{Q^{N-j}}{<M_o>} \qquad \text{(E12)}$$

From which eqn. 6.23 follows.

APPENDIX F

Proposed Experimental Determination of ϕ'_e , ϕ''_e , ϕ'_h and ϕ''_h for a SSPM

We outline here briefly how the quantities ϕ'_e, ϕ''_e, ϕ'_h and ϕ''_h may in principle be determined as a function of the electric field for any SSPM structure by measuring the average gain and noise power associated with both pure hole injection and pure electron injection. This may be achieved experimentally by irradiating light of a specific wavelength on the n^+ region or p^+ region for pure hole or pure electron injection respectively. The wavelength must be chosen such that all the photons are absorbed in the n^+ (or p^+) region.

From gain measurements, ϕ'_e and ϕ'_h can be calculated as follows:

$$\phi'_e \equiv \langle w_e \rangle = \frac{(\langle M_e \rangle - 1)\left[\left(\frac{\langle M_e \rangle}{\langle M_h \rangle}\right)^{1/N} - 1\right]}{\langle M_e \rangle - \langle M_h \rangle} \qquad \text{(F1)}$$

$$\phi'_h = \langle w_h \rangle = \frac{(\langle M_h \rangle - 1)\left[\left(\frac{\langle M_h \rangle}{\langle M_e \rangle}\right)^{1/N} - 1\right]}{\langle M_h \rangle - \langle M_e \rangle}$$

$$= \left(\frac{\langle M_h \rangle}{\langle M_e \rangle}\right)^{1/N} .(1+\phi'_e) - 1 \qquad \text{(F2)}$$

From the noise measurements, $\mathrm{Var}(M_e)$ and $\mathrm{Var}(M_h)$, the parameters ϕ''_e and ϕ''_h can be evaluated as follows:

$$\text{Var}\ (M_e) = \phi''_N \ - \ <M_e>^2 \ + \ <M_e>$$

where ϕ''_N is given in eqn. E9. Thus, Var(M_e) can be expressed as

$$\text{Var}\ (M_e) = a_1 + b_1\phi''_e \ + \ c_1\phi''_h \tag{F3}$$

where

$$a_1 = a_{11} \ + \ 2b_1(\phi'_e - Q^2\phi'_h) \tag{F4a}$$

$$a_{11} = \left[\frac{(Q^N-1)^2}{(Q-1)^2} - \frac{(Q^{2N}-1)}{(Q^2-1)} \right] \frac{\phi'^2_h <M_e>^3}{Q^{2N-2}}$$

$$+ \left[\frac{2\phi'_h(Q^N-1)}{(Q-1)Q^{N-1}} - 1 \right] <M_e>^2 \ + \ <M_e> \tag{F4b}$$

$$b_1 = \left[\frac{Q(Q^{2N}-1)}{(Q+1)} - (Q^N-1) \right] \left[\frac{\phi'_h <M_e>^3}{(1+\phi'_h)(Q-1)^2Q^{2N}} \right]$$

$$+ \frac{(Q^N-1)<M_e>^3}{(Q-1)Q^{N+1}(1+\phi'_h)} \tag{F4c}$$

$$c_1 = c_{11} - Q^2 b_1 \tag{F4d}$$

$$c_{11} = \frac{(Q^{2N}-1)<M_e>^3}{(Q^2-1)Q^{2N-2}} \tag{F4e}$$

In a similar way

$$\text{Var}\ (M_h) = \phi''_0 \ - \ <M_h>^2 \ + \ <M_h> \tag{F5}$$

where ϕ''_0 is defined via eqn. E7. Here

$$\text{Var}\ (M_h) = a_2 \ + \ b_2\phi''_e \ + \ c_2\phi''_h \tag{F6}$$

where

$$a_2 = a_{22} + 2b_2(\phi'_e - Q^2\phi'_h) \tag{F7a}$$

$$a_{22} = \left[\frac{(Q^N-1)^2}{(Q-1)^2} - \frac{(Q^{2N}-1)}{(Q^2-1)} \right] Q^2\phi'_h <M_h>^3$$

$$+ \left[\frac{2\phi'_h (Q^N-1)Q}{(Q-1)} - 1 \right] <M_h>^2 + <M_h> \tag{F7b}$$

$$b_2 = \left[\frac{Q(Q^{2N}-1)}{(Q+1)} - (Q^N-1) \right] \left[\frac{\phi'_h <M_h>^3}{(1+\phi'_h)(Q-1)^2} \right] \tag{F7c}$$

$$c_2 = c_{22} - Q^2 b_2 \tag{F7d}$$

$$c_{22} = \frac{(Q^{2N}-1)Q^2 <M_h>^3}{(Q^2-1)} = Q^{-N}c_{11} \tag{F7e}$$

Solving eqns. F3 and F6 simultaneously yields

$$\phi''_e = \frac{c_2 Var(M_e) - c_1 Var(M_h) + c_1 a_2 - c_2 a_1}{b_1 c_2 - c_1 b_2} \tag{F8}$$

and

$$\phi''_h = \frac{c_1 Var(M_h) - c_2 Var(M_e) + c_2 a_1 - c_1 a_2}{b_2 c_1 - c_2 b_1} \tag{F9}$$

The variance of the number of ionisations per initiating carrier per stage can also be calculated using the relation $Var(w_e) = \phi''_e - \phi'^2_e + \phi'_e$. A similar relation applies for the holes.

REFERENCES

Alabedra, R., Orsal, B., Lecoy, G., Pichard, G., Meslage, J. and Frangnon (1985): "An $Hg_{0.3}Cd_{0.7}Te$ avalanche photodiode for optical fibre transmission systems at $\lambda=1.3$ μm", IEEE Trans. Electron Devices, vol. ED-32, pp. 1302-1306.

Allam, J., Capasso, F., Alavi, K. and Cho, A.Y. (1987): "Near single carrier-type multiplication in multiple graded-well structure for a solid-state photomultiplier", Electron Devices Lett., vol. EDL-8, pp.4-6.

Ando, H. and Kanbe, H. (1985): "Effect of avalanche build-up time on avalanche photodiode sensitivity", IEEE J. Quant. Electron., vol. QE-21, pp. 251-255.

Beltram, F., Allam, J. and Capasso, F. (1987): "GaInAs/InP superlattice avalanche photodiode grown by metalorganic chemical vapour deposition", Appl. Phys. Lett., vol. 50, pp. 1170-1172.

Bennett, W.R. and Davey, J.R. (1965): "Data Transmission", New York: McGraw-Hill, pp. 49-82.

Blauvelt, H., Margalit, S. and Yarif, A. (1982): "Single-carrier-type dominated impact ionisation in multilayer structures", Electron. Lett., vol. 18, pp. 375-376.

Brain, M.C.(1979): "Responsivity and noise characterisation of Ge avalanche photodiode throughout wavelength range 1.1-1.7 μm", Electron. Lett., vol. 15, pp. 821-823.

Brain,M.C. (1981): "Characterisation and estimated performance of commercial n-p Ge APDs for long-wavelength optical receivers", Opt. Quant. Electron., vol. 13, pp. 353-367.

Brain, M.C. (1982): "Comparison of available detectors for digital fibre systems for 1.2-1.55μm wavelength range", IEEE J. Quant. Electron., vol. QE-18, pp. 219-224.

Brennan, K.(1985a): "Theory of electron and hole impact ionisation in quantum well and staircase superlattice avalanche photodiodes structures", IEEE Trans. Electron. Devices, vol.ED-32, pp. 2197-2205.

Brennan, K. (1985b): "Theory of the channelling avalanche photodiode", IEEE Trans. Electron. Devices, vol. ED-32, pp. 2467-2478.

Brennan, K. (1986a): "Theoretical study of multiquantum well avalanche photodiodes made from the GaInAs/A1InAs material system", IEEE Trans. Electron Devices, vol. ED-33, pp. 1502-1510.

Brennan, K. (1986b): "Theory of doped quantum well APD: a new solid-state photomultiplier", IEEE J. Quant. Electron., vol. QE-22, pp. 1999-2016.

Brennan, K. (1986c): "Theory of GaInAs/A1InAs-doped quantum well APD: new low noise solid-state photodetector for lightwave communication systems", IEEE Trans. Electron Devices, vol. ED-33, pp. 1683-1695.

Brennan, K. (1987a): "The p-n junction quantum well APD: a new solid-state photodetector for lightwave communication systems and on-chip detector applications", IEEE Trans. Electron Devices, vol. ED-34, pp. 793-803.

Brennan, K. (1987b): "The p-n heterojunction quantum well APD: a new high-gain low-noise high-speed photodetector suitable for lightwave communications and digital applications", IEEE Trans. Electron Devices, vol. ED-34, pp. 793-803.

Brennan, K. (1987c): "Optimisation and modelling of avalanche photodiode structures: application to a new class of superlattice photodetectors, the p-i-n, p-n homojunction, and p-n heterojunction APDs", IEEE Trans. Electron Devices, vol. ED-34, pp. 1658-1669.

Brennan, K. and Summers, C.J. (1987a): "The variably spaced superlattice energy filter quantum well avalanche photodiode: a solid-state photomultiplier", IEEE J. Quant. Electron., vol. QE-23, pp. 320-327.

Brennan, K. and Summers, C.J. (1987b): "Theory of resonant tunneling in a variably spaced multiquantum well structures: an Airy function approach", J. Appl. Phys., vol. 61, pp. 614-623.

Brennan, K. and Wang, Y. (1988): "Field and spatial geometry dependencies of electron and hole ionisation rates in GaAs/A1GaAs multiquantum well APDs", IEEE Trans. Electron Devices, vol. ED-35, pp. 634-641.

Buckingham, M.J. (1983): "Noise in Electronic Devices and Systems", New York : Halsted Press.

Burns, M.J., Fyath, R.S. and O'Reilly, J.J. (1990a): "Modelling superlattice photodiodes : combinig iscrete ionisation model with experimental data", IEE Colliquium on Modelling of Optoelectronic Devices, London, pp. 3/1-3/3.

Burns, M.J., Fyath, R.S. and O'Reilly, J.J. (1990b): "Modelling of superlattice avalanche photodiodes for optical receivers", to be presented at the Eighth European Fibre Optic Communications and Local Area Network Conference (EFOC/LAN '90), Munich.

Campbell, J.C., Dentai, A.G., Holden, W.S. and Kasper, B.L. (1983): "High performance avalanche photodiode with separate absorption, grading and multiplication regions", Electron. Lett., vol. 19, pp. 818-820.

Campbell, J.C., Tsang, W.T., Qua, G.J. and Johnson, B.C.(1988): "High-speed InP/InGaAsP/InGaAs avalanche photodiodes grown by chemical beam epitaxy", IEEE J. Quant. Electron., vol.QE-24, pp. 496-500.

Campbell, J.C., Chandrasekhar, S., Tsang, W.T., Qua, G.J. and Johnson, B.C. (1989a): "Multiplication noise of wide-bandwidth InP/InGaAsP/InGaAs avalanche photodiodes", J. Lightwave Technol., vol. LT-7, pp. 473-478.

Campbell, J.C., Johnson, B.C., Qua, G.J. and Tsang, W.T. (1989b): "Frequency response of InP/InGaAsP/InGaAs avalanche photodiodes", J. Lightwave Technol., vol. LT-7, pp. 778-784.

Capasso, .F. (1982a): "New ultra-low-noise avalanche photodiode with separated electron and hole avalanche regions", Electron Lett., vol. 18, pp. 12-13.

Capasso, F. (1982b): "Channelling avalanche photodiodes: novel ultra low-noise interdigitated p-n junction detector", IEEE Trans. Electron Devices, vol. ED-29, pp. 1388-1395.

Capasso, F. (1983): "Bandgap engineering via graded gap, superlattice, and periodic doping structures: applications to novel photodetectors and other devices", J. Vac. Sci. Technol. B1, vol. 2, pp. 457-461.

Capasso, F. (1984): "Multilayer avalanche photodiodes and solid-state photomultiplier", Laser Focus/Electron-Optics, July, pp. 84-101.

Capasso, F. (1985): "Physics of avalanche photodiodes", in Semiconductors and Semimetals, Willardson, R.K. and Beers, A.C. (Eds.), vol. 22, pt. D, New York: Academic, pp.1-172.

Capasso, F., Tsang, W.T., Hutchinson, A.L. and Williams, G.F. (1982): "Enhancement of electron impact ionisation in a superlattice: a new avalanche photodiode with a large ionisation rate ratio", Appl. Phys. Lett., vol. 40, pp. 38-40.

Capasso, F., Tsang, W.T. and Williams, G.F. (1983): "Staircase solid-state photomultipliers and avalanche photodiodes with enhanced ionisation rate ratio", IEEE Trans. Electron Devices, vol. ED-30, pp. 381-390.

Capasso, F., Allam, J., Cho., A.Y., Mohammed, K., Malik, R.J. Hutchinson, A.L. and Sivco, D. (1986): "New avalanche multiplication phenomenon in quantum well superlattices: evidence of impact ionisation across the band-edge discontinuity", Appl. Phys. Lett., vol.48, pp. 1294-1296.

Cartledge, J.C. (1987): "A maximum entropy method for lightwave system performance evaluation", J. Lightwave Technol., vol. LT-5, pp. 1613-1617.

Cartledge, J.C. and Coathup, L.W. (1986): "A Gram-Charlier series method of calculating the probability of error in lightwave transmission systems", J. Lightwave Technol., vol. LT-6, pp. 1736-1739.

Cattermole, K.W. (1984): "Generating function methods in probability theory", in Mathematical Topics in Telecommunications, Cattermole, K.W. and O'Reilly, J.J. (Eds.), vol .2, London: Pentech Press, pp. 1-25.

Chin, A. and Bhattacharya, P. (1989): "Theory and operation of a GaAs/AlGaAs/InGaAs superlattice phototransistor with controlled avalanche gain", IEEE Trans. Electron Devices, vol. ED-36, pp. 2183-2190.

Chin, R., Holonyak, N., Stillman, G.E., Tang, J.Y. and Hess, K. (1980): "Impact ionisation in multilayered heterojunction structures", Electron. Lett., vol. 16, pp. 467-469.

Chuang, S.L. and Hess, K. (1986): "Impact ionisation across the conduction-band-edge discontinuity of quantum well hetrostructures", J. Appl. Phys., vol. 59, pp. 2885-2894.

Cohen, L.G. (1986): "Trends in U.S. broad-band fibre optical communication systems", IEEE J. Selected Areas Comm., vol. SAC-4, pp. 488-497.

Da Rocha, J.R.F. and O'Reilly, J.J. (1982): "Modified Chernoff bound for binary optical communication", Electron. Lett., vol. 18, pp. 708-709.

Da Rocha, J.R.F. and O'Reilly, J.J. (1986): "Linear direct-detection fibre-optic receiver optimised in the presence of intersymbol interference", IEEE Trans. Comm., vol. COM-34, pp. 365-374.

Engstrom, R.W. (1980): "RCA Photomultiplier Handbook (PMT-62)", Lancaster, PA:RCA Electroptics and Devices.

Forrest, R.S. (1984): "Gain-bandwidth product-limited response in long wavelength avalanche photodiodes", J. Lightwave Technol., vol. LT-2, pp. 34-39.

Fujihashi, C. (1987): "Dark-current multiplication noise in avalanche photodiodes and optimum gains", J. Lightwave Technol., vol. LT-5, pp. 798-808.

Fujita, S., Henmi, N., Takano, I., Yamaguchi, M., Torikai, T., Suzaki, T., Takano, S., Ishigara, H. and Shikade, M. (1988): "10 Gbit/s - 80km optical fibre transmission experiment using a directly modulated DFB-LD and high speed InGaAs-APD", OFC-88, New Orland, U.S., post-deadline paper.

Fyath, R.S. and O'Reilly, J.J. (1987): "New signal designs for binary optical communications based on APD receivers", 21st Conf. Information Science and Systems, Baltimore, USA, pp. 725-730.

Fyath, R.S. and O'Reilly, J.J. (1988a): "Effective gain and effective excess noise factor associated with dark current in superlattice APDs", Solid-state Electron., vol. 31, pp. 275-277.

Fyath, R.S. and O'Reilly, J.J. (1988b): "Performance of optical receivers incorporating multiemission superlattice avalanche photodiodes", Electron. Lett., vol. 24, pp. 234-235.

Fyath, R.S. and O'Reilly, J.J. (1988c): "Multilayered APDs producing up to two impact ionisations per carrier per stage: optical receiver performance analysis", IEE Proc., pt. J., vol. 135, pp. 101-108.

Fyath, R.S. and O'Reilly, J.J. (1988d): "Effect on the performance of staircase APDs of electron impact ionisation within the graded-gap region", IEEE Trans. Electron Devices, vol. ED-35, pp. 1357-1363.

Fyath, R.S. and O'Reilly, J.J. (1988e): "Optical receivers based on superlattice avalanche photodiodes: effect of number of stages", IEE Proc., pt. J, vol. 135, pp. 298-302.

Fyath, R.S. and O'Reilly, J.J. (1988f): "Gain-bandwidth product considerations for superlattice and multiquantum well avalanche photodiodes", IEE Colloquium on Heterojunction and Quantum Well Devices, London, pp. 11/1-11/4.

Fyath, R.S. and O'Reilly, J.J. (1988g): "Frequency response characterisations of superlattice avalanche photodiodes", IEE Proc., pt. J., vol. 135, pp. 413-422.

Fyath, R.S. and O'Reilly, J.J. (1988h): "Analysis of non-ideal solid-state photomultiplier (SSPM) for optical receivers", IEE Proc., pt. J., vol. 135, pp. 423-434.

Fyath, R.S. and O'Reilly, J.J. (1989a): "Performance degradation of APD-optical receivers due to dark current generated within the multiplication region", J. Lightwave Technol., vol. LT-7, pp. 62-67.

Fyath, R.S. and O'Reilly, J.J. (1989b): "Gain moment generating functions for superlattice APD receivers", 23rd Conf. Information Science and Systems, Baltimore, USA.

Fyath, R.S. and O'Reilly, J.J. (1989c): "Comparison of novel superlattice structures and conventional APDs with implications for performance of optical fibre systems", 2nd IEE National Conf. on Telecommunications, York., U.K., pp. 106-110.

Fyath, R.S. and O'Reilly, J.J. (1989d): "Moment generating function of superlattice avalanche photodiodes as a basis for accurate optical receiver performance evaluation", IEE Proc., pt. J., vol. 136, pp. 118-128.

Gimlett, J.L. (1987): "Low-noise 8GHz p-i-n/FET optical receiver", Electron. Lett., vol. 23, pp. 281-283.

Gimlett, J.L., Iqbal, M.Z., Young, J., Curtis, L., Spleer, R. and Cheung, K.N. (1989): "11 Gbit/s optical transmission experiment using 1540nm DFB with non-return-to-zero-modulation and pin/HEMT receiver", Electron. Lett., vol. 25, pp. 596-597.

Gordon, J.P., Nahory, R.E., Pollack, M.A. and Worlock, J.M. (1979): "Low-noise multistage avalanche photodetector", Electron. Lett., vol. 15, pp. 518-519.

Helstrom, J.C. (1988): "Computing the performance of optical receivers with avalanche diode detectors", IEEE Trans. Comm., vol. COM-36, pp. 61-66.

Hildebrand, O., W. Kuebart, W., Benz, K.W. and Pikuhn, M.H. (1981): "$Ga_{1-x}Al_xSb$ avalanche photodiodes: resonant impact ionisation with very high ratio of ionisation coefficients", IEEE J. Quant. Electron., vol. QE-17, pp. 284-288.

Hollenhorst, J.N. (1986): "Ballistic avalanche photodiode: ultralow noise avalanche photodiode with nearly equal ionisation probabilities", Appl. Phys. Lett., vol. 49, pp. 516-518.

Howard, N.R. (1962): "Avalanche multiplication in silicon junctions", J. Electron. Contr., vol. 13, pp. 537-544.

Jindal, R.P. (1987): "A scheme for ultralow noise avalanche multiplication of fibre-optics signals", IEEE Trans. Electron Devices, vol. ED-34, pp. 301-304.

Juang, F.Y., Das, U., Nashimoto, Y. and Bhattacharya, P.K. (1985): "Electron and hole impact ionisation coefficients in GaAs-$A1_xGa_{1-x}$ superlattices", Appl. Phys. Lett., vol. 47, pp. 972-974.

Kagawa, T., Iwamura, H. and Mikami, O. (1989): "Dependence of the GaAs/A1GaAs superlattice ionisation rate on A1 content", Appl. Phys. Lett., vol. 54, pp. 33-35.

Kasper, B.L. and Campbell, J.C. (1987): "Multigigabit-per-second avalanche photodiode lightwave receivers", J. Lightwave Technol., vol. LT-5, pp. 1351-1364.

Kimara, T. (1985): "Factors affecting fibre-optic transmission", J. Lightwave Technol., vol. LT-6, pp. 611-619.

Knabe, K. and Grosskoph, G. (1980): "Dark current properties on a germanium avalanche photodiode", Japan J. Appl. Phys. Lett., vol. 19, pp. L767-L770.

Knabe, K., Grosskoph, G., Mikami, O. and Machida, S. (1981): "Dark current noise characteristics and their temperature dependence in germanium avalanche photodiodes", IEEE J. Quant. Electron., vol. QE-17, pp. 1534-1539.

Kuvås, R. and Lee, C.A. (1970a): "Quaistatic approximation for semiconductor avalanches", J. Appl. Phys., vol. 41, pp. 1743-1755.

Kuvås, R. and Lee., C.A. (1970b): "Carrier diffusion in semiconductor avalanches", J. Appl. Phys., vol. 41, pp. 3108-3116.

Lee, C.A. Batdorf, R.L., Wiegmann, W. and Kaminsky, G.K. (1967): "Time dependence of avalanche process in silicon", J. Appl. Phys., vol. 38, pp. 2787-2796.

Li, W-Q., Bhattacharya, P.K. and Juang, F-U., (1987): "Demonstration of dual gain mechanism in an InGaAs/InA1As superlattice photodiode", Appl. Phys. Lett., vol. 50, pp. 1176-1178.

Lukaszek, W., van der Ziel, A. and Chenette, E.R. (1976): "Investigation of transition from tunneling to impact ionisation multiplication in silicon p-n junctions", Solid-state Electron., vol. 19, pp. 57-71.

MacBean, M.D.A. (1990a): "The influence of photodiode design on receiver sensitivity", IEE Colloquium on Optical Detectrors", London, pp. 7/1-7/4.

MacBean, M.D.A. (1990b): "Lucky drift theory applied to InP/GaInAs and AlInAs/GaInAs multilayer avalanche photodetectors", IEE Colloquium on Modelling of Optical Devices, London, pp. 2/1-2/4.

Mansuripur, M., Goodman, J.W., Rawson, E.G. and Norton, R.E. (1980): "Fibre optics receiver error rate prediction using the Gram-Charlier series", IEEE Trans. Comm., vol. COM-28, pp. 402-407.

Marsland, J.S. and Woods, R.C. (1987): "Lucky drift models of multilayered structures and approximate forms of lucky drift expressions", IEE Proc., pt. J., vol. 134, pp. 313-322.

Mattera, U.D., Capasso, F., Allam, J., Hutchinson, A.L., Dick, J., Brown, J.M. and Westaphal, A. (1986): "High speed InP/$Ga_{0.47}In_{0.53}As$ superlattice avalanche photodiodes with very low background doping grown by continuous trichloride vapor phase epitaxy", J. Appl. Phys. Lett., vol. 60, pp. 2609-2612.

Matsuo, K., Teich, M.C. and Saleh, B.E. (1985): "Noise properties and time response of the staircase avalanche photodiode", J. Lightwave Technol., vol. LT-3, pp. 1223-1231.

Mazo, J.E. and Salz, J. (1976): "On optical data communication via direct detection of light pulses", Bell Syst. Tech. J., vol. 55, pp. 347-369.

McIntyre, R.J. (1966): "Multiplication noise in uniform avalanche diodes", IEEE Trans. Electron. Devices, vol. ED-13, pp. 164-168.

Mohammed, K., Capasso, F., Allam, J., Cho. A.Y. and Hutchinson, A.L. (1985): " New high-speed long-wavelength $Al_{0.48}In_{0.52}As$/ $Ga_{0.47}In_{0.53}As$ multiquantum well avalanche photodiodes", Appl. Phys. Lett., vol. 47, pp. 597-599.

Mon, K.K. and Hess, K. (1982): "Resonant impact ionisation in superlattices", Solid-state Electron., vol. 25, pp. 491-492.

Moseley, A.J., Urquhart, J. and Riffat, J.R. (1988): "High-speed GaInAsP/GaInAs avalance photodiodes grown by atmospheric-pressure MOCVD", Electron. Lett., vol. 24, pp. 313-315.

Muoi, T.V. (1984): "Receiver design for high speed optical-fiber system", J. Lightwave Technol., vol. LT-2, pp. 243-267.

Naqavi, I.M. (1973): "Effects of time dependence of multiplication on avalanche noise", Solid-state Electron., vol. 16, pp. 19-28.

Nyquist, H.(1928): "Certain Topics in telegraph theory", Trans. AIEE, vol. 47, pp. 617-644.

O'Reilly, J.J. (1984): "Generating functions, bounds and approximations in optical communications" in Mathematical Topics in Telecommunications, Cattermole, K.W. and O'Reilly, J.J. (Eds.), vol. 2, London: Pentech Press, pp. 119-123.

O'Reilly, J.J. and Cochrane, P. (1980): "Potential role of untimed repeaters in optical submarine systems", IEE Int. Conf. on Submarine Telecommunication Systems", U.K., pp. 165-169.

O'Reilly, J.J. and da Rocha, J.R.F. (1987): "Improved error probability evaluation methods for direct detection optical communication systems", IEEE Trans. Inform. Theory, vol. IT-33, pp. 839-848.

O'Reilly, J.J., da Rocha, J.R.F. and Schumacher, K. (1985): "Influence of timing errors on the performance of direct detection optical fibre communication systems", IEE Proc., pt. J., vol. 132, pp. 309-313.

O'Reilly, J.J., da Rocha, J.R.F. and Schumacher, K. (1986): "Optical fibre direct detection receivers optimally tolerant to jitter", IEEE Trans. Comm., vol. COM-34, pp. 1141-1147.

O'Reilly, J.J. and Fyath, R.S. (1988a): "Analysis of the influence of dark current on the performance of optical receivers employing superlattice APDs, IEE Proc., pt. J, vol. 135, pp. 109-118.

O'Reilly, J.J. and Fyath, R.S. (1988b): "New APD-based receivers providing tolerance to alignment jitter for binary optical communications", IEE Proc., pt. J, vol. 135, pp. 119-125.

O'Reilly, J.J. and Fyath, R.S. (1988c): "Performance of optical receivers employing ultra low noise APDs", J. Opt. Comm., vol. 9, pp. 82-84.

O'Reilly, J.J. and Fyath, R.S. (1989): "Performace aspects of superlattice and multiquantum well APDs", Symposium on Quantum Well Structures: Chemistry and Electronics, STL Harlow, U.K., paper 8.

Osaka, F. and Mikawa, T. (1986): "Excess noise design of InP/GaInAsP/GaInAs avalanche photodiodes", IEEE J. Quant. Electron., vol. QE-22, pp. 471-478.

Osaka, F., Mikawa, T. and Wada, O. (1986): "Electron and hole impact ionisation rates in InP/$Ga_{0.47}In_{0.53}As$ superlattice", IEEE J. Quant. Electron., vol. QE-22, pp. 1986-1991.

Pearsall, T.P., Temkin, H., Bean, J.C. and Luryi, S. (1986): "Avalanche gain in Ge_xSi_{i-x}/Si infrared waveguide detectors", Electron Devices Lett., vol. EDL-7, pp. 330-332.

Personick, S.D.(1973): "Receiver design for digital fibre optical communication systems", Pt.I and II, Bell Syst. Tech. J., vol.52, pp. 843-886.

Personick, S.D., Balaban, P., Bobsin, J. and Kumer, P. (1977): "Detailed comparison of four approaches to the calculation of the sensitivity of optical fibre system receivers", IEEE Trans. Comm., vol. COM-25, pp. 541-549.

Petroff, M.D., Staplebroek, M.G. and Kleinhans, W.A. (1987): "Detection of individual 0.4-28 μm wavelength photons via impurity-impact ionisation in a solid-state photomultiplier", Appl. Phys. Lett., vol. 51, pp. 406-408.

Prabhu, U.K. (1982): "Modified Chernoff bounds for PAM system with noise and interference", IEEE Trans. Inform. Theory, vol. IT-28, pp. 95-100.

Rideley, B.K.(1985): "Factors affecting impact ionisation in multilayer avalanche photodiodes", IEE Proc., pt. J., vol. 132, pp. 177-183.

Robbins, V.M., Wang, T., Brennan, K.F., Hess, K. and Stillman, G.E. (1985): "Impact ionisation coefficients in (100) and (111) silicon", J. Appl. Phys., vol. 58, pp. 4614-4617.

Rucker, L.M. and van der Ziel (1987): "Noise associated with JFET gate current resulting from avalanching in the channel", Solid-state Electron., vol. 21, pp.7 98-799.

Shikada, M., Fujita, S., Henmi, N., Mito, I., Taguchi, K. and Minemura, K. (1987): "Long-distance gigabit-range optical fibre transmission experiments employing DFB-LDs and InGaAs-APDs; J. Lightwave Technol., vol. LT-5, pp. 1488-1497.

Smith, R.G. and Personick, S.D. (1980): "Receiver design for digital fibre communication systems", in Semiconductor Devices for Optical Communication, Kressel, H. (Ed.), Brelin: Springer-Verlag, pp. 89-160.

Smith, R.G. and Forrest, S.R. (1982): "Sensitivity of avalanche photodetector receivers for long wavelength optical communications", Bell Syst. Tech. J., vol. 61, pp. 2929-2946.

Smith, J.S., Chin, L.C., Margalit, S. and Yariv, A. (1983): "A new infrared detector using electron emission from multiplequantum wells",. J. Vac. Sci. and Technol., vol. 1, pp. 376-378.

Snyder, D.L. (1975): "Random Point Processes", New York: Wiley.

Stillman, G.E. and Wolfe, C.M. (1977): "Avalanche photodiodes", in Semiconductors and Semimetals, Willardso, R.K. and Beers, A.C. (Eds.), vol. 12, New York: Academic, pp.291-393.

Stillman, G.E., Robbins, V.M. and Tabatabaie, N. (1984): "III-V compound semiconductor devices: optical detectors", IEEE Trans. Electron Devices, vol. ED-31, pp. 1643-1655.

Summers, C.J. and Brennan, K. 1986): "Variably spaced superlattice energy filter, a new device design concept for high energy electron injection", Appl. Phys. Lett., vol. 48, pp. 806-808.

Tager, A.S. (1965): "Current fluctuations in a semiconductor under the conditions of impact ionisation and avalanche breakdown", Sov. Phys.-Solid State, vol. 8, pp. 1919-1925.

Tanoue, T. and Sakaki, H. (1982): "A new method to control impact ionisation rate ratio by spatial separation of avalanching carriers in multilayered heterostructures", Appl. Phys. Lett., vol. 41, pp. 67-70.

Teich, M., Matsuo, K. and Saleh, B.E. (1986a): "Excess noise factors for c ontventional and superlattice avalanche photodiodes and photomultiplier tubes", IEEE J. Quant. Electron., vol. QE-22, pp. 1184-1193.

Teich, M., Matsuo, K. and Saleh, B.E. (1986b): "Counting distributions of error probabilities for optical receivers incorporating superlattice avalanche photodiodes", IEEE Trans. Electron Devices, vol. ED-33, pp. 1475-1488.

Teich, M.C., Matsuo, K. and Saleh, B.E. (1986c): "Time and frequency response of the conventional avalanche photodiode", IEEE Trans. Electron Devices, vol. ED-33, pp. 1511-1517.

Van der Ziel, A. and Chenette, E.R. (1987): "Noise in solid state devices", in Advances in Electron Physics, Marton, L. (Ed.), vol. 46, pp. 313-383.

Van der Ziel, A., Yu, Y.J., Bosman, G. and van Vliet, C.M. (1986): "Two simple proofs of Capasso's excess noise factor F_N of an ideal N-stage staircase multiplier", IEEE Trans. Electron Devices, vol. QE-33, pp. 1816-1817.

Van Vliet, K.M. and Rucker, L.M. (1979): "Theory of carrier multiplication and noise in avalanche devices, pt. I: one-carrier processes", IEEE Trans. Electron Devices, vol. ED-26, pp. 746-751.

Van Vliet, K.M. Friedmann, A. and Rucker, L.M. (1979): "Theory of carrier multiplication and noise in avalanche devices, pt. II: two-carrier processes", IEEE Trans. Electron Devices, vol. ED-26, pp. 752-764.

Webb, P.P., McIntyre, R.J. and Conradi, J. (1974): "Properties of avalanche photodiodes", RCA. Rev., vol. 35, pp. 234-278.

Williams, G.F., Capasso, F. and Tsang, W.T. (1982): "The graded bandgap multilayer avalanche photodiode: a new low-noise detector", IEEE Electron Devices Lett., vol. EDL-3, pp. 71-73.

Wu, J., Wu, I-Fan and Lee, S-L (1988): "Calculation of error probability for optical fibre communication systems by Edgeworth series", J. Opt. Comm., vol. 19, pp. 67-71.

Yu, Y.-J, Bosman, G. and Bhattacharya, P.K. (1987): "Impact ionisation coefficient ratio in InGaAs/InA1As superlattice avalanche photodiodes determined from noise measurement", Appl. Phys. Lett., vol. 51, pp. 1433-1435.